Exploiting Process Topology for Optimal Process Monitoring

by

Brian Siegfried Lindner

Thesis presented in partial fulfilment
of the requirements for the Degree

of

MASTER OF ENGINEERING

(EXTRACTIVE METALLURGICAL ENGINEERING)

in the Faculty of Engineering
at Stellenbosch University

Supervisor
Dr. Lidia Auret

December 2014

Declaration

By submitting this thesis electronically, I declare that the entirety of the work contained therein is my own, original work, that I am the sole author thereof (save to the extent explicitly otherwise stated), that reproduction and publication thereof by Stellenbosch University will not infringe any third party rights and that I have not previously in its entirety or in part submitted it for obtaining any qualification.

Date: December 2014

Summary

Modern mineral processing plants are characterised by a large number of measured variables, interacting through numerous processing units, control loops and often recycle streams. Consequentially, faults in these plants propagate throughout the system, causing significant degradation in performance. Fault diagnosis therefore forms an essential part of performance monitoring in such processes.

The use of feature extraction methods for fault diagnosis has been proven in literature to be useful in application to chemical or minerals processes. However, the ability of these methods to identify the causes of the faults is limited to identifying variables that display symptoms of the fault. Since faults propagate throughout the system, these results can be misleading and further fault identification has to be applied. Faults propagate through the system along material, energy or information flow paths, therefore process topology information can be used to aid fault identification. Topology information can be used to separate the process into multiple blocks to be analysed separately for fault diagnosis; the change in topology caused by fault conditions can be exploited to identify symptom variables; a topology map of the process can be used to trace faults back from their symptoms to possible root causes.

The aim of this project, therefore, was to develop a process monitoring strategy that exploits process topology for fault detection and identification. Three methods for extracting topology from historical process data were compared: linear cross-correlation (LC), partial cross-correlation (PC) and transfer entropy (TE). The connectivity graphs obtained from these methods were used to divide process into multiple blocks. Two feature extraction methods were then applied for fault detection: principal components analysis (PCA), a linear method, was compared with kernel PCA (KPCA), a nonlinear method. In addition, three types of monitoring chart methods were compared: Shewhart charts; exponentially weighted moving average (EWMA) charts; and cumulative sum (CUSUM) monitoring charts. Two methods for identifying symptom variables for fault identification were then compared: using contributions of individual variables to the PCA SPE; and considering the change in connectivity. The topology graphs were then used to trace faults to their root causes.

It was found that topology information was useful for fault identification in most of the fault scenarios considered. However, the performance was inconsistent, being dependent on the accuracy of the topology extraction. It was also concluded that blocking using topology information substantially improved fault detection and fault identification performance. A recommended fault diagnosis strategy was presented based on the results obtained from application of all the fault diagnosis methods considered.

Opsomming

Moderne mineraalprosesseringsaanlegte word gekarakteriseer deur 'n groot aantal gemete veranderlikes, wat in wisselwerking tree met mekaar deur verskeie proseseenhede, beheerlusse en hersirkulasiestrome. As gevolg hiervan kan foute in aanlegte deur die hele sisteem propageer, wat prosesprestasie kan laat afneem. Foutdiagnose vorm dus 'n noodsaaklike deel van prestasiemonitering.

Volgens literatuur is die gebruik van kenmerkekstraksie metodes vir foutdiagnose nuttig in chemiese en mineraalprosesseringsaanlegte. Die vermoë van hierdie metodes om die fout te kan identifiseer is egter beperk tot die identifikasie van veranderlikes wat simptome van die fout vertoon. Aangesien foute deur die sisteem propageer kan resultate misleidend wees, en moet verdere foutidentifikasie metodes dus toegepas word. Foute propageer deur die proses deur materiaal-, energie- of inligtingvloeipaaie, daarom kan prosestopologie inligting gebruik word om foutidentifikasie te steun. Topologie inligting kan gebruik word om die proses in veelvoudige blokke te skei om die blokke apart te ontleed. Die verandering in topologie veroorsaak deur fouttoestande kan dan analiseer word om simptoomveranderlikes te identifiseer. 'n Topologiekaart van die proses kan ontleed word om moontlike hoofoorsake van foute op te spoor.

Die doel van hierdie projek was dus om 'n prosesmoniteringstrategie te ontwikkel wat prosestopologie benut vir fout-opspooring en foutidentifikasie. Drie metodes vir topologie-ekstraksie van historiese prosesdata is met mekaar vergelyk: liniêre kruiskorrelasie, parsiële kruiskorrelasie en oordrag-entropie. Konnektiwiteitsgrafieke verkry deur hierdie ekstraksie-metodes is gebruik om die proses in veelvoudige blokke te skei. Twee kenmerkekstraksiemetodes is hierna toegepas om foutdeteksie te bewerkstellig: hoofkomponentanalise (HKA), 'n liniêre metode; en kernhoofkomponentanalise (KHKA), 'n nie-lineêre metode. Boonop was drie tipes moniteringskaart metodes vergelyk: Shewhart kaarte, eksponensieel-geweegde bewegende gemiddelde kaarte en kumulatiewe som kaarte. Twee metodes om simptoom veranderlikes te identifiseer vir foutidentifikasie was daarna vergelyk: gebruik van individuele veranderlikes; en inagneming van die verandering in konnektiwiteit. Die konnektiwiteitgrafieke was daarna gebruik om hoofoorsake van foute op te spoor.

Dit is gevind dat topologie informasie nuttig was vir foutidentifikasie vir meeste van die fouttoestande ondersoek. Nogtans was die prestasie onsamehangend, aangesien dit afhanklik is van die akkuraatheid waarmee topologie ekstraksie uitgevoer is. Daar was ook afgelei dat die gebruik van topologie blokke beduidend die fout-opspooring en foutidentifikasie prestasie verbeter het. 'n Aanbevole foutdiagnose strategie is voorgestel.

Acknowledgements

I would like to express my appreciation to those who made this project possible:

- To my supervisor, Dr. Lidia Auret, for all the patient guidance, inspiration, motivation and advice. Even though I'm not too sure why I chose one of your topics for my skripsie, I'm glad I did, since it helped me find a field of research I'm passionate about.
- To Anglo American Platinum for their financial support of this project.
- To both my parents, for your unwavering support and encouragement.
- To my brothers, Bernie, Gerard and Vincent, for your words of encouragement whenever I needed it most. In every endeavour that I've undertaken you've gone before me and paved the way for me and walked with me, and this project was no different.
- To God, the ever-present benefactor in my life, for His guidance. Everything in my life, including this project, is a testimony to his grace and love.

Table of Contents

Nomenclature

Acronyms	Description
AM	Adjacency Matrix
AUC	Area Under ROC Curve
CM	Connectivity Matrix
CUSUM	Cumulative Sum
DD	Detection Delay
EWMA	Exponentially Weighted Moving Average
FAR	False Alarm Rate
FEM	Feature Extraction Method
FIM	Fault Identification Method
KPCA	Kernel Principal Component Analysis
KPI	Key Performance Indicator
LC	Linear Cross-correlation
MAR	Missing Alarm Rate
MCM	Monitoring Chart Method
MFR	Mass Flow Rate
NOC	Normal Operating Conditions
PC	Partial Cross-correlation
PCA	Principal Component Analysis
PID	Proportional Integral Derivative
PPM	Pre-processing Method
PSD	Particle Size Distribution
ROC	Receiver Operator Characteristic curve
SA	Shared Ancestors
SCC	Strongly Connected Components
SD	Shortest Distance
SPE	Squared Prediction Error
TAR	True Alarm Rate
TE	Transfer Entropy
TEM	Topology Extraction Method

Symbols	Description
A	Number of retained components. (A<M)
C	Covariance matrix
c	Kernel width
C^{SPE}	Contribution of single variables to the SPE
h	Transfer entropy prediction horizon
$\tilde{\mathbf{K}}$	Scaled kernel matrix
K	Kernel matrix (NxN)
k	Number of lags for cross-correlation
k_{max}	Lag corresponding to maximum correlation
lx	Embedding dimension for vector **x** in transfer entropy calculation
ly	Embedding dimension for vector **y** in transfer entropy calculation
M	Number of variables
N	Number of samples
P	MxM principal components loadings matrix
p(**x**,**y**)	Joint probability density function of **x** and **y**
p(**z**|**x**,**y**)	Joint conditional probability of **x** and **y** conditioning on **z**
$\mathbf{P_A}$	MxA matrix of retained principal components loadings
$\mathbf{p_m}$	m^{th} principal component (Mx1 vector)
r	EWMA weighting
T	NxM Matrix of principal component scores for training data
t(**x**|**y**)	Transfer entropy from **y** to **x**
$\mathbf{T_A}$	NxA matrix of retained scores
T_A^2	Modified Hoteling's T^2 statistic
$\mathbf{t_m}$	m^{th} principal component score (Nx1 vector)
$\mathbf{T^{test}}$	NxM matrix of test scores
$t_{\mathbf{x}\rightarrow\mathbf{y}}$	Transfer entropy causality measure
x	single sample scalar
x	Nx1 vector of a single measured variable
X	NxM matrix of historical process data
$\hat{\mathbf{X}}$	Reconstructed data matrix
X	NxM matrix of historical process data
z	Represents either SPE or T_A^2 statistic

Greek Symbols	Description
$\boldsymbol{\alpha_m}$	KPCA loading vector
$\alpha_{n,m}$	KPCA loading coefficient
λ_m	variance of m^{th} principal component
$\tilde{\lambda}_m$	Scaled eigenvalue
μ	Mean
σ	standard deviation
ρ_k^{LC}	Linear correlation for lag k
ρ_{kmax}^{LC}	Maximum Linear correlation over all lags
σ^2	variance
$\Phi(x)$	mapping from input space to feature space

List of Figures

List of Tables

Chapter 1 - Introduction

1.1. Introduction to Process Monitoring

Modern processing plants are characterised by a large number of consecutive processing units often with recycle of material streams between them. The chemical processes within these units are often complex, and the processes tend to have a high overall throughput.

In recent years monitoring of large numbers of measured variables and key performance indicators has become possible as a result of improvements made in sensors to measure the variables, large data historians to collect and store the historical process measurements, as well as improvements in the techniques to analyse the collected data.

Abnormal process behaviour, for example faulty sensors, malfunctioning valves or disturbances in feed conditions, may have a profound effect on the performance and safety of a process. Numerous control strategies are also typically implemented to ensure that the processes run safely and economically, according to the following objectives:

- Limiting unexpected downtime
- Preventing reduction of throughput/quality of product
- Reducing the risk of damage to equipment
- Improving operational efficiency and reliability
- Safe operation

These control strategies are implemented in multiple concentric layers to achieve the above-mentioned objectives. Figure 1-1 provides an illustration of these layers.

The first layer in Figure 1-1 entails the basic process control systems (BPCS). This involves basic process control at the plant level with standard sensors to measure flow rates, temperatures…etc. and various (feedback) control loops. The purpose of this layer is to keep process variables within safe and profitable operating windows by adjusting manipulated variables associated with them.

The second layer entails the automatic signalling of alarms when the process begins to move outside its specified operating window. This indicates an abnormal event, or a “fault” occurring in the process. Alarms alert the operator(s) of the fault in the process so that corrective actions can be manually administered.

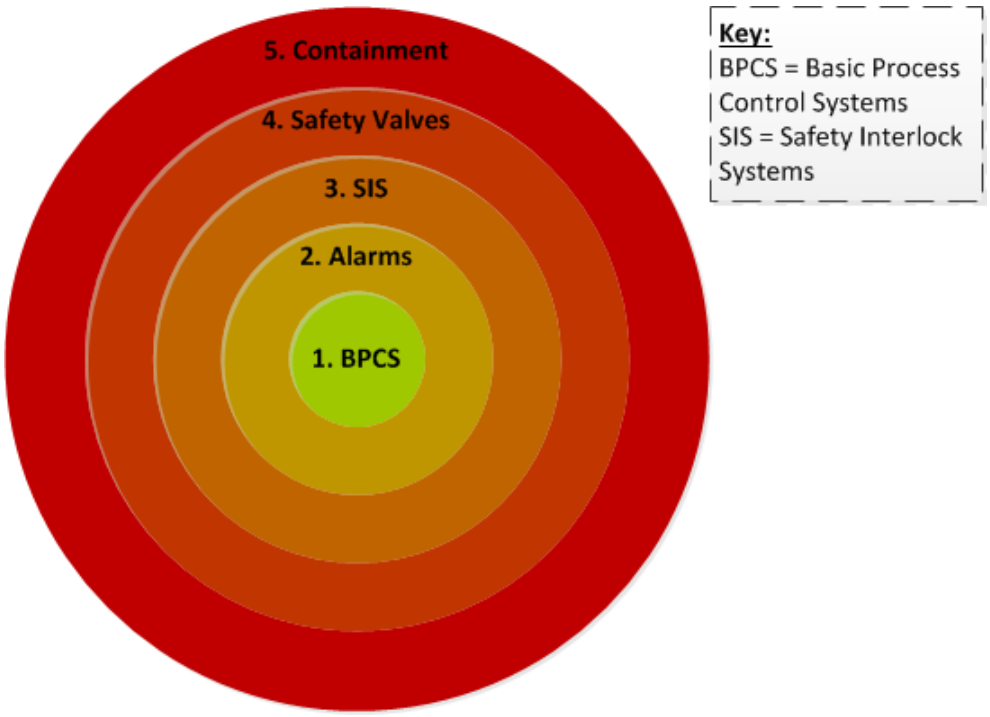

Figure 1-1: Layers of control for performance and safety in processing plants

The third layer entails safety interlock system (SIS) (occasionally called emergency shutdown systems). These systems employ automatic feedback control when process variables come close to exceeding the safe limits of operation; violation of which could cause harm to people, the environment or processing equipment. Preventing such situations is of extreme importance, so the automatic control actions will disrupt process operation: typically shutting down the whole process or sections of it by immediately closing or opening specific valves.

The fourth layer, safety valves (relief valves), entails feedback loops that are automatic and self-actuating. This means that these systems do not require electrical, pneumatic or hydraulic power sources. For example a pressure valve held closed by a spring, which opens when the pressure exceeds the force of the spring to relieve the build-up of pressure in a container.

The fifth and final layer entails containment of hazardous flows, or perhaps fires. This layer does not prevent incidents, but rather limits its effect to a certain section of the plant or prevents harming areas surrounding the plant.

Process monitoring is implemented at the second level: alarms. A large number of process variables can be measured using sensors, and these measurements may be recorded, generating historical process data. The performance of the process can be monitored by analysing this data. For short-term process monitoring, the measured variables can be monitored online and an alarm can be signalled when it is observed that the process has moved outside the bounds of acceptable or desirable operating conditions. The long-term implementation of process monitoring involves

analysing the historical data to determine the reasons for periods of improvement or degradation of performance.

1.2. Fault Diagnosis

A fault in a processing plant is an abnormal event that results in deviation of measured variables or key performance indicators (KPIs) from an acceptable or desirable range. Fault diagnosis forms a part of process monitoring that includes fault detection, to detect the presence of abnormal events, and fault identification, to obtain further details about the abnormal events.

1.3. Use of Feature Extraction for Fault Diagnosis

Modern processing plants have a large number of measured variables that are highly interconnected through process units, recycle streams and control loops. This degree of interconnection results in faults propagating throughout the process and affecting a large number of variables, therefore it is necessary to monitor multiple variables simultaneously so that no information is lost when determining whether the behaviour of the process has altered from its normal operating conditions (NOC). Feature extraction methods, such as principal component analysis (PCA), may be employed to reduce the large intercorrelated data sets to a lower dimensional space that retains only the essential information and is easier to analyse.

1.3.1. Linear vs. nonlinear feature extraction for fault detection

One limitation of standard PCA is that it is a linear method and may lead to inadequate results when applied to processes that show nonlinear behaviour. Nonlinear feature extraction algorithms, such as kernel principal components analysis (KPCA), can be applied to improve fault detection.

1.3.2. Modifications to standard monitoring charts for feature extraction statistics

PCA and KPCA allow multivariate statistics, namely the modified Hotteling's (T_A^2) and squared prediction error (SPE) statistics to be calculated to measure the deviation of the process data from NOC. The T_A^2 and SPE statistics are typically monitored using simple Shewhart charts, which only take into account current time information. Incorporation of cumulative sum (CUSUM) and exponentially weighted moving average (EWMA) charts may be more suitable for detection of small shifts in the process since both take into account previous values of the statistics.

1.3.3. Multiblock process monitoring to improve fault diagnosis

Although PCA and KPCA are effective at analysing combined data from the whole process, some information may be obscured by the effects of the other variables. Additionally, the results from the feature extraction may not allow for ready interpretation of where in the process the fault occurred.

Separating the data into multiple blocks to be monitored separately may therefore improve detection, as well as identification, in comparison to plant-wide monitoring. This is known as multiblock monitoring, decentralised monitoring or distributed monitoring. Typically the variables are separated into blocks according to units or sub-sections of the process. However, since effects propagate through the system and the systems are connected, the effects of the fault may be spread over multiple units, therefore blocking solely accordin to process units may result in inadequate detection performance.

1.3.4. Limitations of feature extraction for fault identification

Standard methods used for identifying faults detected using PCA involve contribution plots, where the contributions of each variable to the SPE statistic under fault conditions are calculated. This allows identification of a group of variables that are either key contributors to the fault, or that show symptoms of the fault as a result of the fault propagating through these variables from some upstream cause. Unfortunately, the high degree of intercorrelation of process units and variables results in faults propagating throughout the system, meaning that it is unlikely that the variables highlighted by the contribution plots are the root causes of the faults. In addition, not all faults correspond to a single process variable that represents the root cause. The root cause might be a change in some variable or property that is not measured. For example if the fault were caused by fouling of cooling coils in a process, there is no measurement that would indicate directly that fouling has occurred. The temperatures in the process might show large contributions and be identified as symptoms. For this reason additional information about the system is required to identify the fault.

1.4. Use of Process Topology to Aid Fault Diagnosis

Once a fault has been detected it is necessary to perform fault identification to determine the location of the fault The location of the fault refers to where in the process the fault originated, or its root cause; this could mean isolation of a unit or part of the process, or a single variable that indicates the origin of the fault. This information allows the operator to identify where in the plant the problem lies and where to take corrective action.

1.4.1. Use of topology for fault identification

Since the ability of the feature extraction methods introduced to identify fault conditions is limited, further fault identification methods need to be applied. Process topology information, which describes how variables and units are connected to each other, can be used to aid fault identification in two ways. Firstly, topology can be used to trace a fault back from variables that have been identified as symptoms to a possible root cause by tracing back along connections between

variables. Secondly, the topology structure of process changes with the presence of a fault, this can be used to gain some information about the fault.

1.4.2. Use of topology for pre-processing

In addition to its use for fault identification, topology information can be used for pre-processing of the data to aid both fault detection and fault identification. Topology information can be used in application to multiblock monitoring methods since the process can be separated into blocks according to strongly connected groups of variables.

1.4.3. Extracting topology from process data

Historical process data can be used to extract process topology information through a number of methods, such as linear cross-correlation (LC), partial cross-correlation (PC) or transfer entropy (TE).

1.5. Aims of this Project

The aim of this project is to develop, test and compare data-based process monitoring approaches that exploit process topology to aid fault detection and identification in order to develop an optimal approach to process monitoring. Performance of the monitoring strategy will be judged according to the fault detection performance (specifically in terms of false alarm rates, missing alarm rates, detection speed) as well as fault identification performance (specifically in terms of the ability to determine the location of the fault). Additionally the general performance of each method well be judged according to consistency and robustness.

1.6. Objectives of this Project

1) Determination of whether topology information can be used to aid fault identification using connectivity change and back propagation in connectivity graphs.
2) Determination of whether automatic blocking of data according to connected components in connectivity graphs improves fault diagnosis.
3) Testing of all possible combinations of fault diagnosis methods considered to determine which combination provides best fault detection performance and best fault identification performance.

1.7. Scope of Work for this Project

1) Only Linear correlation, partial correlation and transfer entropy topology extraction methods will be considered. These are sufficient for the purposes of this project since this includes a non-linear method (TE) and a method that focuses on elimination of indirect connections (PC).

2) Only PCA and KPCA fault detection methods will be considered since this allows comparison of linear and nonlinear techniques. Additionally, the focus of the project is not to compare different types of feature extraction methods, rather to demonstrate and test the incorporation of feature extractive methods with process topology to aid fault diagnosis.
3) Three case studies are considered for the testing of the fault diagnosis methods. The first case study includes four differnet faults, the second case study includes two different faults and the final case study considers only one fault.

1.8. Outline of this Thesis

The outline of this thesis is as follows:

- Chapter 2 gives a description of the feature extraction methods and related fault detection techniques considered and a discussion of their use in literature.
- Chapter 3 follows with a description of topology extraction methods considered and the application of topology to fault diagnosis with a discussion of the available literature.
- Chapter 4 presents the fault diagnosis methodology with different combinations of the considered methods and discusses how the methodology will be tested in subsequent chapters.
- Chapter 5 presents the results of application of this methodology to the first case study, which is a dynamic simulation of Two-Tanks with heat exchange.
- Chapter 6 presents the results of application of this methodology to the second case study, which is a dynamic simulation of a pressure leaching system in a base metals refinery.
- Chapter 7 presents the results of application of this methodology to the third case study, which is a real industrial case study of a concentrator process.
- Chapter 8 then presents conclusions reached on the optimal diagnosis strategy in light of the results for each case study.
- Chapter 9 presents the recommended fault diagnosis strategy in view of the results, as well as recommendations for further study.

Chapter 2 - Feature Extraction for Fault Diagnosis

Processing plants continuously collect and store large amounts of data from sensors measuring process variables, which can be analysed to monitor the performance of the process. Through such data-based analysis, alarms can be signalled to indicate when the process is behaving abnormally, indicating the presence of a fault.

2.1. Definition of a Fault

Before the detection of faults is discussed it is first necessary to define what is meant by the term "fault". A fault in a processing plant is an abnormal event that results in deviation of measured variables or key performance indicators (KPIs) from an acceptable or desirable range. Therefore a fault is an event that causes the process to depart from normal operating conditions (NOC). The definition of what constitutes normal conditions is subjective, and classification between faulty and normal conditions is dependent on a number of factors, including: characteristics of the process under consideration, the aims of the process defines what is acceptable deviation; the behaviour of the measured variables chosen for performance monitoring; the accuracy of the statistic used for performance monitoring (Himmelblau, 1978).

To be able to monitor the performance of a process therefore it is necessary to monitor some KPIs or have some statistic that is representative of the process performance.

2.2. Univariate Process Monitoring

Recording of the measurements data from the sensors on the plant results in a data matrix represented in Equation 2-1.

$$\mathbf{X} = \begin{bmatrix} \mathbf{x}_{1,1} & \mathbf{x}_{1,2} & \cdots & \mathbf{x}_{1,M} \\ \mathbf{x}_{2,1} & \mathbf{x}_{2,2} & \cdots & \mathbf{x}_{2,M} \\ \cdots & \cdots & \cdots & \cdots \\ \mathbf{x}_{N,1} & \mathbf{x}_{N,2} & \cdots & \mathbf{x}_{N,M} \end{bmatrix} \qquad \textbf{Equation 2-1}$$

The result is an NxM data matrix represented by the symbol **X**, where N is the number of observations and M is the number of variables.

As mentioned in section 2.1, performance monitoring requires monitoring of some KPIs in the process or some statistic that is representative of the process performance. In the past, most industrial process monitoring strategies used univariate (single variable) control charts to monitor process performance (Kourti, 2002). In such strategies a few key process variables are selected for monitoring. Limits are set for these variables demarcating the normal window of operation; when these limits are violated an alarm is signalled, notifying the operator of a possible fault. However,

this strategy is impractical since plants typically have a large number of variables that can be measured. Selecting which measured variables to analyse to give a good representation of the process performance, without ignoring valuable information that may be contained in other variables, is therefore difficult. Monitoring multiple variables individually can lead to poor design of an alarm system; the operator may receive an unmanageable number of alarms. The standard for the acceptable number of alarms per hour, as specified in ISA, Management of Alarm Systems for the Process Industries, ANSI/ISA Standard 18.2, 2009, is 6 alarms per hour per operator, with the maximum manageable alarms being 12. Izadi et al. (2011) compiled the data shown in Table 2-1 to show how many alarms are typically received per hour in various chemical industries. Clearly the number of alarms is far too high, indicating that univariate monitoring may be a poor design.

Table 2-1: Typical number of alarms signalled to operators (redrawn from Izadi et al. (2011))

	ISA Standard	Oil & Gas	Petrochemical	Power	Other
Average No. of Alarms per hour per operator	6	36	54	48	30
Average no. of standing alarms		50	100	65	35
Peak Alarms per hour	12	1320	1080	2100	1080

A high degree of intercorrelation between variables also typically exists due to the fact that they are connected by processing units, recycle streams and control loops. This means that variables are not independent of each other and single variables may not supply adequate information for the detection of a fault; the presence of a fault can affect the interaction of multiple variables and is therefore a multivariate approach may be required.

Figure 2-1, redrawn from Kourti (2002), illustrates why using separate univariate control charts may give inaccurate monitoring results. Two variables, X1 and X2, are plotted against each other in Figure 2-1. a) (note that the two are correlated). The ellipse represents a (1-α)% confidence limit under the assumption of a multivariate normal distribution for the two variables. The same variables are plotted individually with each of their upper and lower limits: X2 in Figure 2-1. b) and X1 in Figure 2-1. c). Consider the measurement represented by the blue **x** symbol. In both univariate charts it appears as if that measurement is well within the operating limits, therefore with univariate monitoring no alarm would be signalled. However, it is clearly outside of the operating limits when plotted on a multivariate chart. Along the same vein, the measurement represented by the red symbol ◊ is outside of both variables' operating limits, yet still within the joint limits. Therefore with univariate monitoring, in this case the measurement would trigger an alarm even though the process is behaving normally, i.e. a false alarm would be triggered.

The design of a monitoring system may therefore be improved by employing multivariate (as opposed to univariate) monitoring.

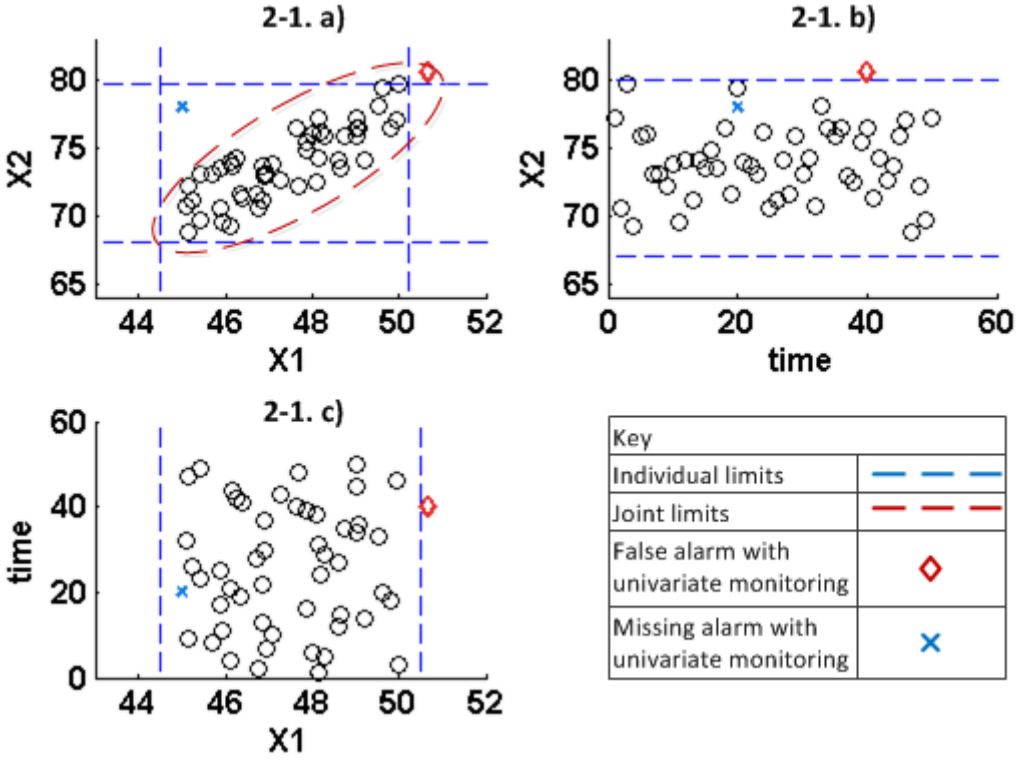

Figure 2-1: Problem associated using separate univariate control charts for process monitoring. a) shows two cocorrelated variables plotted against each other with their joint confidence limits, b) and c) show each variable plotted individually against time with their individual confidence limits. Redrawn from Kourti (2002)

2.3. Multivariate Process Monitoring

Due to the limitations of unviariate monitoring, discussed section 2.2, multivariate monitoring may be incorporated for improved fault detection ability. When a process is behaving well, under normal operating conditions (NOC), the data have a probability distribution corresponding to these NOC. When a fault occurs, the process deviates from NOC and the underlying distribution changes; so fault detection strategies aim to detect such deviations, allowing inference that a fault has occurred.

Numerous multivariate monitoring methods exist. As mentioned in section 2.2, the measured variables are highly intercorrelated, which means that most of the variation in the data is caused by only a few underlying events and all the measurements are only varying manifestations of these events (Kourti, 2002). These underlying events could be fluctuations in the feed stream flow rates, temperatures or compositions, small process disturbances or any other common cause variations. Feature extraction can be employed to effectively isolate these underlying events, or features. This effectively reduces the dimensionality of the large data sets comprised of a large number of

variables to only a few features that contain most of the essential information, allowing for easier and more effective analysis.

Feature extraction approaches based on historical process data that have been applied to process monitoring can be divided into two groups: multivariate statistical methods and neural networks (Venkatasubramanian et al., 2003b).

These methods are applied by training the feature extraction models on data obtained from the process during NOC. When the new data is projected onto the feature space, the presence of a fault can be inferred when the new data points show different behaviour in the feature space. Additionally, movement off of this feature space implies that the model is no longer valid, also allowing inference that a different type of change has occurred.

2.4. Linear feature extraction methods

Principal component analysis (PCA) is a multivariate statistical approach that has been widely applied for fault detection in chemical and mineral processes. PCA extracts the features by projecting the data onto orthogonal vectors, called principal components, in the directions that explain the maximum variation of the data (Venkatasubramanian et al., 2003b). Another perspective of this explanation is that PCA is an orthogonal transformation of the data from its normal coordinate system (or space) to a new coordinate system defined by the principal components (Schölkopf et al., 1998). Typically, most of the variation in the data is captured in the first few principal components, therefore only these components have to be considered. This means that the feature space is of a lower dimension than the original space.

The extraction of features using PCA is described in this section, while the actual application for fault detection is described in detail in chapter 4.

2.4.1. Principal components analysis calculation

In PCA calculation, the first principal component explains the most variation in the data and subsequent components explain progressively less of the variation. The m^{th} principal component is defined by calculating the linear combination represented by Equation 2-2.

$$\mathbf{t^m} = \mathbf{X}\mathbf{p^m} \qquad \textbf{Equation 2-2}$$

where $\mathbf{p^m}$ represents the m^{th} principal components loading and $\mathbf{t^m}$ represents the m^{th} principal component score, that gives the maximum variance subject to $|\mathbf{p^m}| = 1$ and with $\mathbf{t^m}$ being orthogonal to all other components. The orthogonality criterion ensures that the m^{th} component is completely uncorrelated with all other components. Spectral decomposition of the covariance matrix of **X** gives the principal component loading vectors, $\mathbf{p^m}$, as the eigenvectors of the covariance matrix. The

corresponding eigenvalues, λ_m, represent the variance of the principal components. Typically, most of the variance in the data is accounted for by the first few principal components. Therefore the data set, **X**, can be approximately reconstructed as, $\widehat{\mathbf{X}}$, as shown in Equation 2-3 by retaining only the first A principal components, where A < M, without significant loss of information essential to describing the trends in the data. This calculation presents a reconstruction of the data onto its original space from the feature space.

$$\widehat{\mathbf{X}} = \mathbf{T_A P_A^T} \qquad \textbf{Equation 2-3}$$

In Equation 2-3 the T superscript indicates matrix transpose. Some authors (Dong and McAvoy, 1996; MacGregor and Kourti, 1995) suggest cross-validation as the most reliable method of selecting the appropriate number of principal components to retain. A simpler method is to calculate the fraction of variance accounted for by each principal component. The cumulative sum of these fractions by retaining A principal components can then be calculated and a selection can be made based on a certain fraction of variance, e.g. at least 0.9. This method was used by Dong and McAvoy (1996).

The matrix of principal component loadings, **P,**is used to project unseen data (also referred to as test data) onto the retained principal components to give the test principal component scores, $\mathbf{T_A^{test}}$, in the feature space. **P** consists of the loading vectors of the retained principal components, $\mathbf{p^1},\ldots,\mathbf{p^A}$. This projection is performed according to Equation 2-4.

$$\mathbf{T_A^{test}} = \mathbf{X^{test} P_A} \qquad \textbf{Equation 2-4}$$

The test data can then be reconstructed using the loading matrix of retained principal components, and the matrix of retained principal component scores, according to Equation 2-5.

$$\widehat{\mathbf{X}}^{\mathbf{test}} = \mathbf{T_A^{test} P_A^T} \qquad \textbf{Equation 2-5}$$

2.4.2. Principal component analysis monitoring statistics

Monitoring is achieved by comparing the distribution of the test features to the distribution of the features obtained by the projection of the NOC training data. When the groupings or patterns of the test data projected onto the feature space are different than those of the NOC scores this may indicate abnormal conditions. This can be visualised by plotting the retained scores, or features, against each other to see their configuration in the feature space.

Such visual inspection may provide qualitative evidence that a fault has occurred, but the deviation of the test scores from the NOC scores can be quantitatively defined using two statistics based on the retained features: the modified Hotelling's T_A^2 statistic and the squared prediction error (SPE) statistic (Kourti, 2002).

Comparison of the **t** scores for the test data with those of the training data allow detection of behaviour that is different from that under which the PCA model was trained. The modified Hotelling's T_A^2 statistic can be used for this comparison. For a specific sample, n, the T_A^2 statistic is calculated by taking the square of the score for sample n, for the a^{th} retained component, dividing it by the variance for the a^{th} retained component and then summing that over all components, as shown in Equation 2-6.

$$T_{A,n}^2 = \sum_{a=1}^{A} \frac{\mathbf{t}_{n,a}^2}{\lambda_a} \qquad \textbf{Equation 2-6}$$

Monitoring of the T_A^2 statistic allows determination of whether the new observation has moved from the centre of the feature distribution described by the NOC training data (Dunia and Qin, 1998), i.e. the distance from the centre of the space defined by the NOC data in the feature space. When the statistic calculated for the test scores is significantly larger than that for the training scores it indicates that the variation in the test data in the feature space is greater than that of the training data, and therefore greater than that under NOC. The test of whether a sample's T_A^2 value is significantly large is determined by whether or not it exceeds the control limits set for this statistic. The selection of this limit is discussed in section 2.7.5. The presence of a fault can be inferred from this.

However, when the covariance between the measured variables is altered by a completely new type of event the test observation will move off the feature plane. The T_A^2 statistic will therefore not be able to detect such an event. Another statistic, the squared prediction error (SPE), calculates the distance of the new observation from the feature plane, and can thereby detect such events. The SPE for a single sample, n, sums the square of the error between the actual test data sample and the reconstructed data sample across all *M* variables, as shown in Equation 2-7.

$$SPE_n = \sum_{m=1}^{M} \left(x_{n,m}^{test} - \hat{x}_{n,m}^{test}\right)^2 \qquad \textbf{Equation 2-7}$$

The SPE represents the squared perpendicular distance of a new observation from the plane defined by the retained PCs (MacGregor and Kourti, 1995), i.e. the distance in the residual space. Under fault conditions the covariance between measured variables is altered from that observed under NOC, therefore the PCA model based on the training data can no longer predict the values of the variables correctly. The data reconstructed from this erroneous model will then be significantly different from the actual data, resulting in a large SPE. The test for whether a sample's SPE is significantly large is defined by the control limits set for this statistic, which is further discussed in section 2.7.5.

Figure 2-2, redrawn from Auret (2010), provides an illustration of the score space and the residual space confidence limits (represented by the cylinder) in the feature space projection of data. The blue sample points represent sample that would be classified as indicating NOC. The red points at the bottom of Figure 2-2 represent samples that would indicate fault conditions because of their large values for the T_A^2 statistic. The red points at the top of Figure 2-2 represent samples that would indicate fault conditions because of their large values for the SPE.

Although some authors suggest only the use of SPE (Dunia and Qin, 1998), it is clear that both the SPE and the T_A^2 statistics need to be used for a comprehensive and robust fault detection strategy, so that faults caused by new events and faults that are caused by variations of normal events can both be detected.

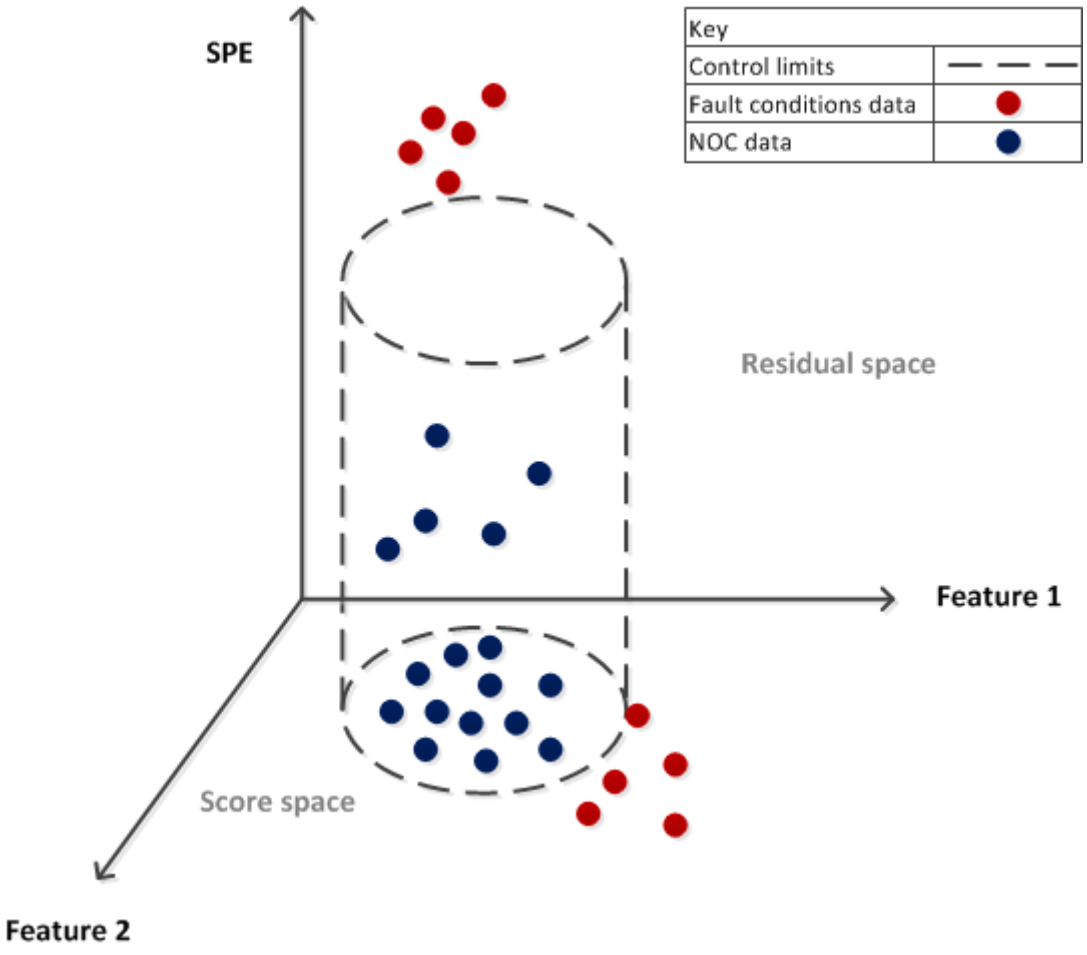

Figure 2-2: Data in feature and residual space with confidence limits. Redrawn from Auret (2010)

Application of standard PCA to process monitoring of industrial processing plants has been investigated by numerous authors (Dunia and Qin, 1998; Kano et al., 2002; Ku et al., 1995; MacGregor and Kourti, 1995; Wise and Gallagher, 1996).

Nomikos and MacGregor (1995) modified the PCA approach for application to batch processes using multiway PCA. Historical data from batch process will have multiple batches of data, with each batch having multiple variables with numerous samples collected in time; resulting in a three-dimensional matrix. Multiway PCA unfolds the matrix into a large two-dimensional matrix and then performs PCA on this new matrix (Nomikos and MacGregor, 1995).

Another modification to standard PCA is multi-scale PCA, which combines wavelet analysis with PCA so that each time scale can be sensitive to certain faults (Bakshi, 1998; Misra et al., 2002; Venkatasubramanian et al., 2003b). Variations within the time scale can be ignored since the wavelet analysis filters the data. The disadvantage of this variation is that it increases the dimension of the analysis since each variable is split into multiple scale-dependent variables (Venkatasubramanian et al., 2003b).

2.4.3. Contribution plots of variables to the squared prediction error

Once a fault has been detected the contribution of each variable to the SPE can be calculated in order to provide an idea as to which variables showed symptoms of the fault (i.e. which variables cause the PCA model to poorly predict the data). The fraction of the contribution of variable m to the SPE of a specific sample, n, can be calculated by dividing the SPE for that variable by the total SPE, as shown in Equation 2-8.

$$C_{n,m}^{SPE} = \frac{\left(x_{n,m}^{test} - \hat{x}_{n,m}^{test}\right)^2}{\sum_{m=1}^{M}\left(x_{n,m}^{test} - \hat{x}_{n,m}^{test}\right)^2} \qquad \textbf{Equation 2-8}$$

The average contribution for all samples can then be calculated. This information can be used to aid fault identification; the variables with large contributions can be highlighted as symptoms variables (variables that display symptoms of the fault). However, fault identification using only contributions obtained from the feature extraction method has some shortcomings. Faults occurring in large, interconnected processes can propagate throughout the process. Therefore a variable that displays symptoms of the fault does not necessarily correspond to a root cause of the fault, which may be further upstream. Additionally, the root cause of a fault does not necessarily correspond to any specific measured variable. For example if the fault were fouling in cooling coils of a process, no measured variable exists that corresponds to fouling; the symptoms displayed might indicate that a temperature fault has occurred. It is therefore necessary to incorporate further fault identification methods to determine more accurately the cause of the fault. This is discussed in Chapter 3.

2.5. Nonlinear feature extraction methods

One of the possible limitations of PCA is that, since it is a linear method, it may give inadequate results when applied to data from processes that show significant non-linear behaviour (Dong and

McAvoy, 1996). The minor components, that typically represent insignificant variance for linear processes, may contain important information in nonlinear processes (Xu et al., 1992). More components would have to be retained to ensure that all the important variation is captured, but this negates the advantage of dimension reduction gained by application of PCA.

Various nonlinear PCA algorithms have been developed. These include incorporating neural networks with PCA (Kramer, 1992), using principal curves and neural nets (Dong and McAvoy, 1996) and kernel principal components analysis (KPCA) (Lee et al., 2004; Schölkopf et al., 1998).

The problem with the neural network-PCA combination suggested by Kramer (1992) is that the proposed network consists of five layers, which would present significant difficulty for training; optimisation of the weights has to be performed where the results could be complicated by local optima, also the number of nodes for each layer has to be selected.

Application of Dong and McAvoy's (1996) method using principal curves and neural nets is limited to certain types of nonlinear behaviour; their principal curve algorithm assumes that nonlinear functions can be represented as a sum of nonlinear functions of the individual variables (Lee et al., 2004). Therefore nonlinear behaviour involving interaction between variables would be ignored. In addition, nonlinear optimisation has to be performed to compute the principal curves and train the neural networks, further complicating this method. An even further disadvantage is that in this method the number of PCs must be set before-hand, i.e. when the number of PCs retained is changed to account for all the important variation, the optimisation must be performed again.

KPCA first maps the input space nonlinearly into a higher dimensional feature space and then performs linear PCA in that feature space (Lee et al., 2004). The nonlinear data in the input space is more likely to be linear after mapping to this higher dimensional feature space (Lee et al., 2004) and the result is principal components of features that are nonlinearly related to the input variables. A kernel function maps the data from the input space to the nonlinear feature space, resulting in the dot-products in feature space (Schölkopf et al., 1998). Figure 2-3 (Lindner et al., 2014) provides an illustration of the extraction of 3D data onto a linear feature space (manifold) by PCA and onto a nonlinear feature space by KPCA.

Application of the kernel function approach using KPCA presents a more robust method of handling nonlinear data. Since it involves only linear algebra, without the added complexity introduced by nonlinear optimisation associated with the other methods, it is almost as simple as standard PCA. The only added complications are that the type of kernel function and its associated kernel parameters have to be selected.

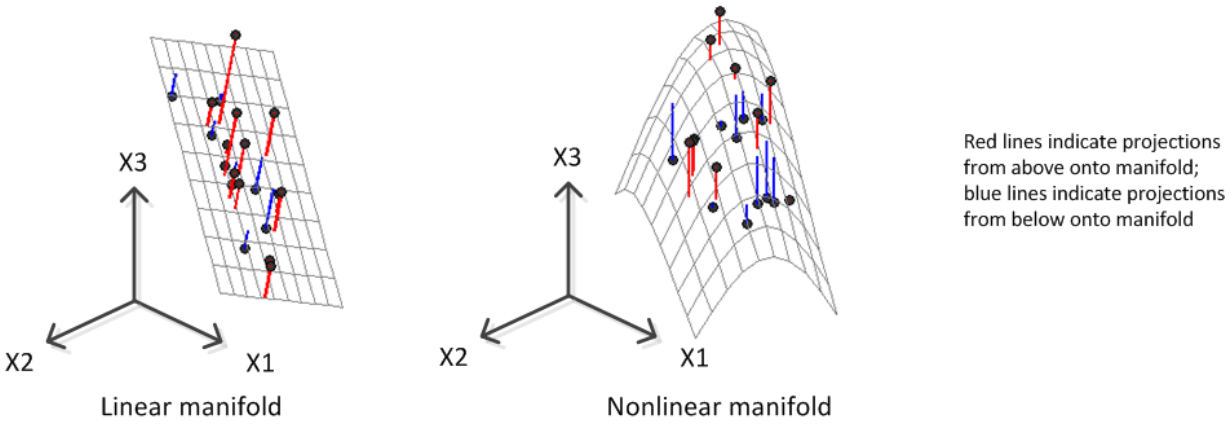

Figure 2-3: Illustration of linear and nonlinear 2D manifolds obtained by means of feature extraction for 3D data (Lindner et al., 2014)

2.5.1. Kernel principal component analysus calculation

When an algorithm can be solely expressed in terms of dot-products, the dot-products can be replaced by a kernel function (Schölkopf et al., 1998). This replacement is known as the kernel trick; it allows a linear function that can be expressed in terms of dot-products to be extended as a nonlinear algorithm with replacement by an appropriate kernel function. Using the kernel trick, KPCA finds orthogonal vectors in a dot-product space, $\mathcal{H}$, without having to explicitly calculate the dot-products for the mapping from the input space, $\mathcal{X}$, to $\mathcal{H}$.

The covariance matrix, **C**, in the dot-product space, $\mathcal{H}$, can be determined according to Equation 2-9 (Lee et al., 2004).

$$\mathbf{C} = \frac{1}{N}\sum_{n=1}^{N} \Phi(x_n)\Phi(x_n)^T \qquad \textbf{Equation 2-9}$$

In Equation 2-9, $\Phi(x)$ is the mapping from the input space to the feature space, whose dimensionality may be arbitrarily large, or even infinite (Schölkopf et al., 1998). It is assumed that $\sum_{n=1}^{N} \Phi(x_n) = 0$

The diagonalisation of the covariance matrix is achieved through eigendecomposition in the feature space, as shown in Equation 2-10 (Lee et al., 2004).

$$\mathbf{C}\mathbf{p}_m = \lambda_m \mathbf{p}_m \qquad \textbf{Equation 2-10}$$

In Equation 2-10, λ_m is the m^{th} eigenvalue associated with the m^{th} eigenvector $\mathbf{p}_m$. The eigenvectors become the principal components, ordered from the first principal component to the last principal component according to largest to smallest λ_m. There exist coefficients α_n such that:

$$\mathbf{p}_m = \sum_{n=1}^{N} \alpha_n \Phi(x_n) \qquad \textbf{Equation 2-11}$$

Combination of Equation 2-9, Equation 2-10 and Equation 2-11 results in Equation 2-12.

$$\lambda_m \sum_{j=1}^{N} \alpha_j \Phi(x_n) \cdot \Phi(x_j)^T = \frac{1}{N} \sum_{j=1}^{N} \alpha_{j,m} \Phi(x_n) \cdot \left(\sum_{i=1}^{N} \Phi(x_i) \Phi(x_i) \cdot \Phi(x_j) \right) \quad \textbf{Equation 2-12}$$

In Equation 2-12, n = 1,…,N. It can be seen in the above equation that the problem involves only dot-products of mapped vectors in the feature space; therefore if a kernel matrix, **K**, is defined so that:

$$\mathbf{K_{i,j}} = \Phi(x_i) \cdot \Phi(x_j) \quad \textbf{Equation 2-13}$$

Subsiuting Equation 2-13 into Equation 2-12 results in Equation 2-14.

$$\lambda_m \sum_{j=1}^{N} \alpha_{j,m} K_{n,j} = \frac{1}{N} \sum_{j=1}^{N} \alpha_{j,m} \sum_{i=1}^{N} K_{n,j} K_{j,i} \quad \textbf{Equation 2-14}$$

Equation 2-14 then reduces to Equation 2-15.

$$N\tilde{\lambda}_m \mathbf{K}\boldsymbol{\alpha_m} = \mathbf{K}^2 \boldsymbol{\alpha_m} \quad \textbf{Equation 2-15}$$

In Equation 2-15, $\tilde{\lambda}_m$ is the scaled eigenvalue $\tilde{\lambda}_m = \frac{\lambda_m}{N}$. Solution of Equation 2-15 is equivalent to solution of the eigenvalue problem (Schölkopf et al., 1998) represented by Equation 2-16.

$$N\tilde{\lambda}_m \boldsymbol{\alpha_m} = \mathbf{K}\boldsymbol{\alpha_m} \quad \textbf{Equation 2-16}$$

The m[th] feature score can then be calculated by projecting the mapping $\Phi(x)$ onto the eigenvector $\mathbf{p_m}$ as shown in Equation 2-17.

$$\mathbf{t^m} = \frac{1}{\sqrt{\tilde{\lambda}_m}} \sum_{n=1}^{N} \alpha_{n,m} k(\mathbf{x_n}, \mathbf{x}) \quad \textbf{Equation 2-17}$$

Similar to standard PCA, retaining only a few principal components still provides most of the information required, thereby reducing the dimensionality of the problem.

The kernel matrix, **K**, in Equation 2-13 is defined by a kernel function as shown in Equation 2-18.

$$\mathbf{K_{i,j}} = k(\mathbf{x_i}, \mathbf{x_j}) \quad \textbf{Equation 2-18}$$

A number of kernel functions exist, such as polynomial, sigmoid and Gaussian (also known as radial basis) kernels. In process monitoring applications, the Gaussian kernel is the most common. Calculation of the Gaussian kernel is shown in Equation 2-19.

$$k(\mathbf{x_i}, \mathbf{x_j}) = \exp\left(-\frac{\|\mathbf{x_i} - \mathbf{x_j}\|^2}{2c^2} \right) \quad \textbf{Equation 2-19}$$

In Equation 2-19, $\|\mathbf{x_i} - \mathbf{x_j}\|$ represents the norm between two sample vectors (a sample vector consists of values of all variables for that sample), and c represents the kernel width. Selection of the kernel width is discussed in 2.5.3.

It is assumed that mapped data are centred in $\mathcal{H}$, therefore the kernel matrices need to be centred as shown in Equation 2-20.

$$\widetilde{\mathbf{K}} = \mathbf{K} - \mathbf{K}\frac{\mathbf{1}_{N\times N}}{N} - \frac{\mathbf{1}_{N\times N}}{N}\mathbf{K} + \frac{\mathbf{1}_{N\times N}}{N}\mathbf{K}\frac{\mathbf{1}_{N\times N}}{N} \qquad \textbf{Equation 2-20}$$

In Equation 2-20, $\mathbf{1}_{NxN}$ denotes an N x N matrix of ones.

Test data can be projected onto the weight vectors obtained from the training data, giving the KPCA features of the new data. To perform this projection, the kernel matrix for the test data, $\mathbf{K^{test}}$, must first be calculated using the kernel function as shown in Equation 2-21.

$$\mathbf{K}_{\mathbf{i,j}}^{\mathbf{test}} = k\left(\mathbf{x_i}, \mathbf{x}_{\mathbf{j}}^{test}\right) \qquad \textbf{Equation 2-21}$$

In Equation 2-21, the vector $\mathbf{x_i}$ represents a sample vector from the training data, and $\mathbf{x_j^{test}}$ represents a sample vector from the training data

This matrix must also be centred:

$$\widetilde{\mathbf{K}}^{test} = \mathbf{K}^{test} - \mathbf{K}^{test}\frac{\mathbf{1}_{N\times N}}{N} - \frac{\mathbf{1}_{N^{test}\times N}}{N}\mathbf{K} + \frac{\mathbf{1}_{N^{test}\times N}}{N}\mathbf{K}\frac{\mathbf{1}_{N\times N}}{N} \qquad \textbf{Equation 2-22}$$

The m^{th} feature score for a test sample can be calculated by:

$$\mathbf{t_m} = \frac{1}{\sqrt{\tilde{\lambda}^m}}\sum_{n=1}^{N}\alpha_{n,m}\widetilde{K}_{n,j}^{test} \qquad \textbf{Equation 2-23}$$

2.5.2. Kernel principal components analysis monitoring statistics

As with linear feature extraction, monitoring statistics need to be calculated to quantify the distance in the feature and residual spaces to determine whether the process has deviated from NOC.

The Hotelling's T_A^2 statistic can be calculated in a manner identical to that of PCA, as shown in Equation 2-6.

With standard PCA reconstruction of the data from the feature space to input space is straightforward, as demonstrated by Equation 2-3 and Equation 2-5. With KPCA it is more complicated; applying the same reconstruction will give the reconstruction of the mapped data in $\mathcal{H}$, not the input space, $\mathcal{X}$. However, Lee et al. (2004) presented a simple method to calculate the SPE in the feature space, $\mathcal{H}$, without having to perform this explicit reconstruction. Their proposed SPE can be calculated as shown in Equation 2-24 (Lee et al., 2004).

$$SPE_n = \sum_{j=1}^{M} \left(t_n^j\right)^2 - \sum_{j=1}^{A} \left(t_n^j\right)^2 \qquad \textbf{Equation 2-24}$$

Where M is the total number of components and A is the number of retained components; i.e. the SPE is approximated as the difference between the sum of squared scores when all components are retained and the sum of squared score when only A components are retained.

2.5.3. Kernel width selection

The selection of the parameter, c, in Equation 2-19 affects the ability of KPCA to capture nonlinear features. When the kernel width chosen is too small it may separate single points. When it is too large, on the other hand, it encompasses all points and thus approximates PCA. The kernel width should at least be larger than the minimum distance between points to avoid separation of single points.

Various suggestions are provided for selection of the kernel width. Lee et al. (2004) used a heuristic based on the dimension of the input data (M), the variance of the data (σ^2) and a constant that depends on the specific process. Nguyen and Golinval (2010) suggest selecting the kernel parameter so that the variance accounted for by the first eigenvalue is above 50%. A more rigorous (robust) method is recommended by Aldrich and Auret (2013), that uses cross validation to select the kernel width.

2.6. Multiblock Process Monitoring

Monitoring the data from the entire process may lead to ineffective fault diagnosis, since the process may have a large number of units and the faults may have propagated throughout the system. Multiblock monitoring methods, where the process is divided into multiple blocks to be analysed separately and hierarchically, have been developed in order to improve fault diagnosis. Methods for dividing the process into blocks will be discussed in Chapter 3, while in this section the application of feature extraction once the data has been separated is discussed.

2.6.1. Consensus and hierarchical principal components analysis

There are two main variations of the multiblock modification of PCA: consensus PCA (CPCA) and hierarchical PCA (HPCA) (Qin et al., 2001; Westerhuis et al., 1998). In CPCA principal component scores and loadings are determined for each individual block and then the information is combined into “super scores”. HPCA is identical to CPCA, except the method in which the block scores and loadings are combined is different (Westerhuis et al., 1998). However, Westerhuis et al. (1998) proved that super scores from CPCA are identical to the scores of standard PCA, so the step of

combining the information is unnecessary; PCA (or KPCA) can be applied to each block separately to perform multiblock detection.

2.6.2. Application of multiblock process monitoring in literature

AlGhazzawi and Lennox (2008) applied CPCA for the monitoring of a complex refining process, separating the process into two blocks. The multiblock modification showed an improvement on monitoring without blocking and they were able to narrow the faults down to their blocks and then find the key contributing variables for each fault using contribution plots. Liu et al. (2013) extended CPCA to include multiple levels; i.e. blocking was performed and then these blocks were further subdivided. They found that this presented an improvement on CPCA which involves only the super level and the blocked level. Zhang et al. (2010) applied a multiblock KPCA approach to the Tennessee Eastman process. They effectively narrowed the faults down to specific blocks using this method.

2.6.3. Using mulitblock monitoring for fault diagnosis

Monitoring charts can be generated for each block, in this way it may be possible to isolate the block in which the fault originated; for example if a fault is detected in the second block, but not the first, then it is clear that the first block can be eliminated as a candidate for containing the root cause of the fault. Further root cause analysis can then be applied to identify the variable within the block that is most associated with the fault. By analysing each block separately, detection performance may be improved, since it eliminates interference from variables that are not so strongly affected by the fault. Additionally, it may improve identification, since if the fault is detected strongly in one block and not so strongly in another, the root cause of the fault can be narrowed down to one block. Root cause analysis can then be performed in this block only. The improvement to fault diagnosis presented by multiblock monitoring can therefore be in terms of both fault detection and fault identification.

2.7. Monitoring Charts

To monitor the performance of the process under observation, the SPE and T_A^2 statistics can be plotted against time on monitoring charts. Three variants of monitoring charts are considered: the Shewhart chart, the Cumulative Sum (CUSUM) chart and the Exponentially Weighted Moving Average (EWMA) chart.

2.7.1. Shewhart chart

The simplest chart is the Shewhart chart, which simply plots the calculated statistics for each sample against time. This method only uses information from the current observation, therefore when the deviation in the process behaviour is fairly small, but persistent the Shewhart chart would only show

that the current sample has slightly deviated from the NOC statistics and is therefore insensitive to slight shifts in the process. However, if it was taken into account that the previous samples also displayed slight deviation, it would indicate that a fault had occurred. The reverse is also true; in some cases a sudden spike in the SPE or T_A^2 can occur, and then return to normal. The Shewhart chart would then give a spurious alarm. In such cases methods that consider not just the current value, but previous values additionally, might improve detection. For this reason the CUSUM and EWMA monitoring charts were developed.

2.7.2. Cumulative sum chart

As the name implies, CUSUM calculates a cumulative sum of past values, usually summing the difference of the observations from the in-control mean. In this way it adds up the effect of small shifts in the process diagnostics. The basis for CUSUM charts is that they are a series of sequential probability ratio tests (MacGregor and Kourti, 1995); this means that it analyses the probability ratios of the statistics in question as they are collected.

CUSUM can be calculated according to Equation 2-25.

$$\mathrm{CUSUM}_n^z = \mathrm{Max}(0, C_{n-1}^z + z_n - \mu_z) \qquad \textbf{Equation 2-25}$$

In Equation 2-25, z may represent either the SPE or the T_A^2 statistic, and μ_z represents the in-control mean of the statistic.

2.7.3. Exponentially weighted moving average chart

EWMA sums past values, but gives progressively less weight to older data. The EWMA statistic can be calculated according to Equation 2-26.

$$\mathrm{EWMA}_n = rz_n + (1-r)\mathrm{EWMA}_{n-1} \qquad \textbf{Equation 2-26}$$

In Equation 2-26, r represents the selected weight (with $0 < r < 1$) and z may represent either the SPE or the T_A^2 statistic. Larger values of r give more smoothing and better detection of slight shifts in the process (MacGregor and Kourti, 1995).

2.7.4. Application of various monitoring charts in literature

Chen and Liao (2001) combined PCA with CUSUM and EWMA control charts for the T^2 and SPE statistics. In their approach they performed the CUSUM and EWMA calculations on the time series for each variable in the data. PCA was then performed on the altered data. The same approach used by Bin Shams et al. (2011) for their CUSUM-based PCA. In both applications the modifications resulted in improved detection with a slight sacrifice to detection speed. The alternative is to first perform PCA and then apply CUSUM and EWMA to the SPE and T^2 statistics. Wold (1994) developed an EWMA-based PCA method that applied EWMA montoring charts to the principal component

scores. Wachs and Lewin (1999) similarly proposed using a CUSUM method that sums the principal component scores over a moving window of observations. However, basing control charts only on the principal component scores individually ignores the importance of simultaneously monitoring the scores, which can be done easily with the SPE and T^2 statistics.

Crosier (1988) developed a CUSUM control chart based on the square root of the T_A^2 statistic that was discussed by Macgregor and Kourti (1995). They found that it improved detection without much sacrifice to detection speed.

2.7.5. Control limits for monitoring charts

In order to determine whether the statistic in one of the monitoring charts is large enough to signal a fault for that sample, significance thresholds, or control limits, have to be set. Figure 2-4 contains an illustrative example of a simple Shewhart chart. The dashed red line indicates the selected threshold, or limit. When the statistic calculated rises above this threshold and alarm is signalled. Analysis of such charts in terms of performance metrics is discussed in Section 2.8.

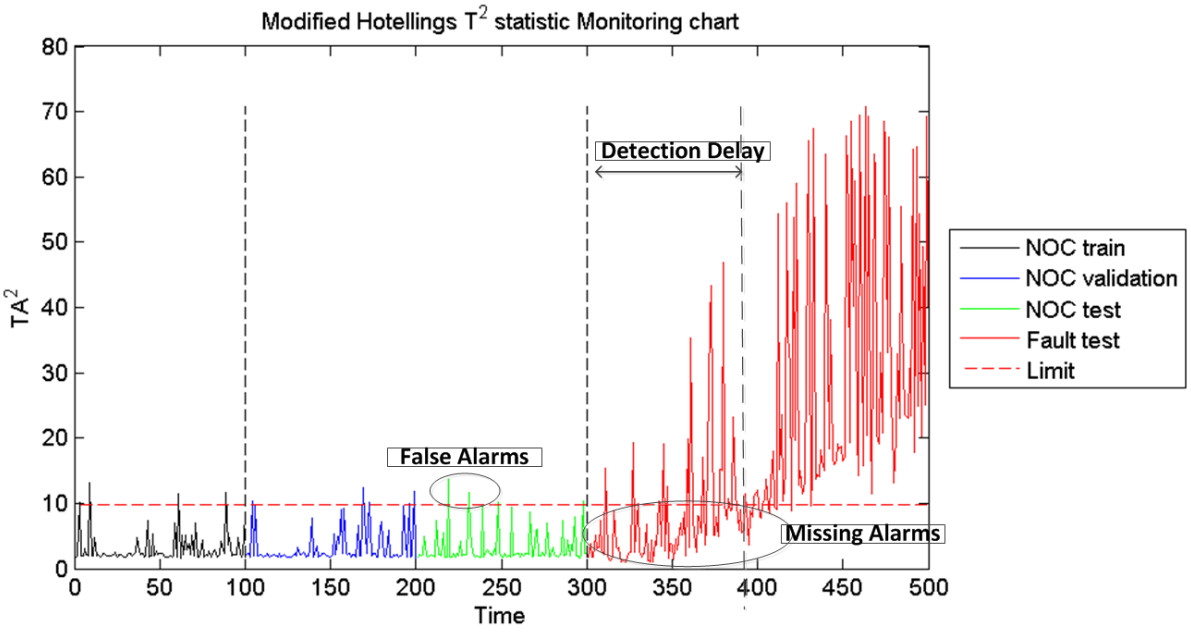

Figure 2-4: Illustrative example of monitoring chart with performance metric definitions

In one threshold selection approach, the value under which 99% (for example) of the statistic calculated for NOC validation data falls is chosen as the threshold. In this way the threshold is defined according to the normal behaviour of the process, to which the new observations are being compared. Another approach is to define thresholds based on the assumption of normally distributed data distribution of the statistic. An α-value threshold is set using the F-distribution for the T_A^2 and the χ^2 distribution for SPE (Aldrich and Auret, 2013).

2.8. Fault Detection Performance Metrics

In order to quantify the performance of a fault detection method, certain performance metrics can be calculated. **Error! Reference source not found.** provides a summary of these performance metrics, and then each of the metrics is discussed in more detail in the following subsections.

Table 2-2: Summary of fault detection performance metrics

Metric	Definition	Measure of good detection
False alarm rate (FAR)	Percentage of NOC Test data > Threshold	Low values
Missing alarm rate (MAR)	Percentage of Fault data < Threshold	Low values
True alarm rate (TAR)	Percentage of fault conditions > Threshold	High values
Receiver operator characteristic (ROC) curve	TAR vs. FAR with Threshold from minimum to maximum	Close to top left corner
Area under curve (AUC)	Area under ROC curve	Values close to 1
Detection delay (DD)	Time since start of fault until three consecutive alarms	Low values

2.8.1. Missing and false alarms

The multivariate statistics, T_A^2 and SPE, allow the test data to be compared to the training data. When these statistics exceed a threshold defined according to the training data, the presence of a fault is indicated. Consider the monitoring chart displayed in Figure 2-4. The chart plots the T_A^2 statistic for four different sets of data: the NOC data on which the feature extraction model is trained; the NOC data that is used for validation of the method; the NOC data that is used for testing of the method; and the fault data that is used for testing of the method.

When the threshold is exceeded for a sample that is known to be under NOC it is called a false alarm. This scenario is illustrated in Figure 2-4where the samples in green, representing the calculated diagnostic for the NOC test data, exceed the dashed red line that represents the limit/threshold. The percentage of the total number of NOC testing samples that give false alarms is called the false alarm rate (FAR).

When the threshold is not exceeded for a sample that is known to be under fault conditions it is called a missing alarm and the percentage of the fault conditions samples that give missing alarms is called the missing alarm rate (MAR). The FAR and MAR are both indications of the fault detection performance of a process monitoring method. So low values of both FAR and MAR indicate that a detection method performs well for a specific fault. The true alarm rate (TAR), which is the percentage of fault conditions sample that gave alarms, can also be calculated as shown in Equation 2-27.

$$\mathrm{TAR} = 100 - \mathrm{MAR}$$ **Equation 2-27**

2.8.2. Receiver operator characteristic curves

Unfortunately the selection of thresholds can lead to some error in fault detection: when the threshold is too high it may give zero false alarms, but also a large number of missing alarms; when the threshold is too low it may give zero missing alarms but also a large number of false alarms. A receiver operator characteristic (ROC) curve can be generated to provide a summary of the possible performance of a diagnostic irrespective of the threshold selected (Aldrich and Auret, 2013).

To generate an ROC curve, such as the one shown in Figure 2-5, the threshold is varied from the minimum to the maximum value of the statistic obtained, and the FARs and MARs are calculated for each threshold. The true alarm rate (TAR, which is just 1-MAR) is then plotted against the FAR. The closer the ROC curve reaches to the top left corner the better the detection performance, since this is the point where FAR is 0% and TAR is 100%. The area under the ROC curve (AUC) can then be calculated as quantitative measure of detection performance, since the closer it is to the top left corner the more area there is under the curve.

The dashed diagonal line in Figure 2-5 represents the random performance line, with an AUC of 0.5. This line represents an imaginary monitoring method that has a 50% chance of either giving an alarm on NOC data or not, and a 50% chance of either giving an alarm on fault data or not. I.e. it performs no better than a random selection of whether or not to give an alarm. An AUC of less than 0.5 would indicate a fault detection method that performs worse than such a random selection; meaning that it picks up NOC data as faulty, and faulty data as normal.

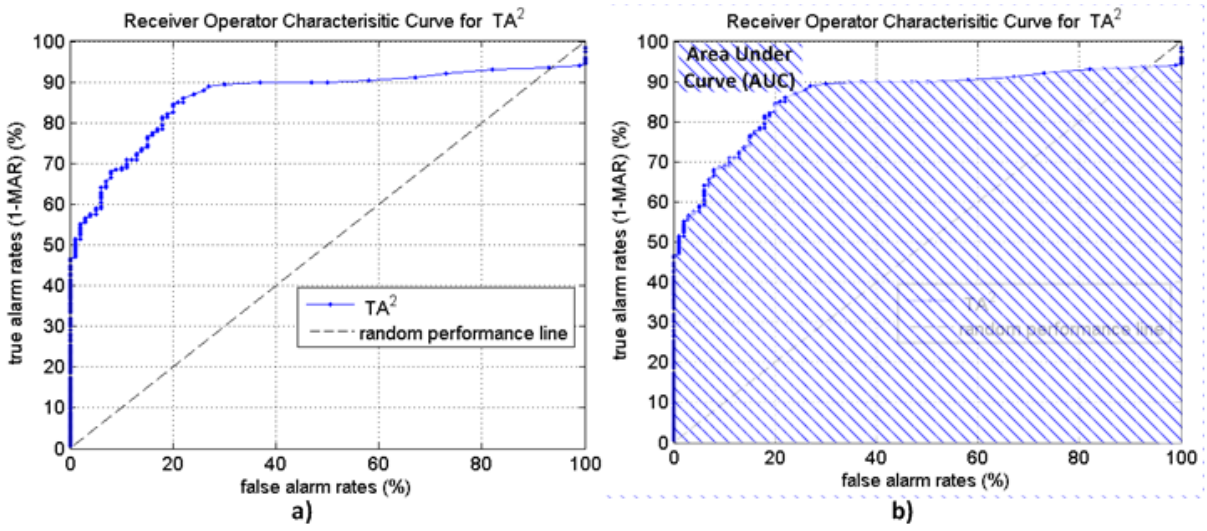

Figure 2-5: a) Illustrative example of receiver operator characteristic curve. b) Illustration of area under curve

2.8.3. Detection delay

When applying monitoring methods for fault detection it is desirable that the fault be detected soon after it has occurred so that the operator can take corrective action before significant degradation of the process performance has occurred. Therefore another performance metric to consider is how rapidly the method is able to detect the fault. This can be quantified by the detection delay (DD), which is defined as the amount of time from the introduction of the fault to the first instance where three consecutive alarms have been signalled (Aldrich and Auret, 2013). The DD gives an indication of how rapidly the method is able to detect the fault. The DD is also illustrated in Figure 2-4.

Chapter 3 - Topology for Fault Diagnosis

In Chapter 2 -, the application of feature extraction methods for fault diagnosis was discussed. Once the fault has been detected, signalling an alarm to the operator, it is necessary for the operator to diagnose the fault conditions in order to make an informed decision of what corrective action should be taken. The feature extraction methods are limited in their fault identification ability, as noted in Chapter 2. For this reason additional information about the system is required to identify the fault.

Process topology information, which describes how variables and units are connected to each other, can be used to aid fault identification in two ways. Firstly, topology can be used to trace the propagation path of a fault from variables that have been identified as symptoms to a possible root variable by tracing back along connections between variables. Secondly, the topology structure of process changes with the presence of a fault, this can be used to gain some information about the fault.Diagnosis of the fault conditions after fault detection can be referred to as fault identification. Fault conditions identified should include the location of the fault. The location of the fault refers to where in the process the fault originated, or its root cause; this could mean isolation of a unit or part of the process, or a single variable that indicates the origin of the fault. This allows the operator to identify where in the plant the problem lies and where to take corrective action.

In addition to use in fault diagnosis, topology information (also referred to here as connectivity information) can be useful in pre-processing of the data before feature extraction to aid both fault detection and fault identification. Topology information can be used in application to multiblock monitoring methods since the process can be separated into blocks according to strongly connected groups of variables.

3.1.Representing Topology Information

Process topology information can be represented by a graph, which can be defined as a representation of structural relationships (connections) between objects (variables). A simple example of such a graph, termed a connectivity graph, is shown in Figure 3-1 a). In a connectivity graph, the nodes represent the variables, and edges between nodes indicate a connection between the variables. When the edges have a direction associated with them (indicated by arrows on the edges), for example the edge between Node a and Node b in Figure 3-1, it means that the direction of the causality is from a to b. The information in a connectivity graph can also be represented by an adjacency matrix (AM), shown in Figure 3-1 b); where the rows and columns both represent the variables (nodes) and where entry i,j is assigned a value of 1 if there is a connection (edge) from variable i to variable j.

The edges in a connectivity graph can also be assigned weights according to the strength of the connection between the two variables. An example of such a weighting applied to the connectivity graph shown above is given in Figure 3-2 a). This can then also be represented in the adjacency matrix by changing the entries with a value of 1 to the weight value of the connection, which is then termed a connectivity matrix (CM), shown in Figure 3-2 b).

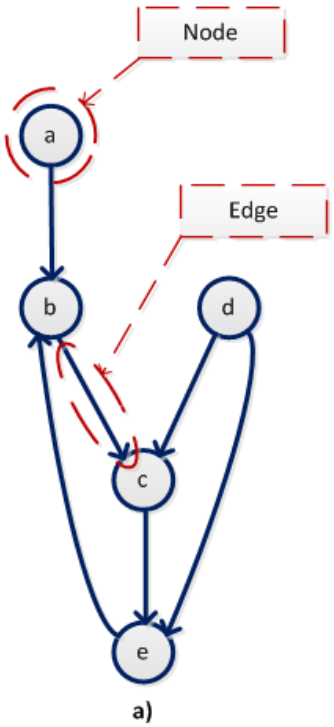

a)

$$AM = \begin{array}{c} \\ a \\ b \\ c \\ d \\ e \end{array} \begin{array}{c} \begin{array}{ccccc} a & b & c & d & e \end{array} \\ \begin{bmatrix} 0 & 1 & 0 & 0 & 0 \\ 0 & 0 & 1 & 0 & 0 \\ 0 & 0 & 0 & 0 & 1 \\ 0 & 0 & 1 & 0 & 1 \\ 0 & 1 & 0 & 0 & 0 \end{bmatrix} \end{array}$$

b)

Figure 3-1: a) Simple connectivity graph with b) its corresponding adjacency matrix (AM)

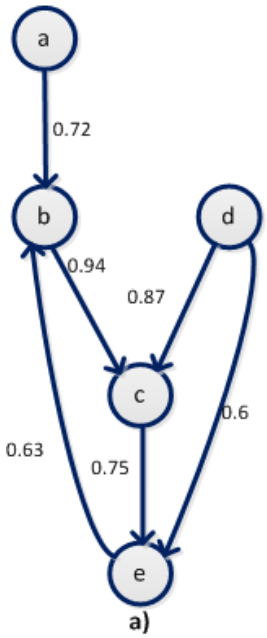

a)

$$CM = \begin{array}{c} \\ a \\ b \\ c \\ d \\ e \end{array} \begin{array}{c} \begin{array}{ccccc} a & b & c & d & e \end{array} \\ \begin{bmatrix} 0 & 0.72 & 0 & 0 & 0 \\ 0 & 0 & 0.94 & 0 & 0 \\ 0 & 0 & 0 & 0 & 0.75 \\ 0 & 0 & 0.87 & 0 & 0.6 \\ 0 & 0.63 & 0 & 0 & 0 \end{bmatrix} \end{array}$$

b)

Figure 3-2: a) Connectivity graph with weights attached to edges b) Corresponding connectivity matrix (CM)

3.2.Topology Extraction from Process Knowledge

Topology can be inferred from knowledge of the process. This can take the form of: fundamental equations (physical or chemical relationships) governing the process; piping and instrumentation diagrams; or simply intuitive or experience based knowledge of how the process functions.

In the field of fault identification in chemical processes, process topology has been incorporated in the form of signed directed graphs (SDGs) (Yang and Xiao, 2012). SDGs represent the topology information with the variables as nodes and the connections between them as edges, but with the additional information of a positive or negative change on each arc, and typically fundamental process models are used to generated these SDGs (Maurya et al., 2003).

3.2.1. Topology extraction from process models

Some processes can be described by differential equations (DEs), algebraic equations (AEs) or differential algebraic equations (DAEs). When a variable can be described by an equation representing it as a function of another variable then, intuitively, a connection between the two variables exists. For example when $x = f(a, b, c)$ or $\frac{dx}{dt} = f(a, b, c)$ then x is connected to a, b and c. The SDG of the process can therefore be developed from these types of model equations.

There are a few issues involved with this method:

- It requires the development of a fundamental model of the process, which may be too complicated or impossible, or otherwise requires a large amount of simplifying assumptions.
- Large plants will have a large number of equations with numerous spurious solutions. Methods have been proposed for reducing the solutions (Maurya et al., 2003), but this can be tedious and time-consuming.
- In many cases, model parameters which might give an indication of the strength of the connections are unknown and have to be estimated or values have to be obtained from literature or estimated from the data (Thornhill and Horch, 2007), which may be unreliable.
- Model parameters often change with changing process conditions, such as fault conditions, which may possibly change the connectivity relationships between variables.
- Connectivity from this method may be incomplete since variables may be connected through control loops, which are not necessarily described in the process model.

Although these systematic analytical solutions to SDG generation are useful and give valuable and substantial insight into the connectivity relationships of variables, the methods may be unnecessarily complicated and they are limited to systems where the fundamental models are known.

3.2.2. Topology extraction from intuitive process knowledge

Process connectivity can also be determined by simple inspection of the process. For example it is obvious that the temperature of an outlet stream of a mixing tank is connected to the temperature of an inlet stream to the tank. This method may be time consuming, especially for large processes, but it provides valuable information that aids process monitoring.

It is often useful to focus on the connections between control loops as well since faults often originate in one control loop and propagate to other control loops due to physical connections or because of control structures. Therefore the root cause may be more effectively determined by analysing connections in the control loops. Connectivity between control loops can be determined by inspection of the process (Jiang et al., 2009). In this method each node in the connectivity graph represents a controller in the system. Arcs between nodes are added if there is direct interaction between the controllers; direct interaction exists if the output of one controller can directly affect the controlled variable of the other without passing through any other controllers first.

3.2.3. Topology extraction using process diagrams

Other authors have used process flow diagrams or piping and instrumentation diagrams embedded with extensible mark-up language (XML) to determine connectivity, allowing automatic identification of connections between variables using commercially available software (Yim et al., 2006). Although the automated nature of this method is very useful, especially for large processes where development of connectivity graphs by simple inspection of the process would be extremely time consuming, it obviously requires an XML description of the process topology, which is not always available.

3.3.Topology Extraction from Data

Process topology information can be derived from historical process data by finding cause-and-effect relationships between variables, also called causality or referred to henceforth as connectivity. Utilising data-based methods provides an automated and systematic technique for developing a connectivity graph that avoids the shortcomings of knowledge-based topology extraction, described in section 3.3.1.

3.3.1. Motivation for data-based methods

The main shortcoming of knowledge-based topology generation is that the development of the graphic models is prone to human error; a systematic method needs to be developed to eliminate the risk of human error (Ram Maurya et al., 2004). The generation of connectivity graphs from process knowledge is a complex task, relying heavily on experience and familiarity with the process (Fan Yang et al., 2010). Therefore the connections determined by these methods need to be

validated using data connectivity methods, since these methods provide systematic and straightforward ways of determining connectivity.

In the minerals processing industry, alterations are often made to plants, such as the replacement of equipment, alterations of processing steps and changes in specific operating conditions. These alterations are often made on an ad-hoc basis, and therefore often are undocumented. Therefore the topology structure of a process may have changed, rendering the topology generated from process knowledge invalid. Through the use of data-based methods applied to the most recent plant data, these alterations in the topology would be automatically captured.

Although methods exist for their treatment (Yang et al., 2009), the presence of control loops and recycle loops common in industrial processes create a problem when using only process-knowledge based connectivity graphs, since control action may alter the connectivity during the presence of a disturbance.

It is therefore desirable to investigate the use of an automated method of capturing topology information. The generation of connectivity graphs from process diagrams, although automated, requires an XML description of the process topology, which is not always available.

With all of the methods described in section 3.2, connections between variables that are not readily apparent by inspection or from the fundamental process knowledge may be obscured or lost. Methods that extract process topology from historical process data may avoid these shortcomings, allowing for automated generation of connectivity graphs that may also capture connections that allow for greater understanding of the process.

3.3.2. Inferring causality from historical process data

A possible approach to estimating connectivity (or causality) between process variables from their historical data is to perform pairwise hypothesis tests of connections between variables and reject those connections where the correlation between their time series is insignificant. However, as the expression that correlation should not be confused with causality is very firmly entrenched in scientific reasoning, it is clear that this is not sufficient information to infer a causal relationship. Fortunately, data from chemical or minerals processing plants exists typically in the form of time series measurements of the variables. Incorporating information about time, or the sequence of events, can improve the validity of casual inference (Bauer and Thornhill, 2008).

Three methods for extracting topology from historical process data were identified for this research: linear cross-correlation (LC) (Bauer and Thornhill, 2008); partial cross-correlation (PC) (de la Fuente et al., 2004; Yang et al., 2011); and transfer entropy (TE) (Bauer et al., 2007; Duan et al., 2012; Hlaváčková-Schindler et al., 2007; Hou et al., 2010). All three of these methods incorporate pair-wise

hypothesis tests and time information in their implementation. In this section these three methods are described and their use in literature is discussed.

3.3.3. Topology extraction using linear cross-correlation

The presence of causality between two variables can be inferred from historical process data by estimating the time delays between their time series (Bauer and Thornhill, 2008). The presence of a time delay implies causality, since physical properties, such as temperatures, levels and flow rates, travel through the process and take time to reach from the measurement point of one variable to that of another. The topology extraction method using LC, presented by Bauer et al. (2008), exploits this fact by estimating time delays between two measured variables' time series and considering that to be an indication of a connection between the two variables.

Calculation of linear cross-correlation

Two time series are compared by shifting one series by a number of different lags and calculating the cross-correlation at different lags. The linear correlation, ρ^{LC}, between two time series, ***x*** and ***y***, is calculated as shown in Equation 3-1.

$$\rho_k^{LC} = \frac{1}{N-k}\sum_{i=1}^{N-k}\frac{(x_i-\mu_x)(y_{i+k}-\mu_y)}{\sigma_x\sigma_y} \qquad \textbf{Equation 3-1}$$

In Equation 3-1, k represents the number of lags, N represents the number of samples and μ and σ represent the mean and standard deviation respectively of the time series. This calculation is done for all pairs of variables, and the maximum correlation, at kmax, is selected. This calculation results in a connectivity matrix with ρ_{kmax}^{LC} for each pair as the entries in the matrix.

Figure 3-3 illustrates the resulting cross-correlation between **x** and **y**. The maximum correlation value, $\rho_{kmax}^{LC}$of all the correlations calculated for different lags is taken as an indication of the strength of the connection between the two variables. The lag, $k_{max,}$ corresponding to this ρ_{kmax}^{LC} gives an estimate of the time delay between the variables. When the value of k_{max} is positive, **x** precedes **y**, and therefore the causal direction is from **x** to **y**. If the value is negative, **y** precedes **x**, and therefore the causal direction is from **y** to **x**.

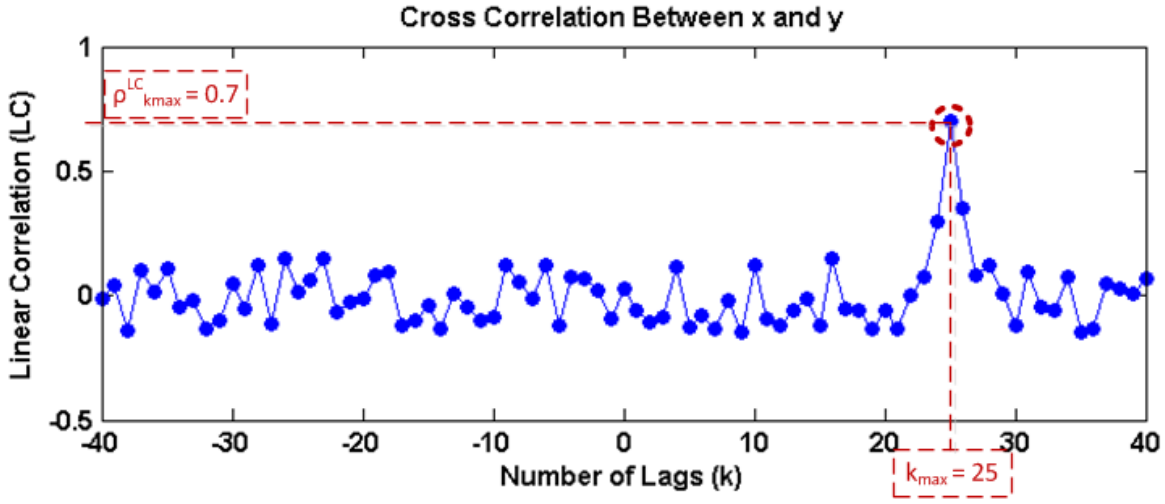

Figure 3-3: Cross-correlation between two variables, showing maximum correlation and maximum lags

Use of linear cross-correlation in literature

Bauer and Thornhill (2008) demonstrated the cross-correlation method described above on two industrial case studies: the first was a distillation column in the Tennessee Eastman process; the second was a petrochemical process. Bauer and Thornhill (2008) found that their LC method could successfully retrace the propagation paths and identify the root causes of the faults. They also verified that the method was able to accurately detect time delays in a process with recycle. However, the processes for both case studies were relatively small; the distillation column had only ten measured variables variables and the petrochemical process had only seven measured variables. In comparison with the concentrator process in a minerals processing plant presented as a case study in this thesis (Chapter 7 -), which had 56 measured variables, these processes are small. In addition, both case studies considered only one fault. Therefore it is uncertain whether the method would perform as well with a larger process or with different types of disturbances.

Chiang and Braatz (2003) proposed a fault diagnosis method incorporating changes in connectivity (discussed in further detail in section 3.5.1) and a connectivity map. The connectivity map was constructed from process knowledge, but the correlation coefficients between pairs of variables were used to validate connections. This is not the cross-correlation discussed here, simply correlation between time series of measured variables.

3.3.4. Topology extraction using partial cross-correlation

Linear cross-correlation may sometimes give misrepresentative results since strong correlation may exist between two variables because of a strong mutual correlation to an intermediate variable. Partial cross-correlation (PC) infers connectivity between two variables, whilst eliminating the effects of the remaining variables. I.e. PC represents only the direct interactions between variables (Yang et al., 2011). This elimination is achieved by calculating the correlation between two variables while

conditioning on any number of other variables in the system. The two variables under consideration are both regressed against all the other variables in the system. The residuals of this regression are the parts of the two variables that are not correlated with the other variables. The partial correlation is then the correlation between these residuals.

For example, the correlation between two variables, **x** and **y**, conditioning on a third variable, **z**, is the correlation between the parts of **x** and **y** that are uncorrelated with **z**. These parts of **x** and **y** are determined by regressing them both separately on **z**. The respective residuals, $\mathbf{e}_x$ and $\mathbf{e}_y$, of said regression are then the parts of **x** and **y** that are uncorrelated with **z**. Calculating the correlation between $\mathbf{e}_x$ and $\mathbf{e}_y$ therefore determines the correlation of **x** and **y** while conditioning on **z** (de la Fuente et al., 2004).

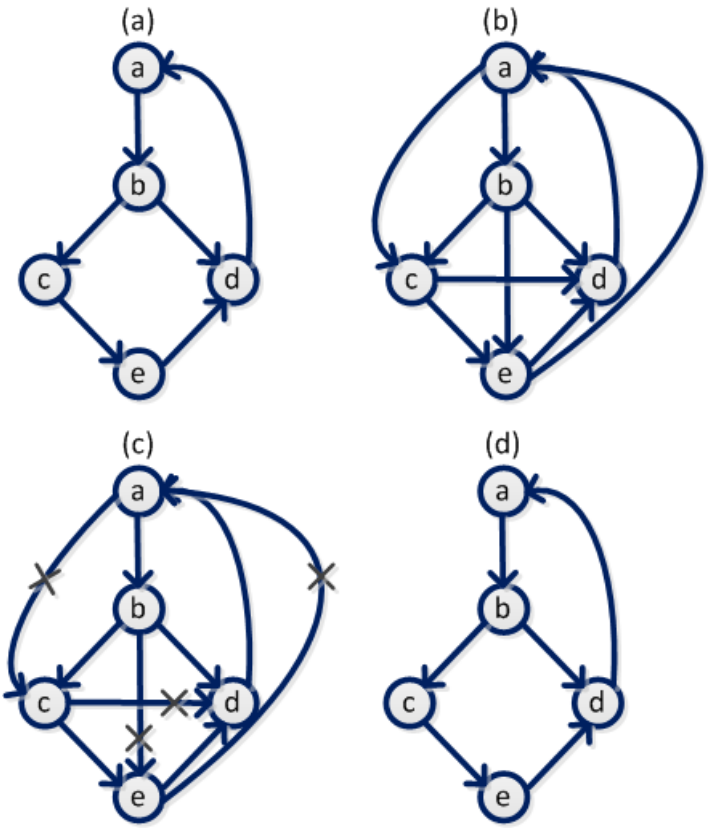

Figure 3-4: Illustration of partial cross-correlation. (a) The actual connectivity graph. (b) Connectivity graph obtained from linear cross-correlation. (c) Edges that exist only because of intermediate variables are removed since they have zero partial cross-correlaiton, resulting in (d); connectivity graph from partial cross-correlation.

Calculation of partial cross-correlation

The order of the partial correlation is defined as the number of variables it is conditioned on. This order can be large enough to include all other variables in the data set under consideration. Equation 3-2, Equation 3-3 and Equation 3-4 demonstrate calculation of PC coefficients, ρ^{PC}, of orders 0-2, which can similarly be extended to any arbitrarily large order (de la Fuente et al., 2004).

0^{th} -order partial correlation (linear correlation)

$$\rho_{xy}^{PC} = \frac{\mathrm{cov}(x, y)}{\sigma_x \sigma_y} \quad \textbf{Equation 3-2}$$

1^{st} -order partial correlation

$$\rho_{xy,z}^{PC} = \frac{\rho_{xy} - \rho_{xz}\rho_{yz}}{\sqrt{(1-\rho_{xz}^2)(1-\rho_{yz}^2)}} \quad \textbf{Equation 3-3}$$

2^{nd} -order partial correlation

$$\rho_{xy,zq}^{PC} = \frac{\rho_{xy,z} - \rho_{xq,z}\rho_{yq,z}}{\sqrt{(1-\rho_{xq,z}^2)(1-\rho_{yq,z}^2)}} \quad \textbf{Equation 3-4}$$

The same procedure as described with LC can then be followed; i.e. calculating the PC over a number of lags, finding the lags at which the PC is at a maximum and using that lag as an estimate of the time delay between variables.

Use of partial cross-correlation in literature

Using PC in the place of LC for the determination of connectivity from process data has not been widely discussed. Fried and Dedelez (2005) used a version of PC to generate causal graphs from time series data in the medical field; i.e. data from vital signs of a patient. Their conclusion was that using partial correlation as opposed to LC eliminated spurious solutions. Yang et al. (2011) applied PC to a number of data sets in the fields of: medicine, agriculture, meteorology, insurance and biology. They concluded that PC is valid as a causal inference procedure.

3.3.5. Topology extraction using transfer entropy

TE provides a quantitative measure of the information transferred from one variable to another by measuring the reduction of uncertainty of the value of ***x*** under the assumption that ***y*** is a good predictor of ***x***. TE adds time information into the causal hypothesis because it tests hypotheses concerning joint and conditional probabilities of current and previous values in the time series pairs (Bauer and Thornhill, 2008). One limitation of both LC and PC is that they are linear methods and therefore may fail to capture nonlinear relationships between variables, and therefore may give incorrect results in nonlinear applications (Yang and Xiao, 2012). The transfer entropy (TE) method does not have this limitation.

Calculation of transfer entropy

A measure of the information transferred from **y** to **x** is given by Equation 3-5.

$$t(\mathbf{x}|\mathbf{y}) = \sum p(\mathbf{x_{i+h}}, \mathbf{x_i}, \mathbf{y_i}) \log\left(\frac{p(\mathbf{x_{i+h}}|\mathbf{x_i}, \mathbf{y_i})}{p(\mathbf{x_{i+h}}|\mathbf{x_i})}\right) \quad \textbf{Equation 3-5}$$

In Equation 3-5, p() represents the probability density function (PDF) and h is the prediction horizon. $\mathbf{x_i}$ and $\mathbf{y_i}$ are embedded vectors given by $\mathbf{x_i} = [\mathbf{x_i}, \mathbf{x_{i-\tau}}, ..., \mathbf{x_{i-(lx-1)\tau}}]$, $\mathbf{y_i} = [\mathbf{y_i}, \mathbf{y_{i-\tau}}, ..., \mathbf{y_{i-(ly-1)\tau}}]$, where τ is the sampling period and lx and ly are embedding dimensions for **x** and **y** respectively. $p(a, b)$ is the joint

PDF between two variables a and b. The transition probability $p(\mathbf{x_{i+h}}|\mathbf{x_i}, \mathbf{y_i})$ is the probability that a future value of **x**, denoted as $\mathbf{x_{i+h}}$, has a certain value when past values $\mathbf{x_i}$ and $\mathbf{y_i}$ are known and can be calculated according to the Bayesian principle as shown in Equation 3-6.

$$p(\mathbf{x_{i+h}}|\mathbf{x_i}, \mathbf{y_i}) = \frac{p(\mathbf{x_{i+h}}, \mathbf{x_i}, \mathbf{y_i})}{p(\mathbf{x_i}, \mathbf{y_i})} \qquad \textbf{Equation 3-6}$$

When $\mathbf{x_{i+h}}$ is independent of $\mathbf{x_i}$ and $\mathbf{y_i}$, the logarithmic term in Equation 3-5 reduces to log(1), which is zero, and there is no information transferred from one variable to another. A quantitative measure of the causality between variables can then be calculated by comparing the influence of **x** on **y** with the influence of **y** on **x**, as shown in Equation 3-7.

$$t_{\mathbf{x}\to\mathbf{y}} = t(\mathbf{y}|\mathbf{x}) - t(\mathbf{x}|\mathbf{y}) \qquad \textbf{Equation 3-7}$$

A positive value of $t_{\mathbf{x}\to\mathbf{y}}$ indicates that the directionality is from **x** to **y**, while a negative value indicates the reverse. Small absolute values indicate little or no connection between the variables

Use of transfer entropy in literature

Bauer et al. (2007) demonstrated the transfer entropy method on two case studies from the Tennessee Eastman benchmark. Using a causal map derived from TE, the root cause was correctly identified in both cases. Again, the processes on which the methods were tested were small, with less than ten measured variables, and each case study considered only one fault. Therefore it is uncertain whether the method would perform well with a larger number of variables or be robust with respect to different faults. A drawback of the TE method is that it involves selection of multiple parameters, namely: the prediction horizon, h; the embedding dimensions, lx and ly; and the sampling period, τ.

Yang et al. (2010) used cross correlation and transfer entropy to validate signed directed graphs developed from process knowledge. Hou et al. (2010) also successfully used TE to construct a SDG which was then used for fault diagnosis. The contribution of their paper was a method of evaluating the severity of the fault based on the SDG. The resulting SDG from application of TE to data from their case study was similar to that obtained from process knowledge. The fault diagnosis method was able to accurately isolate root causes for different faults.

3.4. Use of Topology Information for Blocking

As mentioned in Chapter 2, multiblock fault detection, which divides the process into multiple blocks to be analysed separately can be incorporated to improve fault detection. In typical multiblock process monitoring applications (Ge and Song, 2009; MacGregor et al., 1994; Westerhuis et al., 1998; Wold et al., 1996) the process is divided into blocks according to process knowledge: logical

subsystems such as different processing steps or units are identified and treated as blocks. This dependency on process knowledge is a disadvantage, since the process knowledge required to decide which parts of the process should be grouped together may not always be available or complete. Additionally, this method ignores the fact that there is often a large degree of connectivity between process units, especially in the presence of recycle streams and control loops. Therefore a method that uses the available data and the connectivity information extracted from it to divide the process according to the connections between variables may provide an improvement on multiblock methods.

Ge and Song (2013) presented a multiblock technique that automatically divided the process according to the direction of the principal components. A good block division results in blocks that are as diverse from each other as possible, but when combined make up the entire process. Since PCA results in principal components that are uncorrelated with one another, forming the blocks on the directions of these principal components will satisfy the diversity criteria. The contribution of each variable to each principal component can be calculated, thereby allowing the block to be defined by those variables that displayed the largest contribution.

Process topology information can reveal which groups of variables are strongly interconnected with each other. These groups of variables are known as strongly connected components (SCCs). Therefore the process can be divided into blocks of variables based on this information, already obtained from the process topology extraction methods. This can be performed as a data pre-processing step before feature extraction is applied. To the best of the author's knowledge this technique for selecting blocks in process monitoring has not been applied previously. Ge and Song (2013) stated that, to their best knowledge, theirs was the only blocking method not based on process knowledge. Therefore application and testing of this blocking method is a novel contribution to process monitoring.

3.4.1. Finding connected components in a connectivity graph

Strongly connected components can be identified using Tarjan's algorithm (Tarjan, 1972). This algorithm performs a depth-first search starting from any arbitrary node. Subsequent depth-first searches are conducted on any nodes that have not yet been found. The search visits every node exactly once, i.e. it remembers which nodes it has already visited. Groups of nodes that are mutually reachable without violating edge directions are defined as a strongly connected component. E.g. in Figure 3-5; nodes 1, 2 and 3 form strongly connected component, while 4 is excluded because it cannot be reached without violating edge direction.

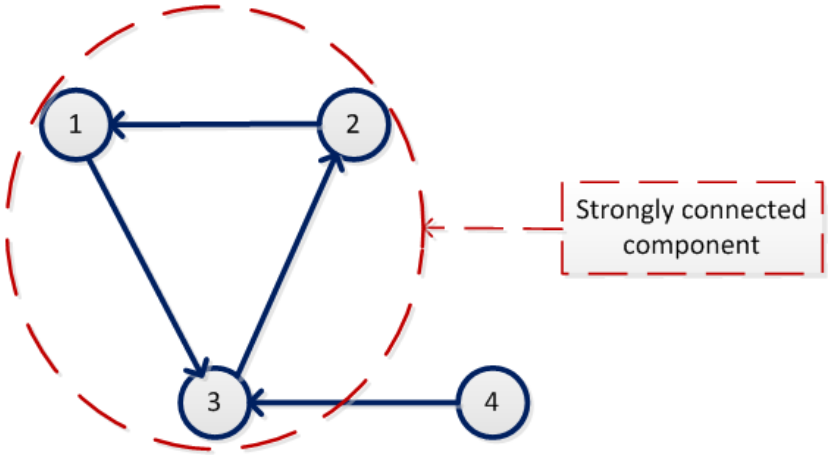

Figure 3-5: Illustration of a strongly connected component defined according to Tarjan's algorithm

A weakly connected component is defined similar to a strongly connected component as a group of nodes that are mutually reachable, except that edge directions may be violated.

Since variables connected to the same unit are linked through mass and energy balances or control loops they will tend to be strongly connected to each other. Therefore it is expected that dividing the process according to connected components will result in blocks will reflect the units in the process.

3.5.Using Topology for Fault Identification

In addition to their use for blocking process data into groups according to strongly connected components, connectivity graphs can be for fault identification to determine possible root causes of faults. This is achieved by tracing faults from variables that showed symptoms of the fault back to variables that were root causes of the fault.

3.5.1. Change in connectivity for identification of symptom nodes

In order to use the connectivity graph to trace faults to their root causes the symptom nodes, i.e. variables that showed symptoms of the fault, have to first be identified. Fault conditions will result in a change in the connectivity structure in a process. This change can be due to a change in the physical or chemical behaviour of the process, or due to a change in the control action, or some other change in the process behaviour. By comparing connectivity extracted from process data under normal operating conditions to that extracted from fault conditions data, information can be gained about the fault conditions to aid root cause analysis.

This change in causality, or connectivity, due to faults was demonstrated by Chiang and Braatz (2003), who used it for detection of faults. They used two causality measures, the modified distance (DI), which is similar to transfer entropy since it is also a measure of mutual information, and the causal dependency (CD) (based on the T_A^2 statistic). They compared the values obtained during fault

conditions to those obtained during NOC. Significant deviation of the observed values from those observed under NOC provided an indication of a fault condition. The variables that showed the highest DI and CD were identified as symptom nodes, and then variables that were highly correlated (connected) with these variables were considered to be possible root nodes. Their method was applied to faults in the Tennessee Eastman Process case study and it was found that it performed very well for fault detection, with MAR of about 15%, but, more importantly, also performed well for fault identification, allowing an expert to highlight propagation paths correctly and allowing the root cause to be identified in most cases.

3.5.2. Back propagation in connectivity graphs for fault identification

Once symptom nodes have been identified, either from contribution plots or from connectivity change, the connectivity graph can be used to trace them back to possible root causes.

Connectivity maps have been widely used for fault diagnosis, typically by identifying possible fault propagation paths. One method for inference of propagation paths uses expert systems. This type of rule-based inference can only be used when a set of expert rules is available (Yang and Xiao, 2012), which makes it a very limited method. Bayesian nets have also been used for inference (Yang and Xiao, 2012); probability and conditional probability of fault conditions is used to make inference on the probability of the fault occurring.

However, the most common method for finding the root cause for the fault using a connectivity map is depth-first traversal on the map (Iri et al., 1979; Venkatasubramanian et al., 2003a; Yang and Xiao, 2012). This method constructs a propagation path by moving to adjacent nodes until no further edges are found. So a node that has been identified as having fault conditions associated with it is taken and possible propagation paths are traced back until a node is found that has no entering edges (a root node). However, applying this method will generally just trace a fault back to the first node in the graph, or the first variable in the process. In a graph that has captured control and recycle loops in its connectivity structure, it would be difficult to determine if a root node was captured inside one of these loops. This method also does not account for the weights of the edges in the graph, or the strength of the connections between the variables. A propagation path that follows strongly connected variables from a possible root node to a symptom node is more likely to be a true representation of the actual fault propagation path.

It is therefore proposed to use a slightly modified back propagation method that involves finding all the shared ancestors of the identified symptom nodes, finding the shortest distances from these ancestors to the symptom nodes by taking into account the weights of the edges in the graph, and then finding the furthest shared ancestors.

Chapter 4 - Fault Diagnosis Methodology

This chapter presents the proposed fault diagnosis methodology combining all the techniques described in chapters 2 and 3 as well as the methodology followed to determine which combination of techniques performed best according to the aims of the project.

4.1. Fault Diagnosis Techniques

The various topology extraction, pre-processing, fault detection and fault identification techniques considered for this research include: three topology extraction methods (TEM) including linear cross-correlation (LC), partial cross-correlation (PC) and transfer entropy (TE); two pre-processing methods (PPM) including the unblocked case (i.e. no pre-processing) and blocking; Two feature extraction methods (FEM) including principal components analysis (PCA) and kernel principal components analysis (KPCA); three monitoring chart methods (MCM) including Shewhart, exponentially weighted moving average (EWMA) and cumulative sum (CUSUM) monitoring charts; two fault identification methods (FIM) including contributions and connectivity change. Figure 4-1 summarises the techniques considered with a reference to where each technique was discussed in Chapter 2 - and Chapter 3 -.

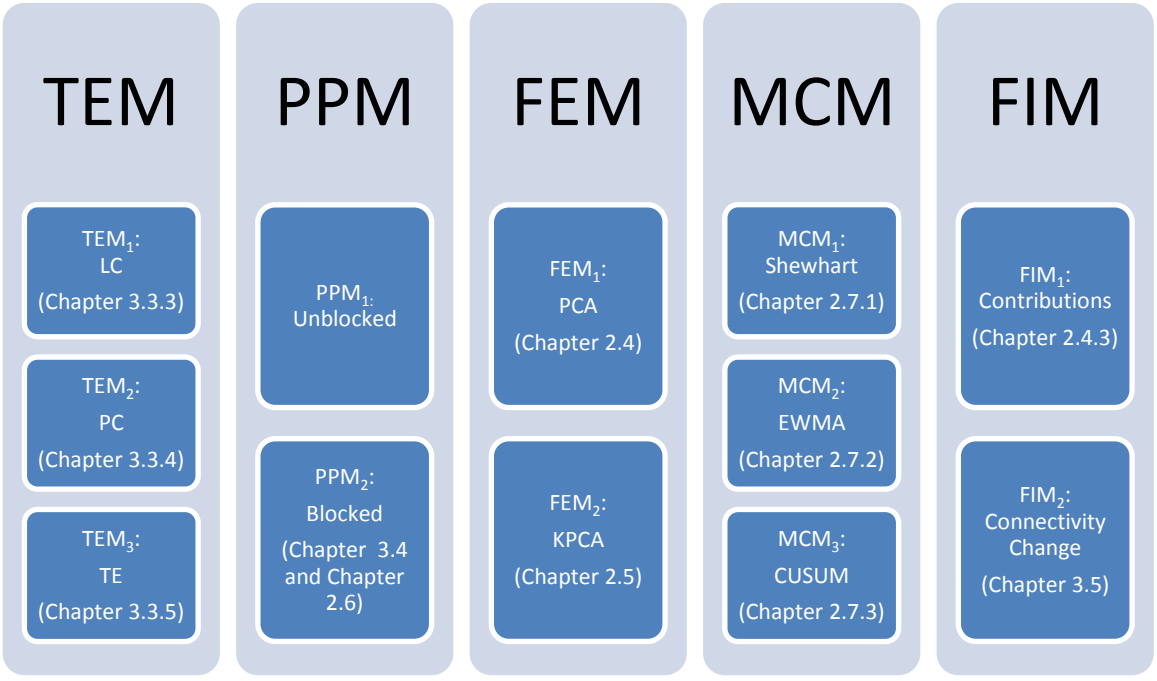

Figure 4-1: Summary of fault diagnosis techniques considered

Each possible combination of methods was applied in order to determine which combination resulted in the best fault detection and identification performance. The performance was evaluated based on the following performance metrics:

- Fault detection: AUCs and DDs
- Fault Identification: Location identified for each fault

4.2. General Fault Diagnosis Procedure

The procedures followed for application of the fault diagnosis methods is described in this section.

4.2.1. Use of different data sets

Application of all the fault diagnosis methods required the methods first to be trained on NOC data. This training provided the training connectivity graph that was used for: blocking, connectivity change, back propagation and for the feature extraction model's loadings onto which test data was be projected. Then the methods were validated so that the limits for the monitoring charts, as well as the limits for the contributions of individual variables in the contribution plots, could be set. Then the FEM had to be tested on NOC data to see if the methods gave false alarms. Finally the fault data could be tested to determine if the methods could detect and identify the fault. Therefore four sets of data were required: training, validation, NOC Test and fault test data. The first three sets were all obtained from normal operating conditions, while the last was under fault conditions.

Validation was performed on a different NOC data set, rather than re-using the training NOC data set. The reason for this was to avoid overfitting the feature extraction models on the training data. Since the feature extraction model would describe the data on which it was trained extremely well, the SPE and T_A^2 values would be small, Therefore if the control limits were set according to these values, the limits would be very strict and slight changes in the process that are not necessarily faults would signal an alarm.

Plants operate under different states, regimes or conditions, depending on changes such as the feed material, the operator on duty. Therefore the definition of NOC can strongly affect the ability of the feature extraction methods to detect faults accurately. If there are varying plant regimes that are normal, but that are not captured in the training data, these alterations may be picked up as a fault. On the other hand, if undetected fault conditions were present in the training data, the fault conditions may not be detected as abnormal when the new data is tested, and no alarm would be signalled. Although the difficulty associated with defining NOC data in real plants is important, it was not considered in this project, since the focus of this work was to improve fault diagnosis after selection of NOC conditions.

4.2.2. Training of fault diagnosis methods

Figure 4-2 provides a diagram illustrating the procedure followed in this research for training of the methods using NOC data, which is described as follows:

1) First one of the TEMs was selected and the NOC data was then used to construct a connectivity graph, using a threshold set according to the procedure described in section 4.3.4. This threshold and the training connectivity graph were saved for later application for TEM and FIM.
2) One of the PPMs was selected. When the method selected was blocking, the connectivity graph was then used to separate the data into separate blocks by finding the strongly connected components (SCC). Otherwise the data was unaltered (unblocked).
3) A FEM was selected and trained on the processed data, resulting in the extracted scores and loadings. For PCA (dashed path), these were then used to reconstruct the data. This reconstruction was then compared to the actual data to give the SPE statistic. For KPCA the scores were used to calculate the SPE approximation according to Equation 2-7. The scores were also used to calculate the T_A^2 statistic according to Equation 2-6.

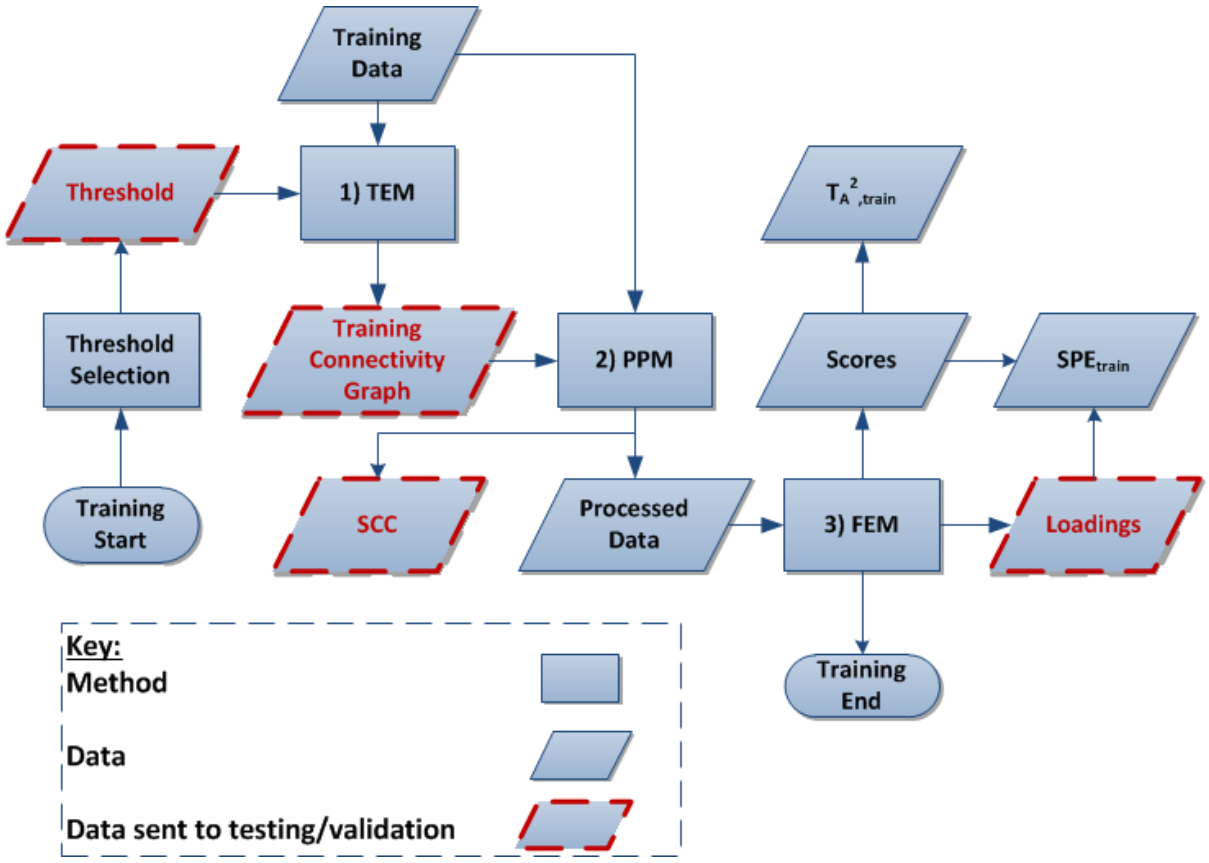

Figure 4-2: Diagram of methodology followed for training of fault diagnosis methods

4.2.3. Validation of fault diagnosis methods

A subset of the NOC data was used for validation of the methods, specifically the feature extraction methods. Figure 4-3 illustrates the methodology followed for validation in the form of a block diagram. This can be described as follows:

1) Pre-processing was first applied to the validation data: either the data was blocked according to the SCCs obtained from the training method's pre-processing, or the data was left unblocked.
2) The processed data was projected onto the feature space using the loadings obtained from feature extraction on the training data. This gave the T_A^2 and the SPE statistics for the validation data.
3) Both statistics were used to generate monitoring charts using the selected MCM. These monitoring statistics were then used to define the monitoring chart thresholds according to the value under which 99% of the statistics fell. These thresholds were later applied for the testing methods.
4) The SPEs were used to generate contribution plots. These individual variables contributions were also used to define the thresholds for the testing contributions.

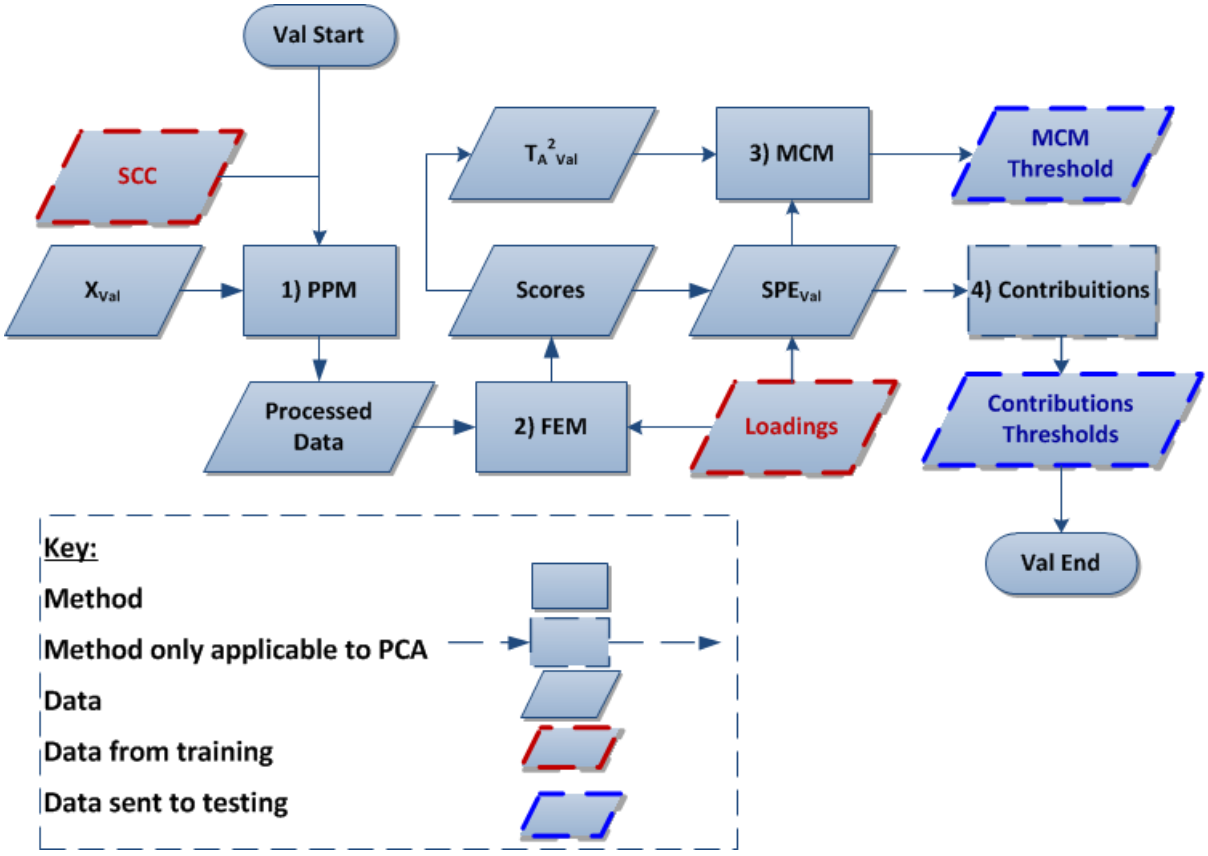

Figure 4-3: Diagram of methodology followed for validation of fault diagnosis methods

4.2.4. Normal operating conditions testing of fault diagnosis methods

A subset of the NOC data was used for testing of the methods, specifically the feature extraction methods. Figure 4-4 illustrates the methodology followed for NOC testing in the form of a block diagram. This can be described as follows:

1) Pre-processing was first applied to the NOC testing data: either the data was blocked according to the SCCs obtained from the training method's pre-processing, or the data was left unblocked.
2) The processed data was projected onto the feature space using the loadings obtained from feature extraction on the training data. This gave the T_A^2 and SPE statistics for the NOC testing data.
3) Both statistics were used to generate monitoring charts. The thresholds from the validation statistics were applied to these charts. The values that rose above the thresholds were identified false alarms, giving the false alarm rate (FAR).

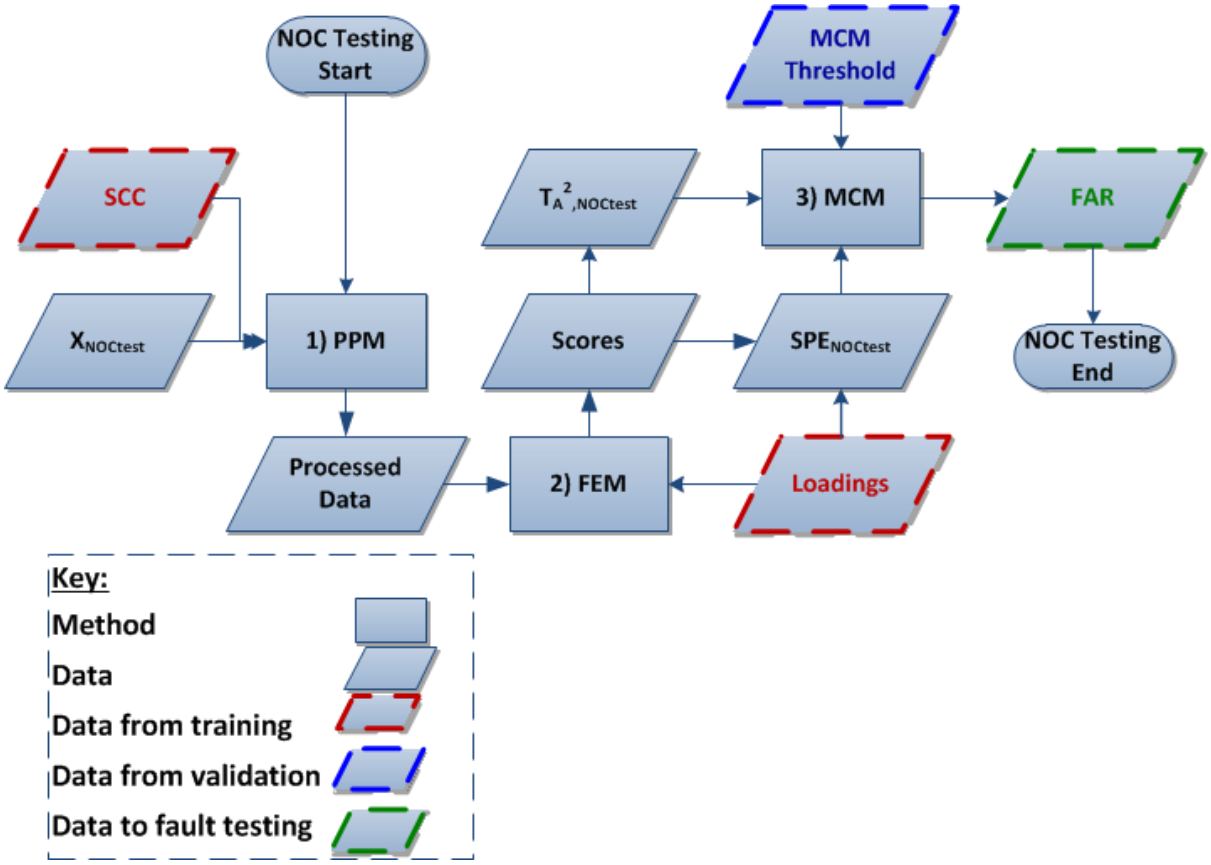

Figure 4-4: Diagram of methodology followed for normal operating conditions testing of fault diagnosis methods

4.2.5. Testing of Methods

Figure 4-5 presents a diagram illustrating the procedure followed for testing of the methods using fault data, which is described as follows:

1) Pre-processing of the data was first performed: either the data was blocked according to the SCCs obtained from the training method's pre-processing, or the data was left unblocked.
2) The processed data was then projected onto the feature space using the loadings obtained from the training FEM, giving the scores. For PCA this was again used to reconstruct the

data, which was then compared to the original data to give the SPE for the test data. For KPCA the approximation from the scores was used to calculate the SPE. The T_A^2 statistic was calculated from the retained scores.

3) Both the SPE and the T_A^2 statistics were then sent to the selected MCM. The alarm threshold determined from the validation data was set and the missing alarm rates (MAR) and detection delay (DD) were calculated.
4) An ROC curve was then generated using the MAR and the FAR from the NOC Testing methods at varying thresholds and the area under the curve (AUC) was calculated. The DD and AUC were the main performance metrics used to determine how well the combination of methods detected the fault.
5) Fault identification was then performed. First the symptom nodes had to be identified, either using contributions or by using connectivity change. For the contributions method the SPE was used to determine the contributions of each variable to the fault conditions. The contributions for the validation data were used as a threshold and the variables exceeding this threshold were highlighted as symptom nodes. For the connectivity change method a TEM method was chosen and used to generate a connectivity graph using the same threshold as for the training data. The training and testing connectivity graphs were compared and the variables that showed the most change were highlighted as symptom nodes.
6) The symptom nodes were then traced back to possible root nodes using back propagation.

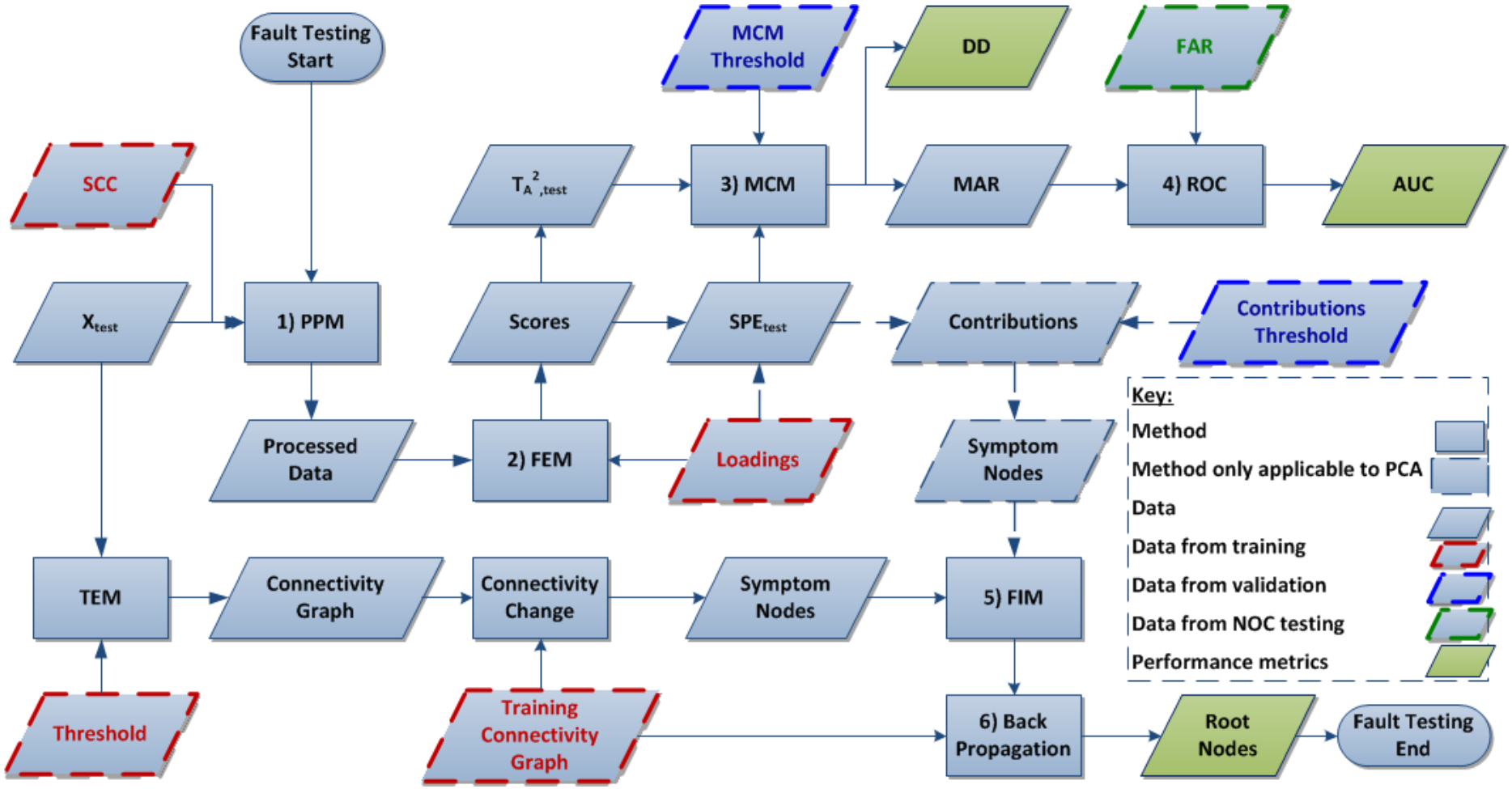

Figure 4-5: Diagram of methodology followed for fault testing of fault diagnosis methods

4.3.Procedure for Topology Extraction Methods

The specific procedure followed to extract topology using each TEM is discussed in this section.

4.3.1. Linear cross-correlation

In order to extract topology from data using the LC method the following procedure was followed:

1) For each possible combination of variable pairs and for the chosen number of lags, Equation 3-1 was applied to each pair of variables in the data matrix. Since this method is symmetrical this only needed to be performed for the upper triangle of the connectivity matrix.
2) This calculation resulted in an MxM connectivity matrix with the maximum correlation for each pair of variables as the entries, as well as a corresponding MxM lag matrix. When the lag was zero it was an indication that there was no causality, so these entries were assigned zero in the CM. When the lag was less than zero it meant the causality was in the other direction, so this entry was then moved below the diagonal.
3) The remaining entries in the CM had to be tested for significance, so the values below the significance level were assigned zeros as well (setting significance threshold is discussed in section 4.3.4).
4) The CM was then used to construct a connectivity graph.

4.3.2. Partial cross-correlation

In order to extract topology from data using the PC method a similar procedure to that for LC was followed:

1) For each possible combination of variable pairs and for the chosen number of lags, Equation 3-4 was applied to each pair of variables in the data matrix, while conditioning on all remaining variables in the data. Since this method is symmetrical this calculation only needed to be performed for the upper triangle of the CM.
2) This calculation gave an MxM connectivity matrix with the maximum correlation for each pair as the entries, as well as a corresponding MxM lag matrix. When the lag was zero it was an indication that there was no causality, so these entries were assigned zero in the CM. When the lag was less than zero it mean the causality was in the other direction, so this entry was then moved below the diagonal.
3) The remaining entries in the CM had to be tested for significance, so the values below the significance level were assigned zeros as well (setting significance threshold is discussed in section 4.3.4).
4) The CM was then used to construct a connectivity graph

4.3.3. Transfer entropy

To extract topology from data using the TE method the following procedure was followed:

1) For each possible combination of variable pairs and for the chosen number of lags Equation 3-5 was applied to each pair of variables in the data matrix to give an MxM matrix with entries $T_{x\to y}$. Values suggested by Bauer et al. (2007) for parameters used in this equation were a prediction horizon, h=4, sampling period, τ =4, and embedding dimensions, lx=ly =1. This method was asymmetrical so it had to be performed on all possible pairs of variables.
2) To give the causality , which was the difference between $T_{x\to y}$ and $T_{y\to x}$ (Equation 3-7), the transpose of the connectivity matrix was subtracted from itself.
3) This calculation gave an MxM connectivity matrix with the TE causality measure for each pair as the entries, as well as a corresponding MxM lag matrix. The significance of each entry had to be tested and the values below the significance threshold were assigned values of zero (setting significance threshold is discussed in section 4.3.4).
4) The CM was then used to construct a connectivity graph.

4.3.4. Setting significance thresholds for topology extraction

Each TEM requires selection of a significance threshold. For LC and PC, the basis of determining causality is that the hypothesis of the presence of a causal relationship between two variables is rejected if there is no evidence of time delay between them and/or if the maximum correlation is not significantly large to indicate causality. For TE the hypothesis of the presence of a causal relationship between two variables is rejected if the difference in the transfer entropy from x to y and y to x is small.

Significance threshold for linear cross-correlation

Bauer and Thornhill (2008) presented a method which can be used for the selection of this significance threshold. This approach empirically estimates the distribution of the correlation under the null hypothesis that two variables, **x** and **y**, are uncorrelated random time sequences. The correlation between two series from the plant data that are connected will be unlikely to have originated from the same distribution; therefore their correlation value should be higher. Using a one-sided hypothesis test, the null hypothesis that two time series are uncorrelated is rejected and the correlation is deemed to be indicative of causality between the variables when the hypothesis presented in Equation 4-1 is valid.

$$\rho_{\max}^{LC} \geq \rho_{\max,rnd}^{LC} = \mu_{\rho_{\max,rnd}^{LC}} + 3\sigma_{\rho_{\max,rnd}^{LC}} \qquad \textbf{Equation 4-1}$$

In Equation 4-1, the subscript rnd indicates values calculated for the random vectors and $\mu_{\rho^{LC}_{max,rnd}}$ and $\sigma_{\rho^{LC}_{max,rnd}}$ are the mean and standard deviation respectively of ρ^{LC}_{max}. The mean and standard deviation are functions of the sample number, or length of the series, N. Therefore to determine an empirical distribution (i.e. μ and σ) of ρ^{LC}_{max}, random time sequences were generated, with varying number of samples N_{rnd}, from 0 to 3000. For each N_{rnd} the correlations of each pair of time series (31x31 pairs) was calculated and the mean and standard deviation of ρ^{LC}_{max} were calculated.

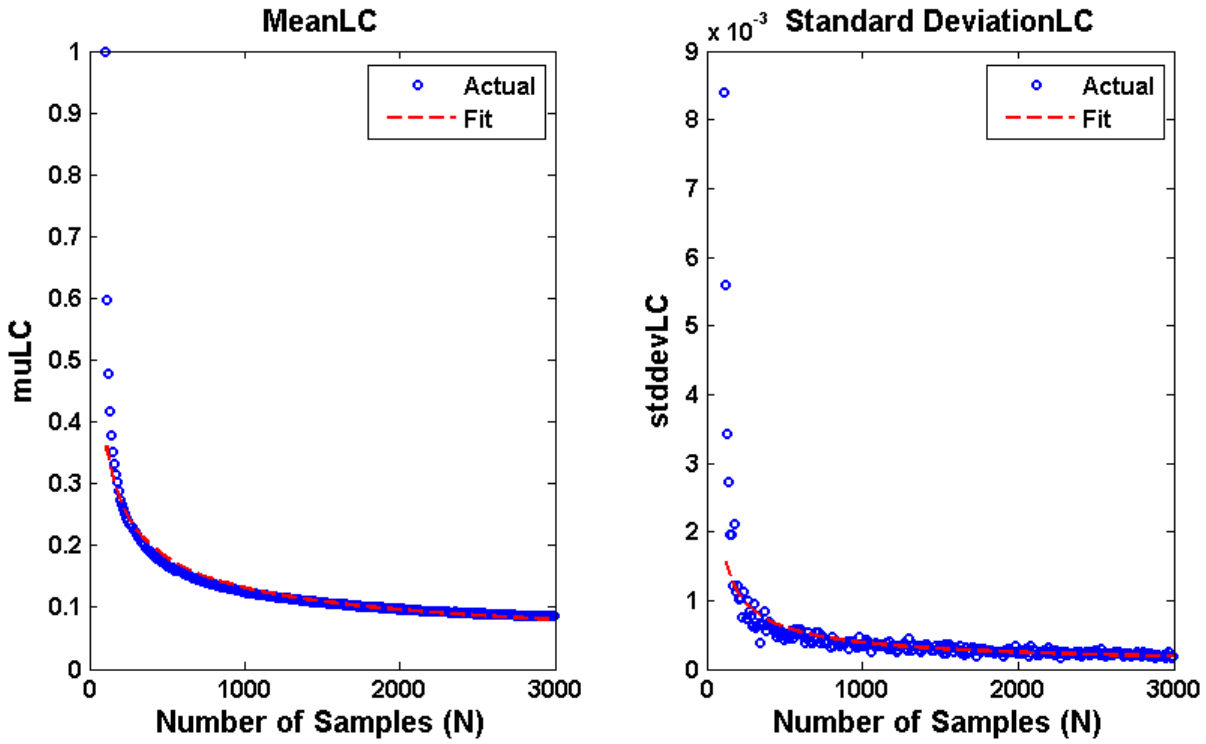

Figure 4-6: Linear cross-coorelation mean and standard deviation for 31 pairs of random sequences with changing sample size

Figure 4-6 shows the plots of the mean and standard deviation against number of samples, N. They both follow a decreasing exponential trend that can be described by the Equation 4-2 and Equation 4-3.

$$\mu_{\rho^{LC}_{max,rnd}} = a_1(N)^{-b_1} \qquad \textbf{Equation 4-2}$$

$$\sigma_{\rho^{LC}_{max,rnd}} = a_2(N)^{-b_2} \qquad \textbf{Equation 4-3}$$

Substituting Equation 4-2 and Equation 4-3into Equation 4-1 results in an equation for $\rho^{LC}_{max,rnd}$, which is now designated as the significance threshold for the correlation, $\rho^{LC}_{max,th}$, as a function of N, as shown in Equation 4-4.

$$\rho^{LC}_{max,th}(N) = a_1 N^{-b_1} + 3a_2 N^{-b_2} \qquad \textbf{Equation 4-4}$$

Curve fitting was used to determine the parameters in Equation 4-4, resulting in the an equation for the threshold as a function of sample size, as shown in Equation 4-5.

$$\rho_{max,th}^{LC}(N) = 3N^{-0.452} + 0.11N^{-0.658} \quad \textbf{Equation 4-5}$$

The fitted curves are also shown as the red dashed lines in Figure 4-6.

Significance threshold for partial cross-correlation

As with LC, PC also requires selection of a threshold to determine the significance of the maximum PC calculated for a pair of variables. The same approach as described for LC can be used for selection of the threshold for PC.

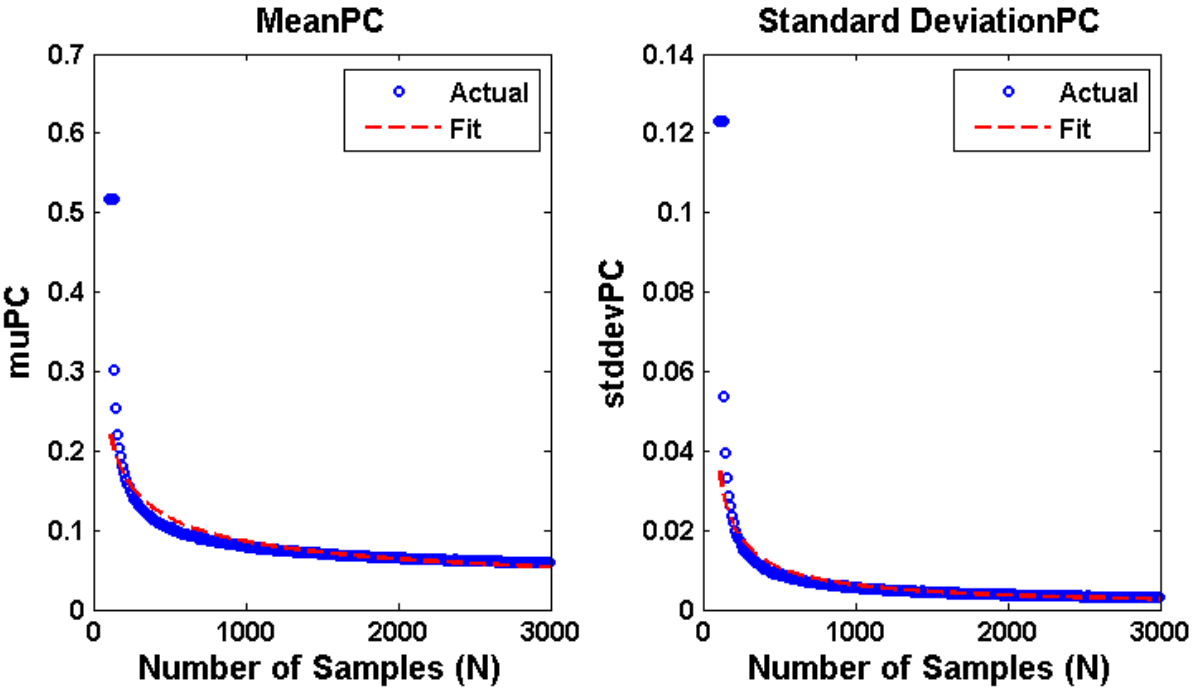

Figure 4-7: Partial cross-correlation mean and standard deviation for 31 pairs of random sequences with changing sample size

Figure 4-7shows the same kind of decreasing exponential trend for the PC as was observed for LC. So the general equation for $\rho_{max,rnd}^{PC}$ as a function of N is similar to Equation 4-4, and is shown in Equation 4-6.

$$\rho_{max,th}^{PC}(N) = a_1N^{-b_1} + 3a_2N^{-b_2} \quad \textbf{Equation 4-6}$$

Curve fitting was used to determine the parameters in Equation 4-6, resulting in an equation for the PC threshold as a function of sample size, shown in Equation 4-7.

$$\rho_{max,th}^{PC}(N) = 1.647N^{-0.428} + 3.864N^{-0.772} \quad \textbf{Equation 4-7}$$

The fitted curves are also shown as the red dashed lines in Figure 4-7.

Significance threshold for transfer entropy

Again the selection of a threshold is required for the hypothesis testing using TE. Bauer et al. (2007) set this threshold using the method suggested by Schreiber and Schmitz (2000). This approach generates surrogate time series data and uses Monte Carlo methods to determine the mean and standard deviation of $t_{x\to y}$. The significance is then defined using a 6 sigma threshold, as shown in Equation 4-8.

$$t_{\mathbf{x}\to\mathbf{y}} \geq t_{\mathbf{x}\to\mathbf{y},\mathrm{th}} = \mu_{t_{\mathbf{x}\to\mathbf{y},\mathrm{rnd}}} + 6\sigma_{t_{\mathbf{x}\to\mathbf{y},\mathrm{rnd}}} \qquad \textbf{Equation 4-8}$$

However, Bauer et al. (2007) did not consider that the TE varies with increasing sample size, as was the case with LC and PC. Using random sequences of increasing sample sizes the TE mean and standard deviation were calculated and plotted against sample size, as shown in Figure 4-8. Figure 4-8 illustrates that TE increases with increasing sample size though.

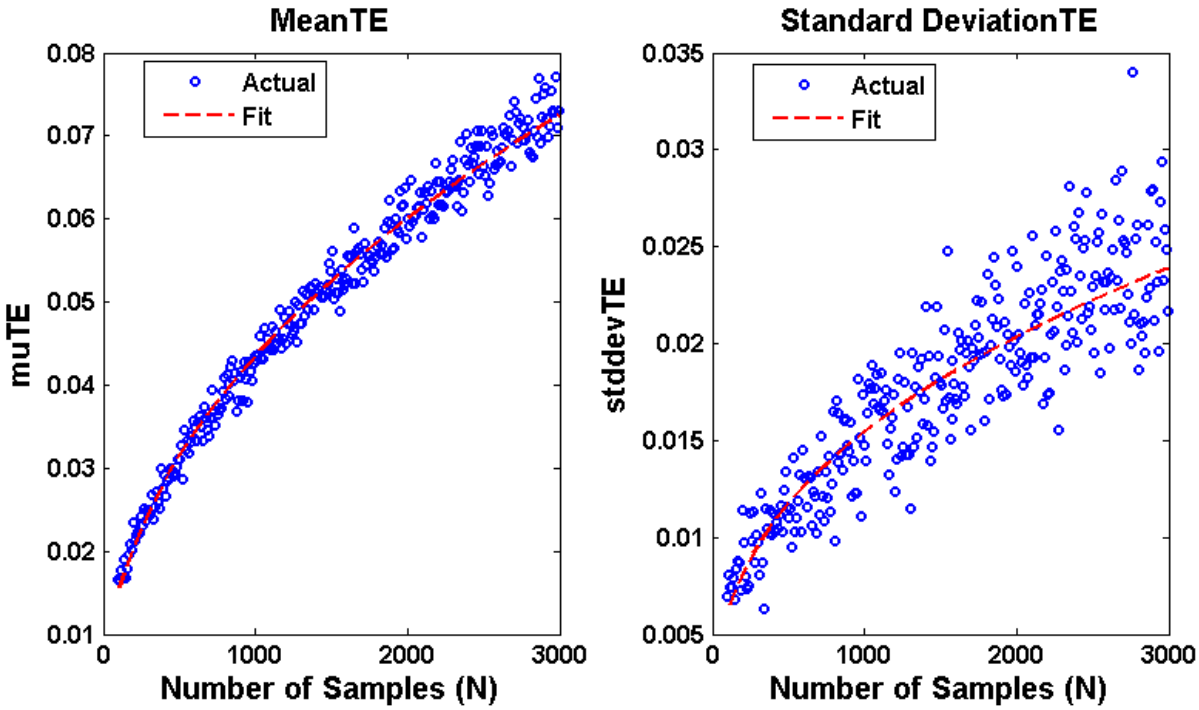

Figure 4-8: Transfer entropy mean and standard deviation for 31 pairs of random sequences with changing sample size

The mean and standard deviation both follow an increasing trend that can be described generally according to Equation 4-9 and Equation 4-10 respectively.

$$\mu_{t_{\mathbf{x}\to\mathbf{y},\mathrm{rnd}}} = a_1(N)^{b_1} \qquad \textbf{Equation 4-9}$$

$$\sigma_{t_{\mathbf{x}\to\mathbf{y},\mathrm{rnd}}} = a_2(N)^{b_2} \qquad \textbf{Equation 4-10}$$

Substituting Equation 4-9 and Equation 4-10 into Equation 4-8 gives a general equation for the threshold as a function of sample size, N, as shown in Equation 4-11.

$$t_{\mathbf{x}\rightarrow\mathbf{y},\mathrm{th}}(N) = a_1 N^{b_1} + 6a_2 N^{b_2} \quad \textbf{Equation 4-11}$$

Curve fitting was used to determine the parameters in Equation 4-11, resulting in an equation for the threshold as a function of sample size, as shown in Equation 4-12.

$$t_{\mathbf{x}\rightarrow\mathbf{y},\mathrm{th}}(N) = 0.0018N^{0.465} + 0.0054N^{0.412} \quad \textbf{Equation 4-12}$$

The fitted curves are also shown as the red dashed lines in Figure 4-8.

4.4. Procedure for Pre-Processing Methods

In this study the only pre-processing method considered was blocking. To divide large process data sets into multiple blocks according to strongly and weakly connected components the following procedure was followed:

1) The strongly connected components in the connectivity graph were found, and the measured variables in these components were grouped into their own blocks.
2) A new connectivity graph was generated using the remaining variables.
3) The weakly connected components in this new connectivity graph were found and the variables in these components were grouped into their own blocks.
4) Any remaining unconnected variables were then lumped together into their own block.

Once the process had been separated into blocks, each block was then be analysed separately for fault detection and identification.

4.5.Procedure for Feature Extraction Methods

The two feature extraction methods considered in this study were PCA and KPCA. In order to apply these methods for fault detection the procedures described in this section were followed.

4.5.1. Principal components analysis procedure

Application of PCA for fault detection can be split up into training of the PCA model (using the NOC training data) and testing of new data on the model (using the validation, NOC testing and Fault testing data):

Training of principal components analysis model

1) Spectral decomposition of the covariance matrix of the training data gave the principal component scores and loadings.
2) Only a few components had to be retained. The method chosen to determine how many components to retain was choosing the number that accounted for 90% explained variance.

Testing of new data on the principal components analysis model

1) The unseen data was then projected onto the feature space defined by the retained principal components to give the principal component scores of the test data according to Equation 2-4.
2) The test data was then reconstructed using the test scores according to Equation 2-5
3) The modified Hotelling's T_A^2 statistic was then calculated, according to Equation 2-6 to determine the distance of each new observation from the centre of the feature space.
4) The SPE statistic was then calculated, using Equation 2-7.

4.5.2. Kernel principal components analysis model

For KPCA the methods are also divided into training (used on NOC training data) of the model and testing of new data on the model (for validation, NOC Testing and fault testing):

Training of kernel principal components analysis model

1) First the data was mapped nonlinearly into a higher-dimensional space through the kernel function according to Equation 2-19. This gave the Kernel matrix **K**. In order to perform this step the kernel width, c, needed to be selected. This was done by performing cross-validation, which is described later in this section.
2) The kernel matrix then had to be centred according to Equation 2-20.
3) Eigenvalue decomposition of **K**, according to Equation 2-15 gave the eigenvectors **P** with eigenvalues λ.
4) Again only a few of these components had to be retained. The number selected was determined again by 90% explained variance.

Testing of new data on the kernel principal components analysis model

1) The new data (test or unseen data) was then be mapped onto the kernel space according to Equation 2-21.
2) The testing kernel matrix also had to be centred on the training data, according to Equation 2-22.
3) Then the scores were calculated according to Equation 2-23.
4) The T_A^2 statistic were calculated according to Equation 2-6(same as PCA).
5) Since KPCA does not allow reconstruction back to the data space the SPE could not be calculated the same as PCA. It had to be approximated according to Equation 2-24

Cross-validation to select kernel width

Cross validation is a parameter selection method commonly used in support vector machine implementation.

1) Training data is divided into five folds.
2) One of the folds is selected for testing, and then the remaining four folds are used to train the KPCA model.
3) This is done for all the folds and is then further repeated for a range of kernel widths.
4) Each time the mean squared prediction error is calculated and the kernel width that resulted in the lowest mean squared prediction error is selected.

4.6. Procedure for Monitoring Chart Methods

The three monitoring chart methods considered for monitoring of the SPE and T_A^2 statistics are discussed here, as well as the ROC curves used to generate the AUC performance metric. Since the methods were all the same with the exception of the first step they are presented as one methodology.

1) The Shewhart chart simply plots the statistic against sample number. EWMA first required calculation of the moving average according to Equation 2-26 and then plotted against sample number. The CUSUM first calculated the cumulative sum over a moving window according to Equation 2-25and then plots it over sample number.
2) The statistics from the validation data were used to set the significance thresholds as the value under which 99% of the statistics for the validation data fell.
3) The percentage of the NOC testing statistics that rose above this threshold was calculated, giving the MAR.
4) The percentage of the fault testing statistics that fell below this threshold were calculated, giving the FAR.
5) The DD was determined by calculating how many samples it took before the fault test data showed three consecutive samples above the threshold.
6) The ROC curve was then used to calculate the AUC. This was done by calculating the MAR and FAR for a range of thresholds and then plotting the MAR against the TAR and calculating the area under this curve using numerical integration, giving the AUC.

4.7. Procedure for Fault Identification Methods

For fault identification the symptom nodes first had to be identified either by connectivity change or contribution plots, and then these symptom nodes were used to trace back in the connectivity graph to identify possible root nodes.

4.7.1. Symptom node identification using connectivity change

The method proposed in this study to incorporate connectivity change into the fault identification procedure was to determine which variables showed a significant change in connectivity from NOC to fault conditions, and highlight these as symptom variables.

1) The connectivity change was determined by subtracting the training data connectivity matrix, CM_{Train} from the testing data connectivity matrix CM_{Test}, as shown in Equation 4-13.

$$\text{ConnChange} = \text{CM}_{\text{Test}} - \text{CM}_{\text{Train}} \qquad \textbf{Equation 4-13}$$

2) The connections that rose above the significance threshold were considered; i.e. where the connection was insignificant in CM_{Train}, but became significant in CM_{Test}. Only these were considered because the fault would propagate through the process and cause large variations in some measured variables and would cause connections that were previously insignificant to become stronger.
3) Then the connectivity changes that were in the top 90^{th} percentile are considered as significant changes. All the nodes associated with these edges were then highlighted as symptom variables.

4.7.2. Symptom node identification using variable contributions

In Chapter 2 the generation of contribution plots was discussed, so it will not be repeated here. The variables whose contributions became larger than the validation data contributions are highlighted as symptom nodes. Since only the contribution plots for the squared prediction error were considered this method could only be applied to PCA, since KPCA does not allow reconstruction of the variables.

4.7.3. Back propagation using connectivity graphs

Figure 4-9 provides a simple illustration of the back propagation method. The symptom nodes were identified, either from contributions or from connectivity change. Then a root node was identified by finding the furthest common ancestor of these nodes, giving an indication of the root cause of the fault.

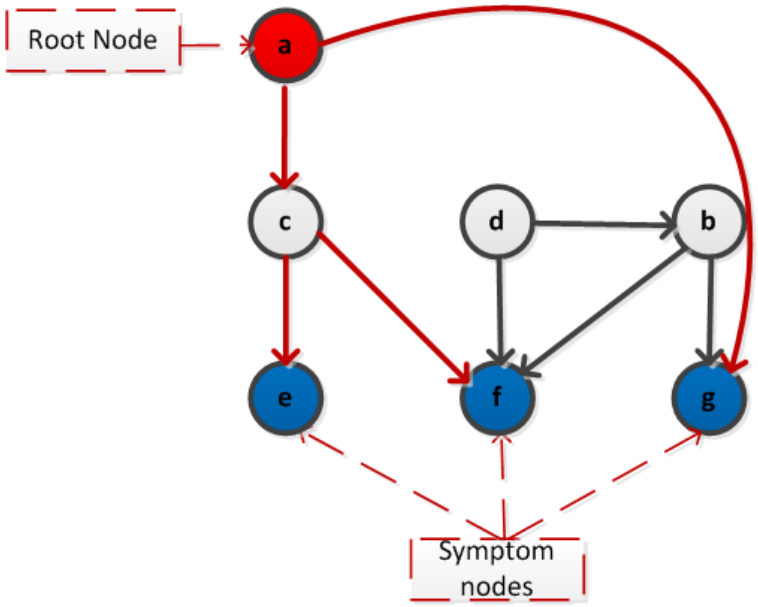

Figure 4-9: Simple illustration of back propagation method. Letters a to g indicate variable names

The back propagation method is described as follows

- The ancestors in the connectivity graph (CG) for each symptom node (SNj) were found.

$$\boldsymbol{Anc_j} = GetAncestors(CG, SN_j) \quad \textbf{Equation 4-14}$$

- The shared ancestors (SA) of all the symptom nodes were found.
- The shortest paths from these shared ancestors to the symptom nodes were determined. The algorithm for determining this takes into account the weights of the edges, so nodes with strongly weighted connections are closer together.

$$SP_{i,j} = ShortestPath(CG, SA_i, SN_j) \quad \textbf{Equation 4-15}$$

- The shared distances (SD) from shared ancestors to all symptom nodes were added up.

$$SD_i = \sum_{j=1}^{Nsn} SP_{i,j} \quad \textbf{Equation 4-16}$$

- The SDs were sorted in descending order according to the distances are to all symptom nodes.

$$\boldsymbol{SD} = sort(\boldsymbol{SD}, descending) \quad \textbf{Equation 4-17}$$

- The first SA node corresponding to the first entry in **SD** is then the furthest common ancestor. To ensure that possible root nodes were not left out the first three furthest ancestors (**SD**(1:3)) were chosen as possible root nodes.

4.8.Missing Data Reconstruction

A problem when using real data is that it may often have missing values or NANs in some entries due to sensor problems, or human error when sampling or operating. Methods exist for the treatment of such data, such as using the mean of the variable's time series as a substitute for the missing value. However, auto associative models, such as PCA, can be used to reconstruct such data. One can use PCA to build a model on a first guess of what the data should look like. The PCA model will capture the major trends in the data due to its feature extraction capability. The model can then be used to reconstruct the data, giving an improved estimate of the values of the missing data. The values obtained from the PCA model can be substituted into the entries where the data had missing values. This next guess can then be used again to train a PCA model and the process can be repeated until suitable convergence is achieved. The initial guess of the missing values can be taken as just the previous sample's value.

4.9.Case Studies

The fault diagnosis methods described were applied to three different case studies:

1) The first was a dynamic simulation of a simple system containing two tanks with heat exchange. This was a small system, with eight measured variables. This system is ideal for the development of the methods
2) The second was a case study a dynamic simulation of a pressure leaching process in the base metals refinery of a platinum processing plant. This simulation s ideal for the testing of the methods because of its complexity: it involves a large number of measured variables; a large number of interconnecting process units; numerous interacting control loops; as well as recycle loops. The high degree of interconnectivity resulting from the control and recycle loops would cause a fault to propagate throughout the large system, so the utility of using connectivity information to trace the faults back to their original causes can be analysed. Also, the large number of variables and process units may make it ideal to test blocking.
3) The third case study involves actual plant data from a concentrator. This case study is useful in that it allows application of the methods to actual plant data and their performance could be gauged.

Detailed descriptions of each case study are provided in their respective results chapters.

Chapter 5 - Case Study: Fault Diagnosis Applied to Two-Tank Simulation

This chapter presents the results of application of the fault diagnosis methods to the first case study.

5.1. Two-Tank Simulation Case Study Description

This first case study is a dynamic simulation of a simple two-tank with heat exchange system. A diagram of the system is presented in **Error! Reference source not found.**. The simulation was developed for this project, since it was ideal for the development of the topology extraction and feature extraction methods. The full details of the modelling and simulation work are provided in Appendix A-. This is a small system, with only eight measured variables. It has four control loops (two for level control and two for temperature control) illustrated by the transmitter and controller symbols (e.g. LT1 and LC2) and the dashed lines. This system has no recycle loops, which means that the resulting connectivity graphs are likely to be quite simple with a mostly hierarchical/sequential structure; i.e. the edges may tend to proceed in one direction, without edges forming a closed loop between a group of variables. However, the presence of control loops may cause such loops to form.

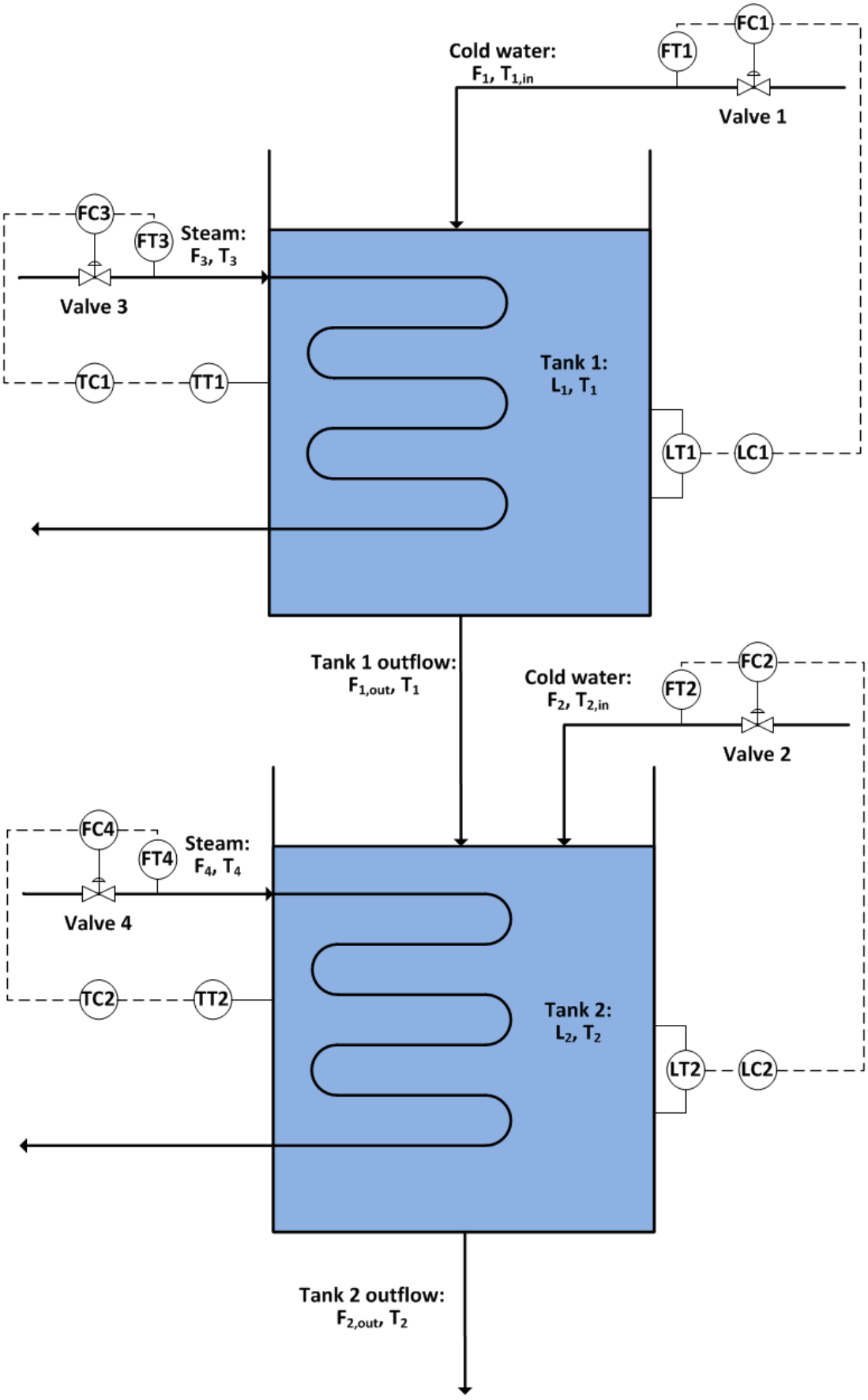

Figure 5-1: Diagram of two-tank with heat exchange process used as a case study, including control loops and measured variable

5.1.1. Description of overall process and control in two-tank system

The chosen example system consists of two tanks in series. The outlet flow from each tank is proportional to the square root of the tank's level. The outlet from the first tank flows into the second tank. Each tank has a cold water supply, which is used to control the level in the tank. Each tank's temperature is controlled by the manipulation of the flow of steam into the heating coils in the tank. All the controllers are simple proportional integral derivative (PID) controllers.

5.1.2. Measured variables in two-tank simulation

The measured variables in the process are shown in **Error! Reference source not found.**by the presence of the transmitter symbol (e.g. Flow Transmitter for F_1 is FT1). These measured variables are: the flow rate of the inlet streams to the tanks, F_1 and F_2; the flow rates of the steam in the heating coils in both tanks, F_3 and F_4; the levels of both tanks, L_1 and L_2; and the temperatures of both tanks, T_1 and T_2. A summary of these variables is also given in Table 5-1.

Table 5-1: List of measured variables in two-tank simulation case study

Variable No.	Variable Name	Description	Units
1	F_1	Volume flow rate of stream 1	[m^3/min]
2	F_2	Volume flow rate of stream 2	[m^3/min]
3	F_3	Volume flow rate of stream 3	[m^3/min]
4	F_4	Volume flow rate of stream 4	[m^3/min]
5	L_1	Level of Tank 1	[m]
6	L_2	Level of Tank 2	[m]
7	T_1	Temperature of Tank 1	[°C]
8	T_2	Temperature of Tank 2	[°C]

5.2.Data from Two-Tank Simulation

NOC data was generated for training, validation and NOC test data sets. Fault conditions were also simulated for a number of faults. The sizes of each data set are given in Table 5-2.

Table 5-2: Summary of sizes of data sets from two-tank simulation

Data Set	Number of samples (N)	Number of variables (M)
Training	343	8
Validation	171	8
NOC Test	169	8
Fault Test	502	8

The different fault scenarios that were simulated are described below. Both step and ramp types of faults were simulated in order to test whether the fault identification methods could distinguish between the two. For each fault, five different sizes of the faults were also simulated to determine whether the fault identification methods could give an indication of the sizes of the faults.

5.2.1. Fault 1: Step disturbance in temperature $T_{1,in}$

A step disturbance in the temperature of the cold water input into the first tank was simulated. This type of fault could occur in a real system due to a change in the source of the feed water, for example. Five different disturbance sizes were introduced: a disturbance of -2°C, -4°C, -6°C, -8°C and -10°C. This fault would cause the temperature of the first tank to deviate from its set-point, and consequently the temperature of the second tank would also deviate from its set-point. This would then cause the temperature controllers to change the flow rates of the steam into the heating coils. The response of the measured variables to the disturbance of -8°C is shown in Figure 5-2.

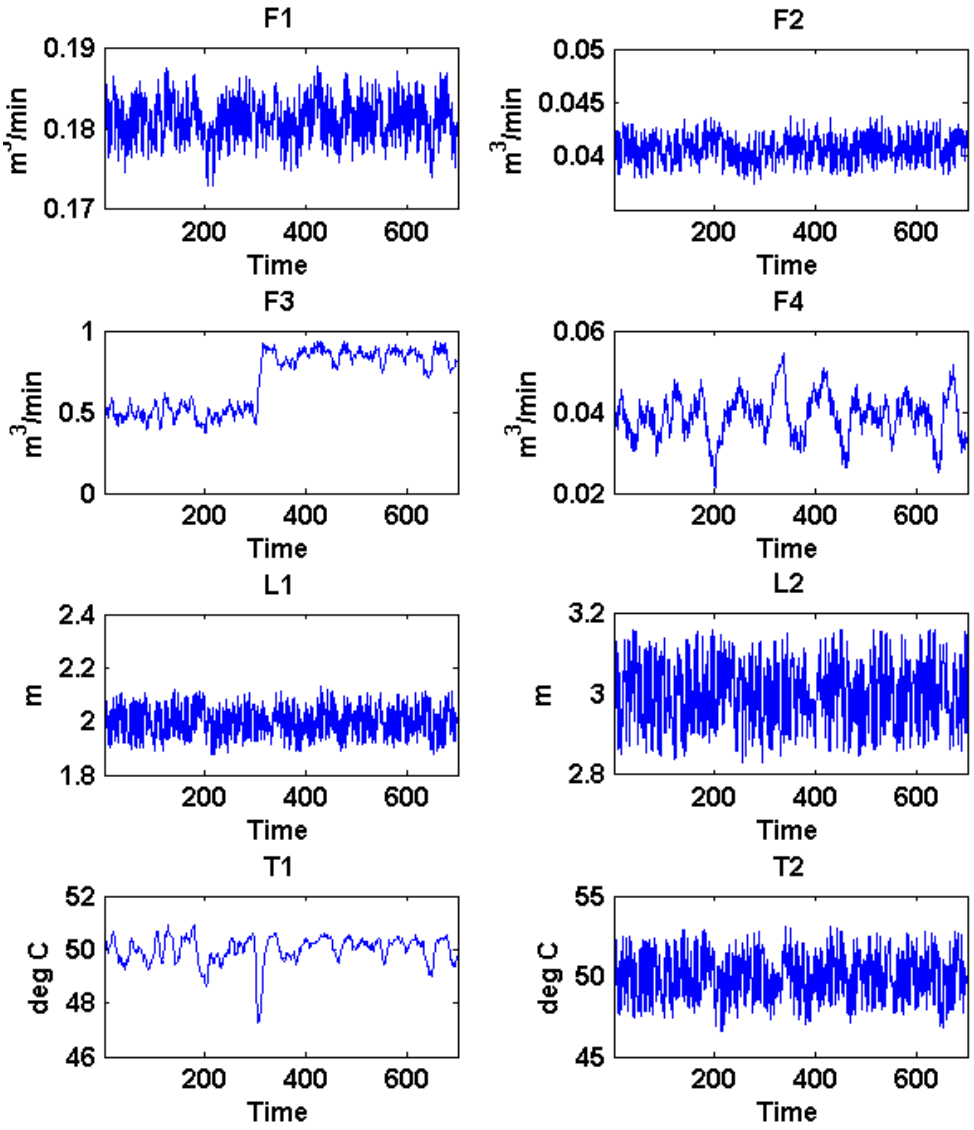

Figure 5-2: Response of measured variables to Step $T_{1,in}$ fault, disturbance of -8°C

5.2.2. Fault 2: Ramp disturbance in temperature $T_{1,in}$

A ramp disturbance in the temperature of the cold water input into the first tank was simulated. This type of fault could occur in a real system due to a change in the surrounding atmosphere's

temperature, for example. Five different ramp sizes were simulated, i.e. five different slopes of the ramp, with the final value being the same. The final values for each fault size were: -2°C, -4°C, -6°C, -8°C and -10°C. The effects of this fault would be the same as for the first fault; causing both tanks' temperatures to deviate from their set-points, in turn causing their controllers to change the flow rates of steam into the heating coils. However, the fact the temperature changed gradually over time means that at first its effects might not be noticeable, but since it keeps changing over a longer period of time would mean that the controller would have to keep making changes over a longer period. The response of the measured variables to this fault is shown in Figure 5-3.

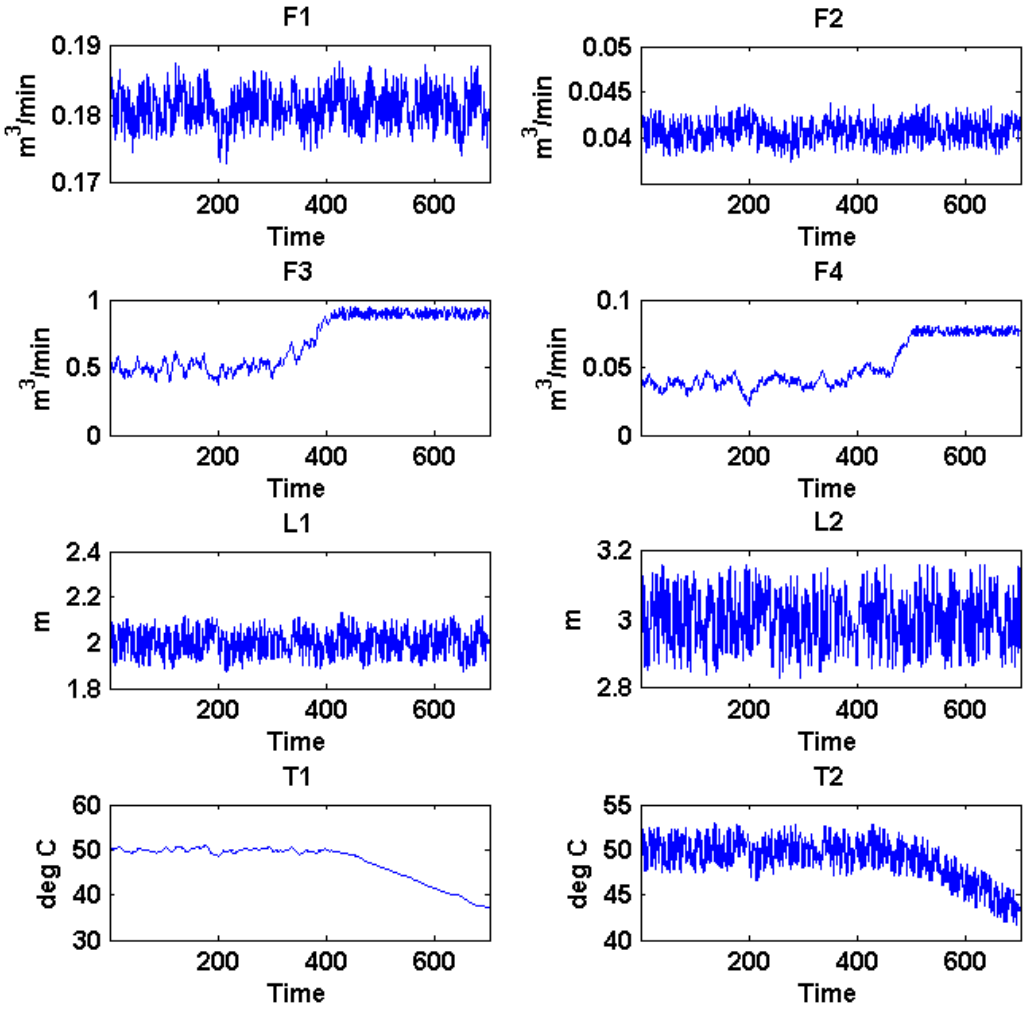

Figure 5-3: Response of measured variables to Ramp $T_{1,in}$ fault with final value of -8°C

5.2.3. Fault 3: Step disturbance in temperature $T_{2,in}$

A step disturbance in the temperature of the cold water input into the second tank was also simulated. This type of fault could occur in a real system due to a change in the source of the feed water, for example. Five different disturbance sizes were introduced: a disturbance of -2°C, -4°C, -6°C, -8°C and -10°C. This fault would cause the temperature of the second tank to deviate from its set-point, which would in turn cause the temperature controller to change the flow rate of the

steam entering the heating coil. Since it only affects the second tank's temperatures, this fault is highly localised in this tank. This makes it ideal for testing if the fault detection would be able to pick up a fault that affects very few variables in the system and if the fault identification can recognise that the fault is localised to the second tank. The response of the measured variables to this fault is shown in Figure 5-4.

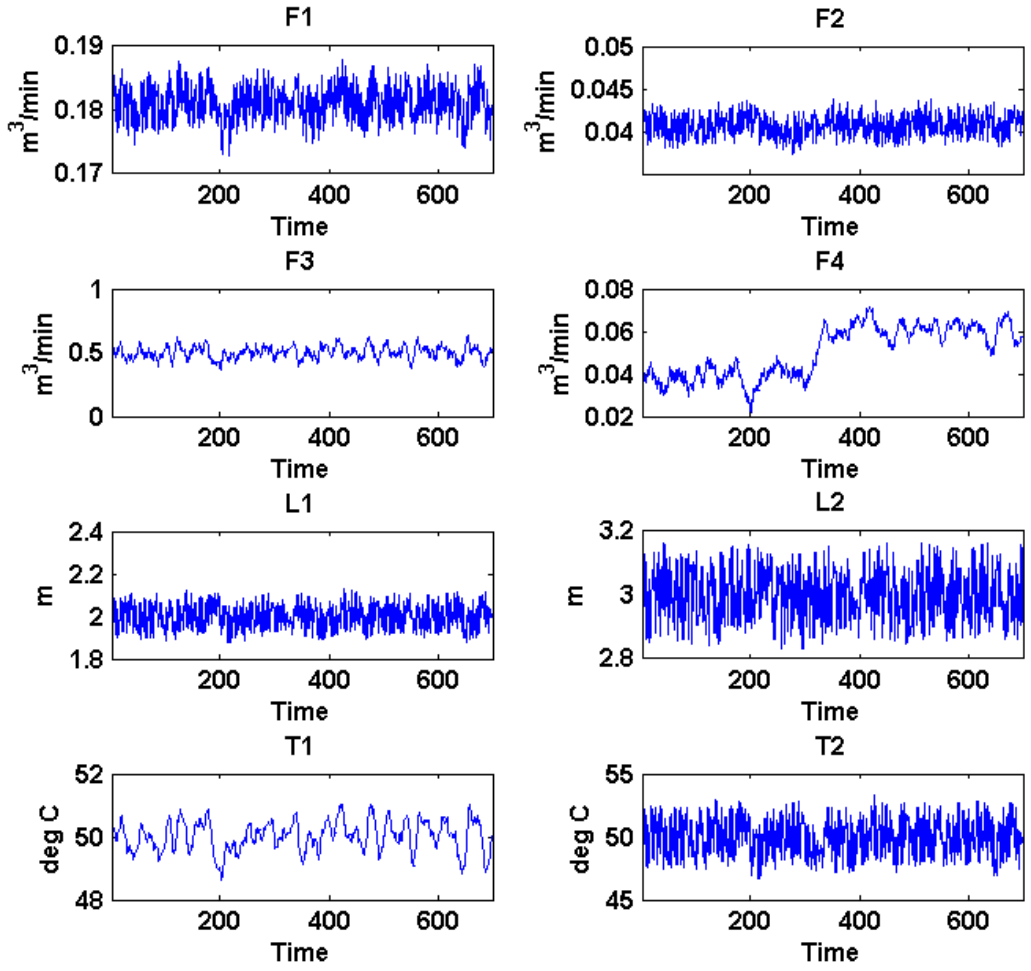

Figure 5-4: Response of measured variables to Step $T_{2,in}$ fault, disturbance of -8°C

5.2.4. Fault 4: Fouling in both heat exchange coils

Fouling conditions were simulated in the heat exchange coils of both tanks. The fouling was simulated by changing the heat exchange constant, aHeat, in the energy balance equations represented by Equation 5-1 and Equation 5-2.

$$V_1 C_p \frac{dT_1}{dt} = \rho C_p \left(F_1 \cdot T_{1,in} - F_{1,out} \cdot T_1\right) - \frac{aHeatF_3^{b+1}}{F_3 + \frac{aHeatF_3^b}{2\rho C_p}} \cdot (T_1 - T_3) \qquad \textbf{Equation 5-1}$$

$$\rho V_2 C_p \frac{dT_2}{dt} = \rho C_p \left(F_{1,out} \cdot T_1 + F_2 \cdot T_{2,in} - F_{2,out} \cdot T_2\right) - \frac{aHeatF_4^{b+1}}{F_4 + \frac{aHeatF_4^b}{2\rho C_p}} \cdot (T_2 - T_4) \quad \textbf{Equation 5-2}$$

A full description of Equation 5-1 and Equation 5-2 and their associated parameters is given in Appendix A.

This disturbance was simulated as a ramp disturbance since fouling would accumulate over time in a real system. Five different fault sizes were simulated by varying the slope of the change in aHeat. The five different slope sizes were: -40, -80, -120, -160 and -200 [cal/min.°C/min]. This fault would also affect the temperatures in both tanks and subsequently cause the controller to change the flow rates of the steam entering the tanks. Since this fault changes parameters in the fundamental relations governing the behaviour of the system it may represent a type of fault where the relations between variables changes, whereas the other faults would show the same relationships, but different behaviour. The response of the measured variables to this fault is shown in Figure 5-5.

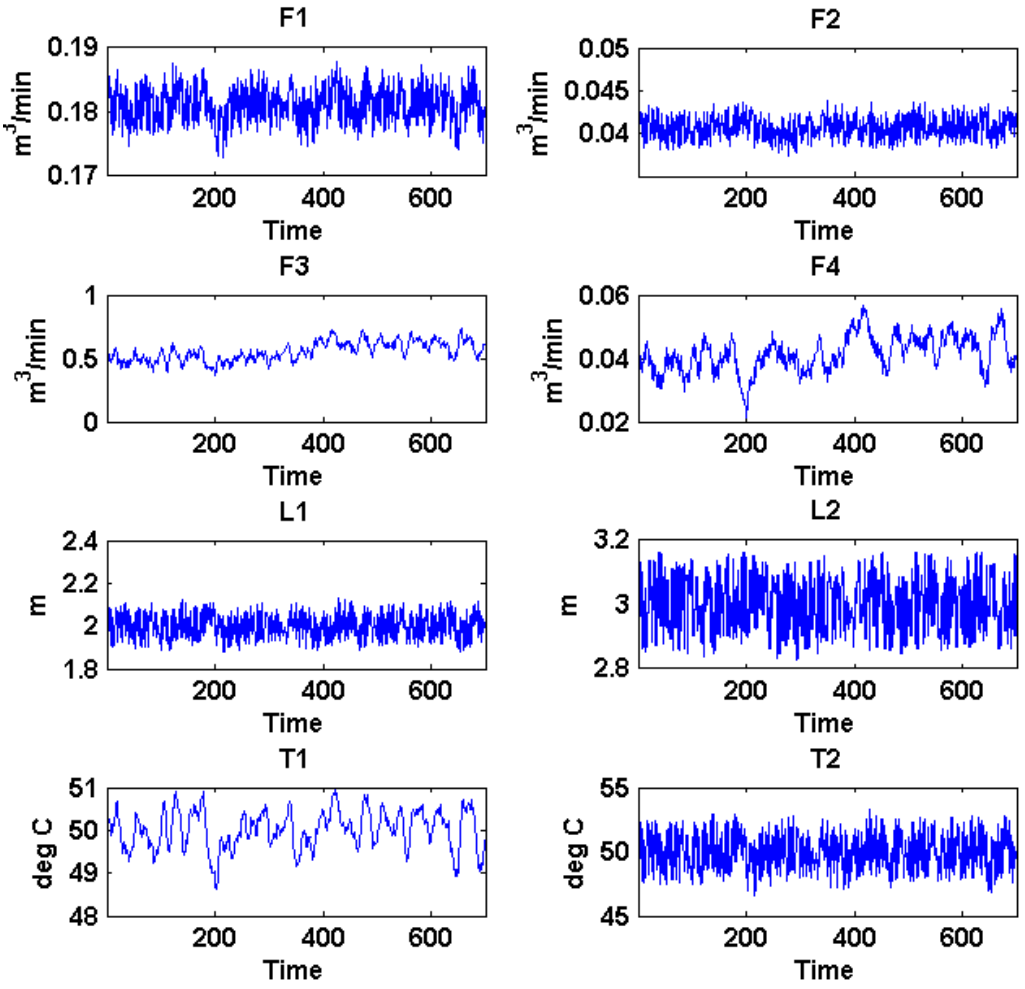

Figure 5-5: Response of measured variables to fouling fault

5.3. Topology Extraction from Two-Tank Data

This section presents the results of the topology extraction methods. Each method's resulting connectivity graph is shown and the validity of each observed connection is discussed.

5.3.1. Linear cross-correlation topology extraction

The number of lags, k, chosen for LC was 200. 200 lags corresponds to 100 minutes, which wass sufficiently long to capture the residence times and dead times in the process. In order to generate the connectivity graph using linear cross-correlation (LC) the significance threshold first had to be determined using the method described in Chapter 4, by substituting the number of samples (N=343) into the equation derived for the threshold as a function of sample number:

$$\rho_{max,th}^{LC}(N) = 3N^{-0.452} + 0.11N^{-0.658} \qquad \textbf{Equation 5-3}$$

$$\rho_{max,th}^{LC}(343) = 0.216 \qquad \textbf{Equation 5-4}$$

The connectivity graph obtained using this threshold of 0.216 was highly connected, with 22 edges in the graph. The connectivity matrix obtained indicated that there were a few correlation values that are very low, less than 0.4, but most of them are above 0.45. The selected threshold was not strict enough to eliminate the majority of the spurious connections, and it was therefore decided to double the threshold. The necessity of this decision indicates that the chosen method for threshold selection is not robust enough to give useful connectivity graphs in all applications. Applying the new threshold of 0.43, the connectivity graph in **Error! Reference source not found.** was generated.

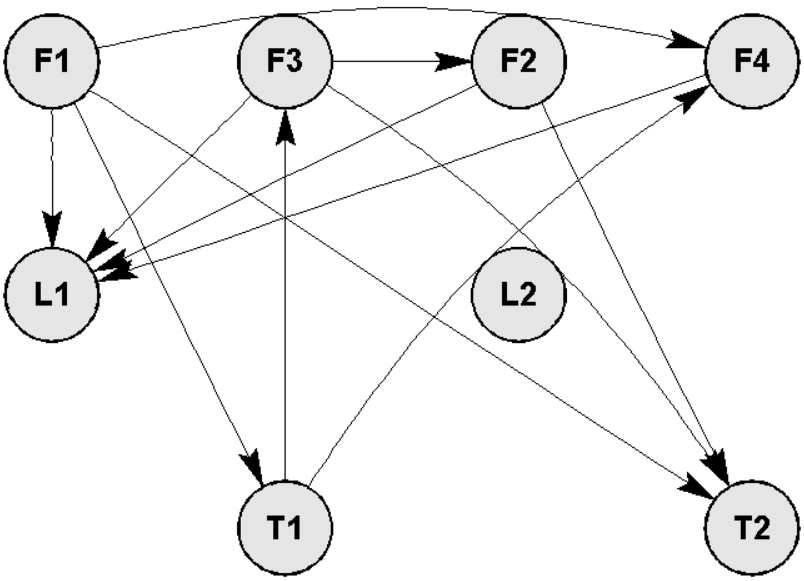

Figure 5-6: Linear cross-correlation connectivity graph from two-tank training data

Table 5-3 contains a systematic validation of each connection observed in this connectivity graph; the first two columns indicate the source and sink nodes of the edge being considered, the third column indicates whether the connection is valid (Y) or spurious (N), and the fourth column supplies the reason why it is considered valid (for example whether it makes sense from a mass or energy balance perspective or a control perspective) or spurious.

Table 5-3: Validation of connections in the linear cross-correlation graph. Y indicates a valid connection, N indicates a spurious connection

Source node	Sink node	Y/N	Reason
F_1	L_1	Y	Control: L_1 is controlled by manipulating F_1
F_1	T_1	Y	Energy balance: The flow rate of cold water into the first tank (F_1) will affect its temperature (T_1)
F_1	T_2	Y	Energy balance: The flow rate of cold water into the first tank (F_1) will affect the temperature of this tank and the temperature of the subsequent tank (T_2)
F_1	F_4	Y	Energy balance/control: The flow rate of cold water into the first tank (F_1) will affect the temperature of the second tank, which will then cause the controller to vary F4
F_2	L_1	N	F_2 cannot affect the level of the tank upstream of it (L_1). The connection should be in the other direction
F_2	T_2	Y	Energy balance: The flow rate of cold water into the second tank (F_2) will affect its temperature (T_2)
F_3	L_1	N	The steam flows only through the heating coils and does not mix with the tank contents. Therefore it is not possible for the flow rate in the heating coils (F_3) to affect the level in the tank (L_1)
F_3	T_2	Y	Energy balance: The flow rate of steam into the first tank's heating coils (F_3) will affect the first tank's temperature and subsequently affect the second tank's temperature (T_2)
F_3	F_2	N	The steam flows only through the heating coils and does not mix with the tank contents. Therefore the flow rate of steam in the heating coils (F_3) cannot affect the flow rate of cold water into the second tank (F_2)
F_4	L_1	N	It is not possible for the flow rate in the heating coils to affect the level in the first tank (L_1)
T_1	F_3	Y	Control: T_1 is controlled by manipulating F_3
T_1	F_4	Y	Control/ Energy balance: T_1 will affect T_2 which is controlled by manipulating F_4

A major discrepancy in the LC graph is that L_2 is not connected to any other node. Also only two of the CV-MV pairs showed direct connections; F_1 to L_1 and T_1 to F_3. However, it still detected indirect effects of the control, for example, the connection from F_1 to F_4 exists because F_1 would affect T_2, causing this controller to vary F_4. Overall the LC connectivity graph does capture most of the mass and energy balance and control loop connections that it should.

5.3.2. Partial cross-correlation topology extraction

The number of lags, k, chosen for PC was the same as for LC, for the same reason. In order to generate the connectivity graph using partial cross-correlation (PC) the significance threshold first had to be determined using the method described in Chapter 4, by substituting the number of samples (N=343) into the equation derived for the threshold as a function of sample number:

$$\rho_{max,th}^{PC}(N) = 1.647N^{-0.428} + 3.864N^{-0.772} \quad \textbf{Equation 5-5}$$

$$\rho_{max,th}^{PC}(343) = 0.221 \quad \textbf{Equation 5-6}$$

As with the LC it was observed that using this threshold of 0.221 resulted in a graph with a large number of spurious connections. The threshold was therefore doubled to give a more accurate connectivity graph. Again this indicates that the selected method for threshold selection is not robust enough for all applications. Using the new threshold of 0.441 the PC connectivity graph shown in Figure 5-7 was generated.

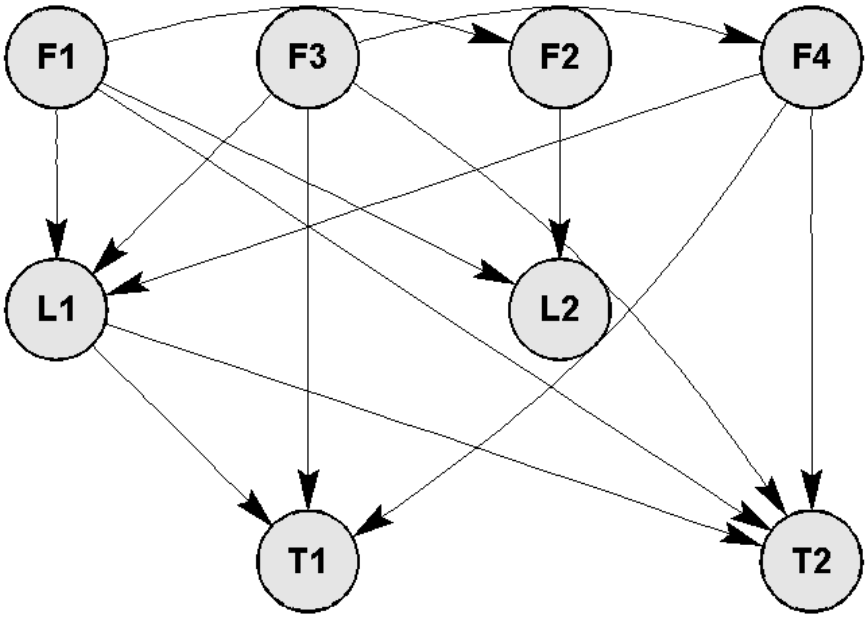

Figure 5-7: Partial cross-correlation connectivity graph from two-tank case study training data

Table 5-4 contains a systematic validation of each connection observed in this connectivity graph; the first two columns indicate the source and sink nodes of the edge being considered, the third column indicates whether the connection is valid (Y) or spurious (N), and the fourth column supplies the reason why it is considered valid (for example whether it makes sense from a mass or energy balance perspective or a control perspective) or spurious.

Table 5-4: Validation of connections in the partial cross-correlation graph. Y indicates a valid connection, N indicates a spurious connection

Source Node	Sink Node	Y/N	Reason
F_1	L_2	Y	Mass Balance: The flow rate into the first tank (F_1) will affect the level of the first tank, causing the outflow of the first tank to change, which then flows into the second tank and changes its level (L_2)
F_1	F_2	Y	Mass Balance/ Control: The flow rate into the first tank (F_1) will affect the levels of both tanks, thereby causing the controller to vary F_2 to control the level of the second tank
F_1	L_1	Y	Control: L_1 is controlled by manipulating F_1
F_1	T_2	Y	Energy balance: The flow rate of cold water into the first tank (F_1) will affect the temperature in the first tank and subsequently the temperature in the second tank (T_2)
F_2	L_2	Y	Control: L_2 is controlled by manipulating F2
F_3	L_1	N	The steam flows only through the heating coils and does not mix with the tank contents. Therefore it is not possible for the flow rate in the heating coils to affect the level in the tank
F_3	T_1	Y	Control: the temperature in the 1st tank is controlled by manipulating F3
F_3	T_2	Y	Energy balance/control: F3 will affect T1 which in turn affects T2
F_3	F_4	Y	Energy balance/Control: F3 will affect T1, which in turn affects T2 which is controlled by varying F4
F_4	T_2	Y	Control: T2 is controlled by manipulating F4
F_4	L_1	N	It is not possible for the flow rate in the heating coils of the second tank to affect the level in the first tank
F_4	T_1	N	The flow rate of steam into the second tank (F_4) cannot change the temperature of the upstream tank (T_1)
L_1	T_1	Y	Energy balance: The temperature in the tank (T_1) is dependent on the amount of liquid in the tank (L_1)
L_1	T_2	Y	Energy balance: The level of the first tank (L_1) determines the flow rate of water at a specific temperature from the first to the second tank, which will affect the second tank's temperature (T_2)

The PC graph was able to detect direct connections between all the CV-MV pairs, which indicates accurate topology capture. The LC graph was only able to detect two out of the four control loops, so in that sense the PC graph is more accurate. In the case of the controller for the second tank's temperature the LC method failed to detect the direct connection between T_2 and F_4, but still detected an indirect connection from F_1 to T_4 that would have T_2 as an intermediate variable. This indicates that PC was effective at eliminating the effects of intermediate variables for that controller connectivity.

The PC graph resulted in a smaller proportion the total connections being spurious, in comparison with the LC graph. Overall the PC graph showed good performance in its ability to capture the topology of this process.

5.3.3. Transfer entropy topology extraction

In order to generate the connectivity graph using transfer entropy (TE) the significance threshold first had to be determined using the method described in Chapter 4, by substituting the number of samples (N=343) into the equation derived for the threshold as a function of sample number:

$$\mathrm{t}_{\mathbf{x}\to\mathbf{y},\mathrm{th}}(N) = 0.0018N^{0.465} + 0.0054N^{0.412} \qquad \textbf{Equation 5-7}$$

$$\mathrm{t}_{\mathbf{x}\to\mathbf{y},\mathrm{th}}(343) = 0.087 \qquad \textbf{Equation 5-8}$$

Using this threshold of 0.087, the connectivity graph shown in Figure 5-8 was generated using transfer entropy. In contrast to LC and PC, the threshold obtained from this method did not result in a connectivity graph with too many connections, and therefore did not need to be changed. This indicates that for this case study the threshold selection method was accurate.

Table 5-5 contains a systematic validation of each connection observed in this connectivity graph; the first two columns indicate the source and sink nodes of the edge being considered, the third column indicates whether the connection is valid (Y) or spurious (N), and the fourth column supplies the reason why it is considered valid (for example whether it makes sense from a mass or energy balance perspective or a control perspective) or spurious.

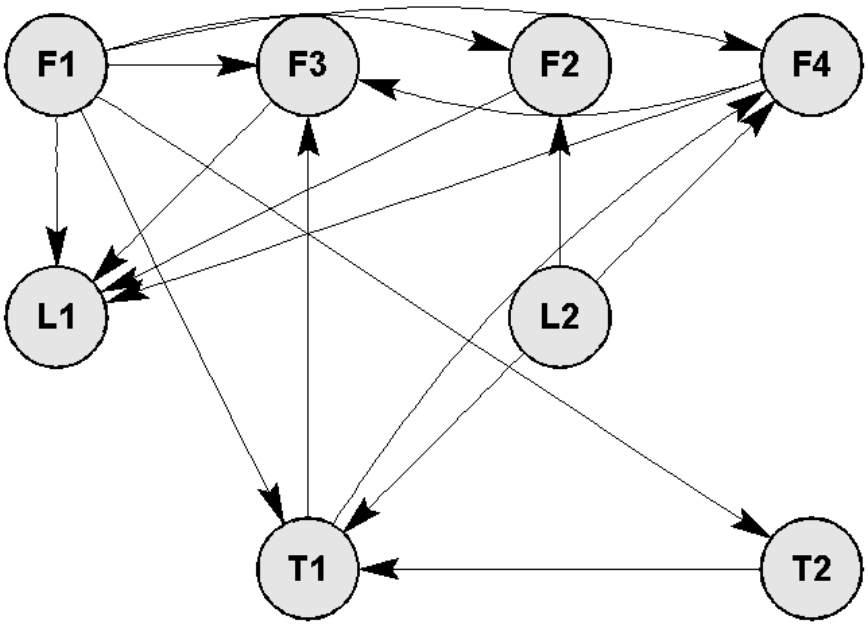

Figure 5-8: Transfer entropy connectivity graph for training data from two-tank case study

Table 5-5: Validation of connections in the transfer entropy graph. Y indicates a valid connection, N indicates a spurious connection

Source	Sink	Y/N	Reason
F_1	L_1	Y	Control: L_1 is controlled by manipulating F_1
F_1	F_2	Y	Mass Balance/ Control: The flow rate into the first tank will affect the levels of both tanks, thereby causing the second tank's level controller to vary F_2
F_1	F_4	Y	Energy balance/control: The flow rate of cold water into the first tank will affect the temperature of the second tank, which will then cause the second tank's temperature controller to vary F_4
F_1	F_3	Y	Energy balance/control: The flow rate of cold water into the tank will affect its temperature, which will cause the temperature controller to vary F_3
F_1	T_1	Y	Energy balance: The flow rate of cold water into the tank will affect its temperature
F_1	T_2	Y	Energy balance: The flow rate of cold water into the first tank will affect the temperature in the first tank and subsequently the temperature in the second tank
F_2	L_1	N	The flow rate into the second tank cannot affect the level of the upstream tank
F_3	L_1	N	The steam flows only through the heating coils and does not mix with the tank contents. Therefore the flow rate in the heating coils cannot affect the level of the tank
F_4	F_3	N	The flow rate of the heating coils in the second tank cannot affect the temperature in the first tank, so it cannot affect F3 either
F_4	L_1	N	The flow rate in the heating coils in the second tank cannot affect the upstream tank's level
L_2	F_2	Y	Control: L_2 is controlled by manipulating F_2
L_2	F_4	Y	Energy balance/control: The temperature of the tank is affected by its level, causing the controller to vary F_4
L_2	T_1	N	The level in the second tank cannot affect the temperature in the first tank
T_1	F_3	Y	Control: T_1 is controlled by manipulating F_3
T_1	F_4	Y	Energy balance/control: The temperature of the first tank affects the temperature of the second, which causes the controller to change F4
T_2	T_1	N	The connection should be in the other direction; the temperature of the second tank cannot affect that of the first tank

The TE graph was able to identify connections between all but one of the CV-MV pairs. That is, it was able to detect connections between F_1 and L_1, F_3 and T_1, F_2 and L_2, but not F_4 and T_2. Compared to LC and PC, the TE graph gave the largest proportion of spurious connections. It appears that many of the connections were in the wrong direction, which may indicate that the method detects causality, but fails to identify the direction of the causality.

5.4.Blocking of Two-Tank Data Using Topology

For this small system it was found that blocking using the proposed method was not possible since none of the graphs had strongly connected components. The connectivity graphs were too small and the connections too sparse for there to be strongly connected components. Also, when attempting to discern the weakly connected components it was found that the whole graph was one weakly connected component. Considering the connectivity graphs, the absence of loops in the connectivity graph meant that no two variables were mutually reachable without violating edge directions. Considering the process itself, this absence of loops is because the variables affect each other in an almost hierarchical manner: F_1 affects all downstream variables, and there is no recycle stream to create a loop that makes these variables mutually reachable.

5.5. Feature Extraction Applied for Fault Detection of Two-Tank System

In this section the results of the feature extraction using PCA and KPCA as well as all the monitoring chart variations are presented for each fault. Since, in this case study, none of the connectivity graphs gave connected components the process was not divisible into multiple blocks according to the proposed method. Therefore the fault detection results presented are for all the variables combined.

The results are presented in terms of the area under the ROC curves (AUCs) and detection delays (DDs). Recall that an AUC close to 1 indicates a fault detection method with a good ability to distinguish between NOC and fault conditions. A low DD indicates rapid detection ability.

5.5.1. Training of feature extraction methods

The details of the feature extraction models developed on the training data are given in this section.

Number of retained features for principal components analysis

Retaining 3 principal components accounted for 90% of the explained variance.

Kernel width selection and retained features for kernel principal components analysis

Cross-validation performed on the training data indicated a decreasing mean squared prediction error for increasing kernel width. This indicates that the data displays mostly linear behaviour. A kernel width of 50 was therefore chosen since at this kernel width the mean squared prediction error had levelled off.

Retaining 3 principal components accounted for 90% of the explained variance.

5.5.2. Detection of Step $T_{1,in}$ Fault

For the first fault the results of the PCA and KPCA detection are shown in Figure 5-9 and Figure 5-10 respectively. An interpretation of these results is presented in this section.

The first thing to note is that the AUCs increased and the DDs decreased with increasing fault size for both PCA and KPCA. This is to be expected since larger disturbances will cause greater deviation from NOC behaviour.

Comparing the PCA results in Figure 5-9 with the KPCA results in Figure 5-10 reveals that the PCA method gave higher AUCs, especially at the smaller fault sizes. However, the DDs were much lower for KPCA. The low DDs are irrelevant when the AUC is less than 0.5, since this indicates that overall the method is more likely to classify fault data as normal and normal data as faulty. The low DDs in this case simply mean that at some point three consecutive samples rose above the threshold.

For PCA the CUSUM T_A^2 and SPE both gave high AUCs, but it is clear that this comes at the sacrifice of detection speed. The higher DDs result from the fact that CUSUM adds up the deviations from the NOC mean of the statistic under consideration (SPE or T_A^2). When the fault occurs the statistic begins to deviate from this mean, but the effect on the cumulative sum is at first small compared to the sum of all past values, then the effect becomes larger and larger. Therefore the CUSUM takes longer to exceed the threshold than the Shewhart would.

The results shown in Figure 5-9 and Figure 5-10 indicate that for this fault that EWMA gives the best detection, for both PCA and KPCA, since it results high AUCs but with much lower DDs than CUSUM. For the smallest fault size, DDs around 110 minutes are observed for the CUSUM, while DDs around 20 minutes are observed for the EWMA. In fact, the DDs are comparable to the Shewhart versions. It may be expected that the EWMA would also come at a sacrifice of detection speed, since it calculates an average of past values and would cause the effect of the sample at the start of fault conditions to be lower. However, since the parameter chose for the weighting, r, was low (0.1), the EWMA chart gave a higher weight to more recent values.

For both PCA and KPCA, the CUSUM T_A^2 and SPE gave the highest AUCs at lower fault sizes, while at the larger fault sizes the EWMA T_A^2 and SPE overtook these. This indicates that the ability of the CUSUM chart to detect slight shifts in the process is better than that of the EWMA chart. In fact the EWMA curves for both figures display an interesting trend with increasing fault size: at smaller fault sizes the performance is poor, with very low AUCs, but as soon as it crosses a certain fault size threshold it experiences a sudden improvement in performance. A possible reason for this is that the moving average causes the effects of small faults to be obscured by averaging the fault samples out with NOC data. However, once the fault size increases, its weight in the moving average is larger and it exerts a stronger influence than the NOC samples and it is then large enough to be detected.

The T_A^2 and the SPE resulted in very similar performance for this fault. In fact, the performance was almost identical. The T_A^2 charts gave slightly higher AUCs, as seen in Figure 5-9 and Figure 5-10. The

effect of this fault is that the temperatures of the first tank would decrease, causing initially a deviation of T_1 from its set-point, followed by the controller manipulating F_3 to correct for this. F_3 would then reach a new steady state value. The same effect would be observed in the second tank with T_2 and F_4. The SPE indicates an increase in the residual distance of the projected test data, the feature extraction models trained on NOC data would fail to predict the correct value for F_3 and F_4 since they achieved a new steady state, also they would fail to predict the behaviour of the temperatures. The T_A^2 statistic indicates wither a change in the relationship between variables or a deviation of variables magnitudes from NOC to fault data. So the deviations of F_3 and F_4 from their original values would cause the T_A^2 to change in much the same way as the SPE did.

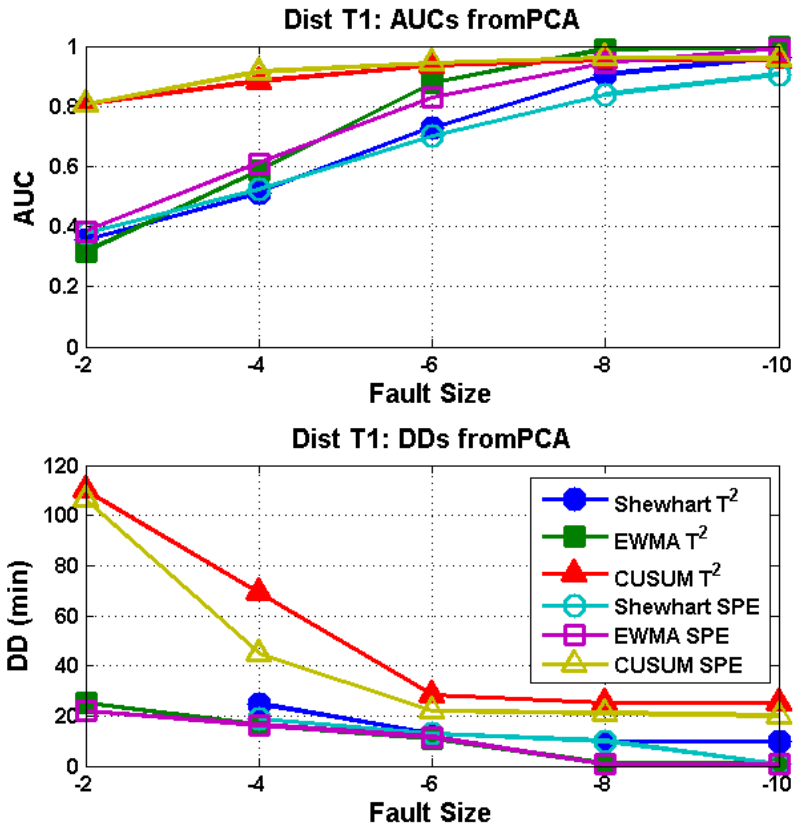

Figure 5-9: AUCs and DDs for PCA for Step $T_{1,in}$ at varying disturbance sizes from -2°C to -10°C

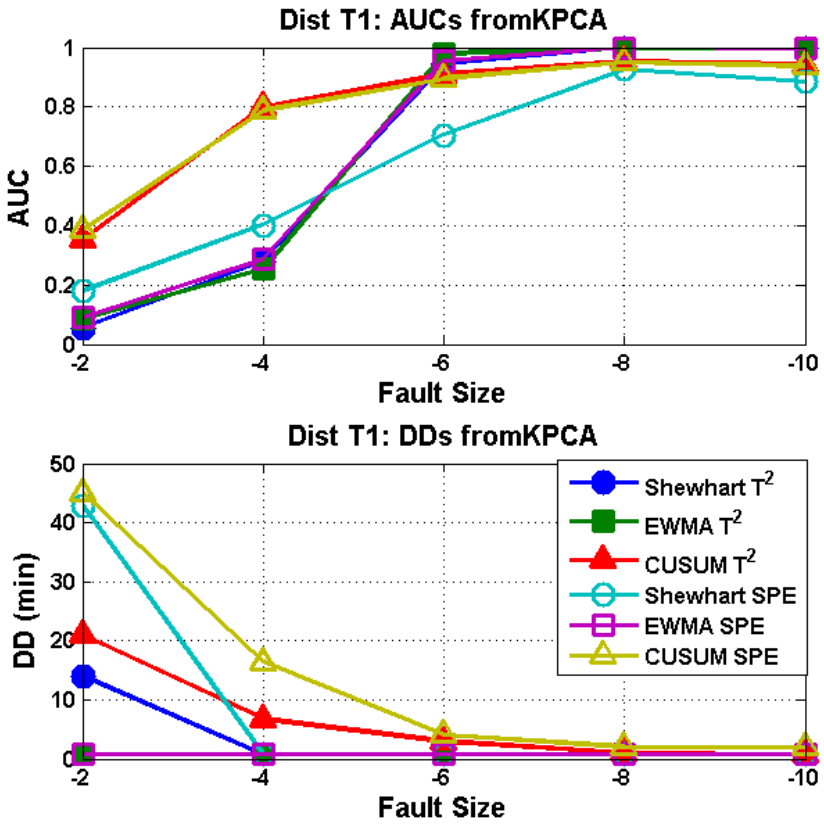

Figure 5-10: AUCs and DDs for KPCA for Step $T_{1,in}$ at varying disturbance sizes from -2°C to -10°C

5.5.3. Detection of Ramp $T_{1,in}$ Fault

For the second fault the results of the PCA and KPCA detection are shown in Figure 5-11 and Figure 5-12 respectively. An interpretation of these results is presented in this section.

Comparing the detection results, shown in Figure 5-9 Figure 5-10, for the Step $T_{1,in}$ to those for this fault, it can be observed that the ramp fault is easier to detect than the step fault, since the AUCs were much higher. The reason for this is that the step fault is a sudden disturbance, so the system immediately begins to apply control to correct for the effects of the fault and the system returns to its new steady state quickly. With the ramp fault, however, the change is gradual, occurring over a longer period of time. Therefore the effect of the fault on the system becomes larger over time until the ramp change levels off. This is supported by the fact that T_1 shows a very large contribution to the PCA's SPE in the contribution plot presented later in Figure 5-21 in section 5.6.2.

Comparing Figure 5-11 with Figure 5-12 reveals that PCA and KPCA gave very similar results in terms of the AUCs, with PCA giving slightly higher AUCs however once again KPCA clearly outperforms PCA in terms of DDs.

Once again the T_A^2 and SPE statistics gave very similar results. The effects of this fault were similar to that of the step disturbance in $T_{1,in}$. The fault caused the temperatures of the first tank to decrease, causing an initial deviation of T_1 from its set-point, followed by the controller manipulating F_3 to

correct for this. F_3 would then reach a new steady state value. The same effect would be observed in the second tank with T_2 and F_4. The SPE indicates an increase in the residual distance of the projected test data. The feature extraction models trained on NOC data would fail to predict the correct value for F_3 and F_4 since they achieved a new steady state, also they would fail to predict the behaviour of the temperatures. The T_A^2 statistic indicates whether a change in the relationship between variables or a deviation of variables magnitudes from NOC to fault data occurred. So the deviations of F_3 and F_4, observed in Figure 5-3, from their original values would cause the T_A^2 to change in much the same way as the SPE did.

Both CUSUM and EWMA charts displayed improved AUCs in Figure 5-11 and Figure 5-12. In this case the EWMA performed better than the CUSUM and Shewhart charts, with higher AUCs (with the exception of that for the smallest fault size) and lower DDs than either of them. The reason the EWMA performed so well for the ramp change is that this fault results in a general increasing trend. The moving average would become large quite quickly. While the CUSUM would also add up the effects quickly, it would still show the influence of the NOC samples for some time after the fault occurred, whereas the EWMA gives less weight to these past values, allowing it to increase faster.

The better performance displayed in Figure 5-11 and Figure 5-12 by the EWMA compared to the CUSUM may also be because the EWMA gave fewer false alarms. With the CUSUM chart, when the NOC statistics deviate slightly from the in-control mean, the deviation is added up and will tend to stay away from its NOC mean for a long time. However, with EWMA, the deviation of past samples has less of an influence over the current EWMA value since past values are given less weight, therefore a deviation in the EWMA would not persist for as long and less false alarms would be signalled.

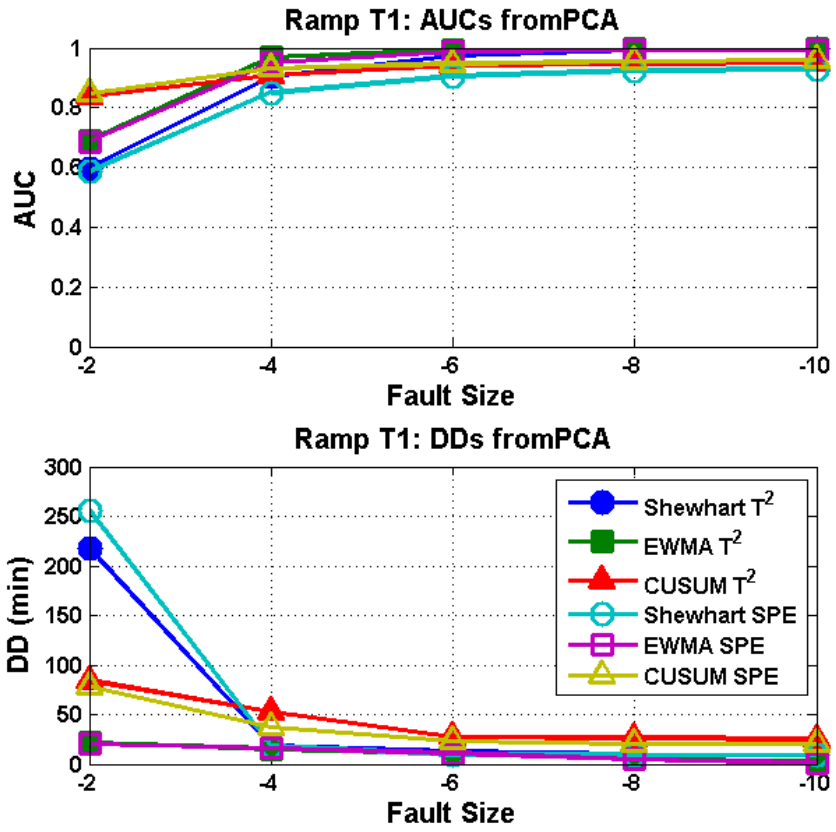

Figure 5-11 AUCs and DDs for PCA for Ramp $T_{1,in}$ at varying final ramp change sizes from -2°C to -10°C

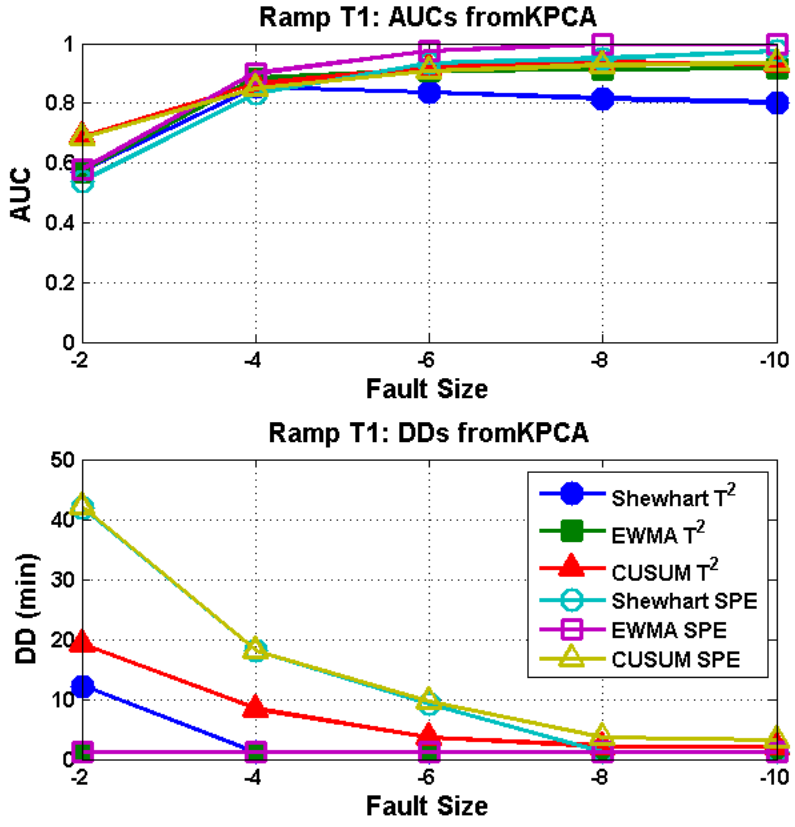

Figure 5-12: AUCs and DDs for KPCA for Ramp $T_{1,in}$ at varying final ramp change sizes from -2°C to -10°C

5.5.4. Detection of Step $T_{2,in}$ Fault

For the third fault the results of the PCA and KPCA detection are shown in Figure 5-13 and Figure 5-14 respectively. An interpretation of these results is presented in this section.

When comparing Figure 5-13 and Figure 5-14 with Figures 5-9 to 5-12, it may be noted that the ability of PCA and KPCA to detect the step $T_{2,in}$ fault was worse than for step $T_{1,in}$ and ramp $T_{1,in}$ faults. The reason for this is that a disturbance in $T_{1,in}$ affects the temperature in the first tank, causing the controller to vary F_3 to compensate, and then this deviation in temperature propagates downstream into the second tank where it also causes the controller to change F_4. For the disturbance in $T_{2,in}$, however, only the second tank is affected, so the fault affects fewer variables and the deviation from NOC to fault conditions is not as pronounced.

Considering Figure 5-13, for PCA the T_A^2 statistic performed consistently better than the SPE with generally higher AUCs and lower DDs for all monitoring chart methods. Interestingly, the opposite was true for the KPCA: in Figure 5-14 the SPE gave higher AUCs, and the difference in DD was not so pronounced.

Comparing Figure 5-13 with Figure 5-14 it appears that for the smaller fault sizes KPCA performed worse, giving very low AUCs (albeit with very low DDs). This is probably because it gave a high FAR. Using the CUSUM and EWMA modification improved this problem significantly. At larger fault sizes however, the KPCA displayed better performance than PCA, with higher AUCs and much lower DDs. Overall it can be concluded that KPCA outperformed PCA for this fault, but neither of the methods was able detect the fault at small fault sizes, since the controller was able to attenuate this disturbance rapidly.

The superior detection performance of the EWMA over the other monitoring charts can once again be observed in Figure 5-13 and Figure 5-14; EWMA gave high AUCs, with no noticeable sacrifice to the detection speed.

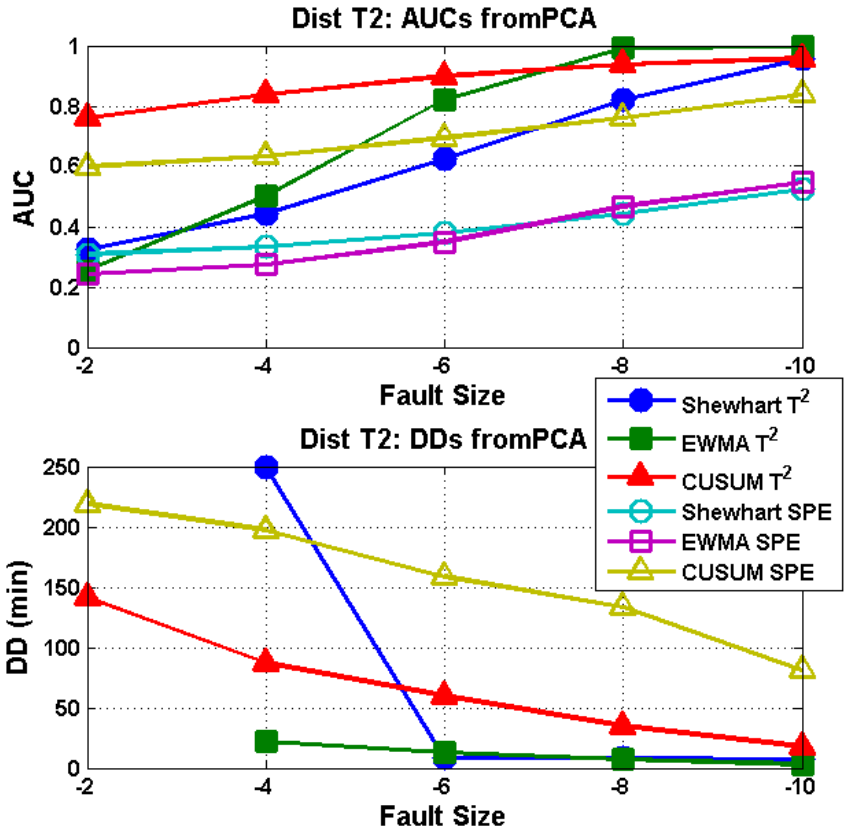

Figure 5-13: AUCs and DDs for PCA for Step $T_{,in}$ varying disturbance sizes from -2°C to -10°C

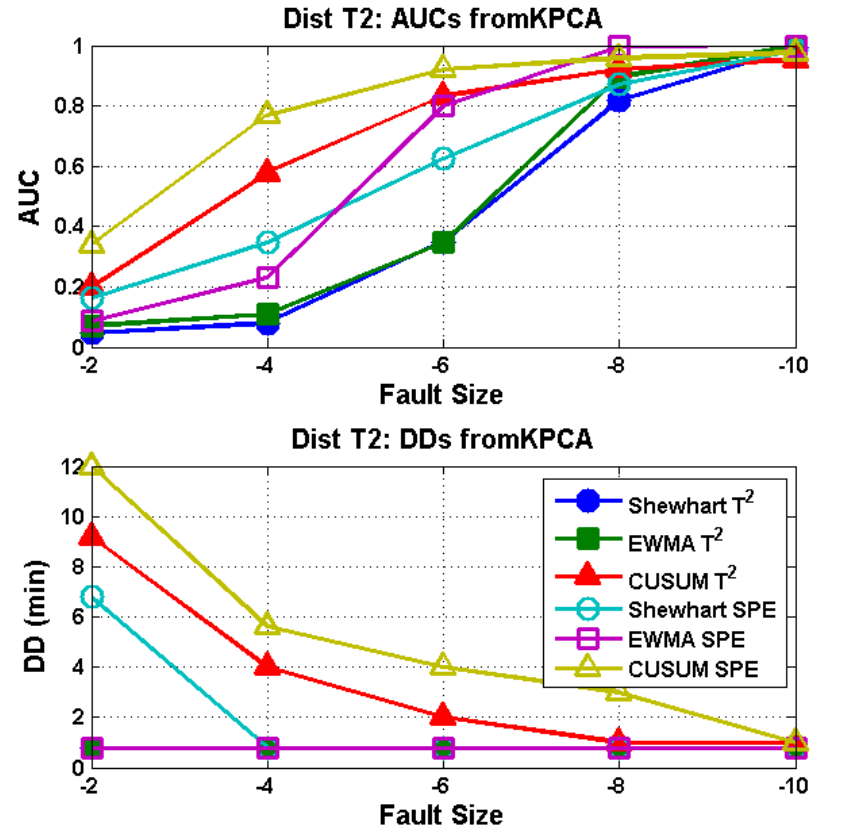

Figure 5-14: AUCs and DDs for KPCA for Step $T_{2,in}$ varying disturbance sizes from -2°C to -10°C

5.5.5. Detection of Fouling Fault

For the fourth fault the results of the PCA and KPCA detection are shown in Figure 5-15 and Figure 5-16 respectively. An interpretation of these results is presented in this section.

Considering Figure 5-15 and Figure 5-16, it may be observed that PCA and KPCA failed to detect this fault accurately. Only the CUSUM T_A^2 and CUSUM SPE for the PCA method, in Figure 5-15 , displayed AUCs larger than 0.5, albeit with high DDs. None of the KPCA monitoring charts were able to detect this fault, showing AUCs below 0.5 in Figure 5-16.

This fault resulted in small shifts in the process behaviour. The effect on the temperatures of the tanks was small, as seen in Figure 5-5. The controller simply increased the flow rate of the steam to account for the lower rate of heat exchange to the tanks' contents. The CUSUM chart's ability to detect slight shifts in the process is therefore evident from these results; the CUSUM would become large since the deviation from the in-control mean would be consistent and would be added up over time. The high DDs show that it takes a long time for this shift to add up to a significantly large CUSUM, however. Increasing fault size did not make much of an impact on the detection ability. This indicates that this fault does not have that much of an effect on the system.

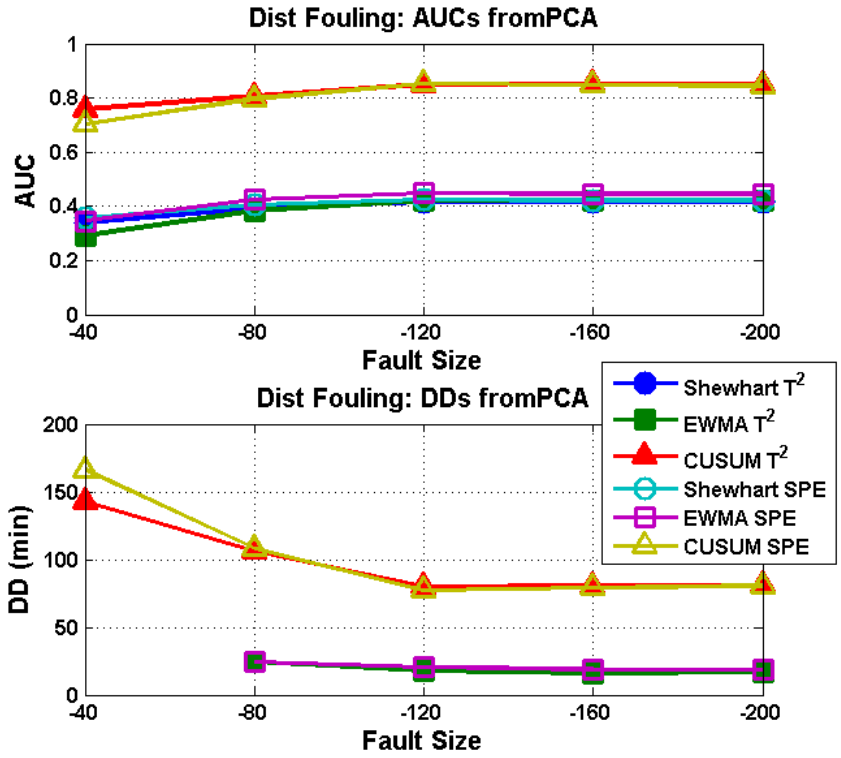

Figure 5-15: AUCs and DDs for PCA for Fouling varying ramp change of aHeat from -40 to -200[cal/min.°C/min]

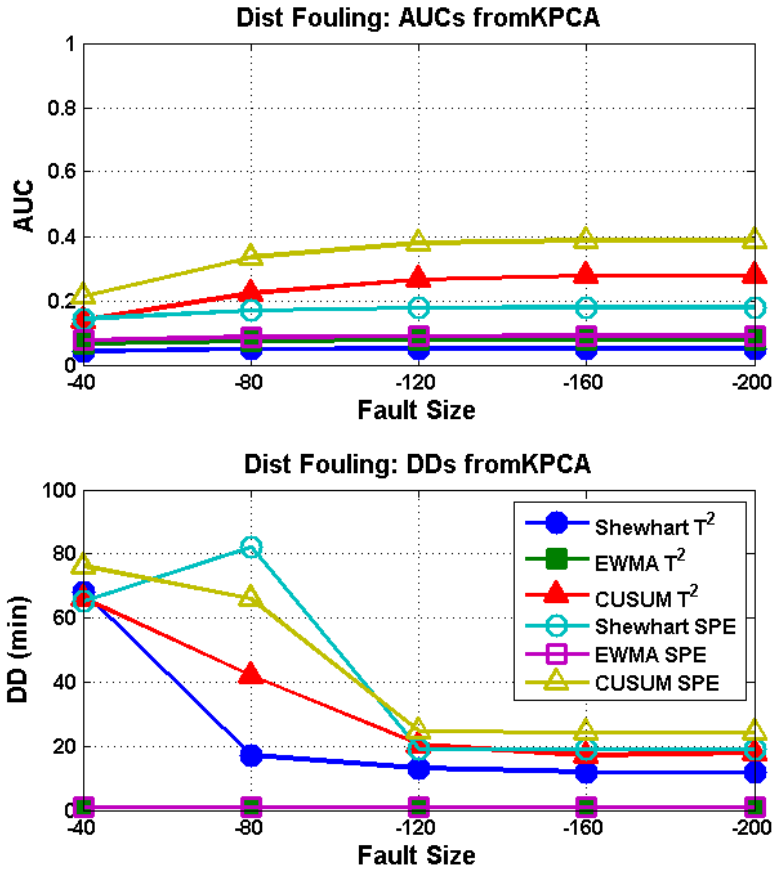

Figure 5-16: AUCs and DDs for KPCA for Fouling varying ramp change of aHeat from -40 to -200[cal/min.°C/min]

5.6. Fault Identification in Two-Tank System

In this section the fault identification results of both FID methods applied to each TEM graph are presented for each fault. First a table is presented summarising the fault identification performance of each method. Then the TEM that gave the best results is used to demonstrate the best FID results obtained, while the rest of the results are presented and discussed in Appendix B-.

The fault identification performance is defined in terms of: the location of the fault, i.e. whether or not the symptom and root nodes identified gave a good indication of the origin of the fault; the type of fault, i.e. whether it is a step or ramp change; and the size of the fault, i.e. whether the method used was able to detect that larger actual fault sizes showed larger changes in root node variables.

For the fault identification method proposed only the measured variables are considered, since the TEMs were data-based. This introduces a limitation in the ability to isolate the root cause since not all root causes of a fault are associated with a single specific measured variable. The objective of the FIMs presented is therefore to point to possible root nodes that are indications of the fault occurring.

5.6.1. Fault identification of step $T_{1,in}$ fault

Table 5-6 displays the summary of the results for the different fault identification methods for one of the fault sizes; a step disturbance of -8°C. A "yes" indicates that the method was able to identify nodes that were representative of the fault, a "no" indicates that it did not, while a "maybe" indicates that it identified suitable nodes, but also some spurious ones. The full results are presented in Appendix B-.

For this fault when F_3, F_4, $T_1$and T_2 were identified as possible root nodes, it was considered to be a successful root cause analysis since this would clearly indicate that the fault was associated with the temperature in the first tank.

Table 5-6 shows that the contribution plot gave suitable symptom nodes that were indicative of the fault conditions. The connectivity change for the LC and PC graphs also gave symptom nodes that were indicative of the fault, while the TE graph's connectivity gave some suitable symptoms, but also some spurious ones.

Table 5-6: Fault identification results for Step $T_{1,in}$ fault for disturbance size of -8°C

TEM	FIM	Symptoms	Roots
LC	**Contributions**	Yes	Maybe
LC	**Connectivity Change**	Yes	Yes
PC	**Contributions**	Yes	Yes
PC	**Connectivity Change**	Yes	Maybe
TE	**Contributions**	Yes	Yes
TE	**Connectivity Change**	Maybe	No

Since it was observed in section 5.3 that PC gave the most accurate connectivity graph, and since Table 5-6 shows that it resulted in accurate identification of this fault using back propagation, the results for PC are presented here.

Identification of symptom nodes using the contribution plot

For the step $T_{1,in}$ disturbance fault, the SPE from the PCA fault detection resulted in the relative contributions shown in Figure 5-17. The plot shows that the contributions of L_1, F_2, T_1 and F_3 in the fault data rose above their contributions in the validation data. Therefore these variables were flagged as possible symptom nodes. The large increase in contribution of L_1 is because the actual behaviour of the system that resulted in temperature changes is different to that expected. Under NOC, when L_1 varied it affected the temperatures of the tanks and the flow rates of the heating steam. Under fault conditions, however, the temperatures changed without the corresponding change in L_1. The same reasoning can be applied to the contribution of F_2. The contributions of these two variables obscure the cause of the fault, since at first glance it appears that they would be more

associated with a change in the flow rate, not temperatures. The large relative contributions of both F_3 and T_1, however, give a good indication that the fault conditions have an effect on the temperature in the first tank.

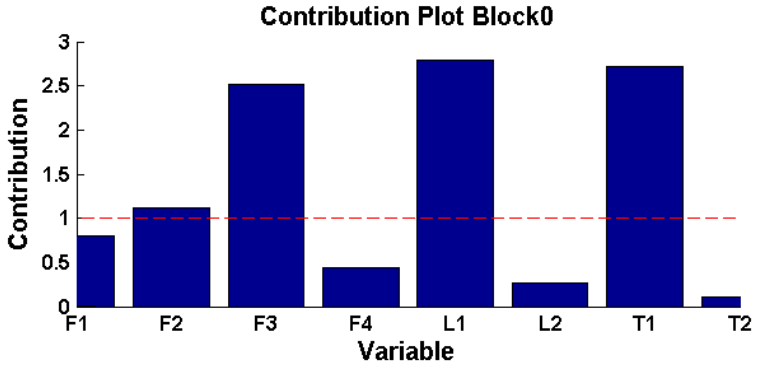

Figure 5-17: Relative contributions of each variable to the PCA SPE for the Step $T_{1,in}$ fault

Fault identification using partial cross-correlation with contributions

Figure 5-18 displays the application of back propagation from the symptom nodes identified from the contribution plots (highlighted in blue) in the PC connectivity graph, resulting in F_3, F_1, and F_4 being identified as possible root nodes (highlighted in red). Since both F_3 and F_4 were identified this is a good indication that a temperature fault in the first tank has occurred. This result allows an operator with fundamental knowledge of the process to focus on the variables associated with the temperature in the first tank (noting that F_3 is upstream of F_4 and therefore closer to the root cause) to identify the root cause of the fault.

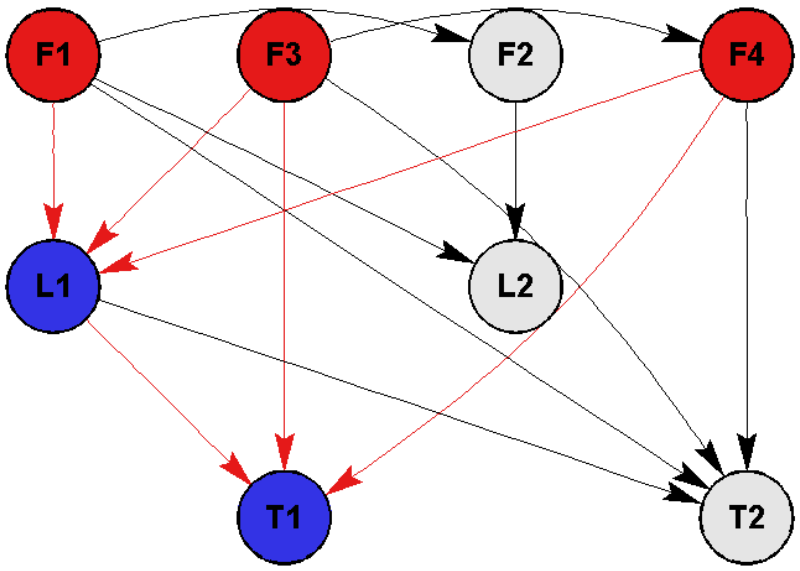

Figure 5-18: Back propagation applied in the PC connectivity for Step $T_{1,in}$ fault using the symptom nodes identified from the contribution plot (in blue), indicating possible root nodes and propagation paths (in red)

Fault identification using partial cross-correlation with connectivity change

Figure 5-19 compares the connectivity obtained using PC on NOC data to that obtained from the fault conditions data. The only edge that became significant after the fault (i.e. which appeared in the fault conditions but was absent in the NOC data) was the edge from T_1 to F_3. This clearly indicates that the causality from T_1 to F_3 has become stronger. This result is consistent with the nature of the fault that has occurred; the temperature disturbance would affect the tank's temperature, causing F_3 to be changed by the controller.

It can also be observed in the figure that F_1 shows less effect on downstream variables once the fault has occurred. This is because under NOC changes in F_1 strongly affect the temperatures of the first and second tanks through mass and energy balances and subsequently affect the flow rates of heating steam in the coils. However, under fault conditions, large changes in the temperatures occur not because of a change in stream 1's flow rate, but because of a change in its temperature. Similarly the connections from F_3 to the temperatures became less significant. Therefore the, connectivity change method automatically identified T_1 (highlighted in blue) as a possible symptom.

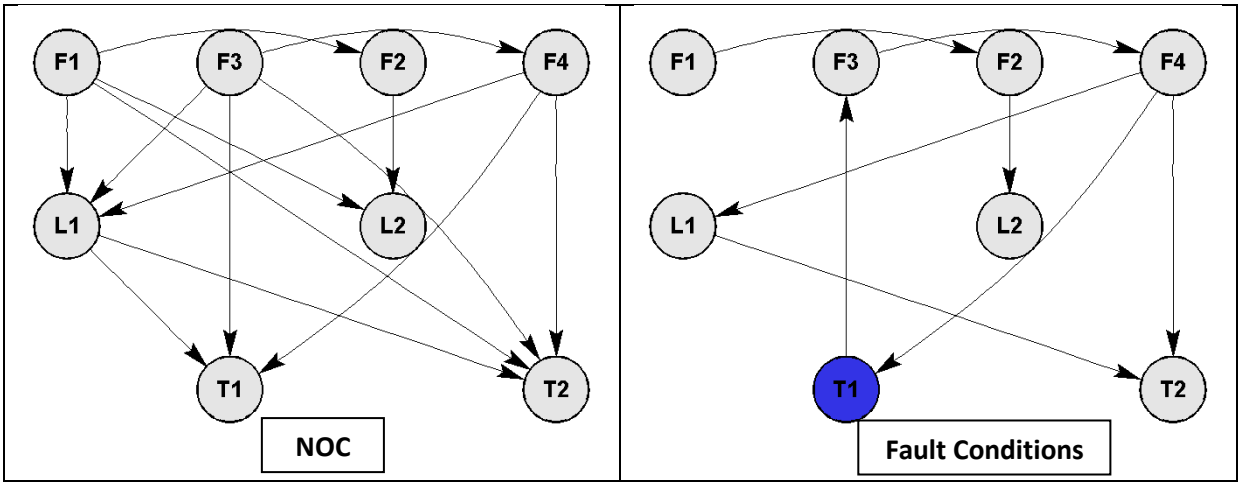

Figure 5-19: Change in connectivity in the PC from NOC (left) to fault conditions (right) for Step $T_{1.in}$ fault

Applying back propagation on the PC NOC connectivity graph from the symptom identified by connectivity change (highlighted in blue) results in F_3, F_4 and L_1 being identified as possible root nodes (highlighted in red). With the exception of L_1 this gives a very good indication that a temperature fault in the first tank has occurred. This allows an expert in the process presented with these results to focus on the first tank's temperature to isolate the root cause of the fault.

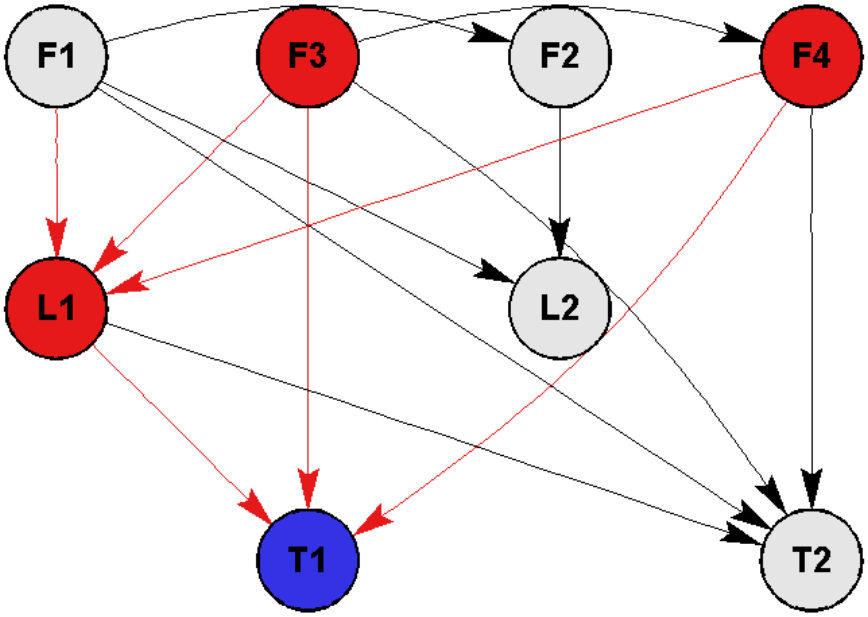

Figure 5-20: Back propagation applied in the PC connectivity for Step $T_{1,in}$ fault using the symptom nodes identified from the connectivity change (in blue), indicating possible root nodes and propagation paths (in red)

5.6.2. Fault identification of ramp $T_{1,in}$ fault

Table 5-7 displays the summary of the results for the different fault identification methods for one of the fault sizes; a final ramp change of -8°C. A "yes" indicates that the method was able to identify nodes that were representative of the fault, a "no" indicates that it did not, while a "maybe" indicates that it identified suitable nodes, but also some spurious ones. The full results are presented in Appendix B-.

For this fault when F_3, F_4, T_1 and T_2 were identified as possible root nodes, it was considered to be a successful root cause analysis since this would clearly indicate that the fault was associated with the temperature in the first tank.

Table 5-7: Fault identification results for Ramp $T_{1,in}$ fault for final ramp change of -8°C

TEM	FIM	Symptoms	Roots
LC	**Contributions**	Yes	Maybe
LC	**Connectivity Change**	Yes	No
PC	**Contributions**	Yes	Maybe
PC	**Connectivity Change**	Yes	Yes
TE	**Contributions**	Yes	No
TE	**Connectivity Change**	Maybe	No

Table 5-7 shows that the LC and PC connectivity change gave suitable symptom nodes, while the TE change did not. Only the back propagation using the PC graph with the symptoms identified from connectivity change gave accurate root cause results.

Again, since it was observed in section 5.3 that PC gave the most accurate connectivity graph and since PC gave the most accurate fault identification results, and therefore PC based fault identification will be discussed in the following subsections.

Identification of symptom nodes using the contribution plot

For the ramp $T_{1,in}$ fault the relative contributions of each variable to the PCA SPE are shown in Figure 5-21. The relative contributions of T_1, F_2, F_3 and F_4 are greater than one, so these variables are highlighted as symptom nodes. The large relative contribution of T_1 gives a very good indication that a temperature fault in the first tank has occurred. It is interesting to note that its contribution to the SPE is higher for the ramp fault than it is for the step fault. This is because the SPE was larger for the ramp fault, as discussed in section 5.5.3. The contributions of F_3 and F_4 also give a good indication of the fault being associated with the temperature of the first tank. The large contribution of F_2 is due to the fact that under NOC changes in F_2 would result in the contribution of F_2 is not consistent with this fault, since the temperature cannot affect the flow rate of cold water into the second tank.

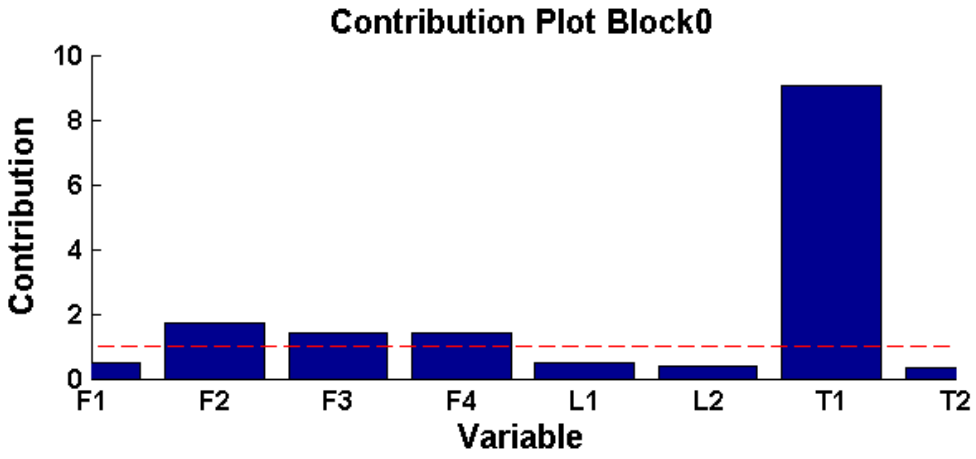

Figure 5-21: Relative contributions of each variable to the PCA SPE for Ramp $T_{1,in}$ fault

Fault identification using partialcross- correlation with contributions

Figure 5-22 displays the results of applying back propagation in the PC graph using the symptom nodes highlighted by the contribution plot. The method resulted in no root nodes being identified. However, upon inspection of the graph it can be observed that if F_2 were not highlighted as a symptom node F3 would have been the furthest common ancestor for F_4 and T_1. Therefore, even though the automated method gave no results, it can be concluded that inspection of the PC graph gave a good indication that the fault was in the temperature of the first tank.

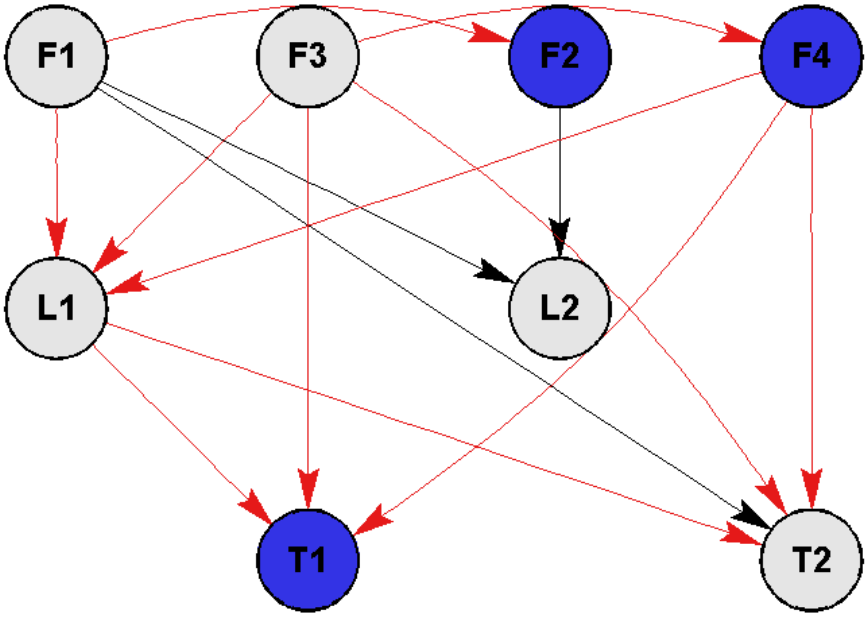

Figure 5-22: Back propagation applied in the PC connectivity for Ramp $T_{1,in}$ fault using the symptom nodes identified from the contribution plot (shown in blue), indicating possible root nodes and propagation paths (shown in red)

Fault identification using partial cross-correlation with connectivity change

Figure 5-23 displays the change in the PC connectivity from NOC to fault conditions. The connectivity change identified T_1 and T_2 as having a significant change in their connectivity. The connection between T_1 and T_2 rose above the significance threshold under the fault conditions because under NOC the temperatures were affected more strongly by changes in the flow rates and levels, while under the fault conditions T_1 was affected strongly by the incoming disturbances, and this had a strong influence on T_2. This gives a good indication that the fault is associated with the temperature of the first tank.

The results of the connectivity change for this fault were very similar to those for the first fault (Figure 5-19). It can again be observed in Figure 5-23 that F_1 shows less effect on downstream variables once the fault has occurred. This is because under NOC, changes in F_1 strongly affect the temperatures of the first and second tanks through mass and energy balances and subsequently affect the flow rates of heating steam in the coils. However, under fault conditions, large changes in the temperatures occur not because of a change in stream 1's flow rate, but because of a change in its temperature. Similarly, the connections from F_3 to the temperatures became less significant.

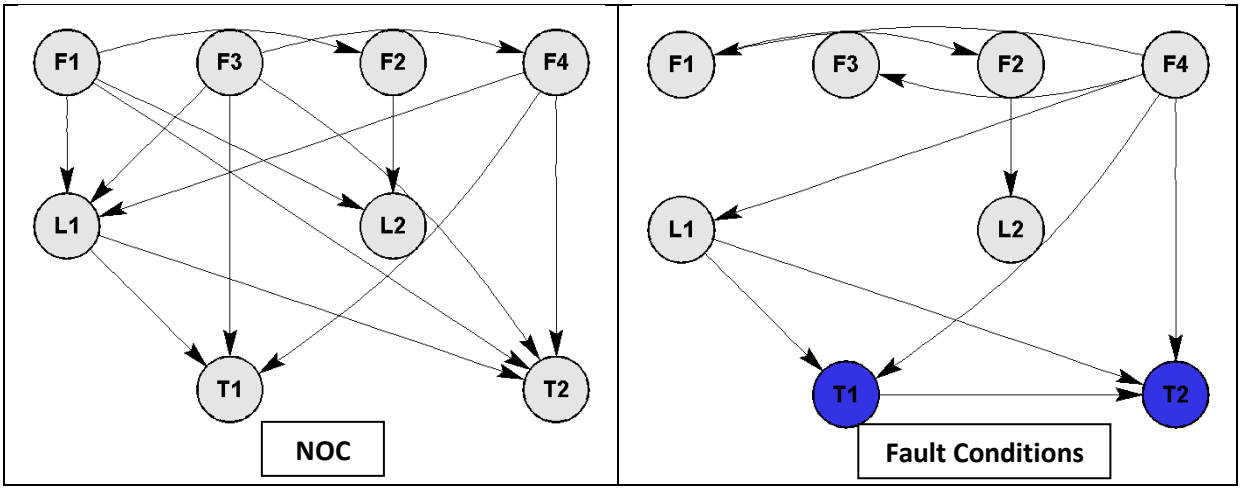

Figure 5-23: Change in connectivity in the PC from NOC (left) to fault conditions (right) for Step $T_{1.in}$ fault

Applying back propagation to the PC graph from the symptoms identified by connectivity change results in L_1, F_4 and F_3 being identified as possible root nodes, as shown in. Apart from the presence of L_1, this gives a good indication that a temperature fault in the first tank occurred, so it can be concluded that root cause analysis using this method was accurate.

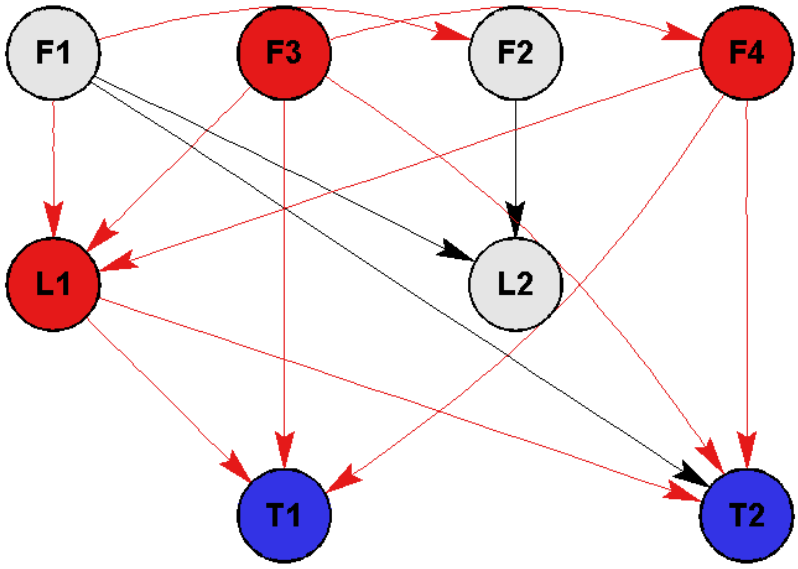

Figure 5-24: Back propagation applied in the PC connectivity for Ramp $T_{1,in}$ fault using the symptom nodes identified from the connectivity change (shown in blue), indicating possible root nodes and propagation paths (shown in red)

5.6.3. Fault identification of step $T_{2,in}$ fault

Table 5-8 displays the summary of the results for the different fault identification methods for one of the fault sizes; a step disturbance of -8°C. A "yes" indicates that the method was able to identify nodes that were representative of the fault, a "no" indicates that it did not, while a "maybe" indicates that it identified suitable nodes, but also some spurious ones. The full results are presented in Appendix B-.

For this fault when F_4 and T_2 were identified as possible root nodes, it was considered to be a successful root cause analysis.

Table 5-8: Fault identification results for Step $T_{2,in}$ fault for disturbance size of -8°C

TEM	FIM	Symptoms	Roots
LC	Contributions	Maybe	No
LC	Connectivity Change	Yes	Maybe
PC	Contributions	Maybe	Yes
PC	Connectivity Change	No	No
TE	Contributions	Maybe	Yes
TE	Connectivity Change	Yes	No

Table 5-8 shows that the contribution plot gave suitable symptom nodes that were indicative of the fault conditions. The connectivity change did not perform as well. Again, since it was observed in section 5.3 that PC gave the most accurate connectivity graph and since PC gave the most accurate fault identification results, and therefore PC based fault identification will be discussed in the following subsections.

Symptom node identification using the contribution plot

For the step $T_{2,in}$ fault the SPE from the PCA fault detection resulted in the relative contributions shown in Figure 5-25. This plot showed large contributions for T_1, F_4 and L_1. The contribution of F_4 makes sense for this fault, since the disturbance in T_2 will cause the controller to vary F_4. The large contribution of T_1 is due to the fact that in the NOC data changes in T_1 would cause changes in T_2, yet the fault resulted in a change in T_2 without a corresponding change in T_1 first. Similarly with L_1; in the NOC data when L_1 changed it caused the temperature in the second tank to change, while in the fault data the change in T_2 occurred without a change in L_1. The reason that T_2 doesn't show a large contribution is that the controller for the second tank's temperature is tightly tuned and is effective at rejecting disturbances.

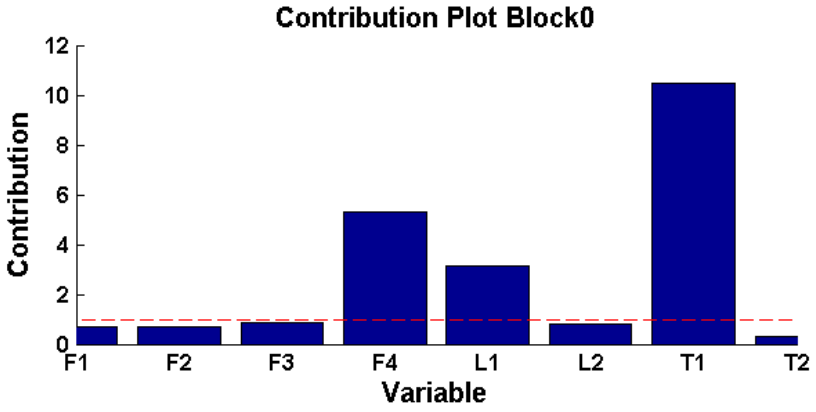

Figure 5-25: Relative contributions of each variable to the SPE for the Step $T_{2,in}$ fault

Fault identification using partial cross-correlation with contributions

Applying back propagation in the PC graph from the symptoms identified by contributions results in F3 and F4 being identified as possible root nodes, as shown in Figure 5-26. Since these both indicate that a temperature fault has occurred, this is a good result for the root cause analysis.

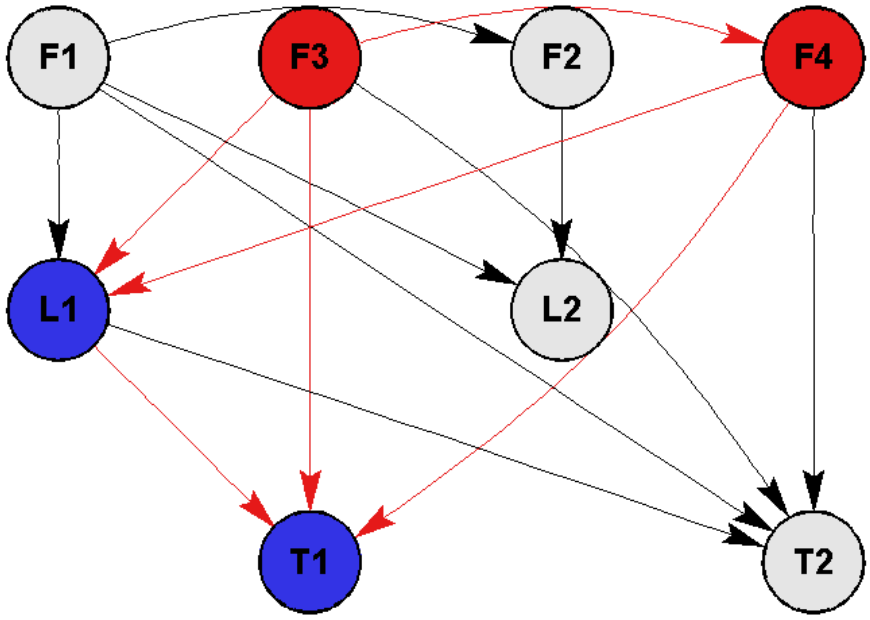

Figure 5-26: Back propagation applied in the PC connectivity for Step $T_{2,in}$ fault using the symptom nodes identified from the contribution plot (shown in blue) , indicating possible root nodes and propagation paths (shown in red)

Fault identification using partial cross-correlation with connectivity change

The change in the PC identified no symptom nodes

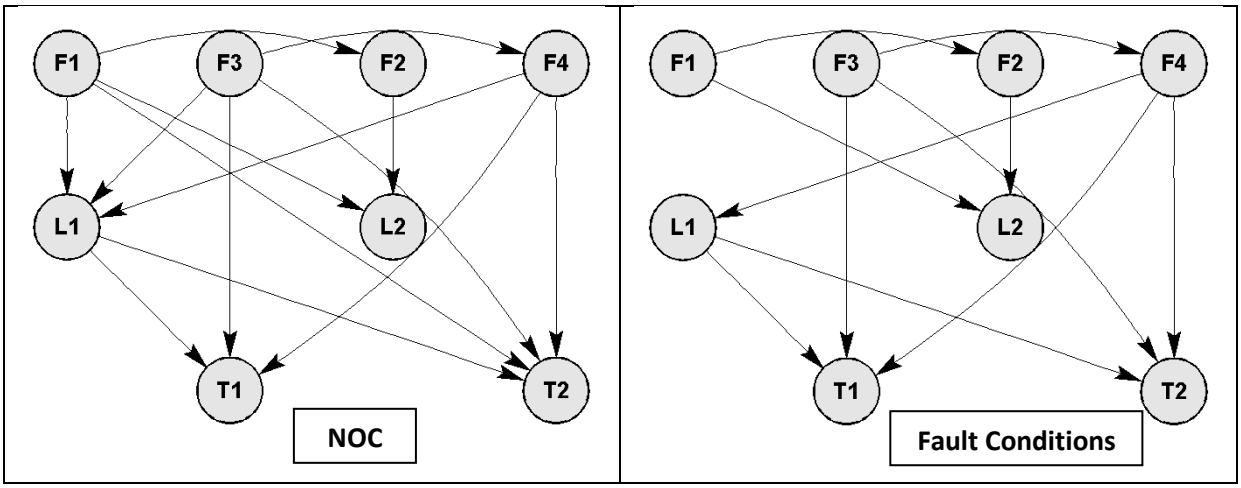

Figure 5-27: Change in connectivity in the PC from NOC (left) to fault conditions (right) for Step $T_{1.in}$ fault

The reason why no symptom nodes were identified is that the only change in connectivity was some of the connections falling below the thresholds, and there were only a couple of them that changed. Therefore, this method gave no extra information for root cause analysis.

5.6.4. Fault identification of fouling fault

For this fault when F_3, F_4, T_1 or T_2 were identified as root nodes it was considered to be a successful root cause analysis. However, since so many variables could be considered as indicators of this fault the results can be misleading.

Table 5-9: Fault identification results for Fouling fault for size -160

TEM	FIM	Symptoms	Roots
LC	**Contributions**	Maybe	Maybe
LC	**Connectivity Change**	Yes	Yes
PC	**Contributions**	Maybe	Yes
PC	**Connectivity Change**	Yes	Maybe
TE	**Contributions**	Maybe	Yes
TE	**Connectivity Change**	Maybe	No

Again, since it was observed in section 5.3 that PC gave the most accurate connectivity graph and since PC gave the most accurate fault identification results, and therefore PC based fault identification will be discussed in the following subsections.

Identifying symptom nodes using the contribution plot

The contributions of the individual variables to the PCA SPE for the fouling fault are shown in Figure 5-28. The relative contributions of F_3 and T_1 were greater than 1, which is consistent with the fouling fault since fouling would influence the temperatures in the tanks (T_1) which would cause the controller to change F_3. The contributions of F_2 and L_1, however, are not consistent with the fault, since the temperatures cannot affect the levels or flow rates of the cold water into the tanks. The fact that T_2 and F_4 are not shown as giving large contributions also doesn't give a good indication of the fouling fault, since these variables should be affected by it. The results of this contribution plot are suspect, however, considering that PCA showed low AUCs for the detection of this fault.

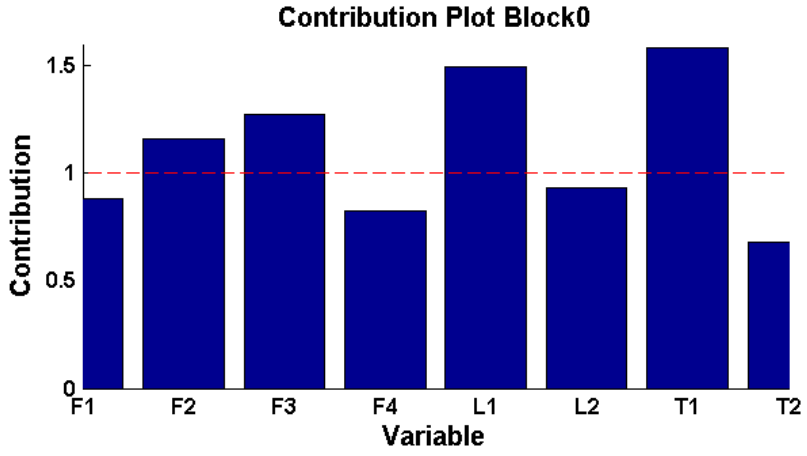

Figure 5-28: Relative contributions of each variable to the SPE for the fouling fault

Fault identification using partial cross-correlation with contributions

Applying back propagation in the PC graph gave F_3, F_1 and F_4 as possible root nodes, as shown in Figure 5-29. This is a very good indication of the fouling fault since both F_3 and F_4 would be affected by it. Especially considering that if L_1 wasn't a symptom node then F_1 wouldn't have been identified as a root node. Therefore, the root cause analysis for this fault using this method may be considered successful.

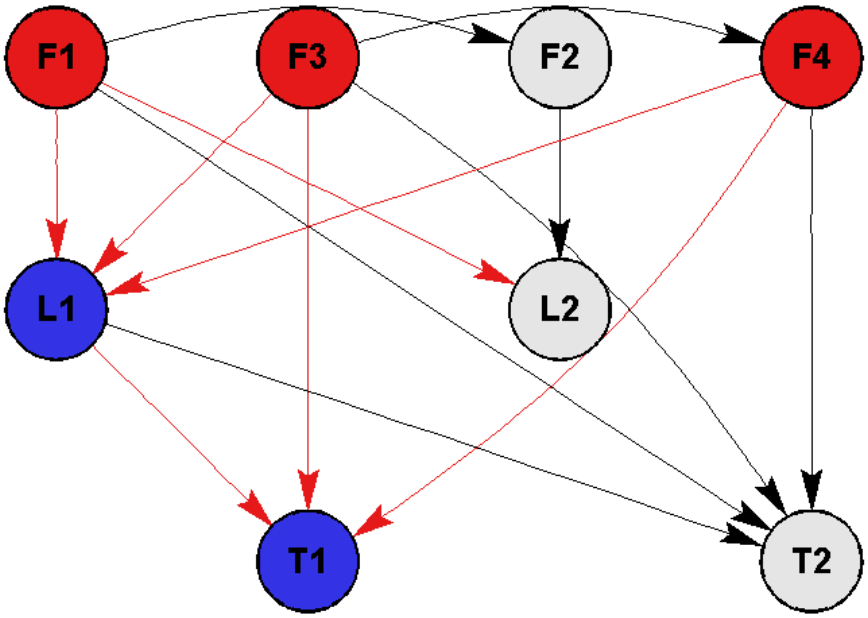

Figure 5-29: Back propagation applied in the PC connectivity for fouling fault using the symptom nodes identified from the contribution plot (shown in blue) , indicating possible root nodes and propagation paths (shown in red)

Fault identification using partial cross-correlation with connectivity change

Figure 5-30 shows the change in connectivity from NOC to fault conditions for PC for the fouling fault. This method identified T_1 as a possible symptom node. This gives a very good indication that a temperature fault has occurred. The only change in connectivity is that the connection from F_1 to T_1 appears, while F_1 to T_2 disappears. The fact that the connectivity graph doesn't change much, compared to Figure 5-23, for example, indicates that this fault had very little effect on this process.

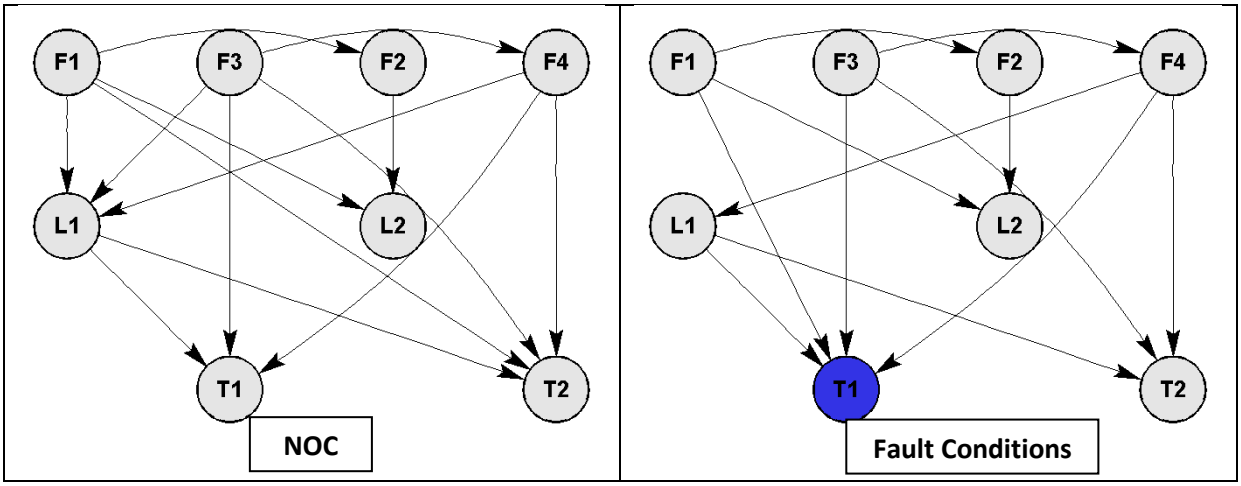

Figure 5-30: Change in connectivity in the PC from NOC (left) to fault conditions (right) for Fouling fault

Applying back propagation in the PC graph from the symptoms identified by connectivity change resulted in F_1, F_3, F_4 and L_1 being identified as possible root nodes, as shown in Figure 5-31. Although F3 and F4 are identified, the presence of F_1 and L_1 confuse the result, so in this case the root cause analysis is not considered successful.

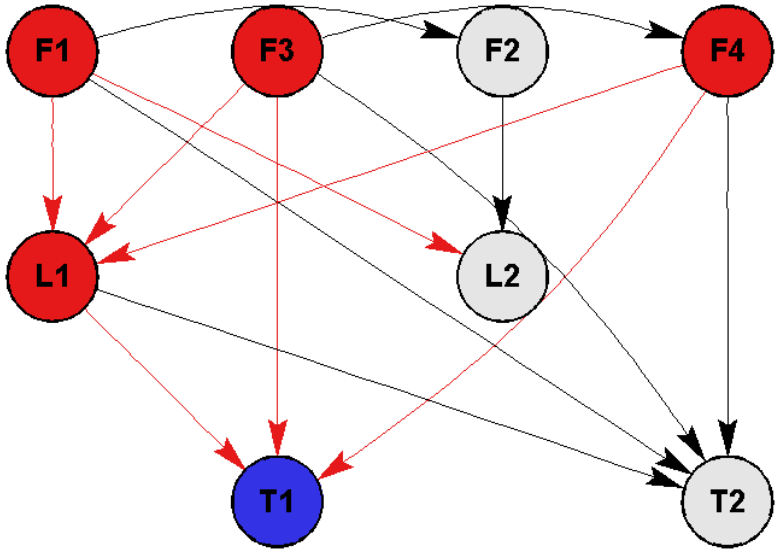

Figure 5-31: Back propagation applied in the PC connectivity for Fouling fault using the symptom nodes identified from the connectivity change (blue), indicating possible root nodes and propagation paths (red)

5.7.Summary of Fault Diagnosis Results in Two-Tank System

This Chapter presented the results of the applications of the various fault diagnosis methods to the Two-tank simulation case study. A summary of these results is presented here. Conclusions drawn from these results are presented in Chapter 8 -

5.7.1. Topology extraction from historical process data

It was observed that of the three TEM, PC gave the most accurate connectivity graph. However, all three graphs showed some spurious connections that may complicate the results of the fault identification methods applied using these connectivity graphs. It was observed that the significance thresholds defined for LC and PC using the method described in chapter 4 resulted in thresholds that were too lax and resulted in a large number of spurious connections. These thresholds had to be increased to extract a useful connectivity graph.

5.7.2. Blocking using topology

It was found that all of the generated connectivity graphs were too small and hierarchical to have any strongly connected components. Therefore blocking according to the strongly connected components was not possible.

5.7.3. Fault detection using feature extraction

Principal components analysis vs. kernel principal components analysis

Of the two feature extraction methods applied for fault detection, KPCA showed the best results overall for the faults considered in this case study; although the AUCs achieved for both methods tended to be similar, the KPCA consistently resulted in lower DDs.

Monitoring charts

The EWMA monitoring chart showed very good detection ability in comparison to the other monitoring charts. EWMA gave larger AUCs than the Shewhart chart, without an increase in the detection delay. And while in some cases it gave slightly lower AUCs than the CUSUM charts, it gave much lower DDs.

5.7.4. Fault identification using topology

Symptom identification using contributions vs. using connectivity change

For fault identification the connectivity change provided suitable symptoms in most cases, with the best results being obtained for the PC graph. The contributions gave better results more consistently than connectivity change, since connectivity change is strongly dependent on the accuracy of the connectivity graph used.

Back propagation using connectivity graphs

In most cases the back propagation resulted in possible root nodes that gave a good indication of the fault conditions. The PC graph gave the best results in general.

Chapter 6 - Case Study: Fault Diagnosis in Second and Third Stage Leaching Simulation

This chapter presents the results of application of the fault diagnosis methods to the second case study.

6.1. Leaching Simulation Case Study Description

For the second case study a dynamic simulation of a pressure leaching process in the base metals refinery of a platinum processing plant was used to generate NOC and fault conditions to test and compare the fault diagnosis methods. The dynamic model for this simulation was developed by Dorfling (2012) and this model was developed into a dynamic simulation by Knoblauch (In Progress).

This simulation is ideal for the testing of the fault diagnosis methods under investigation in this project because of its complexity: it involves a large number of measured variables, 31 variables in total; nine interconnecting process units; ten interacting control loops; as well as recycle loops. The large number of variables and process units may make it ideal to test whether division of the process into multiple blocks would aid detection and/or identification of faults. Along the same vein the presence of the control and recycle loops may result in connectivity graphs with some groups of variables that are strongly connected to each other and mutually reachable, which would result in blocks of variables grouped together that makes sense from a physical perspective of the process. E.g. variables affected by a recycle stream being blocked together.

Additionally, the high degree of interconnectivity resulting from the control and recycle loops would cause a fault to propagate throughout the large system, so the utility of connectivity information to trace the faults back to their original causes can be analysed.

6.1.1. Overall process description

The purpose of the second and third stage pressure leaching in the BMR is mostly to leach the copper from the slurry exiting the first stage atmospheric leach upstream. A block diagram of the process is shown in Figure 6-1.

The solids residue from the first leaching stage enters a preparation tank (MTK10) as slurry, with water, spent electrolyte and acid added. The combined slurry is sent to a flash recycle tank (MTK20) preceding the autoclave, which is used to aid temperature control in the autoclave. The vapour in this tank exits through a vent (MFR6), and the slurry mixture (MFR7) is then fed to the autoclave.

The autoclave consists of four compartments: compartments 1, 2 and 3 making up the 2nd stage leach, and compartment 4 making up the 3rd stage leach. A portion of the slurry (MFR9) and vapour

(MFR8) is recycled from the 2nd stage leaching compartments to the flash recycle tank. Oxygen required by the leaching reactions is supplied to compartments 2, 3 and 4 (MFR10, MFR11 and MFR12, respectively). The contents of the first three compartments are separated by overflow weirs, allowing the slurry to flow through. Slurry from the 2nd stage leach is sent to a discharge tank and then undergoes settling in the 2nd stage leach discharge thickener, producing an overflow of $CuSO_4$ solution (MFR16), and an underflow MFR17. This underflow reports to the 3rd stage slurry preparation tank (MTK50), where further additions (spent electrolyte, water and acid) are made before the slurry enters the 3rd stage leach.

The 3rd and 4th compartments are separated from each other by a partition that prevents slurry transfer, but contains an opening in the vapour space to allow vapour transfer between the 2nd and 3rd stage leach. From the 3rd stage leach, a $CuSO_4$ solution and solids residue stream (MFR22) reports to downstream processing for copper removal and PGM processing.

6.1.2. Control loops in process

Ten process control loops are employed for tank inventory, temperature and pressure control (see Figure 6-1). These control loops are important to take note of since the MV-CV pairs in these loops should display connections in the process topology, giving an indication of how well the topology extraction method captured the process connectivity.

The level in the second stage preparation tank, MTK10, is controlled by MFR1. The level in the flash recycle tank, MTK20, is controlled by varying its outlet stream, MFR7.

The temperature in the first compartment (represented by T9) is controlled using the flash recycle tank: a portion of slurry (MFR9) and vapour (MFR8) is recycled from the 2nd stage leaching compartments to this tank, and when they enter the tank through a flash valve a portion of the liquid being recycled evaporates, losing energy in the process (Dorfling, 2012).

The temperature in the 2nd and 3rd compartments is controlled by cooling water flowing through coils in the autoclave. MFR10 acts as the manipulated variable to control the autoclave pressure, and the other two oxygen streams, MFR11 and MFR12, are varied in proportion to this by ratio control.

The level of the discharge tank, MTK40, is controlled by manipulating its outlet flow rate, MFR15. The level in the 3rd stage preparation tank, MTK50, is controlled by varying its outflow rate (MFR21).

The extents of reactions in the 3rd compartment are relatively small (Dorfling, 2012) so heating is sometimes required to control the temperature. This is achieved by the direct spraying of steam (MFR13) into this compartment.

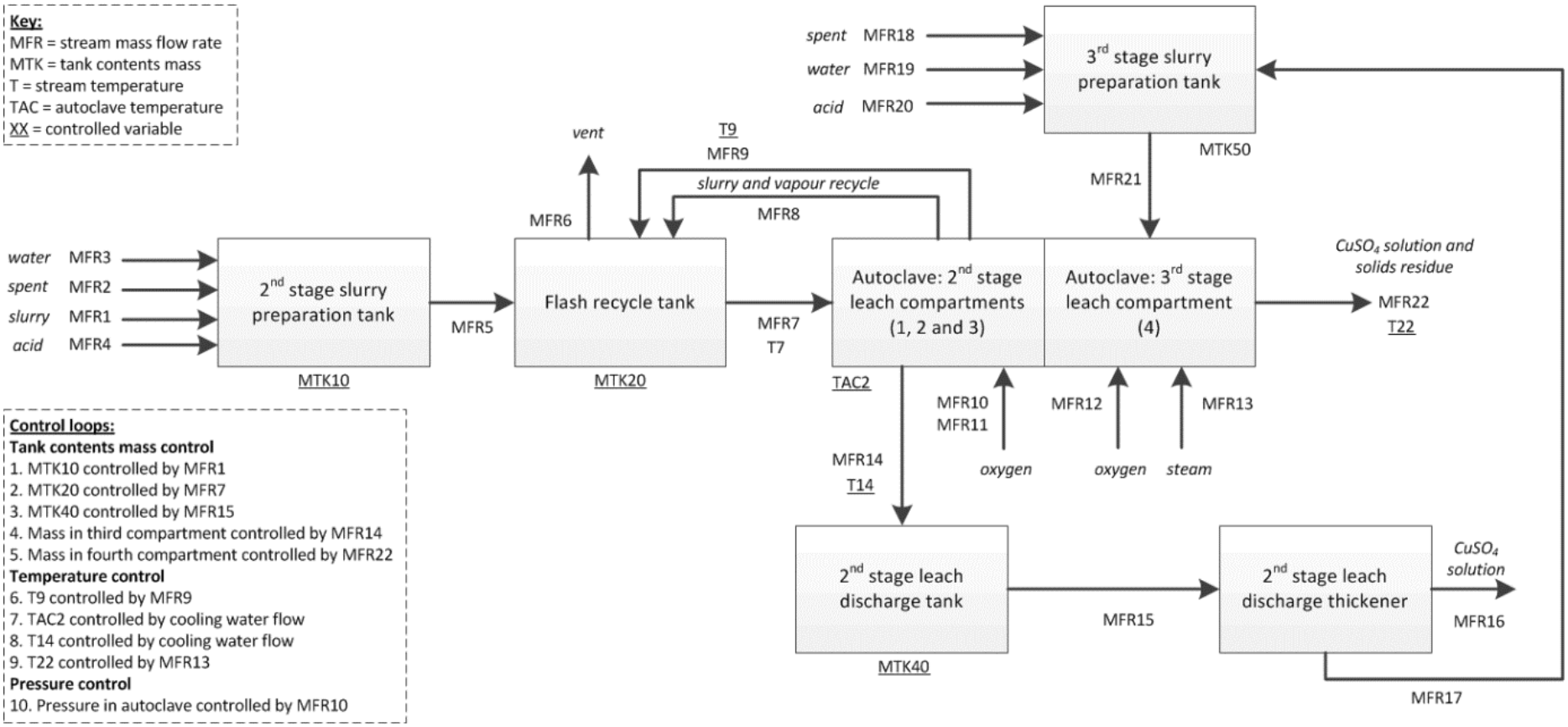

Figure 6-1: Second and third stage leaching process in the BMR (Lindner et al., 2014)

6.2. Data from Leaching Simulation

Normal operating conditions data and fault data were generated for this process. The data consisted of the 31 variables listed in Table 6-2. Three NOC data sets were generated, constituting the training, validation and NOC test data respectively. Then fault test data sets were generated for two fault scenarios and for multiple fault sizes for fault scenario 1, as described in section 6.2.3 and . The sizes of the data sets are summarised in Table 6-1.

Table 6-1: Summary of data set sizes

Data Set	Number of samples (N)	Number of variables (M)
Training	2500	31
Validation	1000	31
NOC Test	1000	31
Fault Test	2000	31

6.2.1. List of variables

A list of the measured variables used for monitoring of this process is given in Table 6-2.

Table 6-2: List of variables in autoclave leaching simulation

Variable No.	Variable Name	Description	Units
1	MFR1	Mass flow rate of stream 1	[kg/hr]
2	MFR2	Mass flow rate of stream 2	[kg/hr]
3	MFR3	Mass flow rate of stream 3	[kg/hr]
4	MFR4	Mass flow rate of stream 4	[kg/hr]
5	MFR5	Mass flow rate of stream 5	[kg/hr]
6	MFR6	Mass flow rate of stream 6	[kg/hr]
7	MFR7	Mass flow rate of stream 7	[kg/hr]
8	MFR8	Mass flow rate of stream 8	[kg/hr]
9	MFR9	Mass flow rate of stream 9	[kg/hr]
10	MFR10	Mass flow rate of stream 10	[kg/hr]
11	MFR11	Mass flow rate of stream 11	[kg/hr]
12	MFR12	Mass flow rate of stream 12	[kg/hr]
13	MFR13	Mass flow rate of stream 13	[kg/hr]
14	MFR14	Mass flow rate of stream 14	[kg/hr]
15	MFR15	Mass flow rate of stream 15	[kg/hr]
16	MFR16	Mass flow rate of stream 16	[kg/hr]
17	MFR17	Mass flow rate of stream 17	[kg/hr]
18	MFR18	Mass flow rate of stream 18	[kg/hr]
19	MFR19	Mass flow rate of stream 19	[kg/hr]
20	MFR20	Mass flow rate of stream 20	[kg/hr]
21	MFR21	Mass flow rate of stream 21	[kg/hr]
22	MFR22	Mass flow rate of stream 22	[kg/hr]
23	MTK10	Mass of tank 2nd stage preparation tank: TK10	[kg]
24	MTK20	Mass of flash recycle tank: (TK20)	[kg]
25	T7	Temperature of stream 7	[°C]
26	T9	Temperature of stream 9	[°C]
27	TAC2	Temperature of second autoclave compartment	[°C]

Variable No.	Variable Name	Description	Units
28	T14	Temperature of stream 14	[°C]
29	MTK40	Mass of 2nd stage discharge tank: TK40	[kg]
30	MTK50	Mass of 3rd stage preparation tank: TK50	[kg]
31	T22	Temperature of stream 22	[°C]

6.2.2. Introduction of noise into process

Included in the modifications made to the original model is the introduction of noisy input signals. This was necessary for two reasons:

1) To approximate actual data as close as possible; real data contains common cause variation from changes in feed compositions, temperatures, sensor noise, etc. Therefore to approximate actual data as close as possible this variation has to be simulated.

2) Without common cause variation the topology extraction methods would be erroneous. If one stream doesn't vary, the streams connected to it won't either, so no correlation or information transfer would occur. I.e. Sufficient excitation in the data is required to show correlation (in the case of LC and PC) and for information to be transferred in the case of the TE method.

The introduction of noise was performed by: analysing the available real process data, finding the mean and standard deviation and reconstructing a signal with a normal distribution with the same mean and standard deviation.

6.2.3. Fault 1: Preparation tank outlet blockage

Data for the first fault condition were generated by simulating a blockage in the outflow of the 2nd stage slurry preparation tank, i.e. stream 5. This blockage causes MTK10 to fluctuate, subsequently causing the level controller to vary MFR1 to correct for this. All downstream flow rates are also affected by this fault, as well as the downstream temperatures.

The flow rate MFR5 is proportional to the level in the tank, so the fault was simulated by multiplying the proportionality constant by a fraction. The flow was restricted for the period of a few hours and then returned to its normal behaviour. The response of the measured variables to this fault is shown in Figure 6-2.

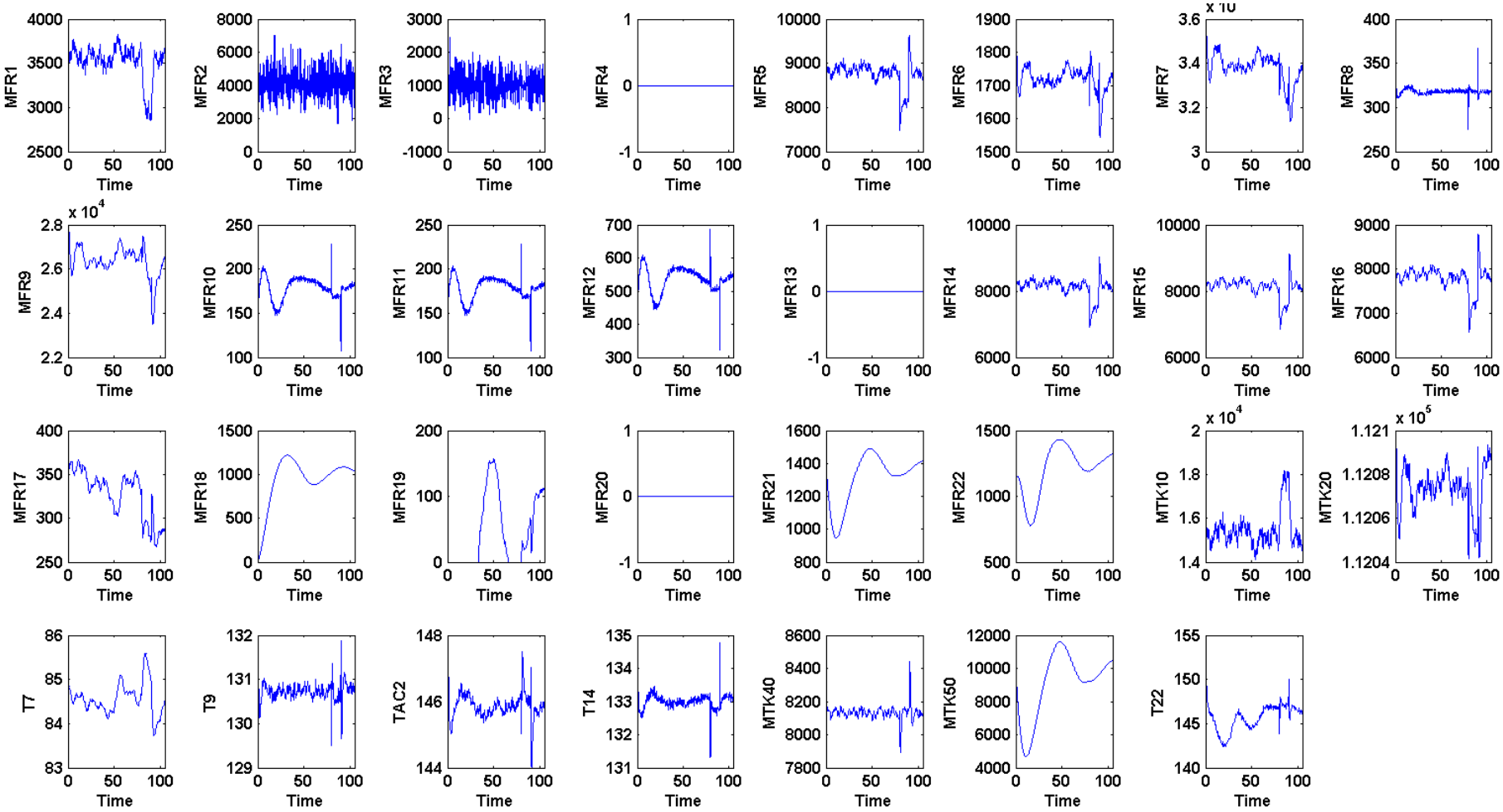

Figure 6-2: Response of measured variables in autoclave leaching simulation to preparation tank blockage fault (Fault 1)

6.2.4. Fault 2: Coiling coil blockage

Data for the second fault condition were generated by simulating a blockage in the coiling coils for the 2nd compartment. This fault affects the temperatures in the autoclave. Temperature within the autoclave have a complex effect in this process; the temperatures affect the exothermic reactions taking place within the compartments, this affects the vapour space in the compartments and these vapours travel back through the compartments and exchange heat with the upstream contents. Since the first compartment's temperature is controlled by varying MFR9 this then has an effect on all flow rates downstream of the flash recycle tank. The response of the measured variables to this fault is shown in Figure 6-3.

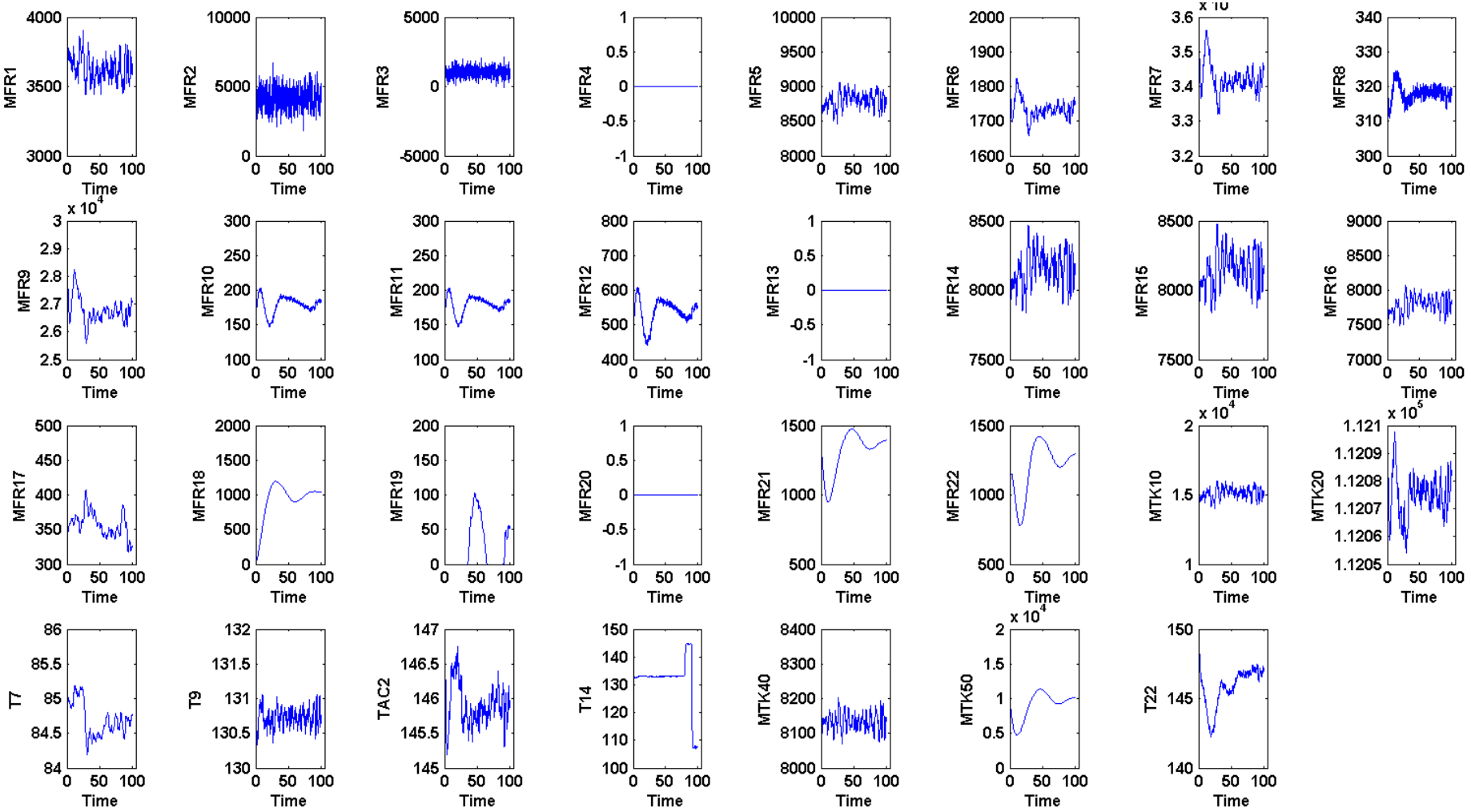

Figure 6-3: Response of measured variables in autoclave leaching simulation to cooling coils blockage fault (Fault 2)

6.3.Topology Extraction from Leaching Simulation Data

This section presents the results of the topology extraction methods. Each method's resulting connectivity graph is displayed and the validity of each observed connection is discussed. Then in section 6.3.4 the connectivity graph generated from process knowledge is presented and each method is compared to this.

6.3.1. Linear cross-correlation topology extraction

The number of lags, k, chosen for LC was 200. 200 lags corresponds to 6 hours, which was sufficiently long to capture the residence times and dead times in the process. In order to generate the connectivity graph using linear cross-correlation (LC) the significance threshold first had to be determined using the method described in Chapter 4, by substituting the number of samples (N=2500) into the equation derived for the threshold as a function of sample number.

$$\rho^{LC}_{max,th}(N) = 3N^{-0.452} + 0.11N^{-0.658} \quad \textbf{Equation 6-1}$$

$$\rho^{LC}_{max,th}(2500) = 0.088 \quad \textbf{Equation 6-2}$$

Applying this threshold for the LC connectivity, however, resulted in a connectivity graph with almost all of the possible connections considered significant. Most of the correlations were above 0.6, in fact the mean correlation for all pairs was above 0.8. Analysing plots of the correlation calculated over a number it was observed that there was a gradual increase in correlation, not a sharp spike as observed for the data in the two-tank case study data. This is likely due to the fact that the process is highly interconnected, but with very slow process dynamics (Dorfling, 2012). This means that a change in one variable will propagate throughout most of the system and affect many variables and this effect will spread out over a long period of time.

In order to generate a useful connectivity graph a more stringent significance threshold had to be selected. This was achieved by finding the 90th percentile for all calculated correlations (for all pairs of variables and for all numbers of lags), whilst omitting correlations equal to zero. For the training data used that resulted in a threshold of 0.775. Applying this threshold resulted in the connectivity graph shown in **Figure 6-4**.

Table 6-3 contains a systematic validation of each connection observed in this connectivity graph; the first two columns indicate the source and sink nodes of the edge being considered, the third column indicates whether the connection is valid (Y) or spurious (N), and the fourth column supplies the reason why it is considered valid (for example whether it makes sense from a mass or energy

balance perspective or a control perspective) or spurious. Some general observations are also presented.

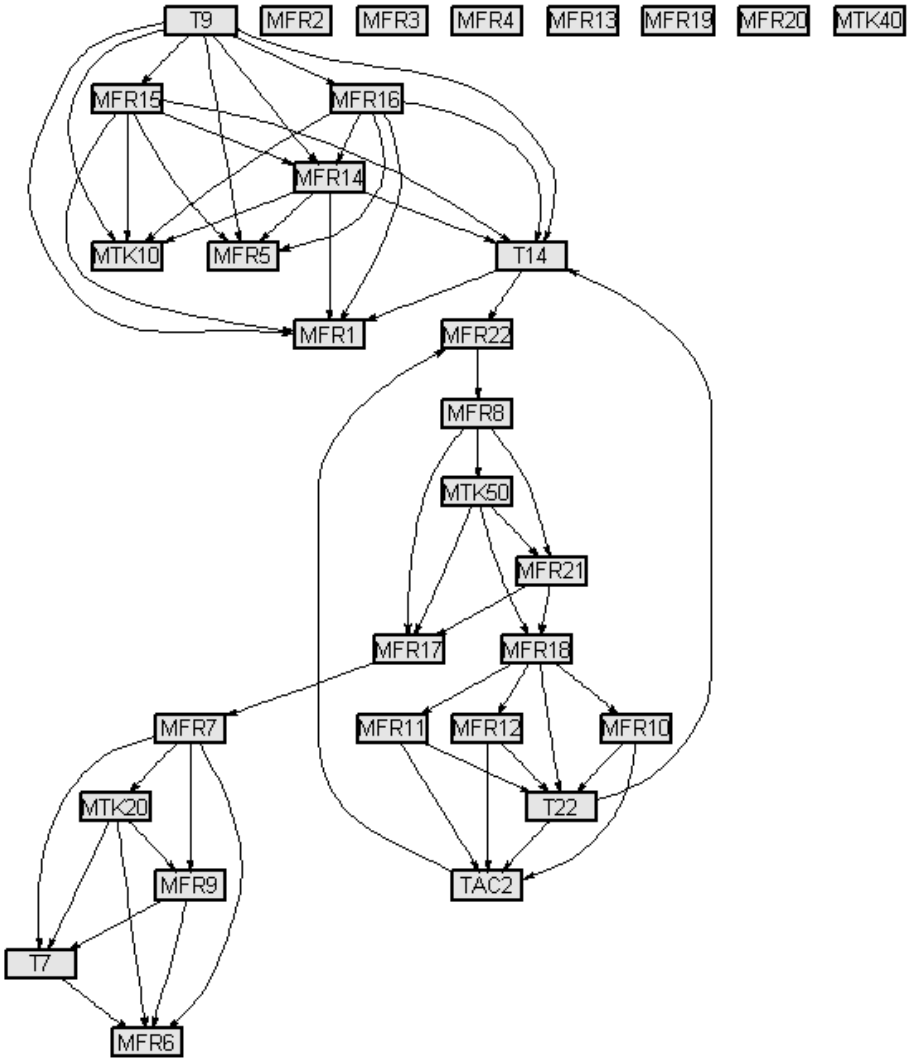

Figure 6-4: Connectivity graph for linear cross-correlation on leaching simulation training data

Table 6-3: Validation of connections in the linear cross-correlation graph (

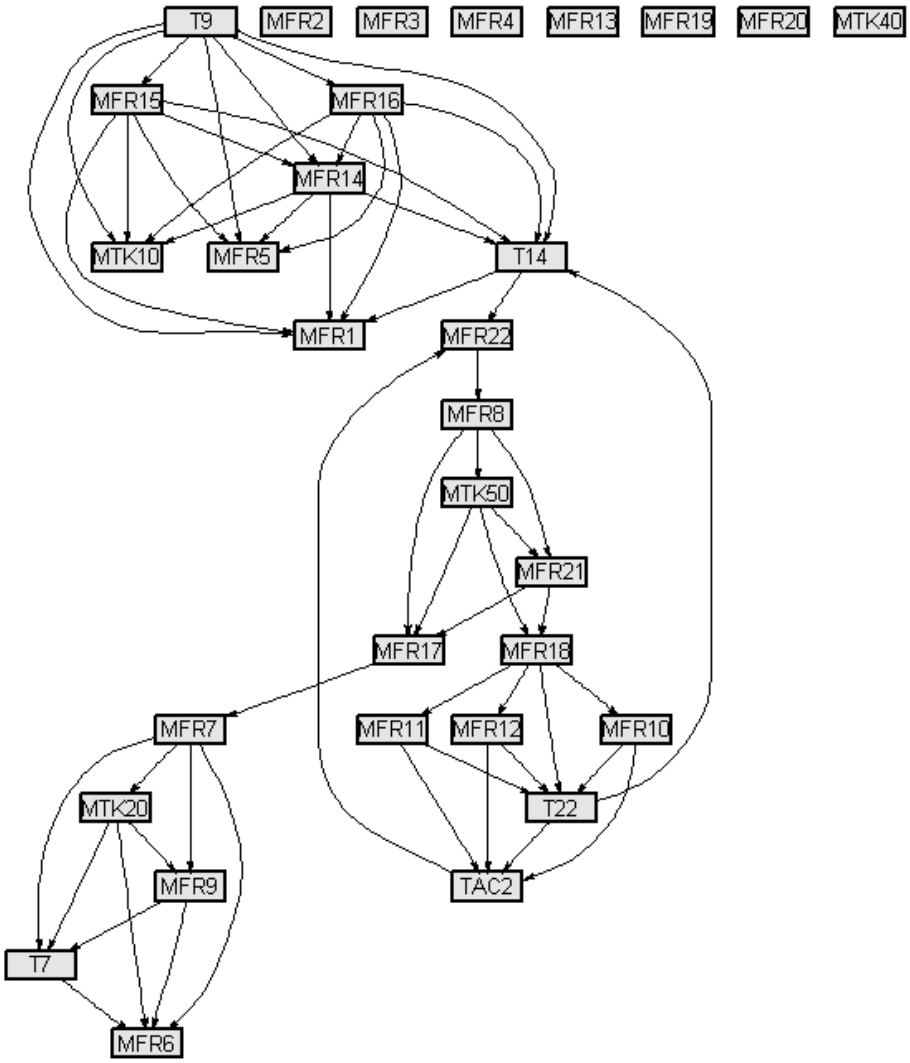

Figure 6-4**). Y indicates a valid connection, N indicates a spurious connection**

Source	Sink	Y/N	Reason
MFR7	T7	Y	Energy balance/Control: MFR7 enters the first compartment, influencing its temperature, causing the controller to vary MFR9, which then affects T7 in the flash recycle tank
MFR7	MTK20	Y	Control/mass balance: MTK20 is controlled by manipulating MFR7
MFR7	MFR9	Y	Control/energy balance: The amount of slurry coming into the autoclave through stream 7 (MFR7) affects the temperature within the autoclave. This temperature is controlled by varying MFR9
MFR7	MFR6	Y	Mass balance/Energy balance/Control: MFR7 affects MFR9 which is recycled back to the flash tank where some of its liquid evaporates and leaves through the vent represented by MFR6

Source	Sink	Y/N	Reason
MFR9	T7	Y	Control/energy balance: Since the recycle stream represented by MFR9 is fed to the flash recycle tank to control the autoclave temperature it will affect the temperature in the flash recycle tank.
MFR9	MFR6	Y	Mass balance: MFR9 enters the recycle tank and some of its liquid

			contents evaporate, adding to MFR6 which represents the mass flow rate of the vent stream exiting the tank
T7	MFR6	Y	Control/mass/energy balance: The temperature entering the autoclave affects MFR9 since this is used to control the autoclave temperature, MFr9 in turn affects MFR6 since the liquid evaporating from stream 9 exits the recycle tank through stream 6
MTK20	T7	Y	Energy balance: the temperature of the recycle tank is dependent on the mass of its contents
MTK20	MFR9	Y	Control/mass/energy balance: MTK20 is controlled by varying MFR7, which causes the temperature in the autoclave to change, causing MFR9 to change to correct this
MTK20	MFR6	Y	Control/mass/energy balance: Following the reasoning above, MTK20 affects MFR9, some of which evaporates in the tank and adds to MFR6
MFR10, 11,12	T22, TAC2	Y	Mass/energy balance: The amount of oxygen entering the autoclave has an effect on the exothermic reactions within the autoclave, which will greatly affect the temperatures
MFR18	MFR10, 11,12	Y	Mass balance: Spent entering the last compartment of the autoclave would affect the composition in the autoclave, affecting the amount of oxygen necessary for the reaction to take place
TAC2	MFR22	Y	Energy balance: the temperature of a stream would be connected to its flow rate
T22	T14,TAC2	Y	Energy balance: The separating screen between the 3rd and 4th compartments allow vapours to pass back to upstream autoclave compartments, so the temperature in the 4th compartment (T22) can affect the temperature in the 2nd (TAC2) and 3rd (T14) compartments
MFR18	T22	y	Mass balance/energy balance: Spent entering the last compartment of the autoclave would affect the composition in the autoclave, affecting the exothermic reactions taking place, affecting the temperature (T22)
MFR17	MFR7	Y	Mass balance/energy balance/control: MFR17 affects the amount of solids entering the 4th autoclave compartment; this affects the reactions taking place, which affects the temperatures in all the autoclave compartments through the vapour stream that exits back through the autoclave. The causes the controller to vary MFR9 to control the temperature, which causes MF7 to change
MTK50	MFR17	N	Connection is in the wrong direction, MFR17 enters the 3rd stage preparation tank, so it should affect MTK50, not the other way round
MTK50	MFR21	Y	Mass balance: MFR21 is dependent on the level in the tank, represented by MTK50
MTK50	MFR18	Y	Control: MTK50 is controlled by varying MFr18

Source	Sink	Y/N	Reason
MFR21	MFR17	N	Connection is in the wrong direction, MFR17 enters the 3rd stage prep tank, so it should affect MTK50 and therefore MFR21, not the other way around
MFR21	MFR18	Y	Control: MFR21 affects the level in MTK50, which is controlled by

			MFR18
MFR8	MTK50, MFR17, MFR21	Y	Mass balance: the amount of vapour leaving the autoclave can affect the flow rates exiting the autoclave, in turn affecting downstream flow rates
MFR22	MFR8	N	Following the reasoning above, this connection should be in the other direction
T14	MFR22	Y	Mass/energy balance/control: T14 will have an effect on the 4th compartment's temperature, which is controlled by injecting steam into the autoclave, which will affect its flow rate. Additionally, T14 affects the reactions taking place in the 3rd compartment, which influences the solids fraction in the stream exiting it, which influences MFR17
MFR14, MFR15, MFR16, T9, T14	MFR1, MFR5, MTK10	N	The variables associated with the 2nd stage preparation tank cannot be affected by downstream variables since there is no control or recycle loop connecting this tank to any variables further downstream
MFR14	T14	Y	Energy balance: MFR14 directly affects MFR15, which affects the amount of slurry entering the 4th autoclave compartment, which affects the reactions taking place in this compartment, which affects the vapour space, which causes the temperature in the upstream compartment to change
MFR15	T14	Y	Energy balance: MFR15 affects the amount of slurry entering the 4th autoclave compartment, which affects the reactions taking place in this compartment, which affects the vapour space, which causes the temperature in the upstream compartment to change
MFR15, 16	MFR14	N	Wrong direction
T9	T14	Y	Energy balance: The temperature of the first autoclave compartment will definitely affect the temperature of the 3rd compartment.
T9	MFR14, MFR15, MFR16	Y	Control/mass balance: T9 is controlled by recycling MFR9, which greatly affects the flow rates downstream of the autoclave compartments

One discrepancy is that MFR1 does not affect any other nodes; it is only affected by them. This is inconsistent because it is the first stream entering the process, and should only be affected my MTK10 (which it isn't) and should drive the variation of downstream variables. The same applies for MTK10 and MFR5.

It can be observed in the connectivity graph that T9 affects a lot of mass flow rates. This displays the effect of the recycle stream. Variation in T9 causes the first compartment's temperature controller to vary MFR9, which has a profound influence on all downstream flow rates. In addition, flow rates and temperatures associated with downstream autoclave compartments can have an effect on upstream temperatures and flow rates because of this recycle stream and because of the partitioning between the compartments that allows a vapour stream to travel back through the compartments. A change in the temperatures of the 4th compartment, for example, affects the

reactions taking place, which affects the vapour stream (MFR8) which exits back through the previous compartments, thereby affecting their temperatures. This then causes the controller to vary MFR9 to control the temperature, which causes MFR7 to change, thereby affecting all downstream flow rates again.

It is interesting to note that the oxygen flow rates (MFR10, MFR11 and MFR12) all have the same connections. This is an accurate representation of how the process works, since these flow rates are controlled by ratio control. This means that their time series trends would be identical and therefore their correlation with other variables would be identical. Additionally, they are not connected to each other because although their correlation would be 1, there would be no time delay between them since they vary simultaneously. When using LC to extract topology one of the criteria for the presence of causality between two variables is that the estimated time delay between them is non-zero.

Overall the LC method gave an accurate representation of the topology of the process; however, its utility is determined by how well it performs for fault identification and for blocking.

6.3.2. Partial cross-correlation topology extraction

The number of lags, k, chosen for PC was 200, which was sufficiently long to capture the residence times and dead times in the process. The same trend as described in section 6.3.1 for the high values of the LC was observed for PC. The correlations calculated were lower than for LC, however, which is to be expected since PC removes the effects of some intermediate variables which would otherwise have increased the correlation. To select the significance threshold the same method was followed as for LC, but selecting the 95^{th} percentile instead. This resulted in a significance threshold of 0.5. Applying this limit resulted in the connectivity graph displayed in Figure 6-5.

Table 6-4 contains a systematic validation of each connection observed in this connectivity graph; the first two columns indicate the source and sink nodes of the edge being considered, the third column indicates whether the connection is valid (Y) or spurious (N), and the fourth column supplies the reason why it is considered valid (for example whether it makes sense from a mass or energy balance perspective or a control perspective) or spurious. Some general observations are also presented.

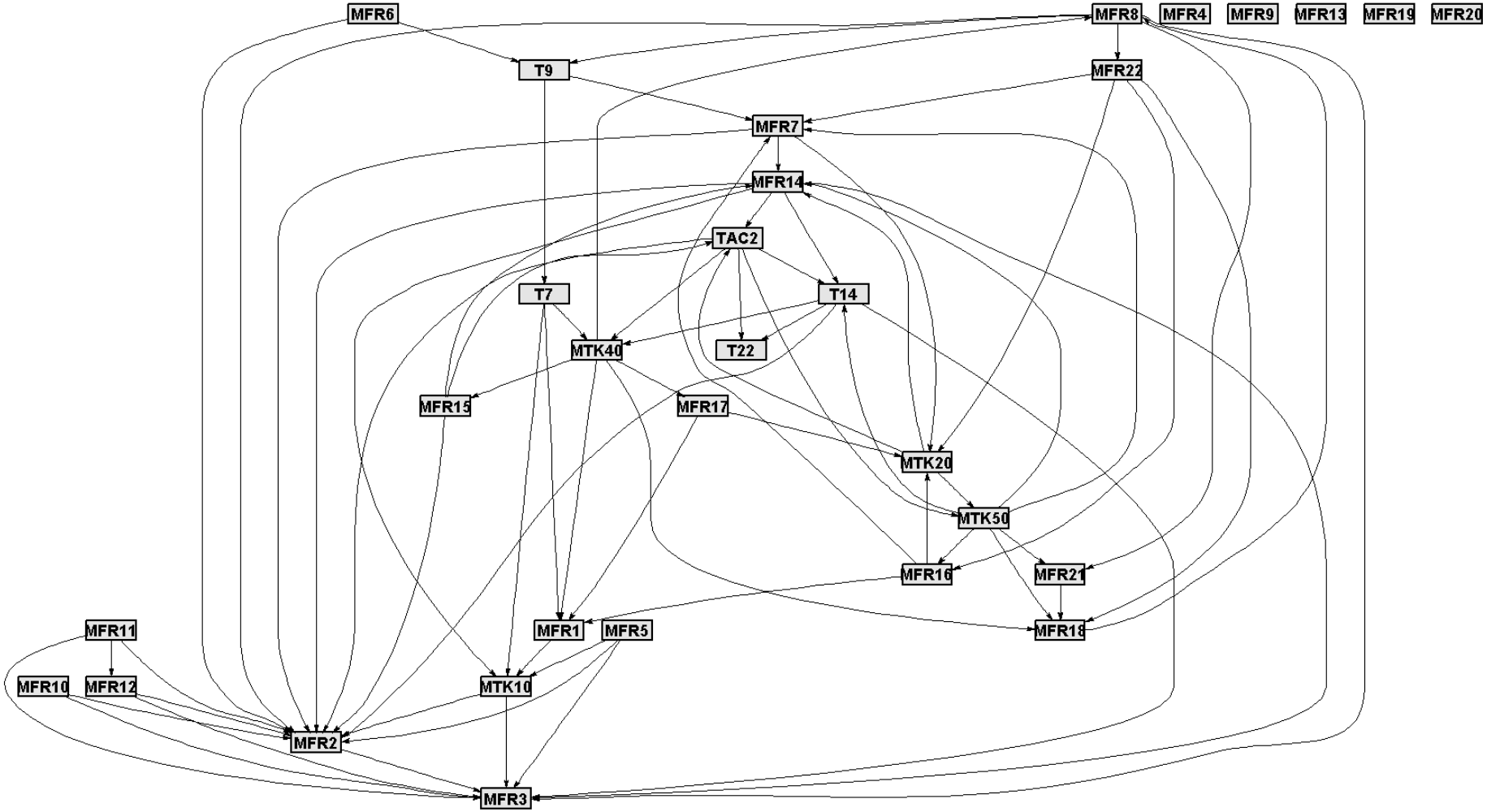

Figure 6-5: Connectivity graph for partial cross-correlation on leaching simulation training data

Table 6-4: Validation of connection in PC graph (Figure 6-5)

Source	Sink	Y/N	Reason
MFR1	MTK10	Y	Control: MTK10 is controlled by varying MFR1
MFR2	MFR3	Y	Mass balance: MFR2 and MFR3 both enter TK10
MTK10	MFR2, MFR3	N	Connection should be in the other direction
MFR5	MTK10, MFR2, MFR3	N	Wrong direction, MTK10 should affect MFR5 by mass balance since MFR5 is dependent on the level in MTK10
MFR6	MFR2	N	MFR2 could affect MFR6, not the other way around
MFR6	T9	Y	Mass/Energy balance: The amount of vapours leaving the recycle stream is an indication of how much energy is released from the recycle stream, which is used to control the temperature
MFR7	MFR2	N	MFR7 cannot affect upstream flow rates
MFR7	MFR14	Y	Mass balance: MFR7 enters the autoclave so it will definitely affect the MFR out of the autoclave
MFR7	MTK20	Y	Control: MTK20 is controlled by varying MFR7
MFR8	MFR2, MFR3	N	MFR8 cannot affect upstream flow rates
MFR8	T9	Y	Energy balance: the vapour stream in the autoclave will affect the temperature of the first compartment
MFR8	MFR21	Y	Mass balance: The vapour stream exiting the autoclave will affect the downstream flow rates
MFR11	MFR12	Y	Control: The two are connected by ratio control
MFR10, MFR11, MFR12	MFR2, MFR3	N	The oxygen streams fed into the autoclave cannot affect the upstream flow rates entering the system
MFR14, MFR15	MFR2, MFR3, MTK10	N	MFR14 and MFR15 cannot affect the flow rates and level of the preparation tank
MFR14	T14	Y	Energy balance: MFR14 directly affects MFR15, which affects the amount of slurry entering the 4th autoclave compartment, which affects the reactions taking place in this compartment, which affects the vapour space, which causes the temperature in the upstream compartment to change
MFR14	TAC2	Y	Energy balance: The flow rate of stream 14 affect the 4th compartment composition, which affects the temperature in all the compartments
MFR15	MFR14	N	Should be the other way around MFR15 should be affected by MTK 40 which should be affected by MFR14
MTK40	MFR15	Y	Control: MTK40 is controlled by varying MFR15
MFR15	TAC2	Y	Energy balance: The flow rate of stream 15 affect the 4th compartment composition, which affects the temperature in all the compartments
MFR16, MFR17	MFR1	N	MFR16 and MFR17 cannot affect the flow rate of slurry entering the system
MFR16	MFR7, MTK20	Y	Mass/Energy balance/Control: The flow rate of stream 16 gives an indication of the composition entering the 4th autoclave

Source	Sink	Y/N	Reason
			compartment (having an inverse relationship to the amount of solids) which will affect the reactions taking place, which affects the temperatures in all the compartments since the vapour stream is allowed to travel back upstream between compartments. This causes the controller to vary MFR9 to control the temperature, which would have a significant effect on the level and flow rates of the recycle tank
MFR17	MTK20	Y	Mass/Energy balance/Control: The flow rate of stream 17 gives an indication of the composition entering the 4th autoclave compartment which will affect the reactions taking place, which affects the temperatures in all the compartments since the vapour stream is allowed to travel back upstream between compartments. This causes the controller to vary MFR9 to control the temperature, which would have a significant effect on the level and flow rates of the recycle tank
MTK40	MFR17	Y	Mass balance: The level of MTK40 affects the flow rate of MFR15 which goes into the thickener and determines how much solids go through stream 17
MFR18	MFR8	Y	Mass balance: The amount of spent entering the autoclave through stream 18 will change the composition within the autoclave, which will greatly influence the stream leaving the vapour space through stream 8.
MFR21	MFR18	Y	Control: MF21 changes the level in the tank, which causes is kept at its set-point by varying MFr18
MFR22	MFR18	N	MFR22 should be influenced by the stream entering the preparation tank since it is dependent on its level
MFR22	MTK20, MFR7, MFR16	N	Mass/Energy balance/Control: The flow rate of stream 22 influences the composition of the 4th autoclave compartment which will affect the reactions taking place, which affects the temperatures in all the compartments since the vapour stream is allowed to travel back upstream between compartments. This causes the controller to vary MFR9 to control the temperature, which would have a significant effect on the level and flow rates of the recycle tank as well as downstream flow rates
MTK20	TAC2	Y	Control/Energy balance: The level of TK20 is an indication of the control actions being taken on MFR9 to control the autoclave temperature, so it would show causality from MTK20 to TAC2
MTK20	MFR14	Y	Control/Mass balance: The level in TK20 determines the flow rate into the autoclave which determines the flow rate out of it
MTK20	MTK50	Y	Control/Mass balance: The level in TK20 determines the flow rate into the autoclave which determines the downstream flow rates and levels
MTK40	MFR1	N	Level of TK40 cannot affect the flow rate of slurry entering the system
MTK40	MFR8	Y	Mass balance: the level of TK40 influences the downstream composition in the autoclave, which will greatly affect the vapour space in the autoclave, represented by MFR8
MTK50	MFR7, MFR14,	Y	Mass/Energy balance/Control: The level of this preparation tank affects the composition in the 4th compartment, thereby influencing

Source	Sink	Y/N	Reason
	MFR16		the reactions taking place, which has an effect on the vapour space which is allowed to move upstream between compartments. This affects the temperatures in all the compartments, which would cause T9 to change, which would affect MFR9 and MFR7 and thereby MFR14 and MFR16
MTK50	MFR18	Y	Control: MFR18 is used along with MFR20 and MFr19 to control the level in this tank
MTK50	MFR21	Y	Mass balance: the level in this tank determines the flow rate out of it
MTK50	T14	Y	Mass/Energy balance/Control: This level affects the flow rates into the 4th compartment, which influences the reactions taking place and thereby the vapour space, which affects the temperature of the upstream compartment
T7	MTK40	Y	Control/Energy/Mass balance: T7 affects the first compartment's temperature, causing MFR9 to vary, which affect MFR7, which will definitely affect all downstream flow rates and levels
T7	MTK10, MFR1	N	This temperature cannot affect the levels and flow rates of the preparation tank
T9	MFR7	Y	Control/Mass balance: T9 is controlled by varying MFR9, which changes the level in the flash recycle tank, which changes MFR7
T9	T7	Y	Energy balance: stream 9 enters the flash tank at T9, which would affect the temperature in the tank, represented by T7
TAC2	T14, T22	Y	Energy balance: the temperature of the second autoclave compartment will have an influence on the 3rd and 4th compartments' temperatures
T14, TAC2	MTK40, MTK50	Y	Mass/Energy balance/Control: These temperatures influence the reactions taking place in the autoclave, which has an effect on the vapour space which is allowed to move upstream between compartments. This affects the temperatures in all the compartments, which would cause T9 to change, which would affect MFR9 and MFR7 and thereby all downstream flow rates and tank levels MFR16
T14	MFR2, MFR3	N	This temperature cannot affect the flow rates entering the system
T14	T22	Y	Energy balance: T14 will have an influence on the next compartment's temperature

Once again the oxygen flow rates all have the same connections. This is an accurate representation of how the process works, because these flow rates are controlled by ratio control, so their time series trends would be identical and therefore their correlation with other variables would be identical. Additionally, they are not connected to each other because although their partial correlation would be 1, there would be no time delay between them since they vary simultaneously. When using PC to extract topology one of the criteria for the presence of causality between two variables is that the estimated time delay between them is non-zero.

Additionally, the significant effect of the recycle stream, T9 is evident from the PC connectivity graph shown in Figure 6-5. The same effect was observed in the LC connectivity graph. The influence can be ascribed to the fact that temperatures of downstream compartments influence those of upstream compartments through the vapour stream (MFR8) that travels backwards. This causes the controller to vary MFR9, which causes all downstream flow rates and levels to vary subsequently.

This graph resulted in a large amount of spurious connections with downstream variables affecting the variables associated with the 2nd stage preparation tank (MFR1, MFR3, MFR5 and MTK10). Since there is not control or recycle stream connecting this unit to downstream process units this is not physically possible.

The resulting connectivity graph is much more convoluted than that obtained from LC. A large amount of spurious connections exist in this graph as well. Consequentially, upon inspection the graph does not provide a very useful representation of the topology of this process. However the utility of the graph remains to be tested in its use for blocking and fault identification.

6.3.3. Transfer entropy topology extraction

In order to generate the connectivity graph using transfer entropy (TE) the significance threshold first had to be determined using the method described in Chapter 4, by substituting the number of samples (N=2500) into the equation derived for the threshold as a function of sample number:

$$\mathrm{t}_{\mathbf{x}\rightarrow\mathbf{y},\mathrm{th}}(N) = 0.0018N^{0.465} + 0.0054N^{0.412} \qquad \textbf{Equation 6-3}$$

$$\mathrm{t}_{\mathbf{x}\rightarrow\mathbf{y},\mathrm{th}}(2500) = 0.2 \qquad \textbf{Equation 6-4}$$

Unlike with PC and LC, the proposed method for threshold selection for TE worked well and the threshold did not have to be increased to obtain a better connectivity graph. Applying the resulting significance threshold of 0.19 resulted in the connectivity graph shown in Figure 6-6.

Table 6-5 contains a systematic validation of each connection observed in this connectivity graph; the first two columns indicate the source and sink nodes of the edge being considered, the third column indicates whether the connection is valid (Y) or spurious (N), and the fourth column supplies the reason why it is considered valid (for example whether it makes sense from a mass or energy balance perspective or a control perspective) or spurious. Some general observations are also presented.

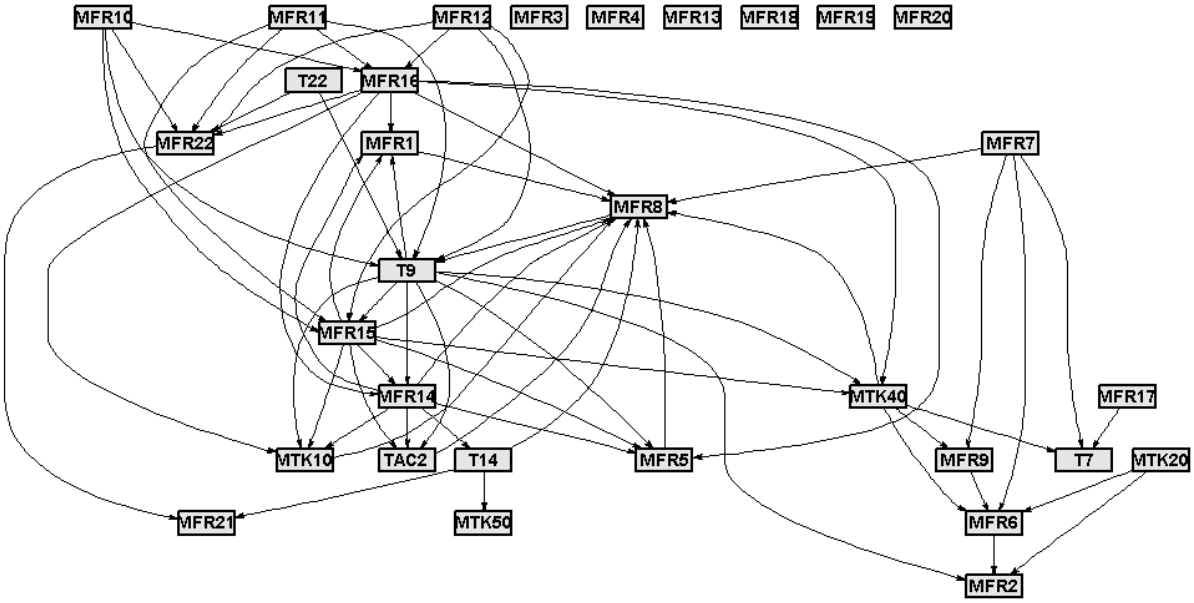

Figure 6-6: Connectivity graph for TE on Leaching simulation training data

Table 6-5: Validation of connections in the TE graph (Figure 6-6)

Source	Sink	Y/N	Reason
MFR1	MFR8	Y	Mass balance: the slurry flow rate entering the process will affect the vapour stream downstream of it
MFR5	MFR8	Y	Mass balance: The flow rate of the slurry in stream 5 will affect the vapour stream downstream of it
MFR6	MFR2	N	Vapour stream exiting the recycle tank cannot affect the spent entering the process
MFR7	MFR8	Y	Mass balance: The flow rate of the slurry entering the autoclave will definitely affect the vapour stream exiting it
MFR7	T7	Y	Energy balance/Control: MFR7 enters the first compartment, influencing its temperature, causing the controller to vary MFR9, which then affects T7 in the flash recycle tank
MFR7	MFR9, MFR6	Y	Control/Mass/Energy balance: The amount of slurry entering the autoclave affects it temperature, which causes the controller to vary Mfr9, which in turn affects MFr6 since some of the recycle stream evaporates and leaves through stream 6
MFR8	T9	Y	Energy balance: The vapour stream in the autoclave will affect the autoclave temperatures
MFR9	MFR6	Y	Mass balance: A portion of the recycle stream (MFr9) evaporates in the flash recycle tank and exits through stream 6
MFR10, MFR11, MFR12	MFR15, MFR16, MFR22	Y	Mass balance: The oxygen flow rates entering the autoclave affect the reactions taking place, which affects the downstream flow rates, it also affects the compositions exiting the 3rd compartment, which affects how much liquids exit through stream 16 and therefore the amount of solids entering into the 4th compartment and the amount exiting it
MFR10, MFR11, MFR12	T9	Y	Mass/Energy balance: The oxygen stream entering the autoclave will affect the reaction taking place and will therefore have a profound influence on the first compartment's temperature

Source	Sink	Y/N	Reason
MFR14, MFR15	MFR8	Y	Mass balance: MFR14 exits the autoclave but affects the flow rate entering the 4th compartment which would affect the vapour stream
MFR14, MFR15, MFR16	MTK10, MFR1, MFR5	N	These flow rates cannot affect the flow rates and levels of the preparation tank
MFR14	T14	Y	Energy balance: A stream's temperature is dependent on its flow rate
MFR14, MFR15	TAC2	Y	Mass/Energy balance: MFR14 affects the flow rate entering the 4th compartment, which affects the reactions within the autoclave. The vapour stream that travels back upstream through the other compartments influences their temperatures
MFR15, MFR16	MFR14	N	MFR14 should influence MFR15, not the other way around
MFR15	MTK40	Y	Control: MTK40 is controlled by varying MFR15
MFR16	MFR8	Y	Mass balance: The flow rate of the liquid stream leaving the thickener is an indication of how much solids are entering the 4th compartment, which will affect the vapour stream exiting it
MFR16	MTK40. MFR14	N	The liquid stream leaving the system cannot affect the upstream level and flow rates, the connection should be in the other direction
MFR16	MFR22	Y	Mass balance: The flow rate of the liquid stream leaving the thickener is an indication of how much solids are entering the 4th compartment, which will determine the flow rate exiting the autoclave
MFR17	T7	Y	Control/Mass/Energy balance: MFR17 affects the flow rate entering the 4th compartment, which affects the vapour space which affects upstream temperatures, which causes MFr9 to vary to control the temperature, which changes the temperature T7 in the flash recycle tank
MFR22	MFR21	N	It should be that MFR21 determines MFR22, not the other way
MTK10	MFR8	Y	Mass balance: The level in the preparation tank determines the flow rate into the autoclave which will affect its vapour stream
MTK20	MFR6	Y	Mass balance: The mass of the flash recycle tank will be connected to the amount of vapour exiting it
MTK20	MFR2	N	The level of the flash tank cannot affect the spent stream entering the process
MTK40	MFR8, MFR6, MFR9, T7	Y	Mass/Energy balance/Control: MTK40 affects the flow rate entering the 4th compartment, which affects the vapour space which affects upstream temperatures, which causes MFR9 to vary to control the temperature, which changes the temperature T7 in the flash recycle tank
T9	MFR1, MFR2, MFR5, MTK10	N	the temperature in the 1st compartment cannot affect the levels and flow rates of the preparation tank
T9	TAC2, T14	Y	Energy balance: the 1st compartment's temperature will affect the subsequent compartment's temperatures

Source	Sink	Y/N	Reason
T9	MFR14, MFR15, MTK40	Y	Control/Mass balance: T9 is controlled by varying MFr9, which will have a profound effect on the downstream flow rates and levels
T14	MFR8	Y	Energy balance: the temperature in the 3rd compartment will affect the reactions in the autoclave, causing the vapour space to change
T14	MTK50	Y	Mass/Energy balance/Control: The temperature in the 3rd compartment influences the upstream compartments' temperatures, which affects the vapour space which affects upstream temperatures, which causes MFR9 to vary to control the temperature, which will affect downstream levels
T22	MFR22	Y	Energy balance: a streams temperature will be connected to tis flow rate
T22	T9	Y	Energy balance: The 4th compartment's temperature affects the previous compartments' temperatures since the vapour stream (MFR8) is allowed to travel upstream between compartments

The influence of the recycle stream is apparent once again when considering the results presented in Figure 6-6 and Table 6-5; T9 is highly connected, and a number of connections exist because of the influence of the recycle stream.

Once again the oxygen flow rates all have the same connections. This is an accurate representation of how the process works, because these flow rates are controlled by ratio control, so their time series trends would be identical and therefore their correlation with other variables would be identical. Additionally, they are not connected to each other because there would be no time delay between them since they vary simultaneously. This means that knowing previous values of MFR10, for example, would not result in a reduction of uncertainty of the values for MFR11. The

The same discrepancy observed with LC and PC connectivity graphs, where the 2nd stage preparation tank's variables were affected by downstream variables, was observed for the TE graph. This is incorrect since no recycle or control loops exist that connect this unit to downstream variables.

In general the TE connectivity graph gives a good representation of the topology of this process. The amount of spurious connections was smaller than for PC. Additionally, the fact that the TE was generated without having to alter the threshold obtained by the proposed method makes it more appealing than using LC or PC.

6.3.4. Comparison of data-based topology to knowledge-based topology

Using knowledge of the process, i.e. considering relationships defined by control loops or CV-MV pairs (as described in section 3.2), mass balances and energy balances, an adjacency matrix was generated. This was then used to construct the connectivity graph shown in Figure 6-7.

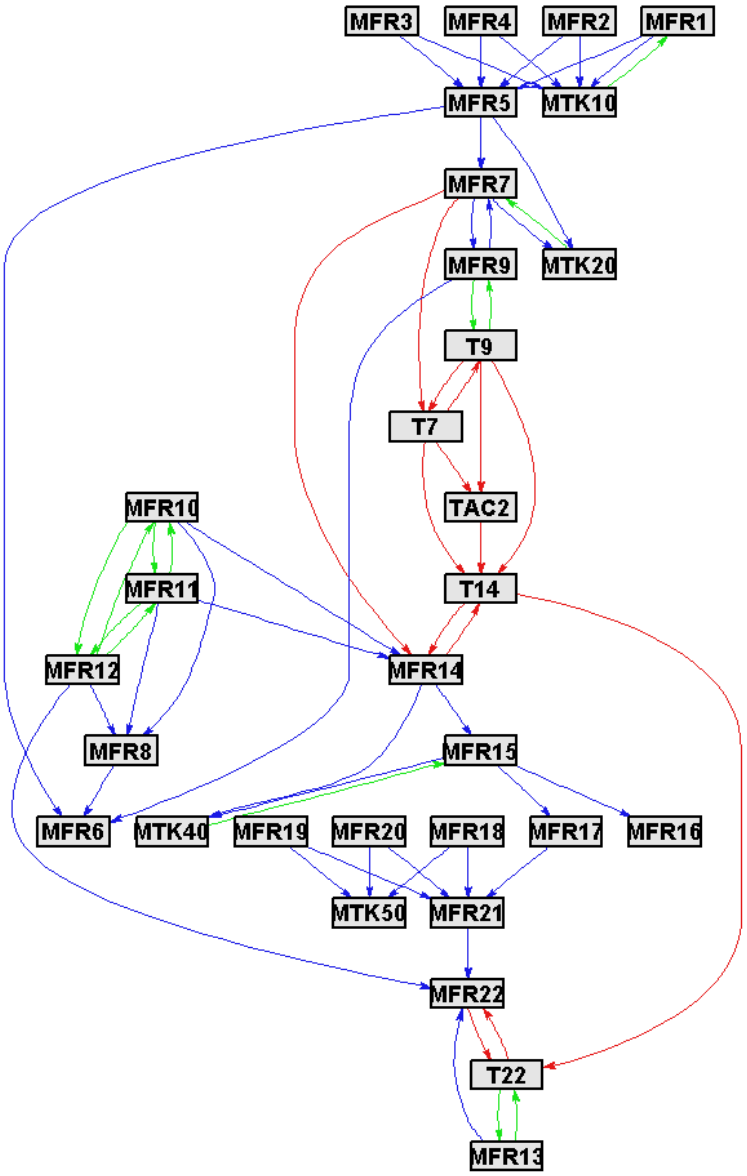

Figure 6-7: Connectivity Graph generated from process knowledge. Red represents energy balance connections, blue represents mass balance connections and green represents control loop connections

Comparing Figure 6-7 with

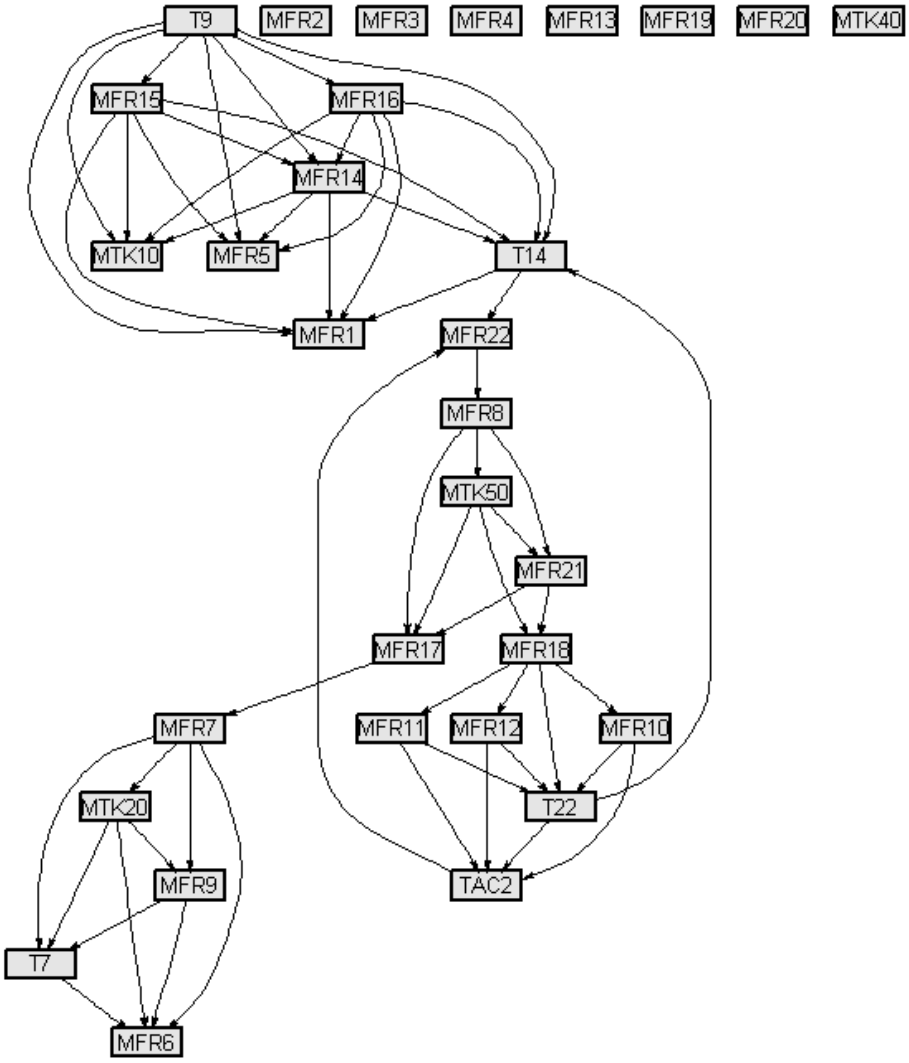

Figure 6-4, Figure 6-5 and Figure 6-6 and considering Table 6-3, Table 6-4 and Table 6-5, what becomes apparent is that using process knowledge may give an accurate and clean representation of the obvious, intuitive topology structure of a process, but the less obvious connections and the strong, indirect connections are lost. Many of the connections shown in the process knowledge graph appear to be missing from the graphs obtained from data-based methods. However, just because the direct connections are missing does not mean the topology extraction method performed poorly. In many case the connections exist through intermediate routes that may actually have stronger connection in the physical system.

Using the data-based topology extraction methods identifies connections that are much less intuitive, but still strong and valid. For example, the effect of the recycle stream, stream 9, that is used to control the temperature in this process. This recycle stream causes strong connections between downstream temperatures and flow rates throughout the process, whether upstream or downstream of where the temperature is measured.

6.4. Blocking of Leaching Simulation Data Using Topology

The connectivity graphs obtained from the three TEM are used in this section to perform blocking on the data. The resulting blocking for each method is presented and discussed.

6.4.1. Blocking using linear cross-correlation topology

Applying the strongly connected components blocking method to the LC connectivity graph results in four blocks, detailed in Table 6-6 and shown on the connectivity graph in Figure 6-8.

The first block contains mostly the autoclave variables, such as the oxygen flow rates, autoclave temperatures and MFR 21 and 22 and the vapour recycle stream. The 3rd stage preparation tank variables are also associated with this block. The second block contains mostly the second stage preparation tank variables, MFR1, MFR5 and MTK10, as well as some flow rates around the discharge tank and the thickener. The third block represents mostly the variables around the flash recycle tank. The remaining unconnected variables constitute the 4th block.

Table 6-6: Division of leaching simulaition variables into separate blocks according to connected components in linear cross-correlation connectivity graph

Block 0	Block 1		Block 2		Block 3		Block 4	
All variables	Variable No.	Variable Name	Variable No.	Variable Name	Variable No.	Variable Name	Variable No.	Variable Name
	1	MFR8	1	MFR1	1	MFR6	1	MFR2
	2	MFR10	2	MFR5	2	MFR7	2	MFR3
	3	MFR11	3	MFR14	3	MFR9	3	MFR4
	4	MFR12	4	MFR15	4	MFR17	4	MFR13
	5	MFR18	5	MFR16	5	MTK20	5	MFR19
	6	MFR21	6	MTK10	6	T7	6	MFR20
	7	MFR22	7	T9			7	MTK40
	8	TAC2						
	9	T14						
	10	MTK50						
	11	T22						

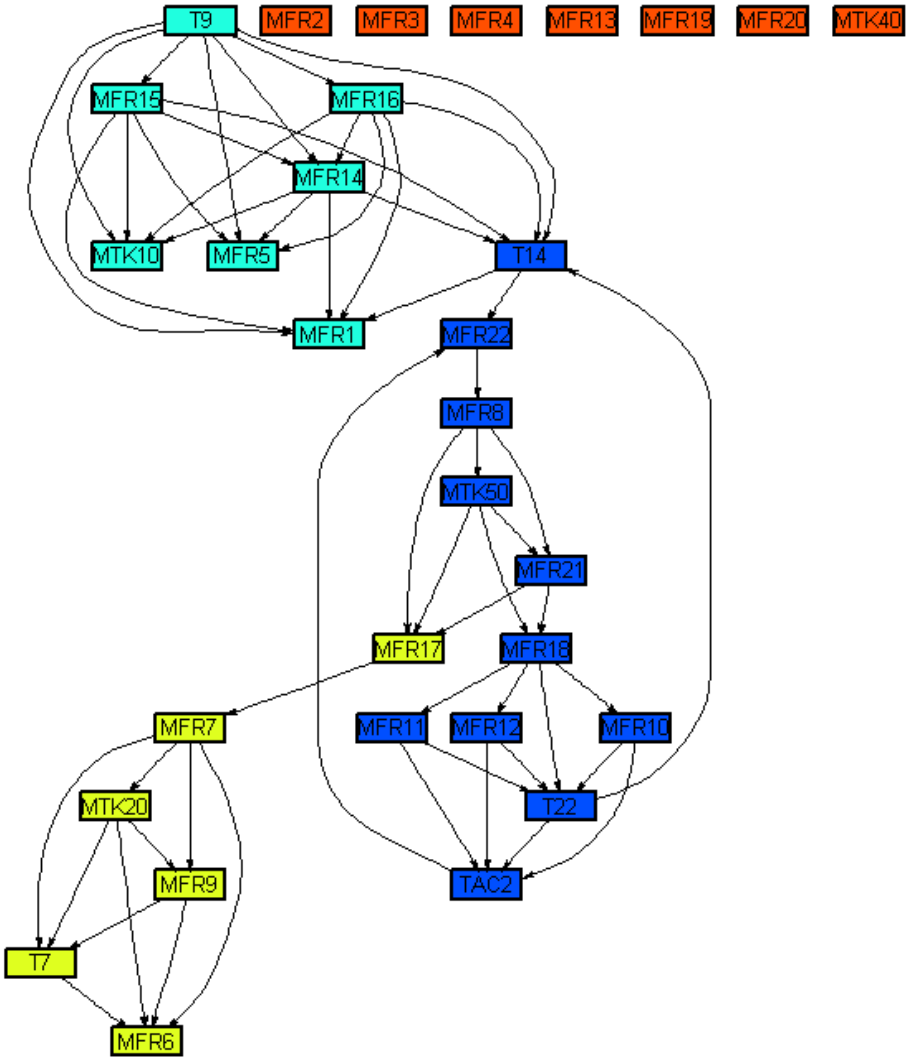

Figure 6-8: Blocked connectivity graph for linear cross-correlation on leaching simulation data. Different colours represent different blocks described in Table 6-6

6.4.2. Blocking using partial cross-correlation topology

Using the PC connectivity graph the blocking resulted in 3 blocks, detailed in Table 6-7 and shown on the connectivity graph in Figure 6-9. Since the connectivity graph for this method showed a high degree of connectivity, the blocking resulted in one large strongly connected block with many variables, Block 1, another less strongly connected block, Block 2, and a third block with the unconnected variables.

Block 1 contains most of the autoclave variables, with the exception of the oxygen flow rates, as well as those of the flash recycle tank and the discharge tank, the thickener and the third stage preparation tank. This encompasses most of the units in the process. Block 2 contains a combination of the variables associated with the first preparation tank and the oxygen flow rates. Since the first block encompasses most of the process it may be reasoned that the blocking would not be useful, or that it didn't really give any new useful information. However, the fact that Block 2 separates the

preparation tank variables from this strongly connected block is promising, especially for detection of the first fault since it originates in this unit.

Table 6-7: Division of leaching simulation variables into separate blocks according to connected components in partial cross-correlation connectivity graph

Block 0	Block 1		Block 2		Block 3	
All variables	Variable No.	Variable Name	Variable No.	Variable Name	Variable No.	Variable Name
	1	'MFR7'	1	'MFR1'	1	'MFR4'
	2	'MFR8'	2	'MFR2'	2	'MFR13'
	3	'MFR14'	3	'MFR3'	3	'MFR19'
	4	'MFR15'	4	'MFR5'	4	'MFR20'
	5	'MFR16'	5	'MFR6'		
	6	'MFR17'	6	'MFR10'		
	7	'MFR18'	7	'MFR11'		
	8	'MFR21'	8	'MFR12'		
	9	'MFR22'	9	'MTK10'		
	10	'MTK20'				
	11	'T7'				
	12	'T9'				
	13	'TAC2'				
	14	'T14'				
	15	'MTK40'				
	16	'MTK50'				

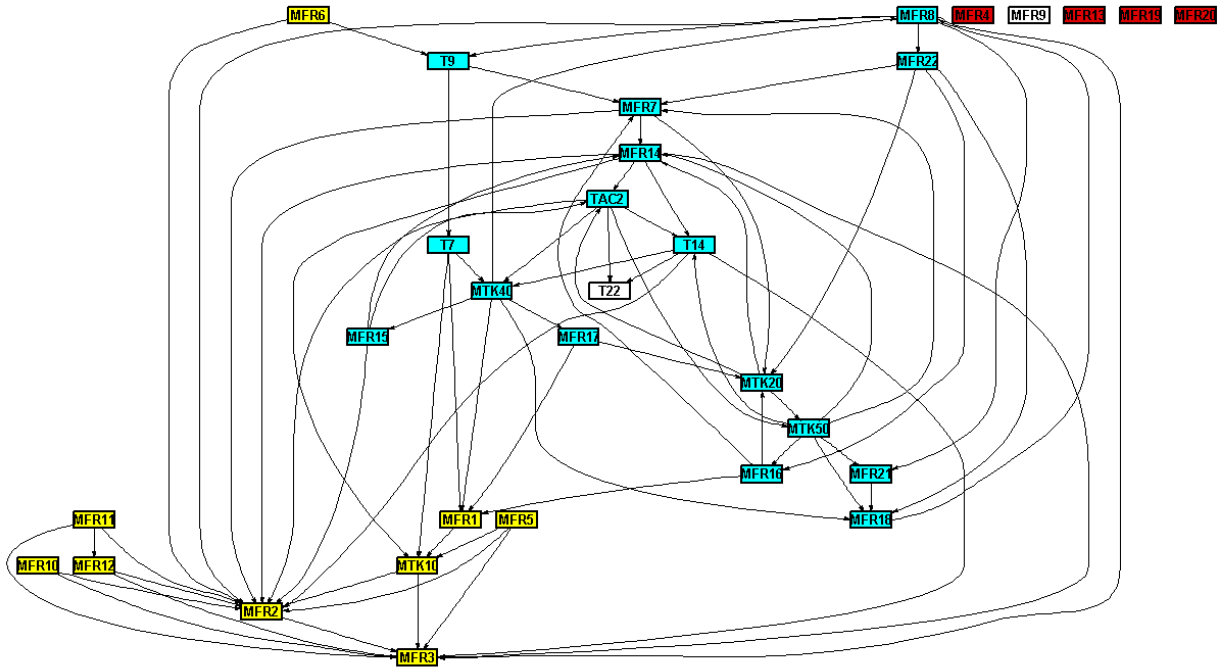

Figure 6-9: Blocked connectivity graph for partial cross-correlation on leaching simulation data. Different colours represent different blocks described in Table 6-7

6.4.3. Blocking using transfer entropy topology

Blocking using the TE connectivity graph results in 4 blocks, detailed in Table 6-8 and shown on the graph in Figure 6-10. Like the LC method this connectivity graph resulted in the variables being reasonably evenly divided over the 4 blocks. The first block contains the variables around the preparation tank, MFR1, MFR5 and MTK10, as well as the discharge and third stage preparation tanks. It also contains the temperatures and flow rates around the first 3 autoclave compartments: T9, TAC2 and T14 and MFR 14. The second block shows a strong association with the flash recycle tank since it consists mostly of the variables around this tank, with the exception of MFR2 and MFR17. The third block contains all the oxygen flow rates, as well as the flow rates abound the 4th autoclave compartment and its temperature. The 4th block contains all the unconnected variables remaining.

Table 6-8:Division of autoclave variables into separate blocks according to connected components in transfer entropy connectivity graph

Block 0	Block 1		Block 2		Block 3		Block 4	
All variables	Variable No.	Variable Name	Variable No.	Variable Name	Variable No.	Variable Name	Variable No.	Variable Name
	1	'MFR1'	1	'MFR2'	1	'MFR10'	1	'MFR3'
	2	'MFR5'	2	'MFR6'	2	'MFR11'	2	'MFR4'
	3	'MFR8'	3	'MFR7'	3	'MFR12'	3	'MFR13'
	4	'MFR14'	4	'MFR9'	4	'MFR16'	4	'MFR18'
	5	'MFR15'	5	'MFR17'	5	'MFR21'	5	'MFR19'
	6	'MTK10'	6	'MTK20'	6	'MFR22'	6	'MFR20'
	7	'T9'	7	'T7'	7	'T22'		
	8	'TAC2'						
	9	'T14'						
	10	'MTK40'						
	11	'MTK50'						

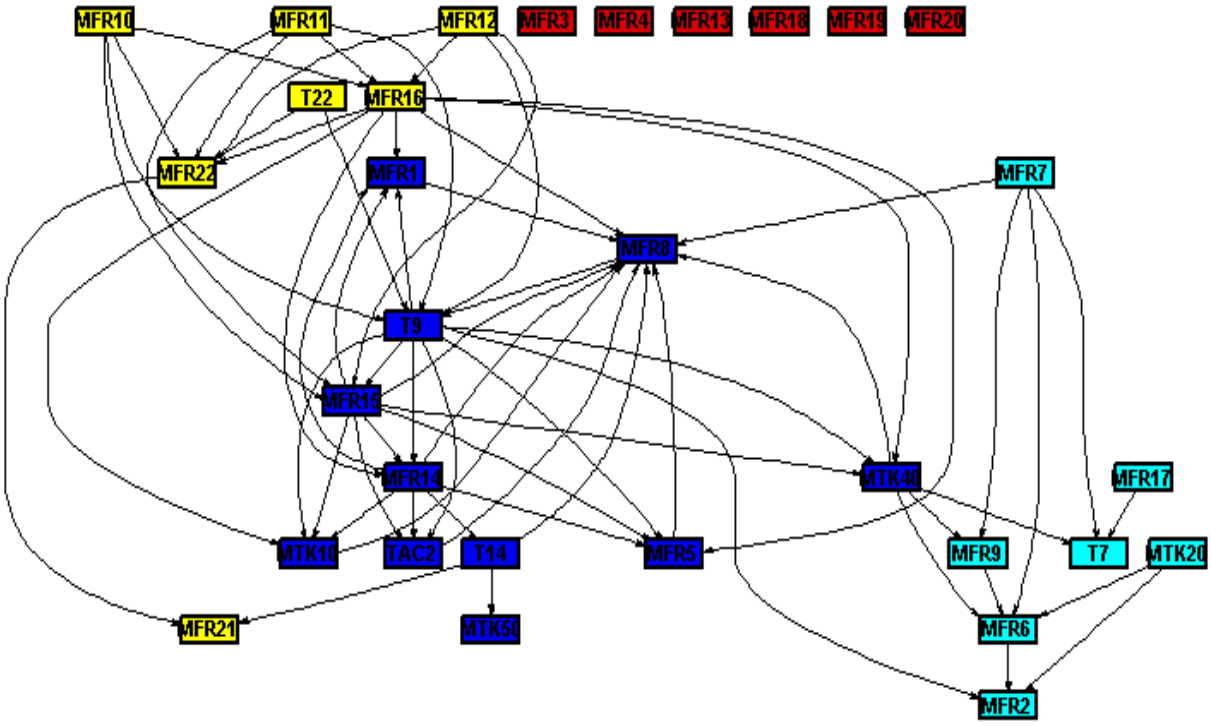

Figure 6-10: Blocked connectivity graph for transfer entropy on leaching simulation data. Different colours represent different blocks described in Table 6-8

6.4.4. Summary of blocking results

Considering the results of blocking using all three connectivity graphs it can be observed that the variables associated with the 2nd stage preparation tank, TK10, tend to form part of the same block. The same applies to the oxygen flow rates. In general the blocking methods result in variables associated with each unit tending to be grouped in the same block. The apparent trend is that the

preparation tank and first three compartments form the most strongly connected component, followed by the flash recycle tank forming a separate block of weakly connected nodes. The oxygen flow rates report to either one of these and the 4th compartment tends to form its own block, with the 3rd stage prep tank and the thickener and discharge tank reporting to either the 2nd stage or 3rd stage compartments. Overall this indicates that the blocking, especially for LC and TE resulted in blocks that actually reflected the units in the process.

6.5. Feature Extraction for Fault Detection in Leaching Simulation

In the previous sections of this chapter the results of topology extraction were presented, followed by the results of using the connectivity graphs obtained to divide the process variables into blocks to be analysed separately. This section presents the fault detection results for both faults considered, applied to the unblocked data (all variables combined) and the blocked data. The results are discussed in order to determine whether blocking improved the fault detection or not. The fault detection results include the use of PCA and KPCA, as well as the three monitoring chart methods, and the different methods are compared to determine which performed best for fault detection.

Summary results are presented here, detailed results are presented in Appendix C-.

6.5.1. Training of feature extraction methods

The details of the feature extraction models developed on the training data are given here.

Number of retained features for principal components analysis

For the unblocked data retention of 5 components resulted in an explained variance of 90%. The number of principal components retained for PCA for the blocked data for each blocking method are given in Table 6-9.

Table 6-9: Retained components giving 90% explained variance for each block for principal components analysis

TEM		Block 1	Block 2	Block 3	Block 4
LC	No. of variables in block	11	7	6	7
	No. of retained components	2	2	3	3
PC	No. of variables	16	9	6	-
	No. of retained components	4	4	0	-
TE	No. of variables	11	7	7	6
	No. of retained components	3	3	2	2

Kernel width selection and number of retained features for kernel principal components analysis

Cross-validation performed on the training data indicated a decreasing mean squared prediction error for increasing kernel width. This indicates that the data displays mostly linear behaviour. A

kernel width of 50 was therefore chosen since at this kernel width the mean squared prediction error had levelled off.

For the unblocked data retention of 3 components resulted in an explained variance of 90%. The number of principal components retained for PCA for the blocked data for each blocking method are given in Table 6-10.

Table 6-10: Retained components giving 90% explained variance for each block for KPCA

TEM		Block 1	Block 2	Block 3	Block 4
LC	No. of variables in block	11	7	6	7
	No. of retained components	3	3	3	3
PC	No. of variables	16	9	6	-
	No. of retained components	3	3	3	-
TE	No. of variables	11	7	7	6
	No. of retained components	3	3	3	3

6.5.2. Fault detection results of preparation tank blockage fault (Fault 1)

Figure 6-11 illustrates the main fault detection results for the first fault, which was the blockage in MFR5 exiting the preparation tank. The figure shows the AUCs and DDs for the unblocked cases first (block0), and then the blocked cases using each TEM. The results presented for the blocked cases display the blocks that gave the best results for the feature extraction method used. A detailed presentation of the results for all blocks is provided in the appendix.

For LC, block 3 showed the best results for both PCA and KPCA. Referring to Table 6-6 and Figure 6-8, this block contains: MFR6, MFR7, MFR9, MFR17, MTK20 and T7. These variables are mostly associated with the flash recycle tank. This is directly downstream of the fault (blockage in MFR5), which would cause MTK20 to deviate from its set-point, causing the behaviour of MFR7, MFR9, T7 and MFR6 to change significantly. Therefore this block displayed the effects of the fault.

Figure 6-11 shows that the KPCA fault detection method displayed much higher AUCs and lower DDs for block 3 than it did for the unblocked case, indicating a significant improvement with the use of blocking in this case. Therefore in terms of fault detection, using LC for blocking resulted in improvement of the detection ability for KPCA. Additionally, considering that the block that showed the best detection results is immediately downstream of the blockage, the blocking fault detection results also provide valuable information as to the location of the fault. Therefore it can be concluded that for this case blocking improved both fault detection and provided useful information for fault identification.

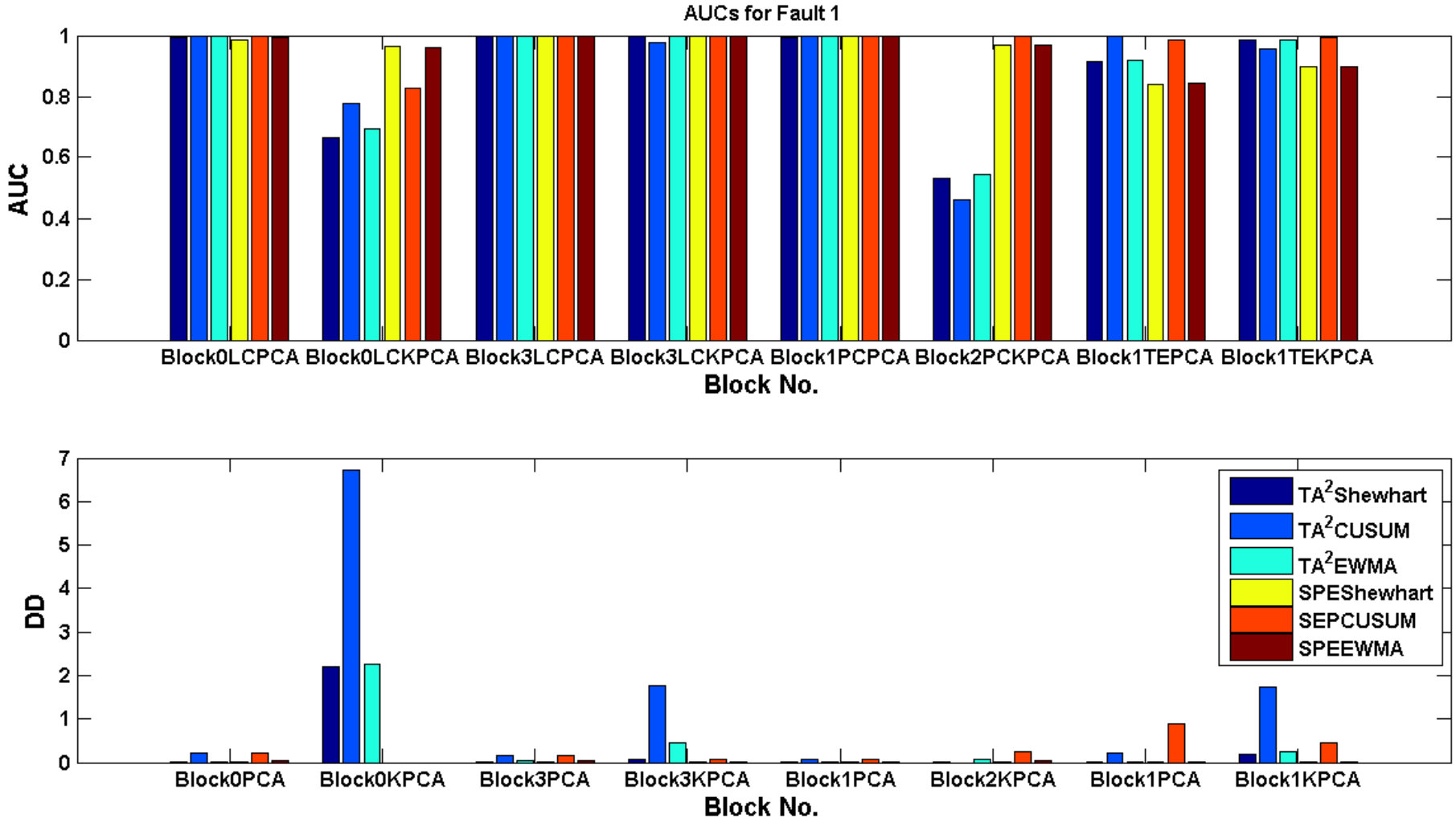

Figure 6-11: Fault detection results for the blockage fault, including AUCs and DDs for blocked and unblocked application. Results from blocks with the best detection results are shown for each topology method.

For PC in Figure 6-11, block 1 showed the best results for PCA. Referring back to Table 6-7 and Figure 6-9, Block 1 contains most of the autoclave variables; with the exception of the oxygen flow rates, as well as those of the flash recycle tank and the discharge tank, the thickener and the third stage preparation tank. These variables are all highly connected, as was observed in section 6.3.2. A blockage in stream 5 would cause a disruption in the flash recycle tank, which would affect flow rates and temperatures of downstream variables significantly. Unfortunately, since this is a large block containing most of the variables in the process, this result does not provide useful information for fault identification.

For KPCA in Figure 6-11, block 2 in the PC blocking method displayed the best detection results. Referring back to Table 6-7 and Figure 6-9, block 2 contained MFR1, MFR2, MFR3, MFR5, MFR6, MFR19, MFR11, MFR12 and MTK10. This block was very strongly associated with the preparation tank where the fault occurred; therefore it would display the effects of the fault very strongly. It can also be observed in the figure that using KCPA in this block resulted in lower AUCs for the T_A^2 statistic than in the unblocked case. Whereas with the SPE statistic, it resulted in higher AUCs than the unblocked case. This result indicates an improvement in fault detection for the KPCA method using blocking, and also provides useful information for fault identification, since the tank where the blockage occurred resulted in the best fault detection results.

In Figure 6-11, TE block 1 showed the highest AUCs and lowest DDs for both PCA and KPCA. Referring to Table 6-8 and Figure 6-10 the first block contains the variables around the preparation tank, MFR1, MFR5 and MTK10, amongst others. Therefore it makes sense that this would show strong effects of the fault. This block also contains the discharge and third stage preparation tanks masses, which would be affected significantly by the upstream blockage, as would the temperatures and flow rates around the first 3 autoclave compartments: T9, TAC2 and T14 and MFR14.

Once again for KPCA the blocking displayed an improvement of the AUCs and DDs of both statistics. This indicates that blocking showed an improvement in the fault detection ability. Additionally, the fact that the block that resulted in the best detection results contains the preparation tank variables indicates that blocking provided useful information for identification of the fault.

For the unblocked results KPCA showed worse AUCs, especially for the T_A^2 statistic. However the AUCs typically improved with blocking, with the exception of the PC blocking results. In the unblocked case the DDs are extremely high. The reason for the poor DDs can be seen in Figure 6-12, which shows an example of one of the monitoring charts for KPCA. The T_A^2 statistic does show an increase from NOC to fault conditions, but the threshold set according to the validation data is quite strict, so it takes some time before the statistic exceeds this threshold consistently The detection is

still adequate when considering the AUCs, however, since the AUC is independent of the threshold set.

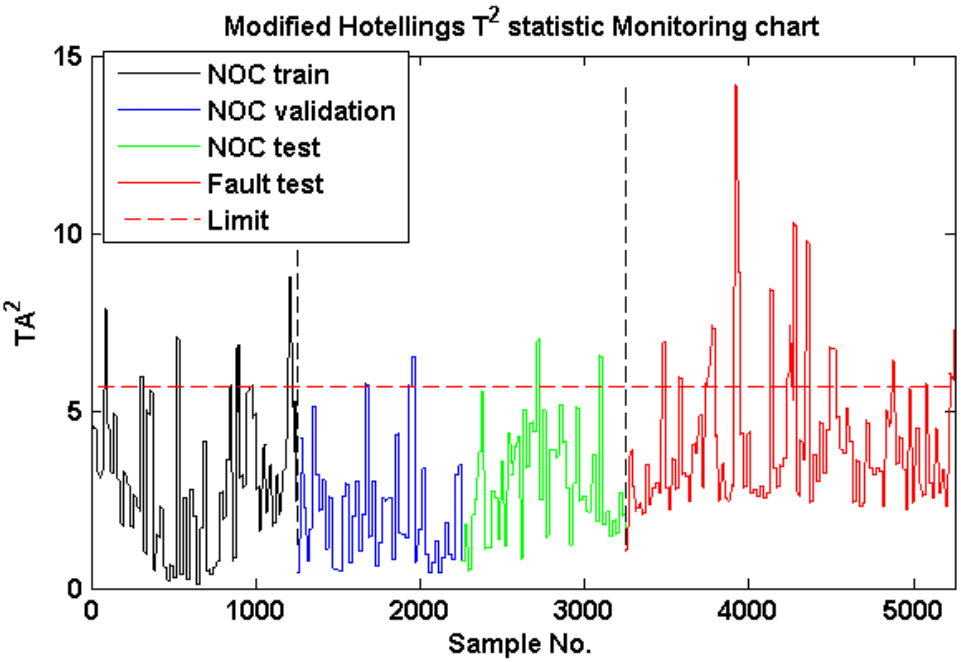

Figure 6-12: Shewhart T_A^2 monitoring chart for kernel principal components analysis for unblocked data for blockage fault

Considering Figure 6-11, in general the SPE charts performed better than the T_A^2 charts, giving larger AUCs. This indicates that the fault does not cause the relationships between variables to change.

In general the CUSUM charts performed the best in terms of AUCs, but this improvement comes at the sacrifice of detection speed, as evidenced by the larger DDs. This is due to the fact that the CUSUM chart adds up the deviation of the statistic from the NOC mean. At first when the fault has occurred this deviation is not very large, and compared to the cumulative sum of past values it does not result in a large increase in the CUSUM. After this deviation has persisted for some time, however, the effect starts to add up and the CUSUM becomes very large.

The results in Figure 6-11 indicate that the EWMA chart resulted in very similar AUCs and DDs to that of the Shewhart charts. The AUCs for the EWMA were slightly larger, and unlike the CUSUM, this did not result in significantly larger DDs. Although it might be expected that the EWMA would also come at a sacrifice of detection speed, since it calculates an average of past values and would cause the effect of the sample at the start of fault conditions to be lower. However, since the parameter chose for the weighting, r, was low (0.1), the EWMA chart gave higher weight to more recent values.

When considering the PCA results in Figure 6-11, there does not appear to be much improvement of fault detection with blocking. The AUCs are similar, although there might be an improvement with DDs. The reason for this is that this fault enters the system right at the start, at the preparation tank.

This affects all downstream variables, i.e. the effects propagate strongly throughout the whole system and aren't isolated in just one part of the system.

However, the utility of applying blocking is not only measured by considering the detection performance, but also in the identification performance. As noted for the LC and TE blocking, the blocks that showed the best detection results were the blocks that were closely associated with the preparation tank, or just downstream of it. This provides valuable insight for fault identification. That information can then be exploited to inspect the contributions, connectivity change and back propagation of the variables for only that block and thereby more accurately find a root cause.

6.5.3. Fault detection of cooling coil fault (Fault 2)

Figure 6-13 illustrates the main fault detection results for the first fault, which was the blockage in the cooling coils. The figure shows the AUCs and DDs for the unblocked cases first (block0), and then the blocked cases using each TEM. The results presented for the blocked cases display the blocks that gave the best results for the feature extraction method used. A detailed presentation of the results for all blocks is provided in Appendix C.

For LC blocking method, block 1 displayed the best results for both PCA and KPCA in Figure 6-13. Referring to Table 6-6 and Figure 6-8, the first block contains mostly the autoclave variables, including the autoclave temperatures TAC2, T14 and T22. Since the blockage in the cooling coils would cause a disruption in the autoclave temperatures, this block would show significant effects of this fault. Blocking using this method displayed higher AUCs for both PCA and KPCA. However, with KPCA the DDs were very high.

For the PC blocking method block 2 displayed the best fault detection results for PCA. Referring back to Table 6-7 and Figure 6-9, block 2 contained MFR1, MFR2, MFR3, MFR5, MFR6, MFR19, MFR11, MFR12 and MTK10. The AUCs were similar to that obtained in the unblocked case, while the DDs were lower.

For the PC blocking method block 1 displayed the best fault detection results for KPCA in Figure 6-13. Referring back to Table 6-7 and Figure 6-9 block 1 contains most of the autoclave variables; with the exception of the oxygen flow rates, as well as those of the flash recycle tank and the discharge tank, the thickener and the third stage preparation tank. These variables are all highly connected, as was observed in section 6.3.2. However, this block contains most of the variables in the autoclave; therefore this result does not provide any insight as to the location of the fault. The AUCs were higher than for the unblocked PCA, but the DDs were also very high.

https://www.youtube.com/watch?v=mXw3jy99w78

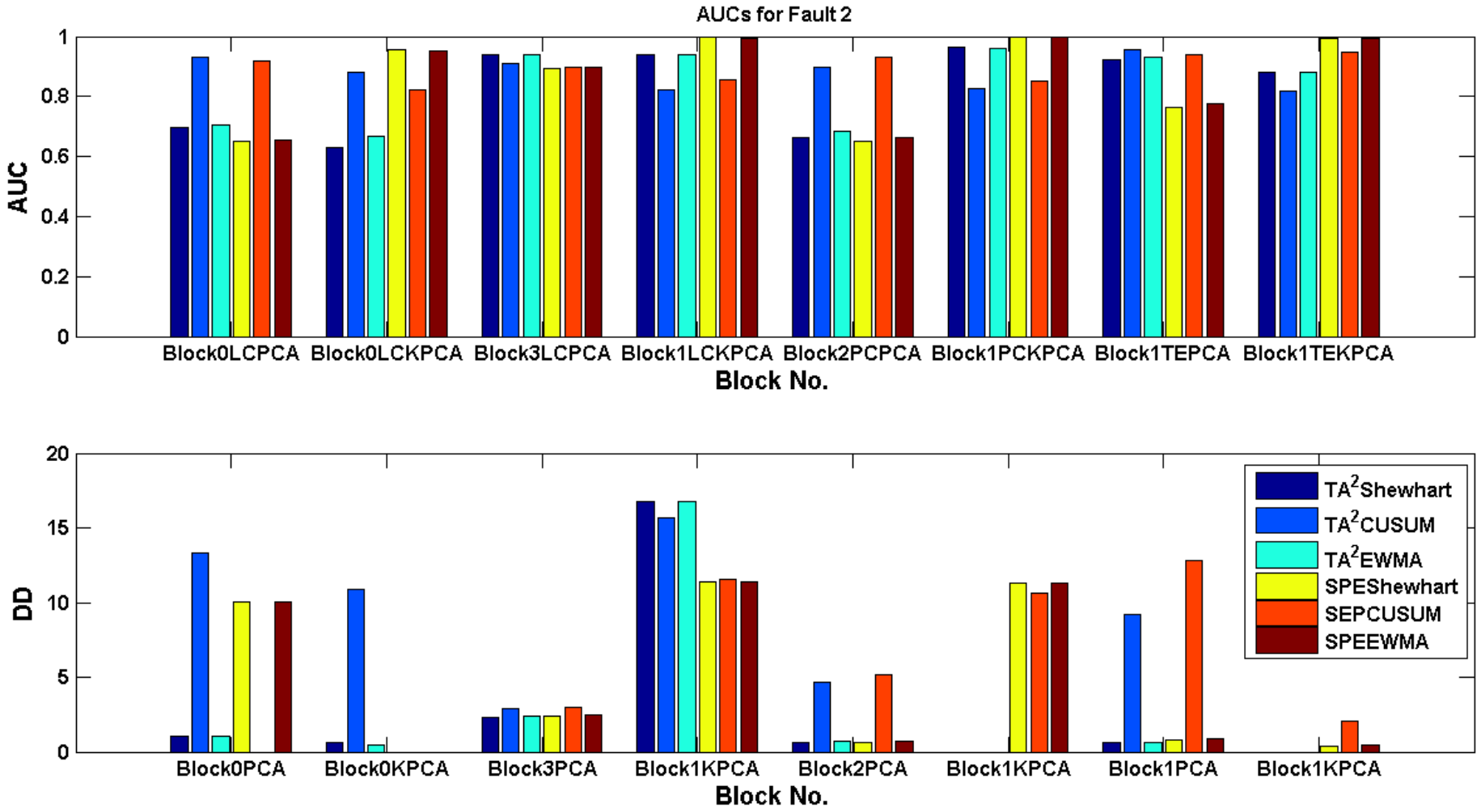

Figure 6-13: AUCs and DDs for different methods for cooling coil fault, including AUCs and DDs for blocked and unblocked application. Results from blocks with the best detection results are shown for each topology method.

For TE block 1 showed the highest AUCs and lowest DDs for both PCA and KPCA. Referring to Table 6-8 and Figure 6-10 the first block contains, amongst others, the temperatures and flow rates around the first 3 autoclave compartments: T9, TAC2 and T14 and MFR 14. Since the blockage in the cooling coils would affect the temperatures in the autoclave, this block would show significant effects of this fault. The PCA and KPCA for this block displayed significantly higher AUCs and low DDs, indicating that using TE blocking resulted in a significant improvement for detecting this fault. Additionally, since this block contains the autoclave temperature variables, this result provided useful information for fault identification as well.

For this fault, Figure 6-13 shows that, CUSUM introduced a significant amount of detection delay, so it really seems like it is not worth the slight improvement in the AUCs.

As with the previous fault, Figure 6-13 shows that the EWMA chart resulted in very similar AUCs and DDs to that of the Shewhart charts. The AUCs for the EWMA were slightly larger, and unlike the CUSUM, this did not result in significantly larger DDs. Although it might be expected that the EWMA would also come at a sacrifice of detection speed, since it calculates an average of past values and would cause the effect of the sample at the start of fault conditions to be lower. However, since the parameter chose for lambda was low (0.1), the EWMA chart gave a much higher weight to more recent values.

Figure 6-13 indicates that KPCA gave higher AUCs than PCA in most cases. However, the DDs are very high, of the order of ten hours in some cases.

If the CUSUM results are ignored, both T_A^2 and SPE gave good results, in most cases the T_A^2 gave better results. This is because the cooling coil blockage fault changes the energy balance in the process. This means that the way the temperatures respond to changes in flow rates, for example, is different, because it will take longer for the controller to return the temperature to its set-point after some deviation. The SPE will also show good detection because some of the relationships in the process are still the same, but the system responds differently to changes in temperatures.

6.6. Fault Identification in Leaching Simulation

In section 6.5 the fault detection results were discussed. Following these results, the results of applying fault identification, either by considering the change in topology from NOC to fault conditions or considering contributions plots for the PCA SPE, are presented in this section. The results are shown for the unblocked case but also for the blocked cases, where the block that displayed the best detection results is used to further investigate the fault conditions.

6.6.1. Fault identification of preparation tank blockage fault

Table 6-11 displays the summary of the results for the different fault identification methods for the first fault. A "yes" indicates that the method was able to identify nodes that were representative of the fault, a "no" indicates that it did not, while a "maybe" indicates that it identified suitable nodes, but also some spurious ones. For this fault when the following variables were identified as possible root nodes it was considered to be a good indication that a blockage fault upstream of the autoclave had occurred: MFR5, MTK10, MFR1, MFR7 and MTK20. A detailed analysis of each fault identification result is given in the Appendix C.

From the results shown in Table 6-11, it can be seen that using LC gave the best results for identifying symptoms, since it gave reasonable symptoms for PCA and KPCA, using contributions as well as connectivity change. Recall from section 6.5.2 for the blocks obtained from the LC graph, block 3 gave the best detection results, and this block was strongly associated with the flash recycle tank downstream from the blockage in stream 5. This illustrates that combining topology information for blocking of the variables with feature extraction already improves fault identification. Further incorporation of topology for identifying symptom nodes and tracing the fault back in the connectivity graph then improves the fault identification even further.

Table 6-11: Summary of fault identification results for preparation tank blockage fault in the leaching simulation

TEM	PPM	FEM	FIM	Symptom	Root
LC	Unblocked	NA	Contributions	Yes	Maybe
			Connectivity Change	Yes	No
	Blocked	PCA	Contributions	Yes	Maybe
			Connectivity Change	Yes	Yes
		KPCA	Connectivity Change	Yes	Yes
PC	Unblocked	NA	Contributions	Yes	Yes
			Connectivity Change	Maybe	Yes
	Blocked	PCA	Contributions	Maybe	Yes
		KPCA	Connectivity Change	No	No
			Connectivity Change	Yes	Yes
TE	Unblocked	NA	Contributions	Yes	No
			Connectivity Change	No	No
	Blocked	PCA	Contributions	Yes	Yes
			Connectivity Change	Maybe	Yes
		KPCA	Connectivity Change	Maybe	Yes

Table 6-11 shows that the TE graph also gave good fault identification results for the blocked case.

Table 6-11 shows that the PC graph gave inaccurate fault identification results in general. This is because the connectivity map generated was highly connected, resulting in a large number of

possible paths to a large number of possible root nodes. In addition, applying blocking to the PC graph did not result in a separation of blocks that would aid fault identification; two large blocks resulted, so applying fault detection in either of them did not narrow down the possible root cause

The results presented in Table 6-11 indicate that in general, connectivity change showed better results once blocking had been applied. The results also show that contributions gave more accurate symptom nodes for most methods, allowing better tracing back to root nodes.

6.6.2. Fault identification of preparation tank blockage using linear cross-correlation

Since it was observed in section 6.6.1 that LC gave the best identification results, these results are presented in this section.

Fault identification using linear cross-correlation with unblocked contributions

Contributions of each variable to the PCA SPE in the unblocked case are plotted in Figure 6-14. Variables whose contributions rose above the contribution from the validation data, i.e. those that rose above the dashed red line are taken to be symptom nodes.

The unblocked contribution plot shown in Figure 6-14 indicates that MFR1, MFR5, MFR13 and MTK10 displayed large contributions. This is consistent with the blockage fault, since the blockage would restrict MFR5, causing MTK10 to deviate from its set-point. Subsequently the level controller would vary MFR1 to correct for this deviation.

https://www.youtube.com/watch?v=mXw3jy99w78

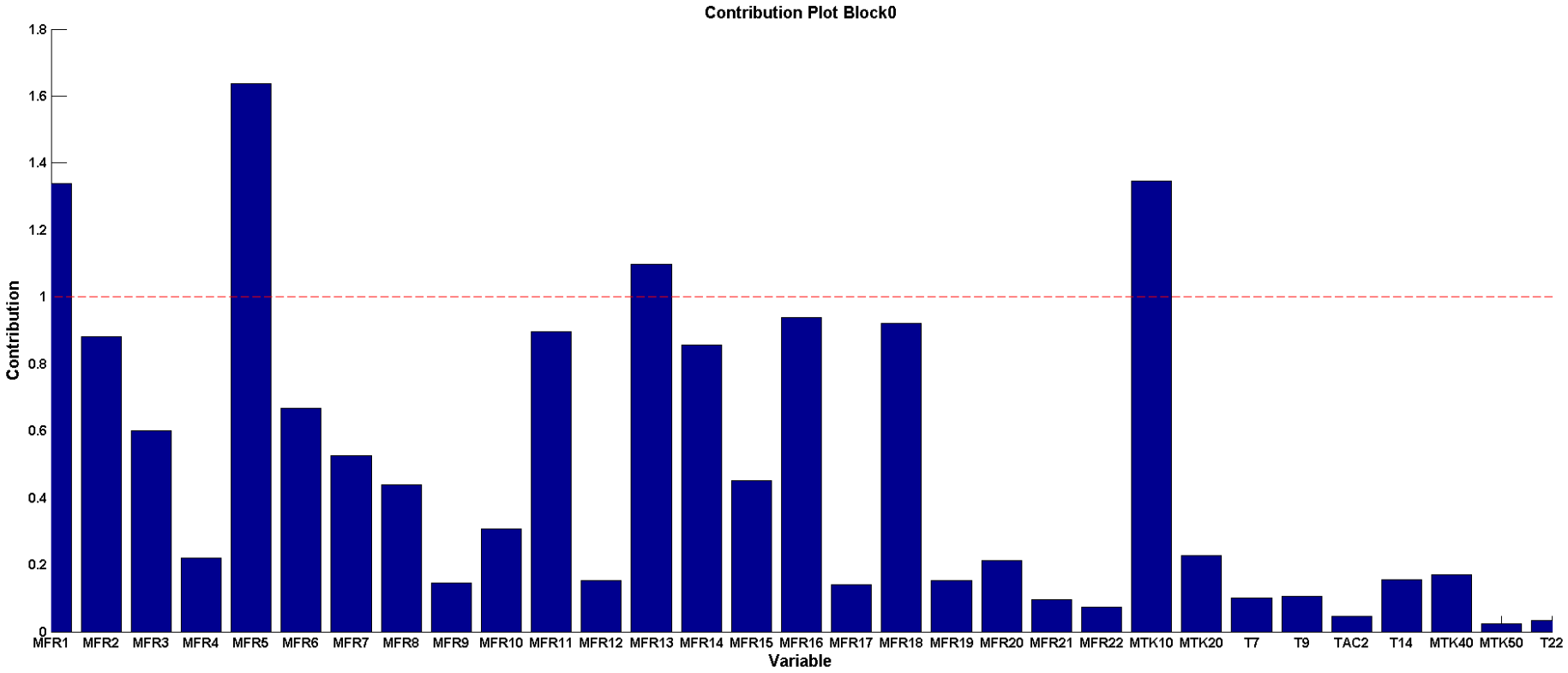

Figure 6-14: Contribution plot for PCA SPE for unblocked data for preparation tank blockage fault

Applying back propagation in the unblocked LC graph from the symptoms identified by contributions plot gives MFR15, T9 and MFR 14 as possible root nodes, as shown in Figure 6-15. It seems that the symptom nodes gave a better indication of the fault conditions. However, as noted earlier, this system's flow rate and temperatures are very sensitive to changes in the flash recycle tank, which cause T9 and MFR9 to fluctuate. Therefore the identified root nodes may be indicative of the fault conditions.

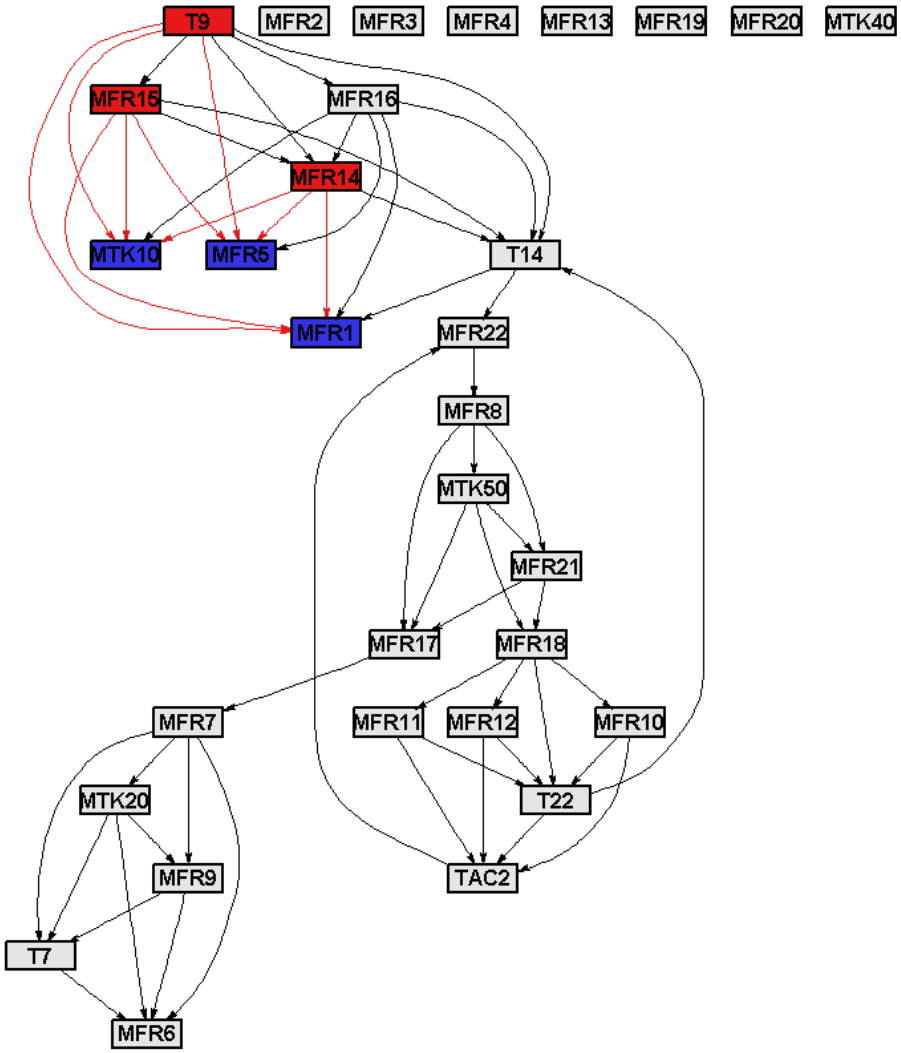

Figure 6-15: Back propagation in the unblocked linear cross-correlation connectivity graph using the symptoms identified from contributions (shown in blue). Possible identified root nodes and propagation paths are shown in red

Fault identification with linear cross-correlation using blocked contributions

The contribution plot for the LC block that showed the best detection results is given in Figure 6-16. This resulted in MFR7 and MFR17 showing increased contributions. Since MFR7 is directly downstream of the blockage, this gives a good indication of the fault conditions. The contribution of MFR17 also indicates that the blockage has a profound effect on downstream flow rates, which is

most likely due to the numerous control loops in the process; a blockage right at the start of the process causes all the flow rates to deviate from their set-points, causing each controller to take aggressive control action which causes the fault to propagate downstream.

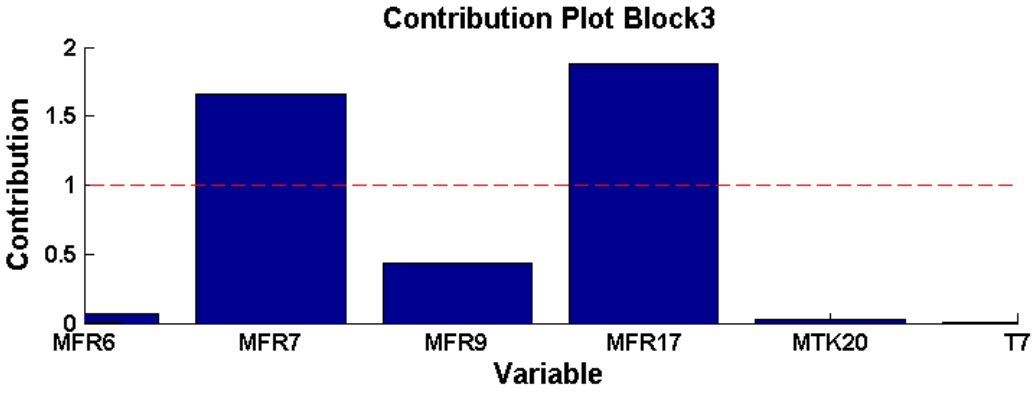

Figure 6-16: Contribution plot for Block 3 from linearcross-correlation

Applying back propagation in the blocked LC graph from the symptoms identified by contributions in this block results in MFR7 being identified as a possible root node, as shown in Figure 6-17. Since this is directly downstream of the blockage, this is a very accurate indication of the fault conditions

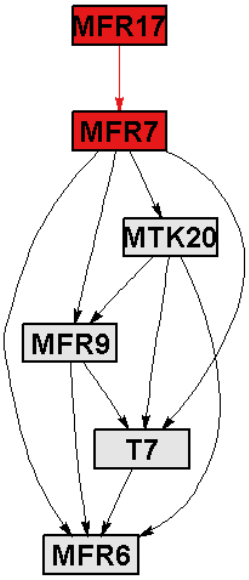

Figure 6-17: Back propagation in linear cross-correlation graph for block 3 using the symptoms identified from contributions. Possible identified root nodes and propagation paths are shown in red

Fault identification with linear cross-correlation using unblocked connectivity changed

Considering the connectivity change in the unblocked LC graph (shown in Figure 6-18), many symptom nodes were identified, including MFR1, MFR5 and MTK10, which gives a good indication that a blockage has occurred.

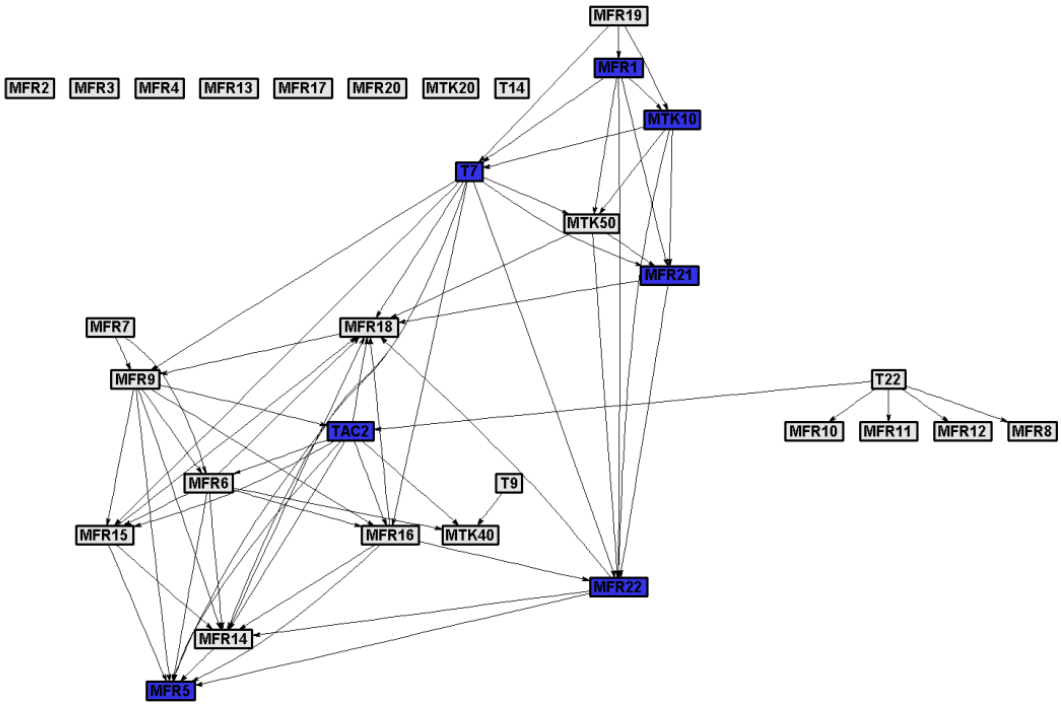

Figure 6-18: Fault conditions linear cross-correlation connectivity for preparation tank blockage fault, showing symptom nodes (highlighted in blue) identified from connectivity change

Applying back propagation in the unblocked connectivity graph from these symptoms did not result any root nodes being identified, as shown in Figure 6-19. Therefore no further fault identification information was revealed. This unsuccessful back propagation is due to the large amount of symptom nodes; no common ancestors could be identified.

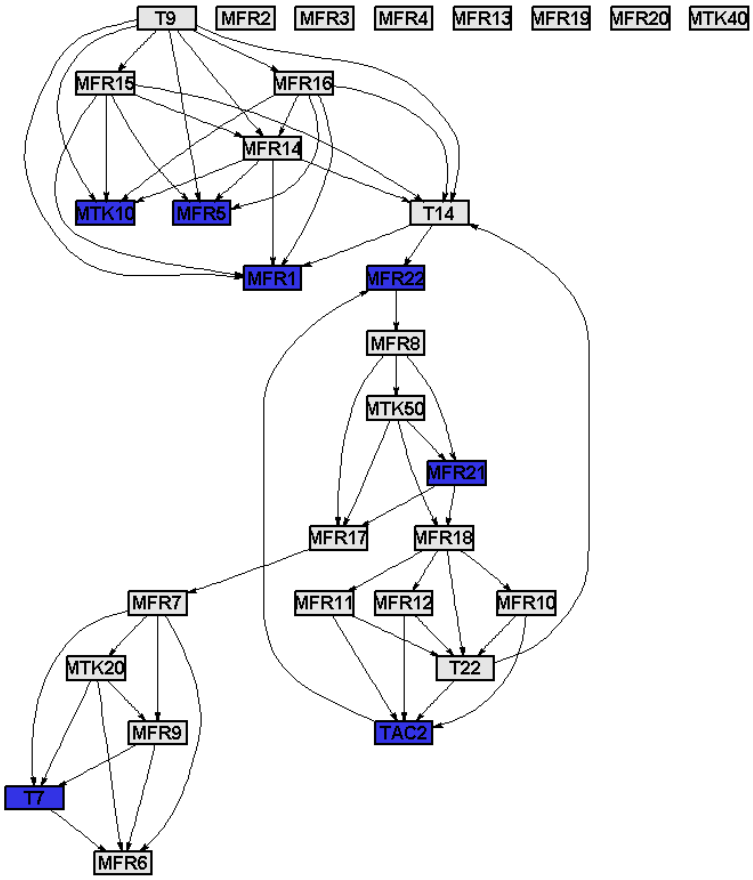

Figure 6-19: Back propagation in the unblocked linear cross-correlation graph using the symptoms (highlighted in blue) identified by connectivity change

Fault identification with linear cross-correlation using blocked connectivity change

Since KCPA and PCA both showed the best results for block 3 the connectivity change results are the same for both. Considering the change in LC from NOC to fault conditions (shown in Figure 6-20) in the block that gave the best results for PCA and KPCA, T7 were identified as symptom nodes and MFR7. This gives a very good indication that a blockage upstream of the recycle tank occurred, since it would strongly affect MFR7 and subsequently the temperatures in the tank.

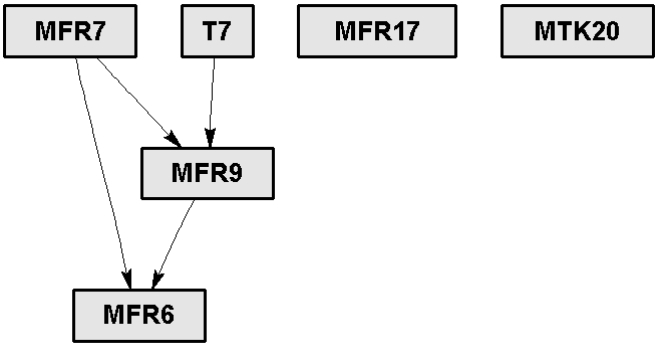

Figure 6-20: Fault conditions linear cross-correlation connectivity for block 3 for preparation tank blockage

MFR7, MTK20 and MFR9 were identified as possible roots using back propagation in the LC graph for block 3, as shown in Figure 6-21. This gives a very good indication of the fault conditions since this affects the tank directly downstream form the blockage.

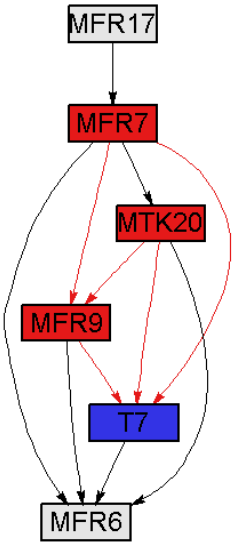

Figure 6-21: Back propagation applied to the linear cross-correlation graph for block 3 using symptoms identified from connectivity change (in blue). Possible root nodes and propagation paths are shown in red

6.6.3. Fault identification for cooling coil fault

Table 6-12 displays the summary of the results for the different fault identification methods for the first fault. A "yes" indicates that the method was able to identify nodes that were representative of the fault, a "no" indicates that it did not, while a "maybe" indicates that it identified suitable nodes, but also some spurious ones. For this fault when the following variables were identified as possible root nodes it was considered to be a good indication that a temperature fault in the autoclave has occurred: T14, TAC2, since these are the temperatures in the autoclave compartments where the fault occurred. T22 since it is a downstream temperature. T9 would also be a good indicator that this was a fouling fault. Firstly the temperature in the first compartment can be affected by the temperatures in the other compartments because of the vapour stream exiting through it; secondly, it is a temperature directly upstream of where the cooling coil fault occurred, so if it was a root node it would indicate that something directly upstream of where the cooling coil might occur was the root cause (not necessarily T9, but in this case we don't have the flow rate of the cooling coils). Also MFR6 and MFR8 would be reasonably accurate symptom nodes since the temperature in the autoclave greatly affects the vapour space, which would affect MFR8 and MFR6. Additionally the temperature in one compartment would affect most of the compartments, so the 1st compartment's temperature would change, resulting in MFR9 to be varied to compensate for this and this would greatly affect MFR6 since some of the liquid in stream 9 evaporates and exits through stream 6.

The results shown in Table 6-12 indicate that using the TE graph for fault identification gave good results, with symptoms and possible root nodes that gave a good indication of the fault conditions. Recall from section 6.5.3 that when PCA and KPCA were applied to the blocks obtained from the TE graph, the best detection results were obtained for block 1. This block contains, amongst others, the temperatures and flow rates around the first 3 autoclave compartments, including T9, TAC2 and T14 and MFR 14.

It appears that connectivity change for TE graphs consistently gave good results.

The PC graph gave the worst results. This is again due to the fact that the connectivity graph obtained was too complex, with too many spurious connections between variables. Additionally, blocking using PC did not provide useful information with regards to narrowing down the variables in the blocks that gave the best detection, since the blocks obtained were large and not representative of physical units in the process.

Table 6-12: Summary of fault identification results for cooling coil fault in the leaching simulation

TEM	PPM	FEM	FIM	Symptom	Root
LC	Unblocked	NA	Contributions	Yes	Yes
			Connectivity Change	No	No
	Blocked	PCA	Contributions	Maybe	No
			Connectivity Change	No	No
		KPCA	Connectivity Change	Yes	No
PC	Unblocked	NA	Contributions	Yes	No
			Connectivity Change	Yes	Maybe
	Blocked	PCA	Contributions	Maybe	No
		KPCA	Connectivity Change	Maybe	Maybe
			Connectivity Change	No	No
TE	Unblocked	NA	Contributions	Yes	Yes
			Connectivity Change	Yes	Yes
	Blocked	PCA	Contributions	Yes	No
			Connectivity Change	Yes	Yes
		KPCA	Connectivity Change	Yes	Yes

6.6.4. Fault identification for cooling coil blockage using transfer entropy

Since the TE method gave the best identification results, as seen in Table 6-12, the fault identification using this method is presented in this section.

Fault identification with transfer entropy using unblocked contributions

The contribution plot for PCA SPE of the second fault for the unblocked data is shown in Figure 6-22.

https://www.youtube.com/watch?v=mXw3jy99w78

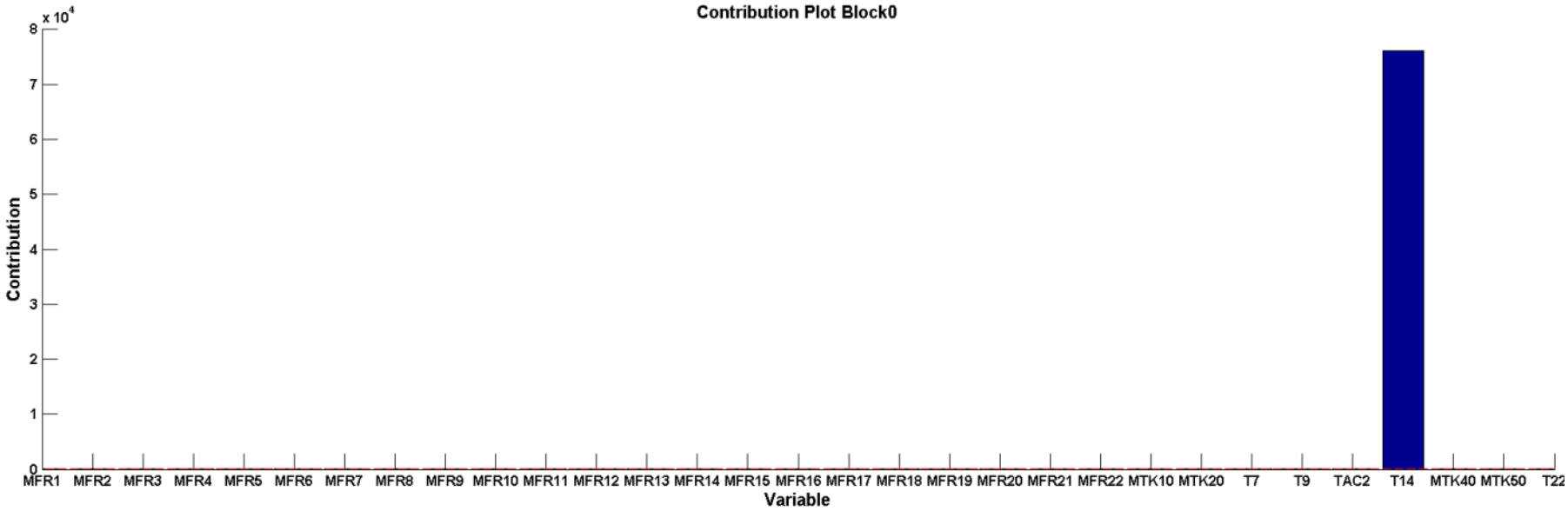

Figure 6-22: Contribution plot for PCA SPE for cooling coil fault

The contribution plot in Figure 6-22 identified T14, MTK40 and T9 as symptom nodes. These variables provide a very good indication that a temperature fault in the autoclave has occurred since T14 and T9 have been highlighted. The contribution of T14 relative to the validation SPE is very large, indicating that the fault that occurred had a profound influence on this variable. In the NOC data on which the PCA model was constructed the measured values for T14 stayed relatively constant, with common cause variation and slight changes when the controller responded to a change in temperature. When the new data was projected onto this model it failed to predict the large upset in the temperature, thereby resulting in such a large change in the SPE for this variable.

Using these variables as symptom nodes, back propagation was applied to the unblocked TE connectivity graph, as shown in Figure 6-23.

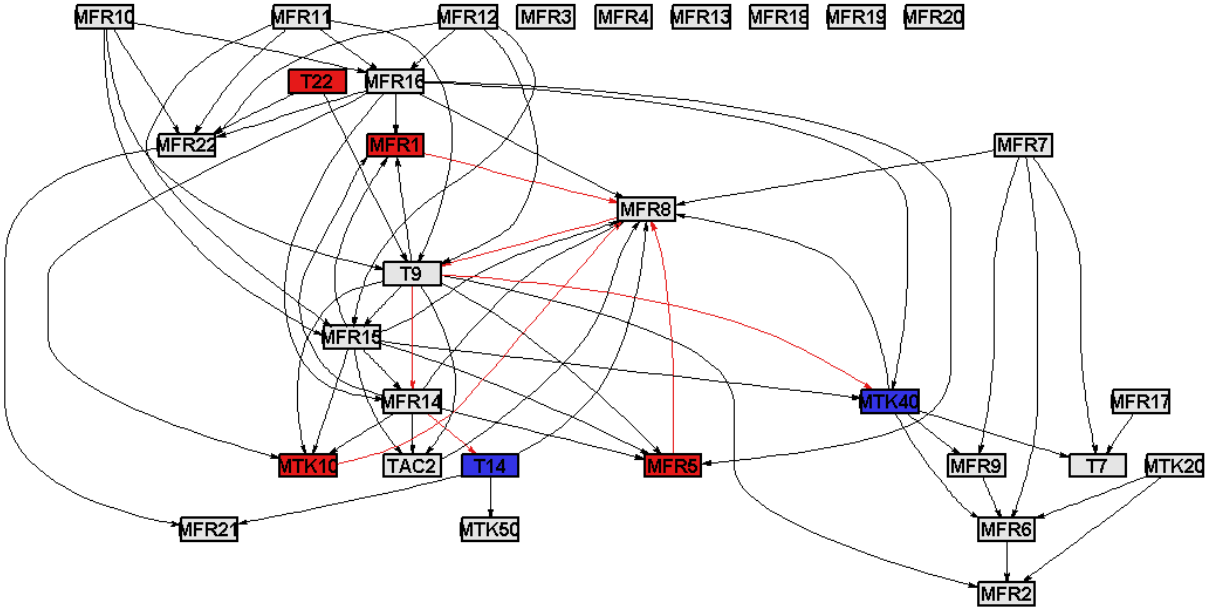

Figure 6-23: Back propagation using the unblocked transfer entropy graph with symptoms from the contributions (in blue). Possible root nodes and propagation paths identified are shown in red

The main root node identified was T22, which gives a good indication that a cooling coil fault occurred. Unfortunately it also identified MFR1, MFR5 and MTK10 as possible root nodes, which complicates the result. Considering the combination of the identified symptoms and the fact that T22 was identified as a possible root node, however, it can be concluded that the symptoms gave a good indication of the cause of the fault and so did the identified roots.

Fault identification with transfer entropy using unblocked connectivity change

Comparing the TE connectivity graph obtained from NOC data with that obtained from the fault data, it was found that the nodes that showed the most change in connectivity were MFR2, MFR6, MFR8, T9, TAC2 and MTK40. The connectivity graph generated from the fault data is shown in Figure 6-24.

MFR2 and MTK40 are not really representative of the fault, but MFR6 and MFR8 would be affected by a temperature fault within the autoclave since the temperature affects its vapour space greatly, which changes MFR8 and MFR6 and also it would change MFR9 which would greatly affect MFR6. Additionally, T9 and TAC2 were identified which directly points to a temperature fault in the autoclave.

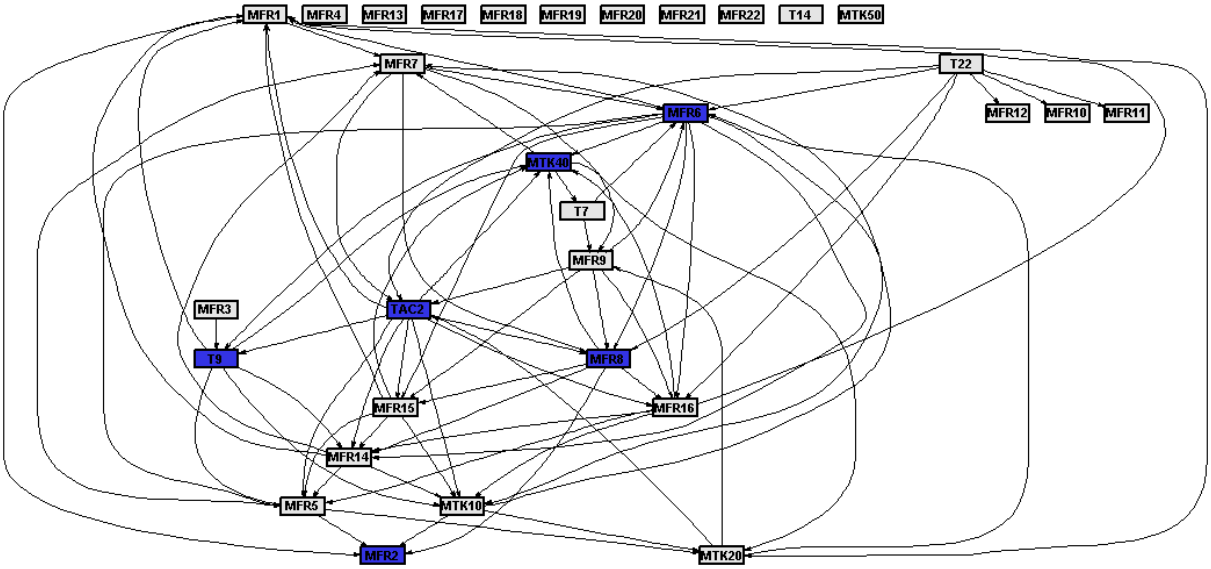

Figure 6-24: Fault conditions transfer entropy connectivity graph for cooling coil fault. Symtpoms identified from connectivity change are highlihgted in blue

Applying back propagation in the training connectivity graph from these fault nodes resulted in T22 being identified as a possible root node, as shown in Figure 6-25. This result, along with the symptoms identified, gives a very good indication that a temperature fault has occurred, which points to a cooling coil fault. So this method identified the symptoms very well and traced these symptoms back to an accurate root cause.

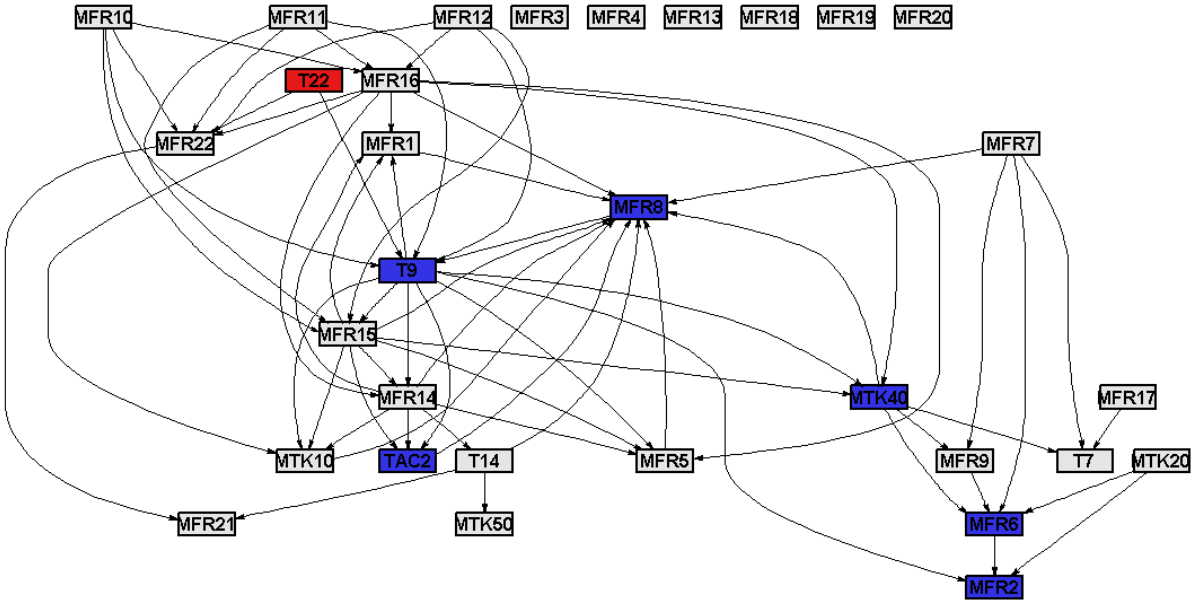

Figure 6-25: Back propagation in the unblocked transfer entropy graph using the symptoms identified by connectivity change (in blue). Possible root nodes and propagation paths identified are shown in red

Fault identification with transfer entropy using blocked using contributions

PCA gave the best detection results for the first block of the TE graph. The contribution plot in this block, shown in Figure 6-26, identified T9, TAC2, T14, MFR5 and MTK40 as possible symptom nodes. Since the blockage in the cooling coils would disrupt the autoclave temperatures, T9, TAC2 and T14 would all be affected. This result provides a very good indication that a temperature fault in the autoclave has occurred, since the temperatures in the autoclave displayed symptoms of the fault. The large contribution of MFR5 and MTK40 is likely due to the fact that variation in these variables previously would have caused variations in the temperatures in NOC data. However, under fault conditions, the change in the temperatures was as a result of the fault, and not these variables, therefore their covariance with the temperatures changed and they displayed large contributions.

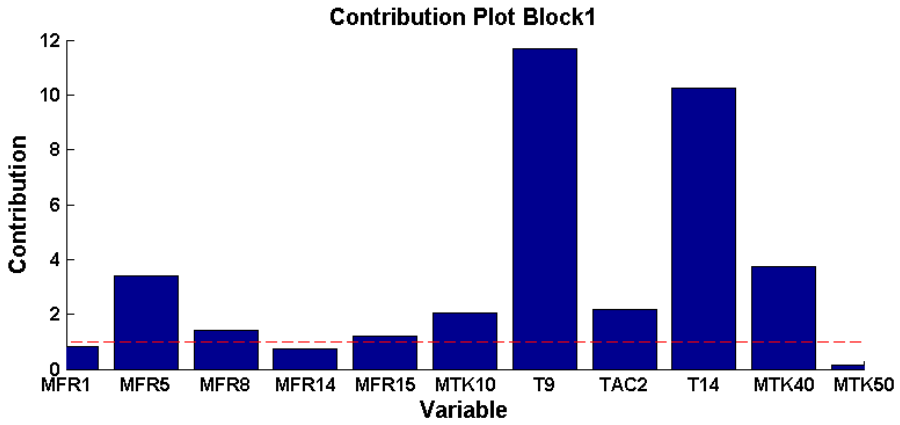

Figure 6-26: Contribution plot for the cooling coil fault in the transfer entropy blocking method's first block

Applying back propagation with TE in this block gives MFR1, MFR5 and MTK10 as possible root nodes, as shown in Figure 6-27. These root nodes give no indication of a temperature fault. However, if MFR1, MTK10 and MFR5 were not direct ancestors of MFR8 the back propagation would have identified MFR8 as a possible root node, which would have been more indicative of the fault being associated with the temperatures in the autoclave. Therefore in this case it can be concluded that the symptoms gave a good indication of the fault, but the roots did not.

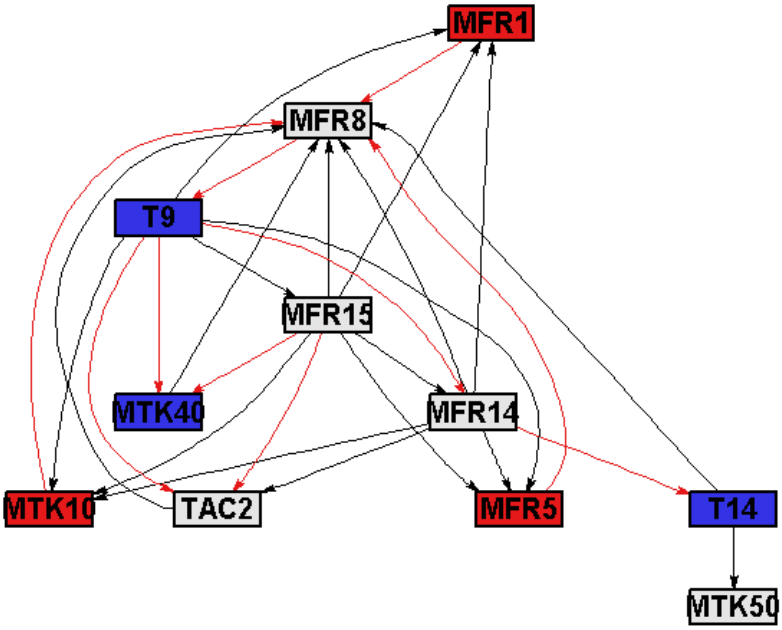

Figure 6-27: Back propagation in the blocked transfer entropy graph using the symptoms identified by contributions (in blue). Possible root nodes and propagation paths identified are shown in red

Fault identification with transfer entropy using blocked connectivity change

Considering the change in the TE connectivity graphs from NOC to fault conditions resulted in TAC2 and MTK40 being identified as possible symptoms, as shown in Figure 6-28. Since TAC2 is present it gives a good indication that a temperature fault in the autoclave has occurred; the causality between this temperature and the other variables would change. Considering the variable T14, it is also clear that this variable experienced a large amount of changes in its connections.

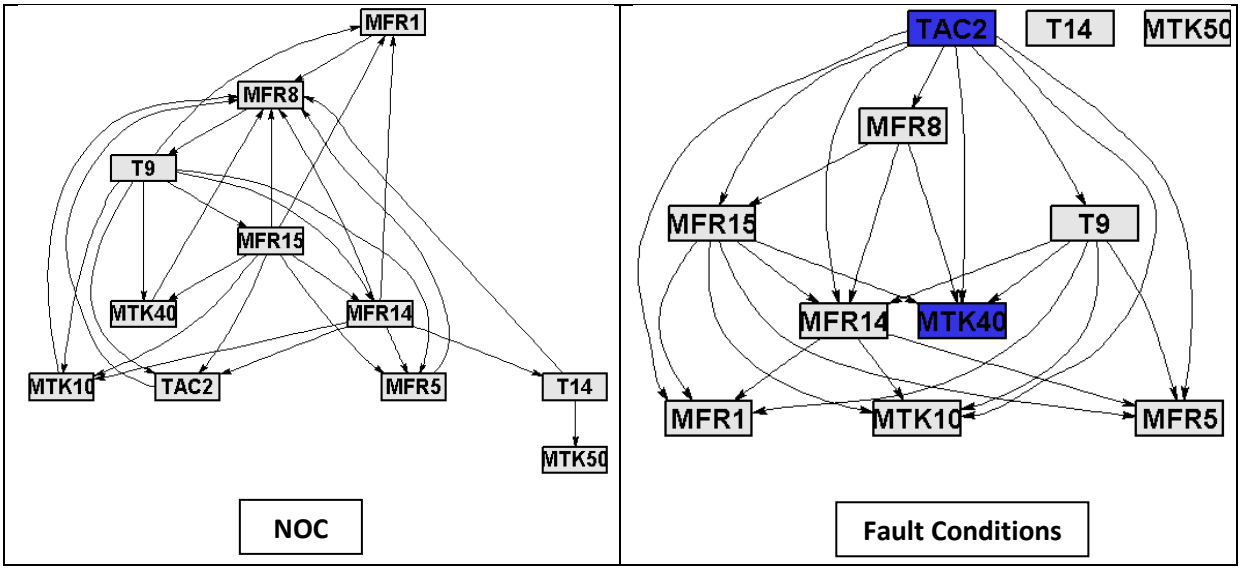

Figure 6-28: Change in transfer entropy connectivity from NOC to fault conditions for cooling coil fault. Symptoms identified are highlighted in blue

Applying back propagation in the training TE graph for block 1 gives T9 and MFR15 as possible root nodes, as shown in Figure 6-29. Since T9 is identified it is a good indication that a temperature fault in the cooling coils has occurred, so this method gave good indications of symptom nodes and root nodes that point to a fault in the autoclave temperatures.

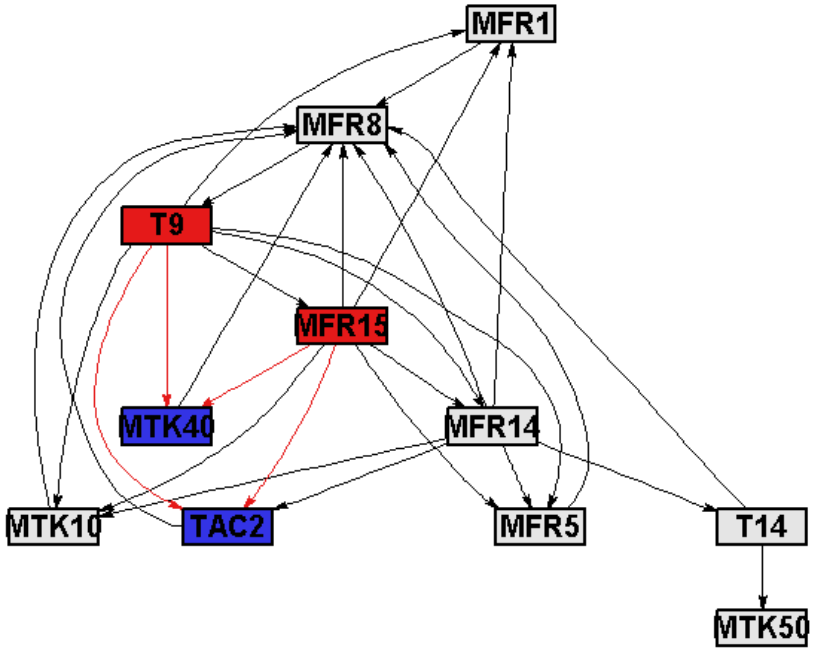

Figure 6-29: Back propagation in the blocked transfer entropy graph using the symptoms identified by connectivity change (in blue). Possible root nodes and propagation paths identified are shown in red

6.7. Summary of Results of Fault Diagnosis in Leaching Simulation

The main results of application of the fault diagnosis methods to the leaching simulation case study already discussed are repeated here to provide a summary of the most important results. Conclusions drawn from these results are presented in Chapter 8 -.

6.7.1. Topology extraction from historical process data

It was observed that of the three TEM, LC and TE resulted in the most accurate connectivity graphs; providing an accurate representation of the physical relations between variables in the process. However, all three graphs showed some spurious connections that may confound the results of the fault identification methods applied using these connectivity graphs. It was observed that the significance thresholds defined for LC and PC using the method described in chapter 4 resulted in thresholds that were too lax and resulted in a large number of spurious connections. These thresholds had to be increased to extract a useful connectivity graph. The method used to choose new thresholds for these graphs provided good results for LC, but poor results for PC; with the PC graph being very convoluted and containing a large number of spurious connections. It was observed that using historical process data to extract process topology provided useful insight into the nature of the process; revealing strong interaction that were not intuitively apparent from process knowledge.

6.7.2. Blocking of process using topology

Using the connectivity graphs for dividing the process into separate blocks worked well for this case study. The blocks obtained for the LC and TE graphs represented the physical process units well; i.e. variables associated with individual units tended to be grouped together into the same blocks. For PC, this was true to some extent, but not as much as for LC and TE. The reason for this is that the PC graph was too convoluted, with too many connections. Therefore the connectivity graph had one very large strongly connected component and just one weakly connected component with a few variables. For all three methods, the most strongly connected component always contained variables associated with the autoclave itself. This provides useful insight into the behaviour of the process since it indicates that there is a large degree of interconnectivity caused by the recycle and control loops associated with the autoclave.

6.7.3. Fault detection using feature extraction

Principal components analysis vs. kernel principal components analysis

For the preparation tank blockage fault, KPCA showed worse results for the unblocked data, giving lower AUCs and larger DDs. However, similar results were obtained for PCA and KPCA in terms of

AUCs and DDs in most cases for the blocked data. For the cooling coil fault KPCA and PCA showed similar AUCs in all cases, but with KPCA showing larger DDs.

Monitoring charts

For both faults the EWMA monitoring chart showed very good detection ability in comparison to the other monitoring charts. It gave larger AUCs than the Shewhart chart, without an increase in the detection delay. And while in some cases it gave slightly lower AUCs than the CUSUM charts, it gave much lower DDs.

Improvement of fault detection with blocking

In most cases for both faults, blocking resulted improvement in the detection performance, with higher AUCs and lower DDs. Additionally, in all cases, the block that gave the best detection results contained variables that would be affected by the fault. This indicates that blocking provided useful information for fault identification.

6.7.4. Fault identification using topology

Symptom node identification using contributions vs. using connectivity change

For fault identification, in some cases the connectivity change resulted in sensible symptom nodes that gave a good indication of the fault, while in other cases it didn't. The ability to provide sensible symptoms is strongly dependent on the accuracy of the connectivity graph.

The contribution plots provided more consistent results in most cases, especially once fault detection had identified the block which gave the best detection results.

Back propagation using connectivity graphs

Back propagation in the LC graph gave the best results for the preparation tank blockage fault, while TE gave the best results for the cooling coil fault. Once again this is strongly dependent on the accuracy of the connectivity graph, and is also dependent on the contributions or connectivity change to identify symptom nodes.

Chapter 7 - Case Study: Fault Diagnosis Applied to Concentrator Process

This chapter presents the results of application of the fault diagnosis methods to a case study of a concentrator in a minerals processing plant.

7.1. Concentrator Case Study Description

The third case study considered for the testing of the fault diagnosis methodology presented in this thesis consists of real data from a minerals processing concentrator plant. The details of the process and the data are considered confidential; therefore any time series plots presented are scaled.

The fact that the data for this case study comes from a real process makes it ideal to determine whether the methodology would perform well in real-life application. The data set is interesting because the plant data is affected by numerous external factors, such as operators making changes to the process.

7.1.1. Overall process description

The process under consideration is concentrator in a minerals processing plant. The case study was used by Groenewald (2014) for the testing of a process performance monitoring methodology for mineral processing plants as part of a doctoral thesis.

A diagram of the process is provided in Figure 7-1. The process consists of three grinding circuits operating in conjunction with their flotation circuits. The feed to the process (stream 1) is first sent ta primary milling circuit (Mill1) for size reduction, and subsequently to a cyclone for classification. The cyclone overflow (stream 3) is sent to the primary floatation cell. The tails from this floatation process (stream 4) is sent to two milling circuits in parallel (Mill2 and Mill3) for further size reduction. The underflow of the cyclone (stream 6) is also sent to a milling circuit (Mill4) for further size reduction, and then to a flash floatation process. The tails from this floatation process and the outlet from the parallel milling circuit are combined (stream 5) and sent to another floatation process, with the tails from this process (stream 10) representing the final tails of the entire concentrator process.

The concentrate from the primary floatation as well as that of the flash floatation are also combined (stream 8) and sent to the secondary floatation process. The concentrate from this floatation and that of the scavenger floatation combined form the final concentrate stream of this process.

https://www.youtube.com/watch?v=mXw3jy99w78

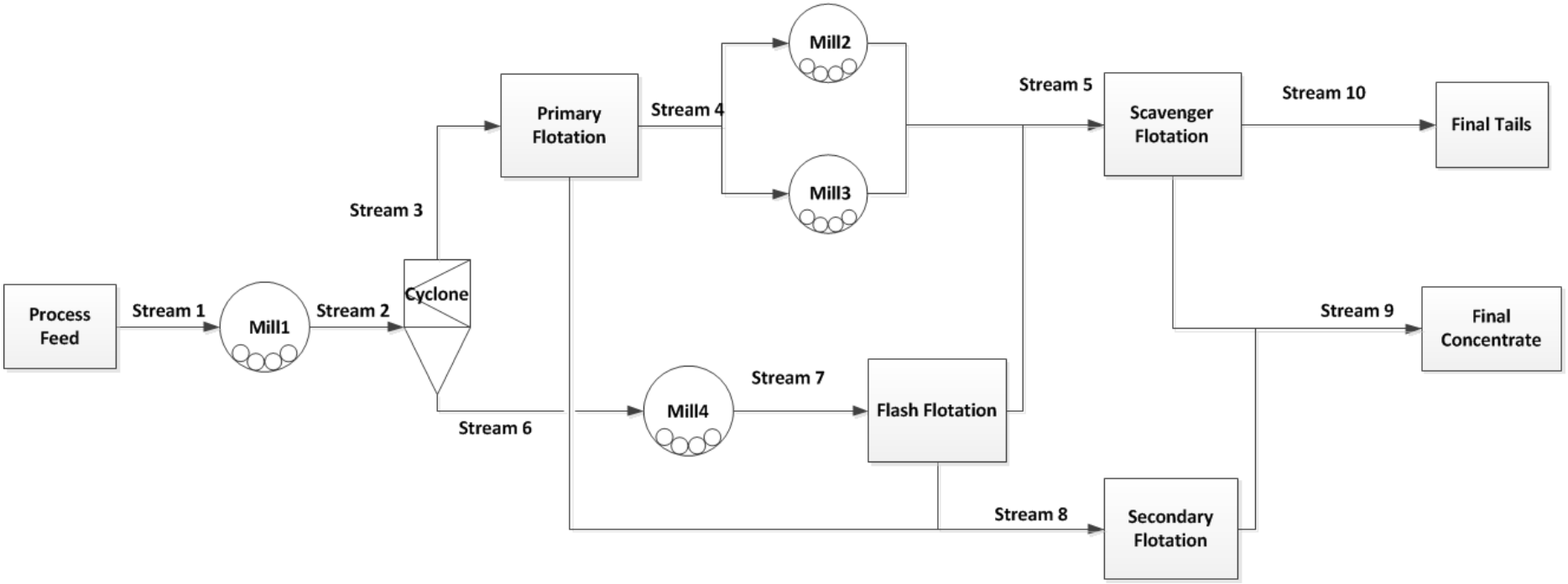

Figure 7-1: Diagram of concentrator process

7.2. Data from Concentrator Case Study

Table 7-1 contains a summary of the sizes of the data sets used for fault diagnosis of the concentrator.

Table 7-1: Summary of data set sizes or concentrator

Data Set	Number of samples (N)	Number of variables (M)
Training	150	56
Validation	60	56
NOC Test	60	56
Fault Test	233	56

7.2.1. List of variables

A list of the measured variables used for monitoring of this process is given in Table 7-2.

Table 7-2: List of variables in concentrator data

Variable No.	Variable Name	Description
1	FeedGrade	Grade of the feed stream to the process
2	FeedFlow	Flow rate of the feed stream to the process
3	FtailGrade	Final tailings grade
4	FTail+425	Final tails particle size distribution (PSD)
5	FTail+300	
6	FTail+150	
7	FTail+106	
8	FTail+75	
9	FTail+45	
10	FTail+38	
11	FTail-38	
12	FTail-45	
13	FTail-75	
14	FTail-106	
15	FTail-150	
16	FTail-300	
17	FTail-425	
18	Masspull	Proportion of feed to floatation cell reporting to concentrate
19	ConcGrade	Final concentrate grade
20	Recovery	Final recovery of mineral
21	Mill23-38	PSD of stream exiting parallel milling circuit (Mill2 and Mill3)
22	Mill23-45	
23	Mill23-75	
24	Mill23-106	
25	Mill23-150	
26	Mill23-300	
27	Mill23-425	
28	FFloat-38	PSD of flash floatation tails
29	FFloat-45	
30	FFloat-75	
31	FFloat-106	

Variable No.	Variable Name	Description
32	FFloat-150	PSD of flash floatation tails
33	FFloat-300	
34	FFloat-425	
35	FFloatGrade	Flash floatation tails Grade
36	MassSplit	Ratio of desired material in overflow and underflow
37	Mill23Grade	Grade of stream exiting parallel milling circuits (Mill2 and Mill3)
38	Mill2Power	Mill2's power
39	Mill3Power	Mill3's power
40	Mill2Stops	Stops for Mill2
41	Mill3Stops	Stops for Mill3
42	Mill2Avail	Availability of Mill2
43	Mill3Avail	Availability of Mill3
44	Split2	d50 particle size of cyclone classification
45	PTail-38	Primary Flotation tails PSD
46	PTail-75	
47	PTail+15	
48	Mill23-38contr	Parallel milling circuits (Mill2 and Mill3) PSD
49	Mill23-75contr	
50	CyclFlow	Feed flow rate to cyclone
51	CyclDens	Density of feed to cyclone
52	CyclPress	Operating pressure of cyclone
53	Mill1Power	Primary mill's power
54	Mill1Load	Primary mill's load
55	Mill1Feedrate	Primary mill's feed rate
56	Mill1H2ORatio	Primary mill inlet water ratio

7.2.2. Description of fault conditions

The challenge posed by this case study is that the origin of the fault is unknown, and therefore the root cause analysis results obtained will give a good indication of the performance of the fault diagnosis methods considered in this project to an unknown fault. The known details of the fault are that the recovery was observed to decrease over time. Previous fault diagnosis work performed by Groenewald (2014) on this case study found that changes to the primary mill inputs (mill inlet water ratio decreasing and feed rate increasing) resulted in changes to the feed to the cyclone, causing the cyclone to underperform in its classification. This then affected the performance of Mill2 and Mill; evidenced by the increase of their measured power, throughput and particle size distribution (PSD). This change in the milling ultimately caused the final tails grade to increase and the final tail PSD to coarsen. This illustrates clearly that a fault in a process can propagate downstream and affect a large number of variables.

7.2.3. Data reconstruction

The data contained a significant amount of missing values. For example Figure 7-2 shows the trend for the recovery, illustrating the gaps in the data.

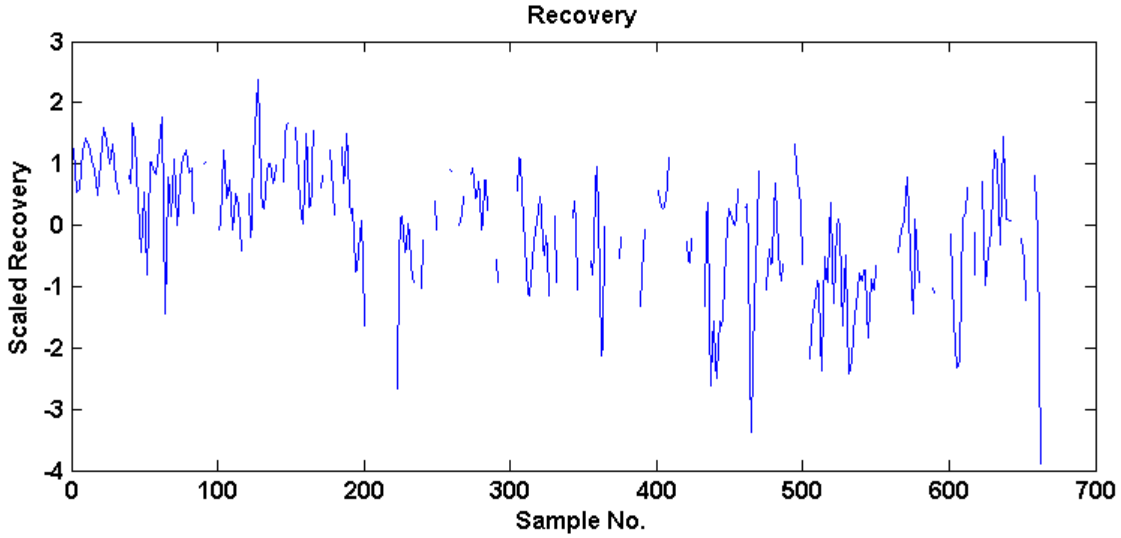

Figure 7-2: Recovery trend from concentrator showing missing data

Missing value reconstruction had to be performed, using the method described in section 4.8, in order to use this data. Figure 7-3 shows the same trend displayed in Figure 7-2 after reconstruction using PCA.

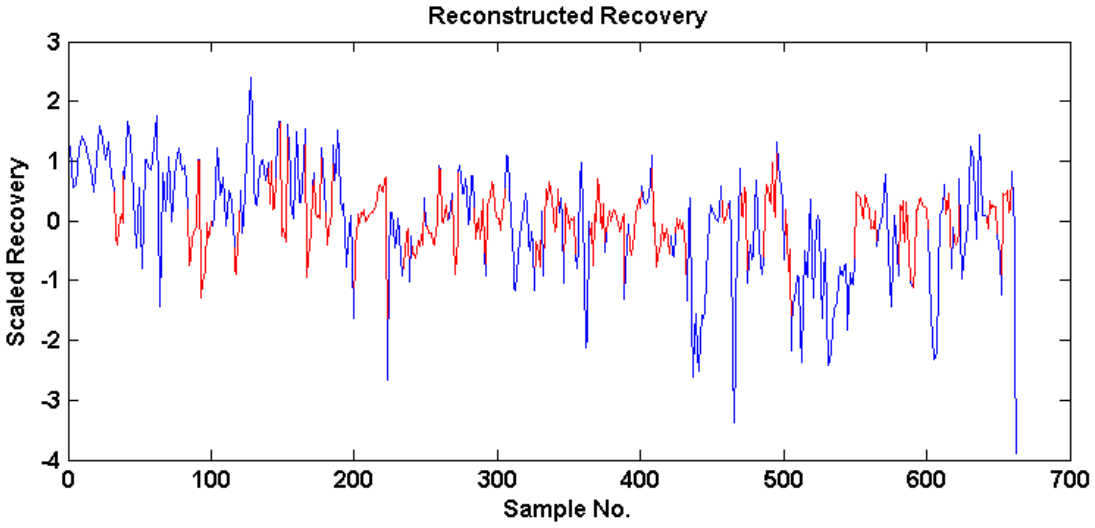

Figure 7-3: Recovery trend from concentrator after data reconstruction. Blue indicates original data, red is reconstructed data

7.3. Topology Extraction from Concentrator Data

This section presents the results of the topology extraction methods applied to the concentrator data. Each method's resulting connectivity graph is shown and the validity of each observed connection is discussed.

7.3.1. Topology generated from process knowledge

Groenewald (2014) provided a thorough hierarchical representation of the causality of each unit in this process from process knowledge. The basic causality maps for individual units generated by Groenewald are shown in Figure 7-4, Figure 7-5 and Figure 7-6. The general causality map focusing on the final tails grade is given in Figure 7-7. For any of the mills, the PSD of the mill product is a function of it power, load and the density of the contents. All these are determined by the throughput, the inlet water ratio, and the feed PSD. For the cyclone it's mass split and cut-point are affected by the feed PSD and pressure, which are determined by the feed flow rate and feed density. For the flotation cells, the recovery and grade are functions of the mass pull, the feed and the reagents. The feed is in turn affected by the density, flow rate and PSD.

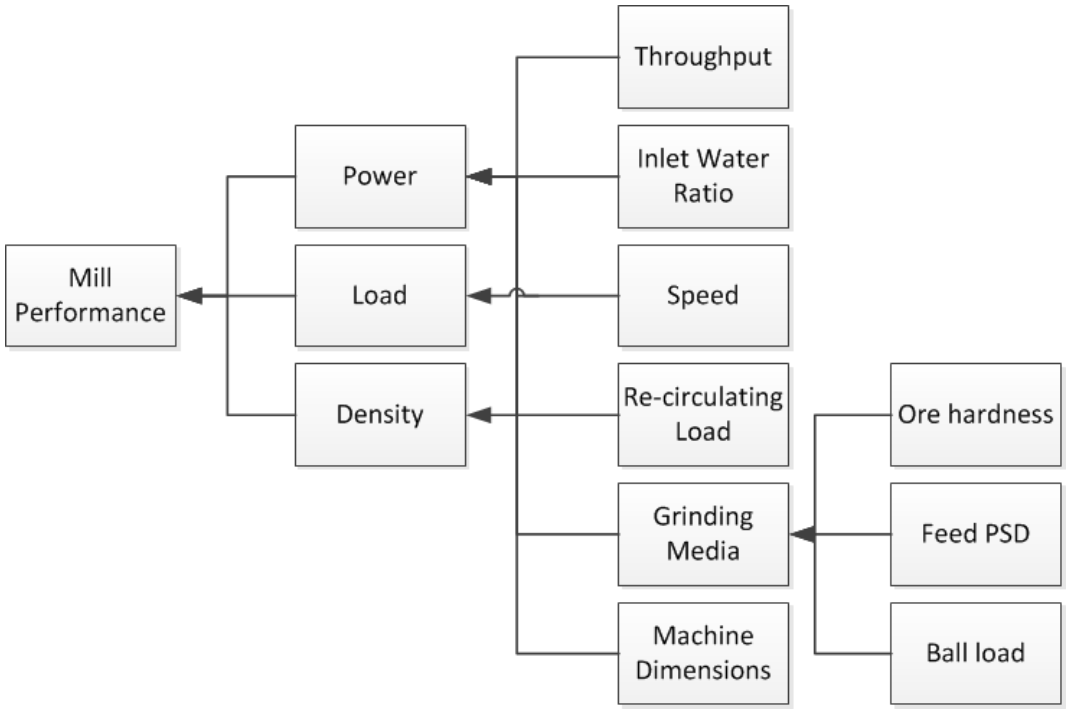

Figure 7-4: Mill performance basic causality map (Redrawn from Groenewald (2014))

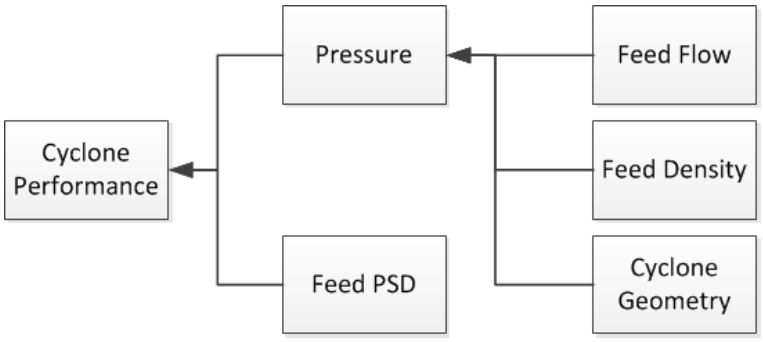

Figure 7-5: Cyclone performance basic causality map (Redrawn from Groenewald (2014))

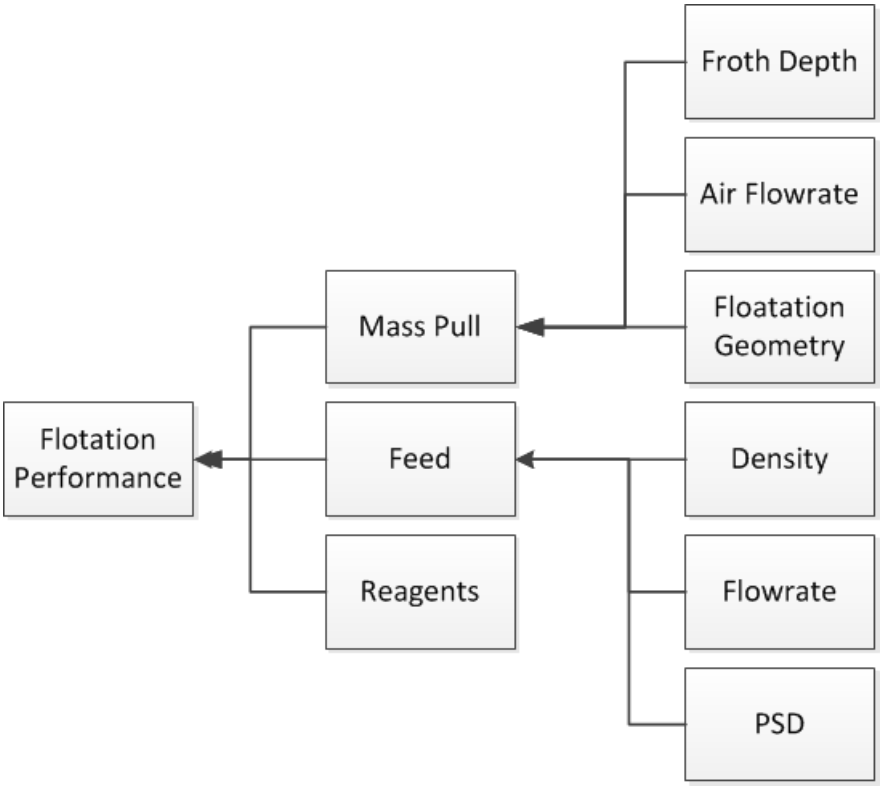

Figure 7-6: Flotation performance basic causality map (Redrawn from Groenewald (2014))

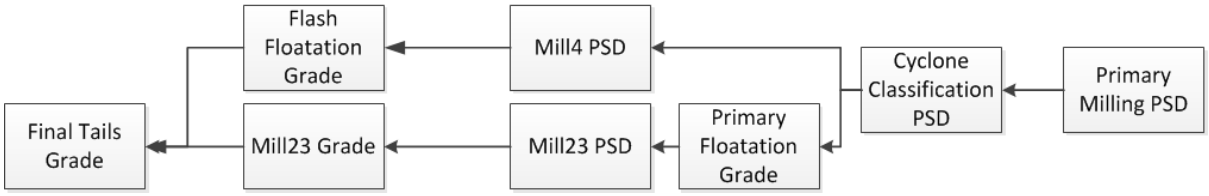

Figure 7-7: General concentrator causality map (Redrawn from Groenewald (2014))

7.3.2. Linear cross-correlation topology extraction

The number of lags, k, chosen for LC was 10. This value was selected since, this corresponded to 40 hours of operation, which is a long enough time period to incorporate the residence times and dead time associated with this process. Using the method described in section 4.3.4 for selection of the significance threshold, the sample size could be used in Equation 7-1 to determine a significance threshold.

$$\rho^{LC}_{max,th}(N) = 3N^{-0.452} + 0.11N^{-0.658} \quad \textbf{Equation 7-1}$$

$$\rho^{LC}_{max,th}(150) = 0.316 \quad \textbf{Equation 7-2}$$

Applying this threshold of 0.316, however, resulted in a connectivity graph with too many connections. It was decided to apply a stricter threshold, so the threshold was rounded up to 0.4. As with the previous case studies the threshold determined from the proposed method was too lax,

resulting in a connectivity graph with too many spurious connections. Figure 7-8 shows the resulting connectivity graph.

Considering the causality presented by Groenewald (2014) the following key connections are discussed for the LC graph shown in Figure 7-8:

- The primary mill water feed affects many key variables, including: mill load, power, the final tails PSD and the concentrate grade. This is accurate, since the feed is at the start of the process and would therefore have a substantial influence on downstream variables.
- The primary mill load affects the concentrate grade, as well as the mass split. This relationship is accurate from a fundamental perspective, since the ability of the mill to reduce the particle size is affected by the load in the mill.
- The flash floatation PSD affects the final tails PSD. Additionally, all the final floatation PSDs are connected.
- All the final tails PSD variables are connected to the same variables. This is accurate since each of the final tails PSD variables represents the same property.
- Mill23 power, availability and stops are all highly connected to Mill23s PSDs and the primary floatation PSDs (Ptails). Since the ability of these mills to reduce the particle size is affected by their operating variables, this is accurate.
- The Mill23s power has a strong connection on the final recovery, indicating that these mills have a strong influence on this KPI.
- The feed mass affects a large number of variables; especially the PSDs. This PSD affects primary mill performance, which, as seen in Figure 7-7, drives the performance of the subsequent units. It also strongly affects the mill power, which is accurate from a fundamental perspective.

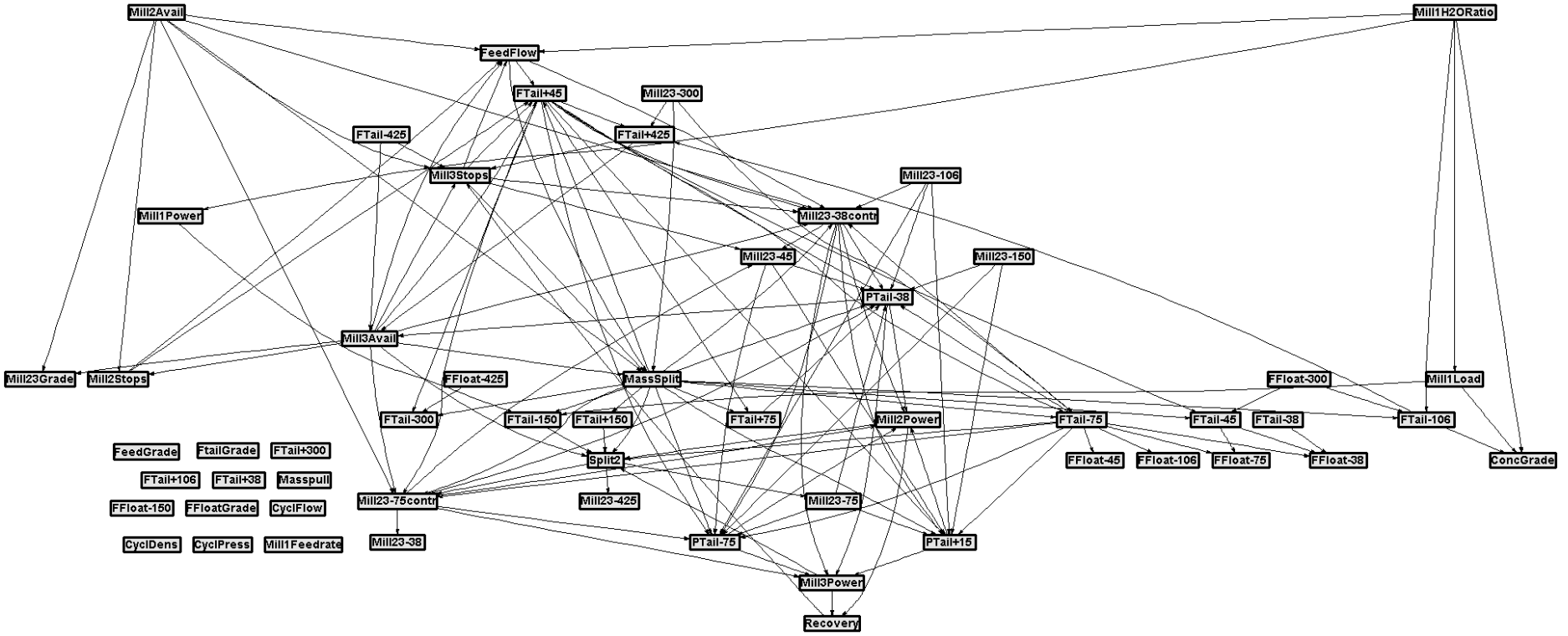

Figure 7-8: Linear cross-correlation connectivity graph on concentrator training data

7.3.3. Partial cross-correlation topology extraction

The number of lags, k, chosen for PC was the same as was chose for LC. Using the method described in section 4.3.4 for selection of the significance threshold, the sample size could be used in Equation 7-3 to determine a value.

$$\rho_{max,th}^{PC}(N) = 1.647N^{-0.428} + 3.864N^{-0.772} \quad \textbf{Equation 7-3}$$

$$\rho_{max,th}^{PC}(150) = 0.274 \quad \textbf{Equation 7-4}$$

It was observed that this threshold of 0.274 was actually too low, giving too many connections. Upon inspection of the connectivity matrix it was observed that many of the entries were between 0.2 and 0.4. It was therefore decided to double the significance threshold to give a more accurate and useful connectivity graph. As with the previous case studies the threshold determined from the proposed method was too lax, resulting in a connectivity graph with too many spurious connections. Using this threshold the connectivity graph shown in Figure 7-9 was generated using partial cross-correlation.

Considering the causality presented by Groenewald (2014) the following key connections are discussed for the PC graph shown in Figure 7-9:

- For the Mill23s their powers, stops availability and PSDs are all connected. The fact their powers affect their PSDs indicates accurate capture of process behaviour, since the operating conditions of these mills will have a strong influence on their ability to reduce size of the particles.
- The primary mill feed rate and its inlet water ratio are connected.
- The MassPull affects the recovery and grade of the tails, which is accurate, since a larger throughput would affect both grade and recovery.
- The final tails PSD variables are all connected, which is accurate since they all represent the particle size of the same stream.
- The final tails grade affects the recovery. These two KPIs are strongly linked, since recovery is dependent on grade.
- The Mill23s variables affect the downstream tails PSD.
- The Cyclone feed flow affects its pressure.
- The primary mill power affects its load. Unfortunately there is no connection between these variables and the mill feed rate and water inlet ratio.
- The cyclone split classification affects the Mill23s. The split classification is affected by the PSD of the primary floatation tails. This may seem like it's in the wrong direction, but as stated in the beginning of the topology extraction section the classification is profoundly

affected by the feed PSD. Unfortunately no measurement is available for that PDS, and the closest estimate of this PSD is that of the primary floatation, so in fact it can be considered accurate. There are no connections between cyclone feed flow and pressure and its splitting unfortunately.

- The PSD exiting the cyclone affects its splitting, which is accurate.

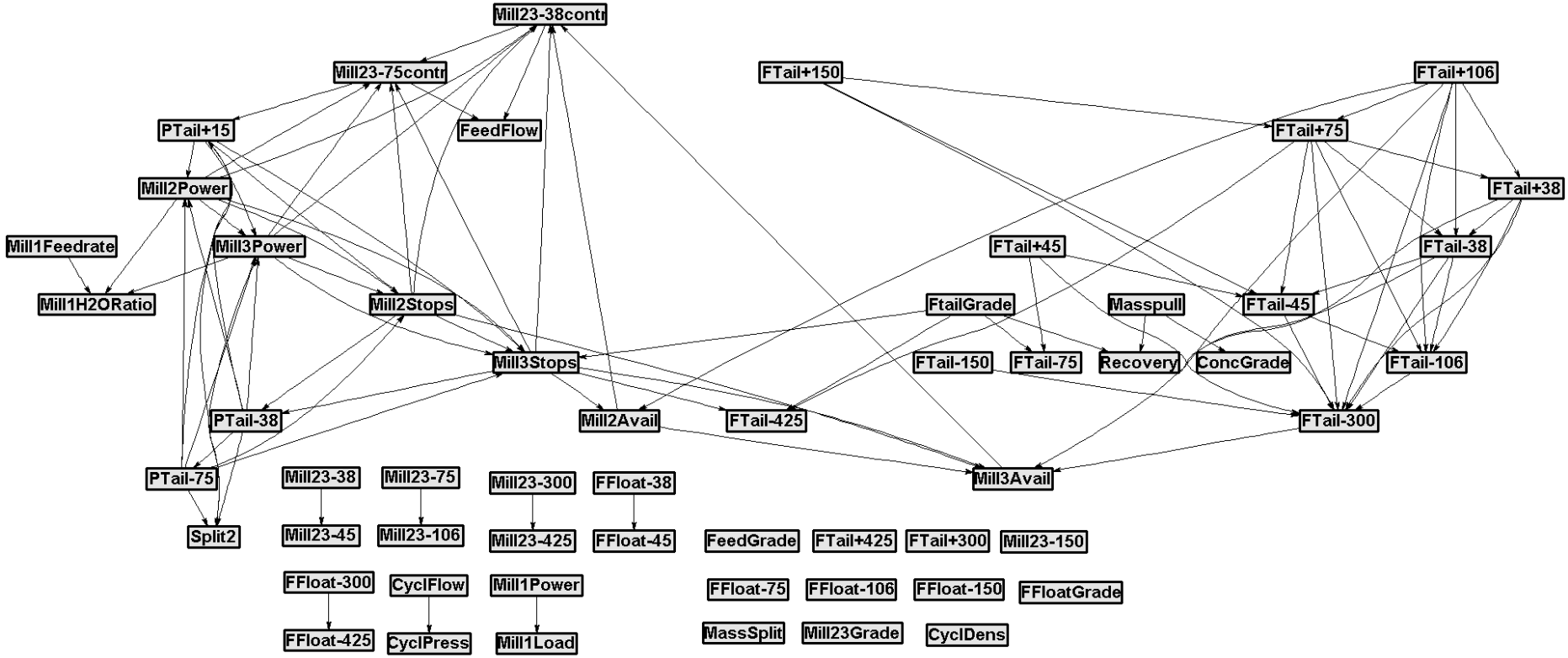

Figure 7-9: Partial cross-correlation connectivity graph for concentrator training data

7.3.4. Transfer entropy topology extraction

Using the method described in section 4.3.4 for selection of the significance threshold, the sample size could be used in Equation 7-5 to determine a value.

$$\mathrm{t}_{\mathbf{x}\rightarrow\mathbf{y},\mathrm{th}}(N) = 0.0018N^{0.465} + 0.0054N^{0.412} \qquad \textbf{Equation 7-5}$$

$$\mathrm{t}_{\mathbf{x}\rightarrow\mathbf{y},\mathrm{th}}(150) = 0.0611 \qquad \textbf{Equation 7-6}$$

Using this threshold of 0.0611 the connectivity graph resulted in a connectivity graph with too many connections. Doubling the threshold and then rounding it up to a value of 0.15 resulted in a more accurate connectivity graph, shown in Figure 7-10.

Considering the causality presented by Groenewald (2014) the following key connections are discussed for the TE graph shown in Figure 7-10:

- The recovery is affected by the flash floatation and Mill23 PSDs, indicating that the particle sizes have a substantial effect on the performance of the process.
- The feed grade is affected by many downstream variables, including the floatation PSDs and concentrate grade. This connection is contrary to the physical process behaviour, since the feed at the start of the process cannot be influenced by downstream variables.
- The cyclone pressure affects the mass pull.
- The mass split affects the tails Grade of Mill2 and Mill3.
- The Split2Cr affects a lot of variables, which makes sense since this is where the process split. It affects the Flash floatation and the Mill23s PSD.
- The Mill23s PSDs affect the mill power, as does the primary mill feed rate.
- In general, for the TE graph, it appears that many of the right connections exist, but possibly in the wrong direction. However, since the data used has a lot of complicated and unknown interactions that may be introduced by the operator, and not just by mass, energy balance and automatic control, this makes it difficult to define the proper direction for the connections.

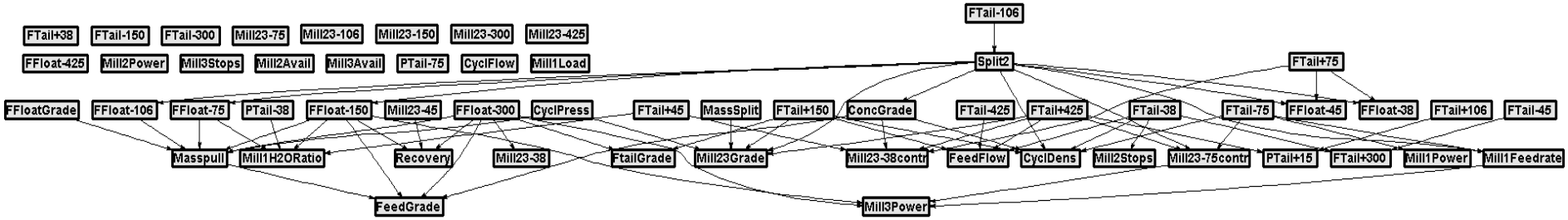

Figure 7-10: Transfer entropy connectivity graph for concentrator training data

7.4. Blocking of Concentrator Data Using Topology

The connectivity graphs obtained from the three TEM were used to perform blocking of the concentrator data. The resulting blocking for each method is presented and discussed in this section.

7.4.1. Blocking using linear cross-correlation topology

Blocking using the connected components in the LC graph resulted in 6 blocks, as shown in Figure 7-11 and Table 7-3.

For this blocking method the connectivity graph had too many connections to provide meaningful and useful blocks that represented the process units. This is evidenced by the fact that it resulted in one very large strongly connected component with 31 of the 56 variables and a number of smaller blocks.

- Block 1 contains the Feed rate to the primary mill, the final tail PSD, the Mill23s PSD, the Mill23s power, the cyclone split, the primary floatation PSD, the flash floatation PSD and the mass split and recovery. This indicates that this block is associated strongly with the Mill23s, but contains a scattering of variables from all over the plant.
- Blocks 2 and 3 contain the final tails PSD.
- Block 4 contains the concentrate grade, and the primary mill variables. This indicates that this block is most associated with the primary mill, but also indicates that the concentrate Grade is strongly associated with the primary mill's operation.
- Block5 contains the Mill23 grade and one of the mill's availability.
- The final block contains all the remaining unconnected variables.

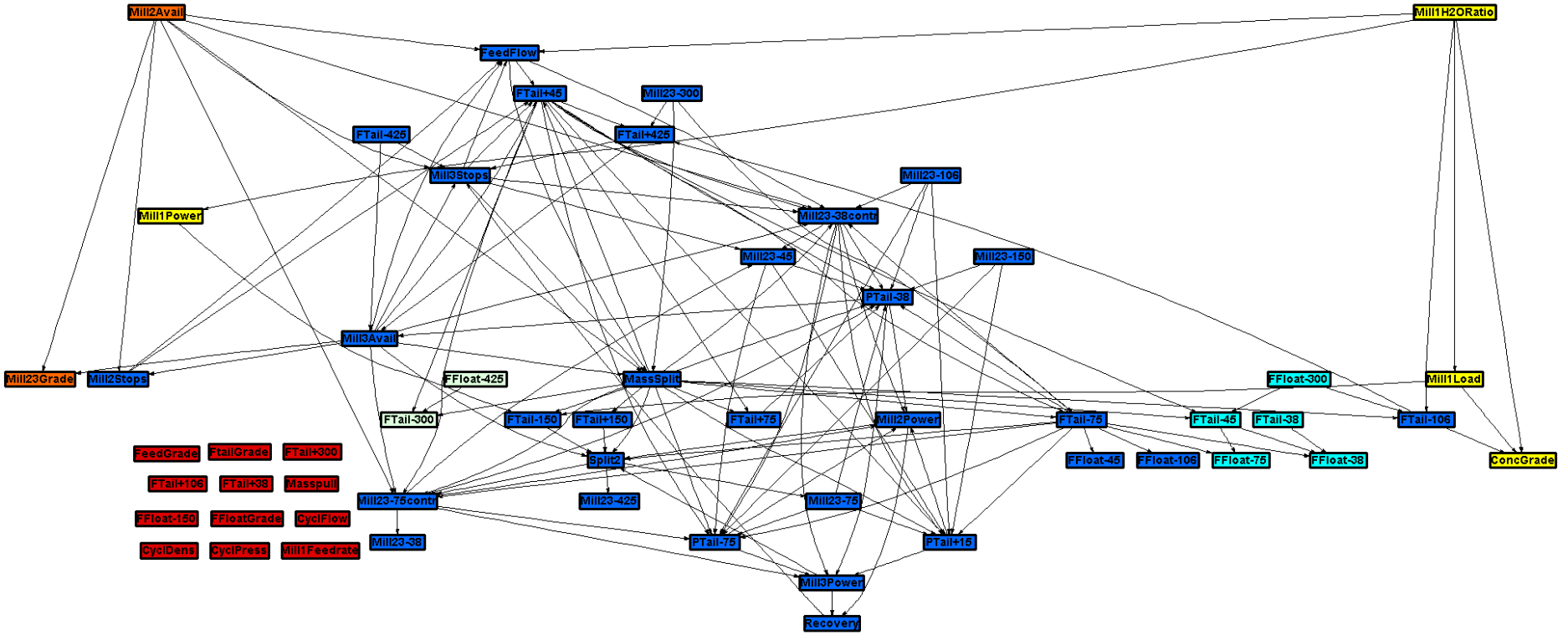

Figure 7-11: Blocking of concentrator data using linear cross-correlation connectivity graph. Different colours represent different blocks, detailed in Table 7-3

Table 7-3: Variables associated with each block in the linear cross-correlation connectivity graph (Figure 7-11)

Variable No.	Block1	Block2	Block3	Block4	Block5	Block6
1	FeedFlow	FTail-38	FTail-300	ConcGrade	Mill23TailGrade	FeedGrade
2	FTail+425	FTail-45	FFloat-425	Mill1Power	Mill2Avail	FTailGrade
3	FTail+150	FFloat-38		Mill1Load		FTail+300
4	FTail+75	FFloat-75		Mill1H2ORatio		FTail+106
5	FTail+45	FFloat-300				FTail+38
6	FTail-75					Masspull

Variable No.	Block1	Block2	Block3	Block4	Block5	Block6
7	FTail-106					FFloat-150
8	FTail-150					FFloatGrade
9	FTail-425					CyclFlow
10	Recovery					CyclDens
11	Mill23-38					CyclPress
12	Mill23-45					Mill1Feedrate
13	Mill23-75					
14	Mill23-106					
15	Mill23-150					
16	Mill23-300					
17	Mill23-425					
18	FFloat-45					
19	FFloat-106					
20	MassSplit					
21	Mill2Power					
22	Mill3Power					
23	Mill2Stops					
24	Mill3Stops					
25	Mill3Avail					
26	Split2Cr					
27	Ptail-38					
27	Ptail-75					
29	Ptail+15					
30	Mill23-38contr					
31	Mill23-75contr					

7.4.2. Blocking using partial cross-correlation topology

Blocking using the connected components in the PC graph resulted in 11 blocks, as shown in Figure 7-12 and Table 7-4. In comparison with LC, this blocking method provided much more meaningful blocks that represented the units in the process.

- The first block, the most strongly connected one, comprised of Mill2 and Mill3 variables, including: mill power, stops and availability as well as the feed PSD to the mills (Ptail PSD). The cyclone classification ability also formed part of this block.
- The second block contains all the final product variables, including: the final tails PSD and grade; the mass pull; the concentrate grade; and the recovery of the process.
- Block 3, 4 and 5 all contain Mill23 PSDs.
- Blocks 6 and 7 contain the flash floatation PSD
- Block 8 contains the cyclone feed and pressure variables
- Block 9 contains the primary mill's power and load, while block10 has the primary mill's feed variables.
- Block 11 contains all the remaining variables

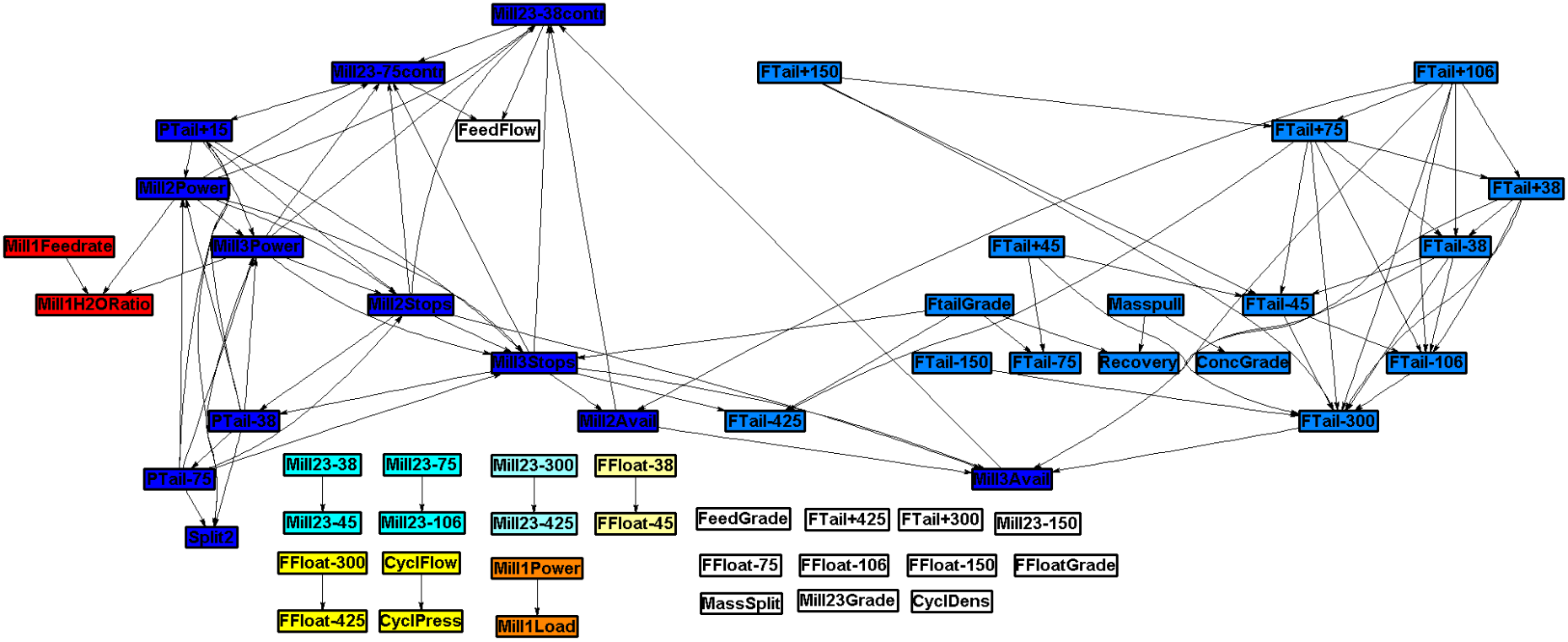

Figure 7-12: Blocking of concentrator data using partial cross-correlation connectivity graph. Different colours represent different blocks, detailed in Table 7-4

Table 7-4: Variables associated with each block in the partial cross-correlation connectivity graph (Figure 7-12)

No.	Block1	Block2	Block3	Block4	Block5	Block6	Block7	Block8	Block9	Block10
1	Mill2Power	FTailGrade	Mill23-38	Mill23-75	Mill23-300	FFloat-38	FFloat-300	CyclFlow	Mill1Power	Mill1Feedrate
2	Mill3Power	FTail+150	Mill23-45	Mill23-106	Mill23-425	FFloat-45	FFloat-425	CyclPress	Mill1Load	Mill1H2ORatio
3	Mill2Stops	FTail+106								
4	Mill3Stops	FTail+75								
5	Mill2Avail	FTail+45								
6	Mill3Avail	FTail+38								
7	Split2Cr	FTail-38								
8	Ptail-38	FTail-45								
9	Ptail-75	FTail-75								
10	Ptail+15	FTail-106								
11	Mill23-38contr	FTail-150								
12	Mill23-75contr	FTail-300								
13		FTail-425								
14		Masspull								
15		ConcGrade								
16		Recovery								

7.4.3. Blocking using transfer entropy topology

The TE blocking method was not able to separate the process into any blocks. This is because the TE connectivity graph did not contain any strongly connected components. This, in turn, is due to the fact that there are no loops in this connectivity graph, so no two variables were mutually reachable without violating edge directions. The graph just forms one weakly connected component. Increasing the threshold has no effect on this result; as the threshold becomes more stringent more and more variables just show no connections to or from them, meaning that the graph just becomes a smaller weakly connected component. Decreasing the threshold just makes it a larger weakly connected component, until the threshold becomes so small that an unmanageable number of connections are present.

7.5. Feature Extraction for Fault Detection in Concentrator Process

In sections 7.3 and 7.4 of this chapter the results of topology extraction were presented, followed by the results of blocking using the connectivity graphs. This section presents the fault detection results, applied to the unblocked data (all variables combined) and the blocked data. The results are discussed in order to determine whether blocking improved the fault detection or not. The fault detection results include the use of PCA and KPCA, as well as the three monitoring chart methods, and the different methods are compared to determine which performed best for fault detection Summary results are presented here, further results are presented in Appendix D.

7.5.1. Training of feature extraction methods

The details of the feature extraction models developed on the training data are given here.

Number of retained features for principal components analysis

For the unblocked data retention of 19 components resulted in an explained variance of 90%. The number of principal components retained for PCA for the blocked data for each blocking method are given in Table 7-5.

Table 7-5: Retained components giving 90% explained variance for each block for principal components analysis

TEM	Block	1	2	3	4	5	6	7	8	9	10
LC	No. of variables in block	31	5	2	4	2	12				
	No. of retained components	12	3	2	2	2	8				
PC	No. of variables in block	12	16	2	2	2	2	2	2	2	2
	No. of retained components	4	8	2	2	2	2	2	2	2	2

Kernel width selection and number of retained features for kernel principal components analysis

Cross-validation performed on the training data indicated a decreasing mean squared prediction error for increasing kernel width. This indicates that the data displays mostly linear behaviour. A kernel width of 50 was therefore chosen since at this kernel width the mean squared prediction error had levelled off.

For the unblocked data retention of 9 components resulted in an explained variance of 90%. The number of principal components retained for PCA for the blocked data for each blocking method are given in Table 7-6.

Table 7-6: Retained components giving 90% explained variance for each block for KPCA

TEM	Block	1	2	3	4	5	6	7	8	9	10
LC	No. of retained components	4	3	3	3	2	6				
PC	No. of retained components	3	6	3	3	3	3	3	3	3	3

7.5.2. Fault detection results for recovery fault in concentrator process

Figure 7-13 illustrates the fault detection results for the concentrator recovery fault for all the methods, with the blocks that showed the best fault detection results as well as the unblocked results. Comparing the unblocked results (Block 0) with the results for PC and LC blocks, blocking noticeably improved the fault detection results. The AUCs achieved when analysing individual blocks were close to 1, and the DDs were of the order of one hour, as opposed to ten hours for the unblocked results.

For LC, block 4 displayed the best fault detection results with PCA. Referring back to Figure 7-11 Table 7-3, block 4 contained the concentrate grade and the primary mill variables. This indicates that this block is most associated with the primary mill. The fact that block 4 gave the best results indicates that the fault affected the primary mill variables strongly, and possibly the final concentrate grade. Comparing the results in this block to that for the unblocked data in Figure 7-13, it can be observed that the AUCs were higher and the DDs much lower, indicating an improvement in performance with the introduction of blocking using LC.

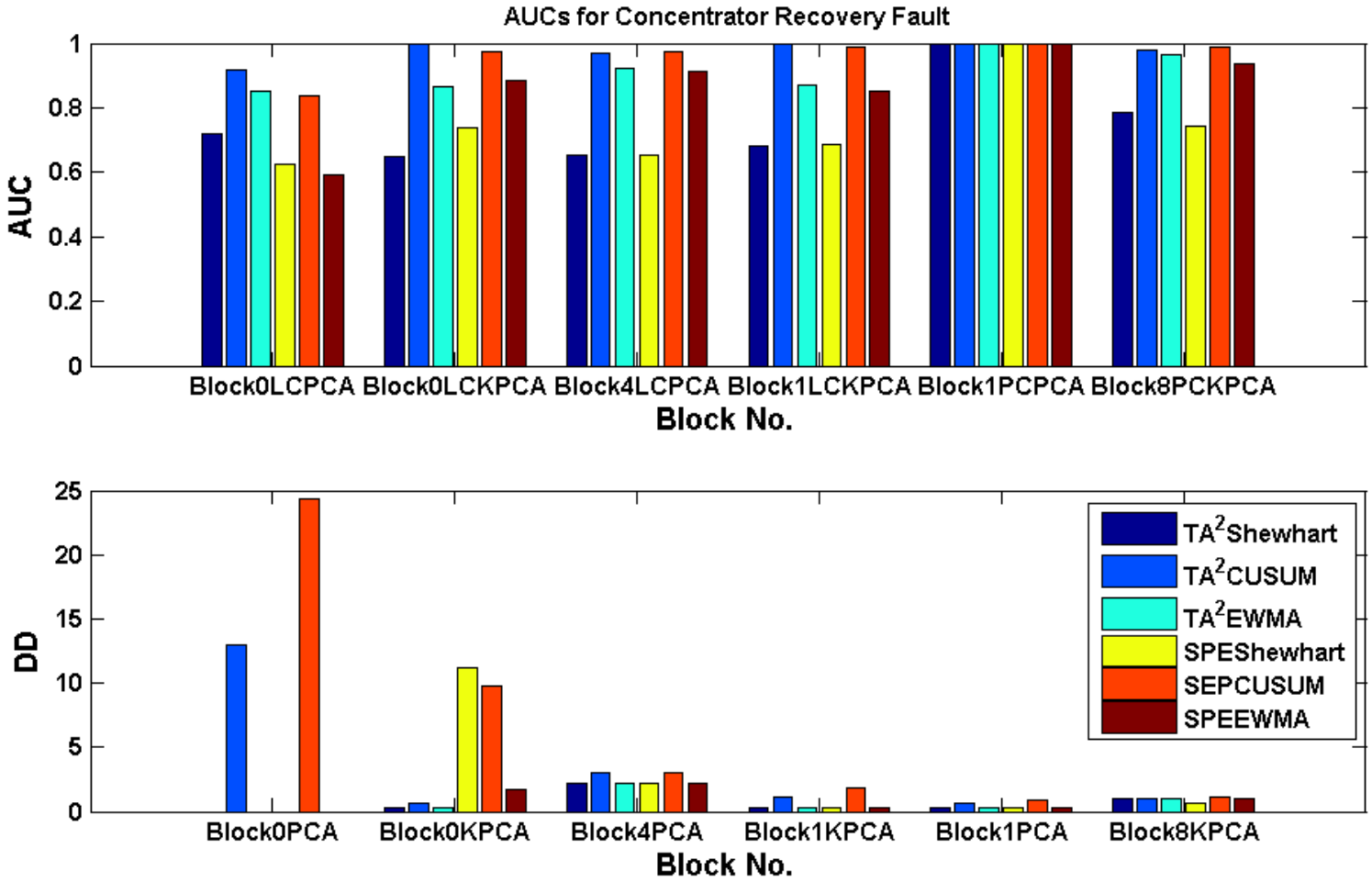

Figure 7-13: Fault detection results for all methods applied to concentrator process recovery fault

For LC block 1 gave the best results for KPCA. Referring back to Figure 7-11 and Table 7-3, block 1 contains a large proportion of the variables in the system, representing variables from various parts of the process. It is however, strongly associated with the parallel milling circuits (Mill2 and Mill3), since it contains their PSD, both their power measurements, as well as their feed PSD, represented by Ptails. The fact that block 1 showed the best detection results for these methods indicates that the fault affected Mill2 and Mill3's performance significantly. Comparing the results in Figure 7-13 for this block with the unblocked KPCA results, it can be observed that the AUCs were not noticeably different, but the DDs were much lower for the blocked case. This indicates that blocking resulted in an improvement in detection performance for this case.

For PC block 1 gave the best results with PCA. Referring to Figure 7-12 and Table 7-4, block 1 comprised of Mill2 and Mill3 variables, including: mill power, stops and availability as well as the feed PSD to the mills (Ptail PSD). The cyclone classification ability also formed part of this block. So this block clearly is associated with Mill2 and Mill3. This indicates that the fault strongly affects the performance of these mills. The AUCs for this block using PCA were very close to one, and the DDs very low. This indicates very good detection performance, which was substantially better than for the unblocked data.

For PC block 8 gave the best detection results with KPCA. Referring to Figure 7-12 and Table 7-4, block 8 contains the cyclone feed flow rate and pressure variables, so it is clearly associated with the cyclone. This indicates that the fault also affected the cyclone performance significantly. Comparison of this block's results with the unblocked results in Figure 7-13 indicates higher AUCs and lower DDs for the KPCA in block 8. This improved detection indicates that blocking in this resulted in improved fault detection results.

Both the CUSUM and the EWMA charts resulted in higher AUCs than the Shewhart charts, and the increase in DD using was not substantial for either of them. The fact that the CUSUM and EWMA charts introduced very little detection delay indicates that the fault was a very gradual one, so the Shewhart charts would not immediately rise above the significance limits. The EWMA charts gave lower DDs than the CUSUM charts. Although it might be expected that the EWMA would also come at a sacrifice of detection speed, since it calculates an average of past values and would cause the effect of the sample at the start of fault conditions to be lower. However, since the value chosen for the EWMA weighting parameter, r, was low (0.1), EWMA gave higher weight to recent values.

For the unblocked case the KPCA showed much better results than PCA; although the AUCs in Figure 7-13 are similar, the DDs are much lower. For the LC blocking, PCA and KPCA resulted in very similar detection performance. For the PC blocking, PCA displayed much higher AUCs than KPCA, while both

resulted in similar DDs. Otherwise, in terms of AUCs and DDs PCA and KPCA performed similarly, indicating no improvement with the introduction of a nonlinear method. However the best performance is clearly shown by the PC blocking method using PCA, with AUCs higher than 0.9 for all monitoring chart methods and low DDs.

7.6. Fault Identification in Concentrator Process

In this section the results of applying fault identification, either by considering the change in topology from NOC to fault conditions or considering contributions plots for the PCA SPE, are presented. The results are shown for the unblocked case, using the unblocked connectivity graphs, but also for the blocked cases, where the block that showed the best detection results for each method is used to further investigate the fault conditions.

Table 7-7 shows the results of fault identification for each different method in terms of the symptoms identified and the possible root nodes associated with these symptoms. This table provides a summary, full analysis of each fault identification result is given in Appendix D.

Considering Table 7-7, a large amount of the fault identification methods identified the Mill23s as a possible cause of the fault, or at least as showing strong symptoms of the fault. This is consistent with the conclusions found by Groenewald (2014), at least in terms of the symptoms identified. Most of the methods also identified the final tails PSD as symptom nodes, as well as many of the variables associated with the cyclone, such as its feed flow, pressure and splitting.

The method that found the root cause with the most accuracy was using combining the blocked LC graph with contribution plots. This method identified the primary mill as a primary cause, and noted that the inlet water ratio is the root variables for the primary mill. In addition, considering the connectivity change for the unblocked PC graph resulted in the feed mass being identified as a root node and as being a primary contributor to the fault. This result is consistent with the results obtained by Groenewald.

In general the same symptoms identified by Groenewald dominate the symptoms and roots found using these methods. This indicates that these methods are useful for identifying the root cause of the recovery fault.

Considering the results in Table 7-7, it can be concluded that PC gave the best fault identification results. This is especially true when considering that PC blocking gave the best detection result for KCPA in the cyclone block, Block 8, resulting in the cyclone feed flow being identified as a possible root cause. Since partial cross-correlation gave the best results for fault identification in general, the rest of this chapter considers these results in more detail.

Table 7-7: Fault Identification results for the recovery fault for different methods

TEM	FEM	FIM	Block	Symptoms			Roots			
LC	na	Contributions	Block0	Mill3Power	Split2Cr	Recovery	FFloat-300	Mill1Load	FTail-106	
LC	na	Connectivity Change	Block0	FTail-75	Mill2Power	Mill3Stops	Mill2Avail			
LC	PCA	Contributions	Block4	Mill1Load	Mill1Power		Mill1H2ORatio			
LC	PCA	Connectivity Change	Block4							
LC	KPCA	Connectivity Change	Block1	FTail-75	Mill2Power	Mill3Stops				
PC	na	Contributions	Block0	Mill3Power	Split2Cr	Recovery	FTailGrade			
PC	na	Connectivity Change	Block0	FFloat PSD	FeedGrade	FeedFlow	FFloat PSD	FeedGrade	FeedFlow	FTailGrade
PC	PCA	Contributions	Block1	Mill3Power	Mill3Stops	Mill3Avail	Mill23-38contr	'Mill2Avail'	'Mill3Avail'	
PC	PCA	Connectivity Change	Block1	Mill2Power	Split2Cr		Ptail PSD			
PC	KPCA	Connectivity Change	Block8	CyclFlow			CyclFlow			
TE	na	Contributions	Block0	Mill3Power	Split2Cr	Recovery	FTail-106	Split2Cr		
TE	na	Connectivity Change	Block0	ConcGrade	FFloat-45	FFloat-75	FTail PSD	Mill23 PSD	FFloat PSD	Split2Cr

7.6.1. Symptom identification using the unblocked contribution plot

In the unblocked case, contributions to SPE of the PCA model showed Mill23Power, Split2Cr and Recovery as the largest contributors to this fault, as illustrated in Figure 7-14. Since the recovery was the symptom of the fault that was recognised by the operators observing the time series trend in the data, this symptom result is accurate. The fact that the Mill23 power and the cyclone classification were also identified is consistent the fault drivers identified by Groenewald (2014).

The other variables that showed increased contributions in Figure 7-14, were the variables 50 to 56, which represent the primary mill and the cyclone variables. Additionally, variables 36 to 46, which represent the Mill23 variables, its PSD and the primary floatation PSD, showed increased contributions.

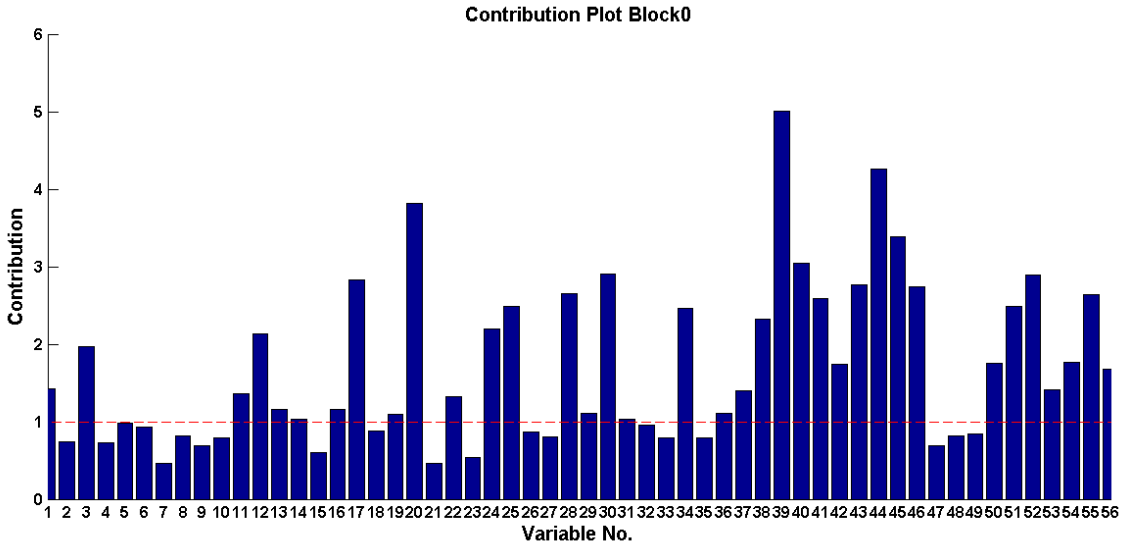

Figure 7-14: Variable contributions to unblocked PCA SPE. Variable number correspond to variables list shown in Table 7-2

7.6.2. Fault identification results using partial cross-correlation

Fault identification using partial cross-correlation with unblocked contributions

Applying back propagation in the unblocked PC graph using the symptoms identified from contributions resulted in FtailGrade, or the final tails grade, being identified as a possible root node, as shown in Figure 7-15. This is more of a symptom than a cause of the fault, considering that this is actually a final performance variable.

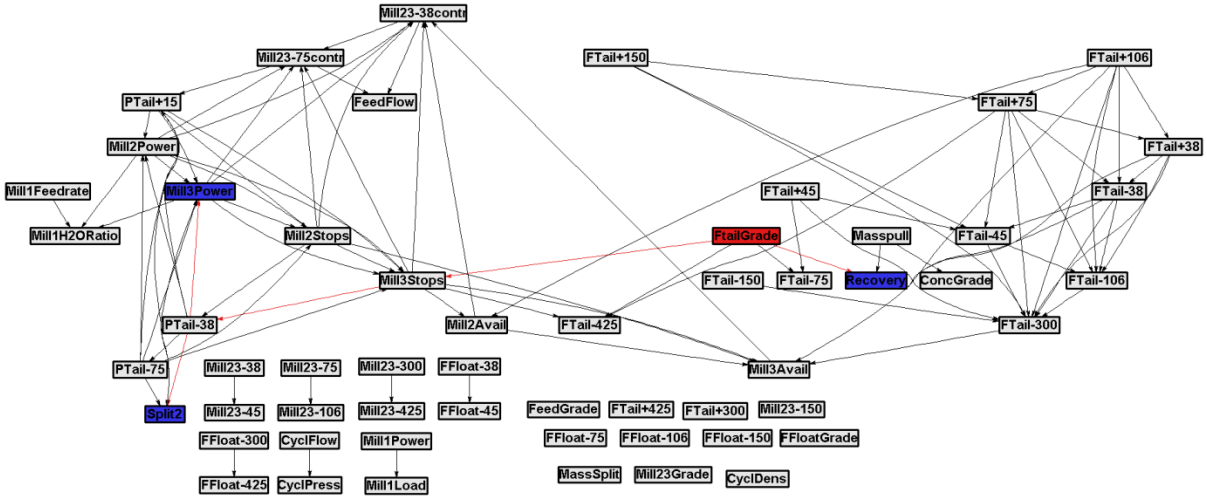

Figure 7-15: Back propagation using unblocked PC graph with symptoms identified by contributions (shown in blue). Possible root nodes and propagation paths are shown in red

Fault identification with partial cross-correlation using unblocked connectivity change

Figure 7-16 shows the fault conditions connectivity graph obtained using partial cross-correlation, illustrating the change in connectivity from NOC.

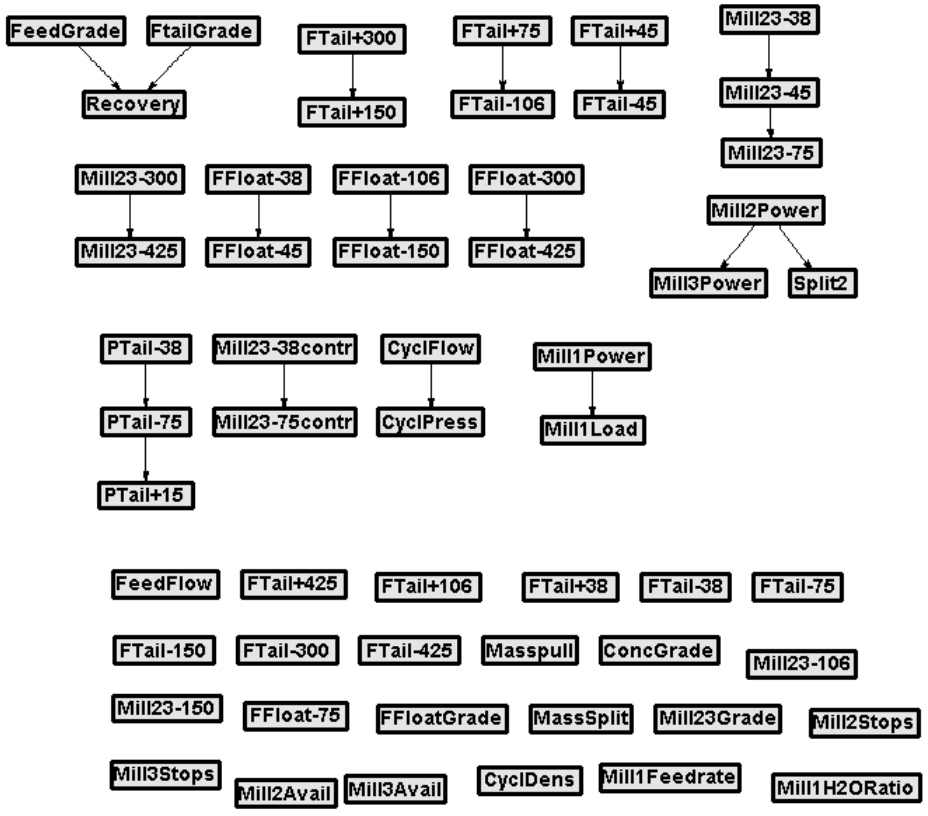

Figure 7-16: Unblocked fault conditions partial cross-correlation connectivity

The change in connectivity indicated a lot of connections becoming insignificant. The possible symptoms identified were the flash floatation PSD, the feed Grade and the final tails Grade.

Applying back propagation in the PC graph from these symptoms resulted in the same variables being identified as possible roots. With the exception of FtailGrade, these variables were not connected to anything else in the graph. So the final tails grade was the possible root identified, the same as with the back propagation from contributions.

Fault identification with partial cross-correlation using blocked contributions

Considering the contributions of individual variables in the block that gave the best detection results for PCA in the PC blocking method, Block 1, gave Mill3Power, Mill3Stops and Mill3Avalil as the largest contributors to the SPE, as shown in Figure 7-17. This block is associated mostly with the Mill23s feed and grind streams and the mill variables, so this indicates that the fault was largely associated with the Mill23s, or at least affected them strongly. These symptoms are consistent with the fault diagnosis performed by Groenewald (2014).

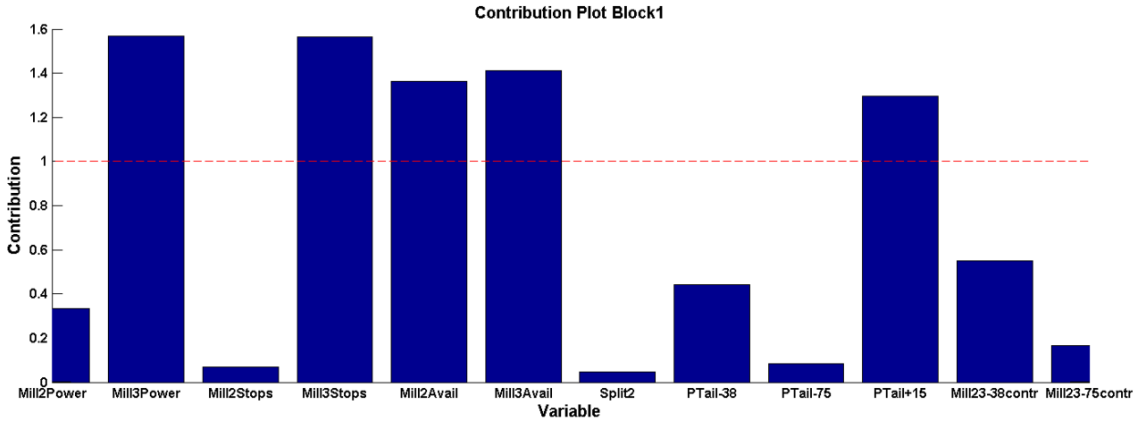

Figure 7-17: Contributions of variable to the PCA SPE for partial cross-correlation block1

Applying back propagation in the PC graph for Block1, using the symptoms identified by contributions then resulted in Mill23-38contr, Mill2Avail and Mill3Avail being identified as possible root nodes, as shown in Figure 7-18. This is similar to the results obtained by using LC unblocked connectivity change. This again indicates that the mills were largely affected by the fault. However, it doesn't point back to the original root cause, which was further upstream.

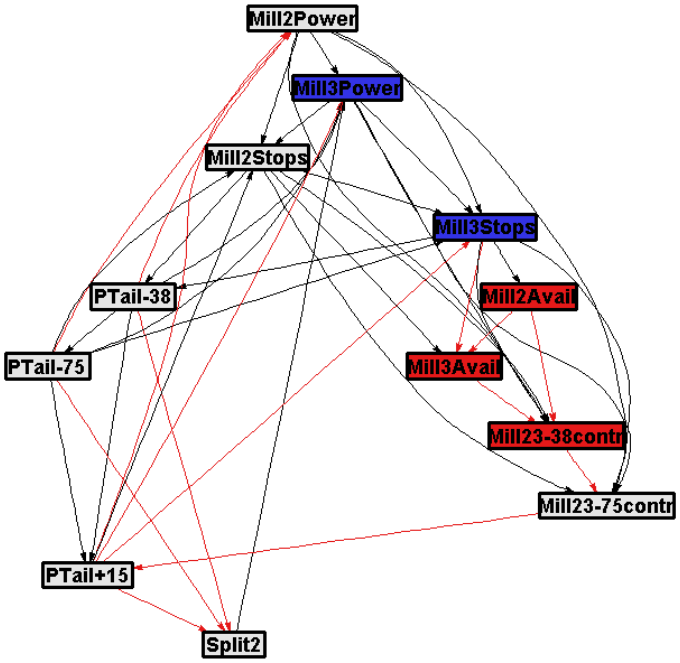

Figure 7-18: Back propagation in the partial cross-correlation graph for block 1 using the symptoms idnetified by contributions (shown in blue). Possible root nodes and propagation paths are shown in red

Fault identification with partial cross-correlation using blocked connectivity change

Considering the change in PC in the block that showed the best detection results for PCA, Block 1, identified Mill2Power and Split2Cr as possible symptom nodes, as shown in Figure 7-19. This again indicates that the Mill23s are associated with the fault.

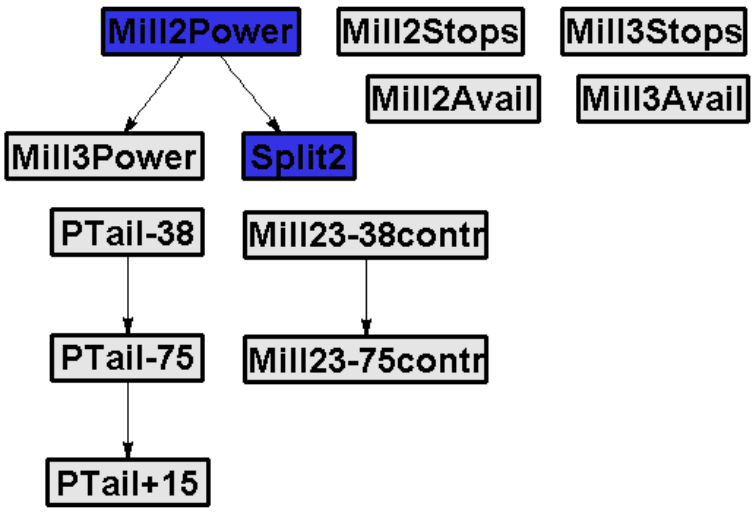

Figure 7-19: Fault conditions partial cross-correlation connectivity graph for block 1. Symptoms identified by connectivity change are highlighted in blue

Applying back propagation in the PC graph for block 1 using the symptoms identified by connectivity change resulted in the primary floatation tails PSD being identified as possible root nodes, as shown in Figure 7-20. Although this is probably still downstream of the actual fault it at least points to the

fact that the performance of some unit upstream of the Mill23s is responsible for the fault conditions.

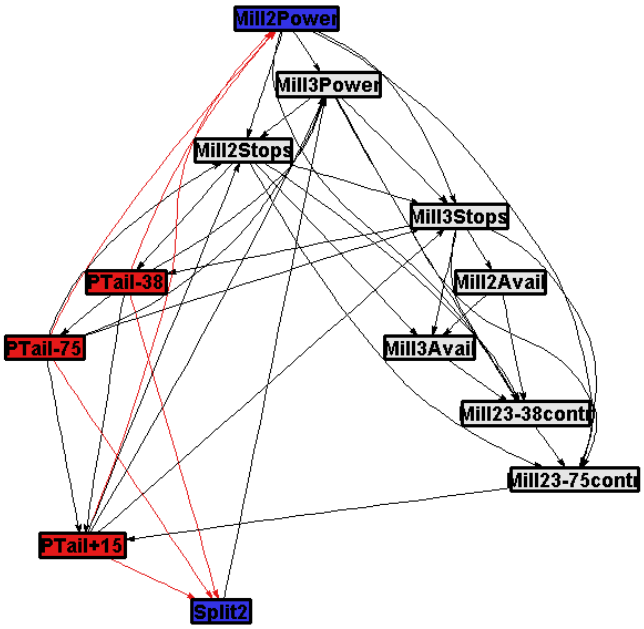

Figure 7-20: Back propagation in the partial cross-correlation graph for block 1 using the symptoms idnetified by connectivity change (in blue). Possible root nodes and propagation paths are shown in red

Fault identification with partial cross-correlation using blocked connectivity change

Considering the change in PC in block8, which showed the best results for KPCA, was used to determine the symptoms. However, block 8 only has two variables, as shown in Figure 7-21. Therefore connectivity change gave no results. However, since the fault is in this block and there are only two nodes, and only one of them is a root node it can be concluded that CyclFlow was the identified root node in this case. This root cause is more consistent with the probable root cause. Groenewald (2014) concluded that a major cause of the degradation in the recovery was a degradation in the performance of the cyclone, so this result points towards that effect.

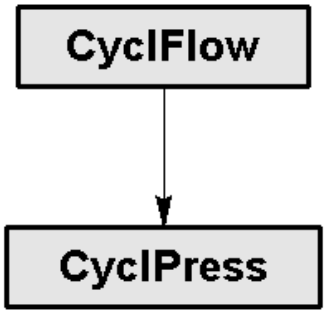

Figure 7-21: Connectivity diagram for partial cross-correlation block 8

7.7. Summary of Results of Fault Diagnosis in Concentrator Process

This section presents a summary of the main results obtained from application of the fault diagnosis methods to the concentrator case study.

7.7.1. Topology extraction from historical process data

All three topology extraction methods (TEMs) performed well for this case study, providing connectivity graphs that were consistent with the physical process. Partial cross-correlation (PC) appeared to give the most accurate connectivity graph. The automated threshold selection for all three TEMs resulted in thresholds that were too low, giving connectivity graphs with a very large number of connections, many of them spurious. The thresholds had to be altered for all of the TEMs, therefore.

7.7.2. Blocking of process using topology

Using the connectivity graphs for blocking of the process provided good results for linear cross-correlation (LC) and PC, with the blocks obtained representing the physical process units well. PC performed better than LC however, since the LC graph had one large strongly connected component with most of the variables in the process, and a few small weakly connected components. The TE graph, however, had no strongly connected components and therefore blocking was not possible. The reason for this is that the resulting TE graph displayed a very hierarchical structure, with no loops in the graph.

7.7.3. Fault detection using feature extraction

Principal components analysis vs. kernel principal components analysis

For the unblocked case the KPCA showed much better results than PCA; although the AUCs are similar, the DDs are much lower. For the LC blocks PCA and KPCA resulted in similar AUCs, with slightly lower DDs for KPCA, indicating slight improvement with KPCA. For the PC blocks, however, For the PC blocking PCA displayed much higher AUCs than KPCA, while both resulted in similar DDs, indicating substantially better performance with PCA in this case.

Monitoring charts

Both the CUSUM and the EWMA charts resulted in higher AUCs than the Shewhart charts, and the increase in DD using was not substantial. This is due to the fact that the fault was a very gradual one, so the Shewhart charts would not show a sudden rise above the significance threshold. The EWMA chart gave the best results, with an improvement in the AUCs over the Shewhart chart and a lower DD than the CUSUM chart.

Improvement with blocking

Applying multiblock fault detection to this case study, especially when using PC for blocking, resulted in substantial improvement in fault detection performance. The AUCs obtained were much higher and the DDs much lower. In addition, the blocks that provided the best detection results contained variables that in previous studies had been identified as showing symptoms of the fault. Therefore the fault identification was also aided with the use of blocking.

7.7.4. Fault identification using topology

Symptom node identification using contributions vs. using connectivity change

Both contributions and connectivity change in all cases resulted in identification of symptoms nodes that had been identified in previous work as showing strong indications of the fault conditions. Overall the PC graph gave the best connectivity change results and also the best results for the contributions in specific blocks.

Back propagation using connectivity graphs

Overall the PC graph gave the best results for identifying possible root causes that were representative of the fault conditions

Chapter 8 - Conclusions

This chapter presents the conclusions drawn from the results obtained in the previous chapters, considering the results from application to all three case studies.

8.1. Topology Extraction Conclusions

Three data-based topology extraction methods (TEM) were considered in this thesis: Linear cross-correlation (LC), partial cross-correlation (PC) and transfer entropy (TE). Although the conclusion of which method aided fault diagnosis most is dependent on their performance in aiding fault detection through blocking and identification through connectivity change and back propagation, general conclusions about the ability of each method to capture process topology are presented here.

8.1.1. Threshold selection

In order to extract topology from historical process data, each method used required setting of a threshold to determine whether a calculated causality measure provided significant evidence for causality between two variables. The method used in this study was to generate a number of random sequences of varying sample numbers (N), calculate the causality measure between all possible pairs for each N and use the mean and standard deviation to obtain the significance threshold as a function of sample number.

When applying this method to the various case studies it was found that: for LC and PC, in each case study the thresholds obtained were too low and resulted in connectivity graphs with too many spurious connections; for TE the method performed very well when applied to the Two-tank simulation case study and the Autoclave leaching simulation case study, but when applied to the Concentrator case study the threshold was also too low. In the cases where the thresholds were too low they had to be raised in order to obtain connectivity graphs that could be used subsequently for blocking and fault identification.

This indicates that this method for threshold selection is not robust enough to be applied in a range of circumstances. For the LC and PC in the Autoclave leaching simulation, the automated method used to strengthen the significance threshold was to determine the 95^{th} percentile of all calculated correlations and use this as the new threshold. This method performed well for LC, resulting in a connectivity graph that represented the physical process very well. However, for PC this threshold may still have been too low, since the resulting connectivity graph was convoluted and a large number of connections were obtained that did not correspond to physical process relationships

In the other case studies the threshold was raised either by doubling the threshold or rounding it up to a value that resulted in good connectivity graphs upon inspection. This approach lacks the rigour that motivated the application of the automated threshold selection method.

8.1.2. Ability to represent process topology

The ability of each TEM to represent process topology was discussed by analysing the connectivity graphs and validating whether the connections obtained were consistent with the physical process from a fundamental perspective. In general for all three methods the large majority of connections identified were considered to be accurate, but the accuracy was largely dependent on the thresholds selected, as mentioned in the previous paragraph

The results obtained indicate that no one of the three TEMs was able to consistently outperform the others. For the leaching simulation the LC method performed better than the PC method, resulting in more accurate representation of physical relations. For the two-tank case study and the concentrator case study the ability of PC to identify direct connections resulted in more accurate connectivity graphs. The TE appears to give the most consistent results; TE did not give a very large amount of spurious connections for any of the case studies. However, for the leaching simulation LC was more accurate than TE, and for the two-tank and concentrator case studies the PC performed better. Therefore at this point, it is difficult to choose one of the methods to be applied to any data set. Each method has strengths and weaknesses dependent on the nature of the data it is being applied to.

Another consideration for the choice of TEM is the computational effort required for each method. PC is by far the most computationally expensive method, since for each pair of variables under consideration it regresses of all other variables on those two and then uses the residuals to compute direct correlation. Additionally, it performs these calculations for a range of lags chosen. Transfer entropy is also quite computationally expensive due to the summing over the prediction horizon. TE also introduces the added complications of choosing the embedding dimensions, lx and ly, as well as the prediction horizon, h, and sampling period, τ. Therefore it is recommended that LC be considered first, in preference to the other methods, since it is the simplest and fastest to compute. If LC gives poor results, the TE can be considered to possibly obtain a better connectivity graph, and finally if neither of those works the PC can be considered.

8.1.3. Ability of blocking results to represent physical process units

The utility of using the topology information obtained from the data-based TEM is determined by whether or not fault detection applied to individual blocks improved the fault detection ability and

whether or not this aided fault identification. First, however, it is necessary to determine whether the methods resulted in grouping of variables that was sensible from a fundamental perspective.

The ability of each blocking method to group variables sensibly is obviously dependent on how well it represented the process. It is also largely dependent on the threshold selected; when the threshold is too low the graph becomes one strongly connected component and cannot be separated into multiple blocks; when the threshold is too strict the variables separate into a number of small blocks.

For the two tanks case study it was found that none of the connectivity graphs allowed for blocking, since the graphs contained no loops allowing for two variables to be mutually reachable. The process under consideration for that case study was a very small process, with few variables that affected each other in a very sequential manner; i.e. changes in the second tank could not cause changes in the first tank, since the process contained no recycle loops. For such a small process then, it does not make sense to separate the variables, and the best fault diagnosis performance would be obtained by analysing the process as a whole.

For the leaching simulation case study, applying blocking to the LC and TE connectivity graphs resulted in blocks that were representative of the process units; i.e. the variables associated with a single process unit tended to group together into the same block. For the PC graph, the fact that it contained such a large number of connections meant that blocking did not provide useful results.

For the concentrator case study, applying blocking to the LC and PC connectivity graphs resulted in sensible separation of variables into groups that were representative of physical process units. For the TE method, however, it was found that the resulting connectivity graph contained no loops and therefore it was not possible to block it according to strongly connected components.

Once again no single TEM method gave the best blocking results consistently. The results were strongly dependent on the nature of the process and on the threshold selection.

8.2.Feature Extraction Methods

The use of the linear feature extraction method, PCA, and the nonlinear method, KPCA, for fault detection were compared in this study. Additionally, modifications to the standard Shewhart monitoring charts for the SPE and T_A^2 statistics were compared.

8.2.1. Principal components analysis vs. kernel principal components analysis

In the two-tank case study there was slight improvement in the fault detection performance obtained through the use of KPCA as opposed to PCA. In all of the cases, however, the difference in performance between the two methods was not very substantial. The reason for this is that in each

case study, applying cross-validation to the training data to select the kernel width parameter for KPCA indicated that the larger the kernel width the lower the mean squared prediction error. Therefore in each case a large kernel width was selected, which means that the KPCA approximated PCA and they achieved similar results. This indicates that the data sets displayed mostly linear behaviour, and the added complexity and computational effort introduced by KPCA is unnecessary.

8.2.2. Monitoring chart methods

Three different monitoring chart methods were applied to the SPE and T_A^2 statistics: the standard Shewhart chart; the cumulative sum (CUSUM) chart; and the exponentially weighted moving average (EWMA) chart. It was observed that both the CUSUM and the EWMA charts resulted in higher AUCs than the Shewhart chart. For the CUSUM chart, this improvement came at the sacrifice of the detection speed, introducing large detection delays. For the EWMA chart however, this improvement in AUCs, although generally smaller than that of the CUSUM, did not result in a substantial increase in the DD. Therefore it can be concluded that the EWMA chart resulted in the best fault detection performance, and it did so consistently.

8.2.3. Improvement in fault detection ability using blocking

For most cases it was found that blocking resulted in improved fault detection ability, with higher AUCs and lower DDs when compared to the detection applied to the unblocked data.

8.3.Fault Identification

After detection of the fault, fault identification methods (FIMs) were employed to further analyse the fault and determine its location. This fault identification was performed using connectivity graphs to trace faults back from variables that displayed symptoms of the fault to variables that possibly represent the root cause of the fault. Two methods for identifying symptoms variables were considered: the first used contributions of individual variables to the PCA SPE; the second considered the change in connectivity from NOC to fault conditions.

8.3.1. Identifying symptom nodes

Both the connectivity change and the contributions displayed good performance in identifying possible symptoms of the fault. In most cases the symptoms identified were consistent with the fault conditions. Both methods have their drawbacks, however. The contributions method can only be used in conjunction with PCA and only considers the SPE. This means that when KPCA performs significantly better, or when the SPE does not give fault detection, the results of this method are questionable. The connectivity change method is dependent on the accuracy of the TEM, and when the TEM results in spurious connections, the results of the connectivity change may be misleading as well. Neither contributions nor connectivity change substantially outperformed the other method in

identifying symptoms. However, the results from contribution plots are perhaps more intuitive to interpret, and therefore are preferable to considering connectivity change. In other words, it is difficult to interpret the change in connectivity to conclusively determine which nodes should be considered symptoms. Further study is required into the changes in connectivity use to fault conditions in order to successfully use the information for fault identification

Both the connectivity change and the contributions gave more useful results once blocking had already narrowed down the part of the process most affected by the fault.

For the connectivity change it is also uncertain which TEM gave the best results.

8.3.2. Back propagation

Using the symptoms identified either by connectivity change or by contributions, the connectivity graphs were used to trace the faults back to possible root causes.

It was observed that a major hindrance for this method is that it considers only measured variables in the system, since the connectivity graphs are extracted from historical data. This is a problem since the root causes of the faults do not always correspond to an individual measured variable. For example, fouling in the heating coils of the two-tank system cannot be measured by a single variable; its effect can be observed in the temperatures of both tanks. Therefore the root cause analysis using this method serves to further isolate possible variables that show effects of the fault, allowing an operator to make a more informed conclusion about where in the plant to proceed with further investigation.

Once again, it is impossible to definitively conclude which TEM's connectivity graph gave the best results for fault identification. Each method performed well in some cases and poorly in others. This performance is once again strongly dependent on how well the TEM represents the topology of the process, and how many of its connections are spurious.

8.3.3. Improvement in fault identification ability using blocking

It was mentioned in section 8.2.3 that blocking showed improvement in the fault detection performance in most cases. It was observed in all cases that, by identifying which block resulted in the best detection performance, useful information of the fault conditions was obtained. In other words blocking displayed substantial utility in fault identification, allowing the variables in a specific block to be identified as displaying the most significant effects of the fault and allowing further fault identification to be performed using this information.

8.4. Fulfilment of Project Objectives

The objectives of the project, as presented in Chapter 1, and a description of how these objectives were fulfilled is given Table 8-1.

Table 8-1: Objectives of the project

	Objective	Description of Fulfilment
1	Determination of whether topology information can be used to aid fault identification using connectivity change and back propagation in connectivity graphs.	Topology information was used to perform fault identification on a number of fault scenarios for different processes. It was found that topology information was useful for fault identification in most of the fault scenarios. However, the performance was inconsistent, being dependent on the accuracy of the topology extraction methods.
2	Determination of whether automatic blocking of data according to connected components in connectivity graphs improves fault diagnosis.	Blocking using connectivity graphs was successfully applied to the leaching simulation and concentrator case studies. It was concluded that blocking substantially improved fault detection and fault identification.
3	Testing of all possible combinations of fault diagnosis methods considered to determine which combination provides best fault detection performance and best fault identification performance.	All possible combinations of fault diagnosis methods considered were tested for fault diagnosis on a number of fault scenarios for different processes. A recommended fault diagnosis methodology based on the results obtained is presented in section 9.1.

Chapter 9 - Recommendations

This chapter presents the recommendations considering the conclusions discussed in Chapter 8 -. The recommendation for the best fault diagnosis strategy, to be used in future case studies, is first presented, and then recommendations for future work are presented.

9.1. Recommended Fault Diagnosis Strategy

Considering the conclusions presented in Chapter 8 - the following strategy for fault diagnosis is recommended:

1) For topology extraction, it is recommended that LC be considered first, in preference to the other methods, since it is the simplest and fastest to compute. If LC gives poor results, the TE can be considered to possibly obtain a better connectivity graph, and finally if neither of those works the PC can be considered.
2) The multiblock process monitoring method proposed clearly improves detection and identification of faults, so blocking should be applied. The connectivity graph that gave the most accurate connectivity should be used for blocking.
3) The difference between PCA and KPCA was not substantial, but the fact that the computational effort associated with KPCA and the added complexity of selecting the kernel width parameter makes PCA the more appealing option. Additionally, PCA allows the use of contribution plots, which gave good fault identification results.
4) The EWMA chart clearly resulted in the best detection performance, giving accurate classification of faulty and normal data, with rapid detection speed. Therefore this monitoring chart should be applied to the T_A^2 and SPE statistics. It is still useful to analyse both the T_A^2 and the SPE statistics, since some faults may show large values for the one and not for the other.
5) Contribution plots generally provided symptoms of the fault that were accurate indicators of the fault conditions. Additionally the results of the connectivity change are more difficult to analyse and interpret.
6) Back propagation using the connectivity graph selected in the first step does provide useful indication of where the fault occurred. However, it is important that these results be considered a tool to aid an expert in the process in identifying the root cause through thorough root cause analysis, the results from back propagation themselves do not result in a definitive root cause identification.

9.2. Possibility of Industrial Application

The first hindrance to real-world implementation of these methods is the issues associated with definition and collection of NOC data. The topology extraction methods require the most representative NOC data, as well as enough data to capture all the NOC behaviour. These criteria ensure accurate representation of the flow in the process, and in turn give accurate fault identification results. The same criteria for NOC apply to training of the feature extraction models.

Once the data has been collected, the data-based methods should be readily applicable without much expert input required to generate the results. The automatic threshold selection for the monitoring charts gave good performance. However, as mentioned in the conclusions, the automatic threshold selection for topology extraction is not robust enough for unsupervised application.

Ideally the fault diagnosis strategy would be suitable for online implementation, so that when a fault occurs, back propagation using topology information happens automatically and root cause analysis results would be immediately available. However, the results of the back propagation using connectivity graphs are not suitable for a non-expert operator to interpret and take corrective action. The techniques considered do not point directly to a fault; they give an indication of the measured variables associated with the root cause of the fault. It requires an expert in the process to then interpret these results as an aid to further root cause analysis, performed offline.

9.3. Recommendations for Future Work

Considering the conclusions presented in Chapter 8 -, the recommendations for focus in future studies on fault diagnosis exploiting process topology are presented.

The automated threshold selection technique for the TEMs was not robust enough to be applied to different case studies; the resulting thresholds had to be increased to generate accurate connectivity graphs. A thorough study on methods for threshold selection is recommended to provide an automated method, or at least a rigorous selection method.

Contribution plots results can be further exploited by setting weights to the symptom variables according to how large their contributions were. I.e. symptoms nodes that showed larger contributions can be given stronger weighting in the identification of possible root nodes.

Fault conditions clearly affect the connectivity of the process, but the results are sensitive to the accuracy of the topology extraction method, as well as the thresholds selected. Therefore further study into the effects of fault conditions on the connectivity is required to improve the use of connectivity change for fault identification.

Chapter 10 - References

1. Aldrich, C., Auret, L., 2013. Unsupervised process monitoring and fault diagnosis with machine learning methods. Springer, London.
2. AlGhazzawi, A., Lennox, B., 2008. Monitoring a complex refining process using multivariate statistics. Control Eng. Pract. 16, 294–307.
3. Auret, L., 2010. Process monitoring and fault diagnosis using random forests (Thesis). Stellenbosch : University of Stellenbosch.
4. Bakshi, B.R., 1998. Multiscale PCA with application to multivariate statistical process monitoring. AIChE J. 44, 1596–1610.
5. Bauer, M., Cox, J.W., Caveness, M.H., Downs, J.J., Thornhill, N.F., 2007. Finding the Direction of Disturbance Propagation in a Chemical Process Using Transfer Entropy. Control Syst. Technol. IEEE Trans. On 15, 12–21.
6. Bauer, M., Thornhill, N.F., 2008. A practical method for identifying the propagation path of plant-wide disturbances. J. Process Control 18, 707–719.
7. Bauer, M., Thornhill, N.F., Meaburn, A., 2004. Specifying the directionality of fault propagation paths using transfer entropy. Proc 7th Int. Symp. Dyn. Control Process Syst. 203–208.
8. Bin Shams, M.A., Budman, H.M., Duever, T.A., 2011. Fault detection, identification and diagnosis using CUSUM based PCA. Chem. Eng. Sci. 66, 4488–4498.
9. Chen, J., Liao, C.-M., Lin, F.R.J., Lu, M.-J., 2001. Principle component analysis based control charts with memory effect for process monitoring. Ind. Eng. Chem. Res. 40, 1516–1527.
10. Chiang, L.H., Braatz, R.D., 2003. Process monitoring using causal map and multivariate statistics: fault detection and identification. Chemom. Intell. Lab. Syst. 65, 159–178.
11. Cho, J.-H., Lee, J.-M., Wook Choi, S., Lee, D., Lee, I.-B., 2005. Fault identification for process monitoring using kernel principal component analysis. Chem. Eng. Sci. 60, 279–288.
12. Crosier, R.B., 1988. Multivariate Generalizations of Cumulative Sum Quality-Control Schemes. Technometrics 30, 291–303.
13. de la Fuente, Bing, N., Hoeschele, I., Mendes, P., 2004. Discovery of meaningful associations in genomic data using partial correlation coefficients. Bioinformatics 20, 3565–3574.
14. Dong, D., McAvoy, T.J., 1996. Nonlinear principal component analysis—Based on principal curves and neural networks. Comput. Chem. Eng. 20, 65–78.
15. Dorfling, C., 2012. Characterisation and dynamic modelling of the behaviour of platinum group metals in high pressure sulphuric acid/oxygen leaching systems (PhD). Stellenbosch University.
16. Duan, P., Yang, F., Chen, T., Shah, S.L., 2012. Detection of direct causality based on process data. Presented at the Proceedings of the American Control Conference, pp. 3522–3527.
17. Dunia, R., Qin, S.J., 1998. Subspace approach to multidimensional fault identification and reconstruction. AIChE J. 44, 1813–1831.
18. Fan Yang, Sirish, L.S., Deyun Xiao, 2010. Signed Directed Graph modeling of industrial processes and their validation by data-based methods. Presented at the Control and Fault-Tolerant Systems (SysTol), 2010 Conference on, pp. 387–392.
19. Fried, R., Didelez, V., 2005. Latent variable analysis and partial correlation graphs for multivariate time series. Stat. Probab. Lett. 73, 287–296.
20. Ge, Z., Song, Z., 2009. Two-level multiblock statistical monitoring for plant-wide processes. Korean J. Chem. Eng. 26, 1467–1475.
21. Ge, Z., Song, Z., 2013. Distributed PCA Model for Plant-Wide Process Monitoring. Ind. Eng. Chem. Res. 52, 1947–1957.
22. Ge, Z., Yang, C., Song, Z., 2009. Improved kernel PCA-based monitoring approach for nonlinear processes. Chem. Eng. Sci. 64, 2245–2255.

23. Groenewald, J.W.D.V., 2014. A Process Performance Monitoring Methodology for Mineral Processing Plants (Thesis). University of Stellenbosch, Stellenbosch.
24. Himmelblau, D.M., 1978. Fault detection and diagnosis in chemical and petrochemical processes. Elsevier Science, Amsterdam.
25. Hlaváčková-Schindler, K., Paluš, M., Vejmelka, M., Bhattacharya, J., 2007. Causality detection based on information-theoretic approaches in time series analysis. Phys. Rep. 441, 1–46.
26. Hou, Q., Wang, L., Lu, N.Y., Jiang, B., Lu, J.H., 2010. A FDD method by combining transfer entropy and signed digraph and its application to air separation unit. Presented at the 11th International Conference on Control, Automation, Robotics and Vision, ICARCV 2010, pp. 352–357.
27. Iri, M., Aoki, K., O'Shima, E., Matsuyama, H., 1979. An algorithm for diagnosis of system failures in the chemical process. Comput. Chem. Eng. 3, 489–493.
28. Izadi, I., Chen, T., Shah, S., 2011. Alarm Systems: Quantitative Analysis and Design.
29. Jiang, H., Patwardhan, R., Shah, S.L., 2009. Root cause diagnosis of plant-wide oscillations using the concept of adjacency matrix. Spec. Sect. Hybrid Syst. Model. Simul. Optim. 19, 1347–1354.
30. Kano, M., Nagao, K., Hasebe, S., Hashimoto, I., Ohno, H., Strauss, R., Bakshi, B.R., 2002. Comparison of multivariate statistical process monitoring methods with applications to the Eastman challenge problem. Comput. Chem. Eng. 26, 161–174.
31. Knoblauch, N., (In Progress). Implementation and analysis of control strategies for second and third stage leach (Master's Thesis). Stellenbosch University.
32. Knoblauch, N., 2012. Preliminary implementation and analysis of control strategies for second and third stage leach (Final Year Project). Stellenbosch University.
33. Kourti, T., 2002. Process analysis and abnormal situation detection: from theory to practice. Control Syst. IEEE 22, 10–25.
34. Kourti, T., MacGregor, J.F., 1995. Process analysis, monitoring and diagnosis, using multivariate projection methods. Chemom. Intell. Lab. Syst. 28, 3–21.
35. Kramer, M.A., 1992. Autoassociative neural networks. Comput. Chem. Eng. 16, 313–328.
36. Ku, W., Storer, R.H., Georgakis, C., 1995. Disturbance detection and isolation by dynamic principal component analysis. Chemom. Intell. Lab. Syst. 30, 179–196.
37. Lee, J.-M., Yoo, C., Choi, S.W., Vanrolleghem, P.A., Lee, I.-B., 2004. Nonlinear process monitoring using kernel principal component analysis. Chem. Eng. Sci. 59, 223–234.
38. Lindner, B., Auret, L., Knoblauch, N., 2014. Exploiting process topology for fault diagnosis in a simulated pressure leaching system. Presented at the International Minerals Processing Conference (IMPC 2014), Santiago, Chilé.
39. Liu, Q., Qin, S.J., Chai, T., 2013. Decentralized Fault Diagnosis of Continuous Annealing Processes Based on Multilevel PCA. IEEE Trans. Autom. Sci. Eng. Early Access Online.
40. MacGregor, J.F., Jaeckle, C., Kiparissides, C., Koutoudi, M., 1994. Process monitoring and diagnosis by multiblock PLS methods. AIChE J. 40, 826–838. doi:10.1002/aic.690400509
41. MacGregor, J.F., Kourti, T., 1995. Statistical process control of multivariate processes. Control Eng. Pract. 3, 403–414.
42. Maurya, M.R., Rengaswamy, R., Venkatasubramanian, V., 2003. A Systematic Framework for the Development and Analysis of Signed Digraphs for Chemical Processes. 1. Algorithms and Analysis. Ind. Eng. Chem. Res. 42, 4789–4810.
43. McNemar, Q., 1947. Note on the sampling error of the difference between correlated proportions or percentages. Psychometrika 12, 153–157. doi:10.1007/BF02295996
44. Misra, M., Yue, H.H., Qin, S.J., Ling, C., 2002. Multivariate process monitoring and fault diagnosis by multi-scale PCA. Comput. Chem. Eng. 26, 1281–1293.
45. Nguyen, V.H., Golinval, J.-C., 2010. Fault detection based on Kernel Principal Component Analysis. Eng. Struct. 32, 3683–3691.

46. Nomikos, P., MacGregor, J.F., 1995. Multivariate SPC Charts for Monitoring Batch Processes. Technometrics 37, pp. 41–59.
47. Prabhu, S.S., Runger, G.C., 1997. Designing a multivariate EWMA control chart. J. Qual. Technol. 29, 8–15.
48. Qin, S.J., Valle, S., Piovoso, M.J., 2001. On unifying multiblock analysis with application to decentralized process monitoring. J. Chemom. 15, 715–742.
49. Ram Maurya, M., Rengaswamy, R., Venkatasubramanian, V., 2004. Application of signed digraphs-based analysis for fault diagnosis of chemical process flowsheets. Eng. Appl. Artif. Intell. 17, 501–518.
50. Schölkopf, B., Smola, A., Müller, K.-R., 1998. Nonlinear Component Analysis as a Kernel Eigenvalue Problem. Neural Comput. 10, 1299–1319.
51. Schreiber, T., Schmitz, A., 2000. Surrogate time series. Phys. Nonlinear Phenom. 142, 346–382.
52. Tarjan, R., 1972. Depth-First Search and Linear Graph Algorithms. SIAM J. Comput. 1, 15.
53. Thornhill, N.F., Horch, A., 2007. Advances and new directions in plant-wide disturbance detection and diagnosis. Spec. Issue - Int. Symp. Adv. Control Chem. Process. ADCHEM ADCHEM 2006 Int. Symp. Adv. Control Chem. Process. ADCHEM 15, 1196–1206.
54. Venkatasubramanian, V., Rengaswamy, R., Kavuri, S.N., 2003a. A review of process fault detection and diagnosis: Part II: Qualitative models and search strategies. Comput. Chem. Eng. 27, 313–326.
55. Venkatasubramanian, V., Rengaswamy, R., Kavuri, S.N., Yin, K., 2003b. A review of process fault detection and diagnosis: Part III: Process history based methods. Comput. Chem. Eng. 27, 327–346.
56. Wachs, A., Lewin, D.R., 1999. Improved PCA methods for process disturbance and failure identification. AIChE J. 45, 1688–1700.
57. Westerhuis, J.A., Kourti, T., MacGregor, J.F., 1998. Analysis of multiblock and hierarchical PCA and PLS models. J. Chemom. 12, 301–321.
58. Wise, B.M., Gallagher, N.B., 1996. The process chemometrics approach to process monitoring and fault detection. J. Process Control 6, 329–348.
59. Wold, S., 1994. Exponentially weighted moving principal components analysis and projections to latent structures. Chemom. Intell. Lab. Syst. 23, 149–161.
60. Wold, S., Kettaneh, N., Tjessem, K., 1996. Hierarchical multiblock PLS and PC models for easier model interpretation and as an alternative to variable selection. J. Chemom. 10, 463–482.
61. Xu, L., Oja, E., Suen, C.Y., 1992. Modified Hebbian learning for curve and surface fitting. Neural Netw. 5, 441–457.
62. Yang, F., Shah, S., Xiao, D., 2009. SDG model-based analysis of fault propagation in control systems, in: Canadian Conference on Electrical and Computer Engineering, 2009. CCECE '09. Presented at the Canadian Conference on Electrical and Computer Engineering, 2009. CCECE '09, pp. 1152–1157.
63. Yang, F., Xiao, D., 2012. Progress in Root Cause and Fault Propagation Analysis of Large-Scale Industrial Processes. J. Control Sci. Eng.
64. Yang, J., Li, L., Wang, A., 2011. A partial correlation-based Bayesian network structure learning algorithm under linear SEM. Knowl.-Based Syst. 24, 963–976.
65. Yim, S.Y., Ananthakumar, H.G., Benabbas, L., Horch, A., Drath, R., Thornhill, N.F., 2006. Using process topology in plant-wide control loop performance assessment. Comput. Chem. Eng. 31, 86–99.
66. Zhang, Y.-W., Zhou, H., Qin, S.J., 2010. Decentralized Fault Diagnosis of Large-scale Processes Using Multiblock Kernel Principal Component Analysis. Acta Autom. Sin. 36, 593–597.

Appendix A- Two-tank Simulation Development

10.1. Model of Example System

An example system was chosen for the development and testing of the methods presented in this report. The fundamental model of this system was derived and the system was modelled in Simulink. A description of this system and the generation of the model is provided here.

A.1.1. Goals

A model of a system containing two tanks with heating coils is to be developed. The dynamic behaviour of all variables in the system is to be modelled so that data generated from this model can be used in the development and testing of data-based monitoring methods and data-based methods of inferring connectivity between variables.

A.1.2. Information

The chosen example system consists of two tanks. A diagram of the system is shown in Figure A-1.

The outlet flow from both tanks is proportional to the square root of the level in each tank. The outlet from the first tank flows into the second tank. Each tank has its own supply of cold water with a control valve to control the level of each tank. Each tank also exchanges heat with a steam line. The temperature in the tanks is controlled using the control valves on the steam lines.

The main variables of interest are the flow rate of the inlet streams to the tanks, F_1 and F_2, the flow rates of the steam in the heating coils in both tanks, F_3 and F_4, the levels of both tanks, L_1 and L_2, and the temperatures of both tanks, T_1 and T_2. F_1 and F_2 are used as manipulated variables (MVs) to control L_1 and L_2 respectively. F_3 and F_4 are used as MVs to control T_1 and T_2 respectively. The controllers used are simple proportional integral derivative (PID) controllers that change the values of the MVs according to the deviation of the controlled variables (CVs) from their set-points (SPs).

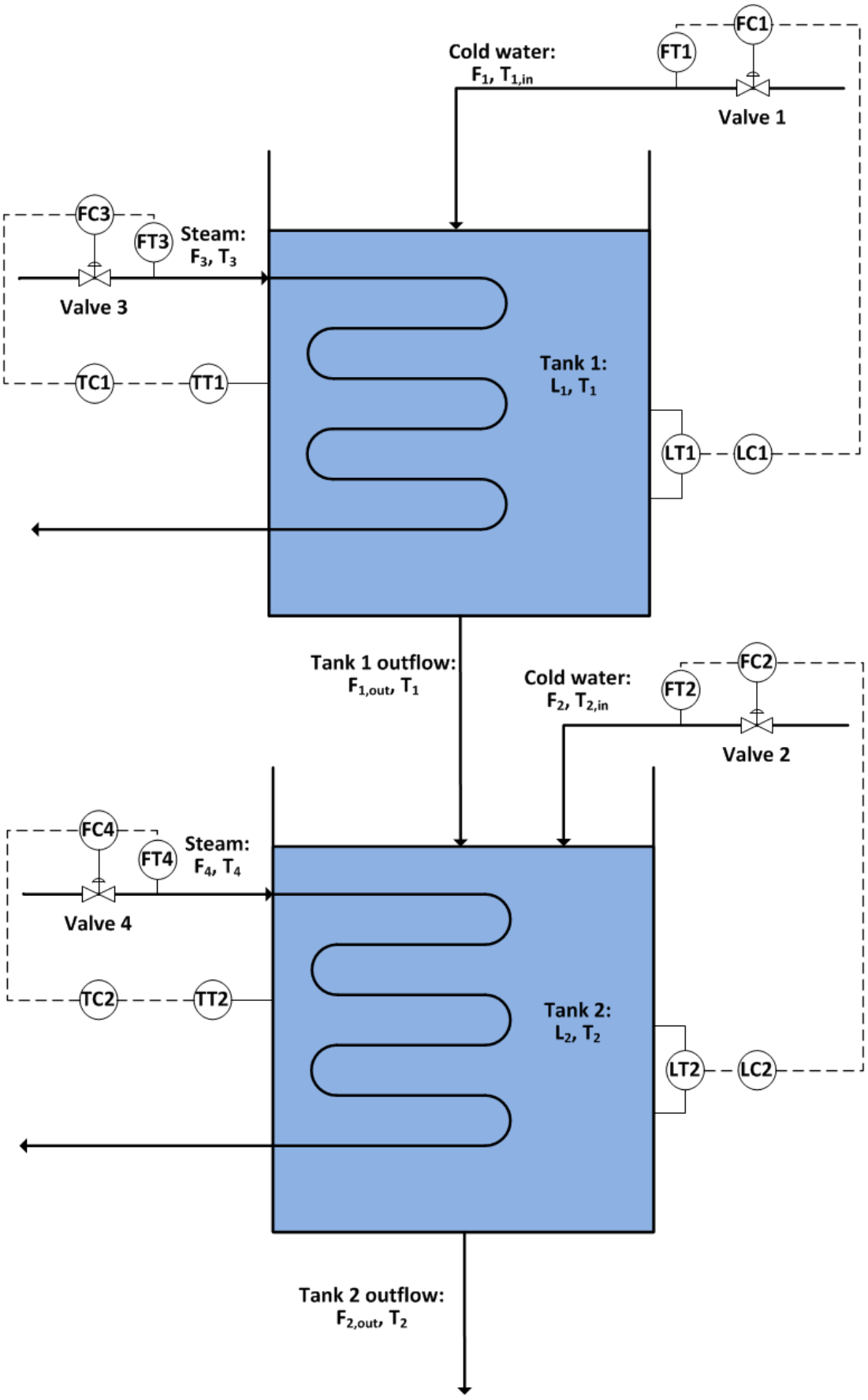

Figure A-1: Diagram of two-tank example system

The measurements obtained from real-life processes such as this would typically display significant amounts of random noise generated by sensors or just normal fluctuations in the values of the properties being measured.

The steady state values for variables in the process are given in Table A-1. The steady state values for the CVs, L_1, L_2, T_1 and T_2, are also their set-point values.

Table A-1: Steady state values for two-tank model

Variable	Value	Units
L_1	2.00	[m]
L_2	3.00	[m]
T_1	50.0	[°C]
T_2	50.0	[°C]
$T_{1,in}$	25.0	[°C]
$T_{2,in}$	25.0	[°C]
T_3	100	[°C]
T_4	100	[°C]
F_1	0.181	[m^3/min]
F_2	0.0408	[m^3/min]
F_3	0.5	[m^3/min]
F_4	0.04	[m^3/min]
F1out	0.191	[m^3/min]
F2out	0.222	[m^3/min]

The values of the parameters used in the model are given in Table A-2. The value for the proportionality constant relating the underflow to the level, K_L, was determined by substituting steady-state values into Equation 10 and solving for K_L (at steady state the differential term is 0). The valve constant for each control valve was simply chosen so that the steady state value of the flow rate being controlled by the valve corresponded to a valve position of 50%.

Table A-2: Parameters used in model of two-tank system

Parameter	Description	Value	Units
aHeat	Constant for heat transfer coefficient calculation	1.41(10^5)	[cal/(min°C)]
b	Constant for heat transfer coefficient calculation	0.5	[ ]
C_p	Heat capacity of water	1	[cal/(g°C)]
ρ	Density of water	10^6	[g/m^3]
A_1	Cross-sectional area of tank 1	1	[m^2]
A_2	Cross-sectional area of tank 2	1	[m^2]
k_L	Level constant	0.128	[m^3/min/$m^{0.5}$]
k_{v1}	Valve 1's constant	0.00363	[m^3/min/%open]
k_{v2}	Valve 2's constant	0.000815	[m^3/min/%open]
k_{v3}	Valve 3's constant	0.01	[m^3/min/%open]
k_{v4}	Valve 4's constant	0.000769	[m^3/min/%open]

A.1.3. Formulation of model

Mass balance

A generalised mass balance on a tank is given by:

Equation 70: Generalised mass balance

$$Accumulation = \sum Flows\ in - \sum Flows\ out$$

The mass balance of the first tank therefore requires determination of the accumulation term, which is the change in volume of the tank with time. There is one stream flowing in, F_1, and one stream flowing out, $F_{1,out}$. The heating steam flow, F_3, flows into and out of the tank in heating coils and does not mix at all with the material in the tank, therefore it does not appear in the mass balance (it will appear in the energy balance since it exchanges heat with the material in the tank). Therefore the mass balance is given by:

Equation 71

$$\frac{dV_1}{dt} = F_1 - F_{1,out}$$

The volume of the tank is given by the level multiplied by the cross sectional area. The level varies, so it remains within the derivative term, but the area can be taken out. The flow rate out of the tank is dependent on the level of the tank. The flow rate is related to the pressure driving force ((Marlin, 2000)), i.e. the static pressure exerted by the liquid. This relationship can be approximated by:

Equation 72 ((Marlin, 2000)**)**

$$F_{1,out} = k_L \cdot \sqrt{L_1}$$

Substitution into Equation 71 results in the mass balance for tank 1:

Equation 10: Tank 1 mass balance

$$A_1 \frac{dL_1}{dt} = F_1 - k_L \cdot \sqrt{L_1}$$

For the second tank the mass balance is similar, except that the underflow from tank 1 also flows into it. The resulting mass balance for tank 2 is given by:

Equation 74: Tank 2 mass balance

$$A_2 \frac{dL_2}{dt} = k_L \cdot \sqrt{L_1} + F_2 - k_L \cdot \sqrt{L_2}$$

Energy balance

Since there is not shaft work in the process, the energy balance is given by:

Equation 75

$$\frac{dU}{dt} = \dot{H}_{in} - \dot{H}_{out} + Q$$

The change in internal energy, U, with time is given by:

Equation 76

$$\frac{dU}{dt} = \rho C_p \frac{dVT}{dt}$$

The enthalpy of stream i, H_i, is given by:

Equation 77

$$H_i = \rho C_p F_i (T_i - T_{ref})$$

Substituting these equations into the energy balance (assuming a value of 0 for T_{ref}) gives the following equation for the first tank:

Equation 78

$$\rho C_p \frac{dV_1 T_1}{dt} = \rho C_p (F_1 \cdot T_{1,in} - F_{1,out} \cdot T_1) + Q$$

Under the assumption of perfect mixing in the tank the temperature of the stream flowing out of the tank is equal to the temperature in the tank. The temperature of the feed stream is designated $T_{1,in}$.

Q represents the heat transferred to the liquid in the tank from the liquid in the heating coils. An energy balance on the liquid in the heating coils gives:

Equation 79

$$Q = \rho C_p F_3 (T_3 - T_{out})$$

F_3 is the flow rate of the heating steam, T_3 is the temperature at which the steam enters the coils and T_{out} is the temperature at which it exits F_3. Rearranging so that T_{out} is the subject of the equation gives:

Equation 80

$$T_{out} = T_3 - \frac{Q}{\rho C_p F_3}$$

The heat transferred can be determined using the overall heat transfer coefficient, UA. Assuming that the inner film resistance dominates the heat transfer through the coils, and that the resistance of the tube walls and the outer film resistance are negligible. An empirical equation relating the heat transfer coefficient to the flow rate of liquid was reported in Marlin as:

Equation 81

$$UA = aF_3^b$$

The heat transfer from the tubes is then given by the heat transfer coefficient multiplied by an approximation of the mean difference of the temperature in the tank and the temperature in the coils.

Equation 82

$$Q = -aF_3^b \left(\frac{(T_1 - T_3) + (T_1 - T_{out})}{2} \right)$$

Combination of Equation 80 and Equation 82 to eliminate T_{out}, gives:

Equation 83

$$Q = -\frac{aHeatF_3^{b+1}}{F_3 + \frac{aHeatF_3^b}{2\rho C_p}} \cdot (T_1 - T_3)$$

Substitution into Equation 78 results in the complete energy balance for tank 1:

Equation 84: Energy balance for tank 1

$$\rho C_p \frac{dV_1 T_1}{dt} = \rho C_p \left(F_1 \cdot T_{1,in} - F_{1,out} \cdot T_1 \right) - \frac{aHeatF_3^{b+1}}{F_3 + \frac{aHeatF_3^b}{2\rho C_p}} \cdot (T_1 - T_3)$$

For tank 2 the energy balance is similar, except that the energy entering the system from the outlet stream of tank 1 has to be included. The flow rate of water into the tank is F_2, entering at a temperature of $T_{2,in}$. The flow rate of steam is F_4, entering at a temperature of T_4. The temperature of the tank is T_2.

Equation 85: Energy balance for tank 2

$$\rho C_p \frac{dV_2 T_2}{dt} = \rho C_p \left(F_{1,out} \cdot T_1 + F_2 \cdot T_{2,in} - F_{2,out} \cdot T_2\right) - \frac{aHeatF_4^{b+1}}{F_4 + \frac{aHeatF_4^b}{2\rho C_p}} \cdot (T_2 - T_4)$$

A.2. Simulink Model

The model developed was simulated in Simulink, with control loops added. The model was divided into four subsystems; one representing each mass balance equation, and one representing each energy balance equation. Four feedback controllers were incorporated into the system to control the levels and temperatures in the tanks. PID control was implemented, and the Ciancone correlations were used to determine appropriate values for the tuning parameters. The tuning results are given in Table A-3. Noise was added to simulate sensor noise by adding noise with amplitude of 5% of the actual value of the variable.

Table A-3: Controller information

Controller	CV	MV	P	I	D
1	L_1	F_1	13.3	1.87	0
2	L_2	F_2	32.9	3.03	0
3	T_1	F_3	5.86	2.30	0
4	T_2	F_4	37.0	11.5	0

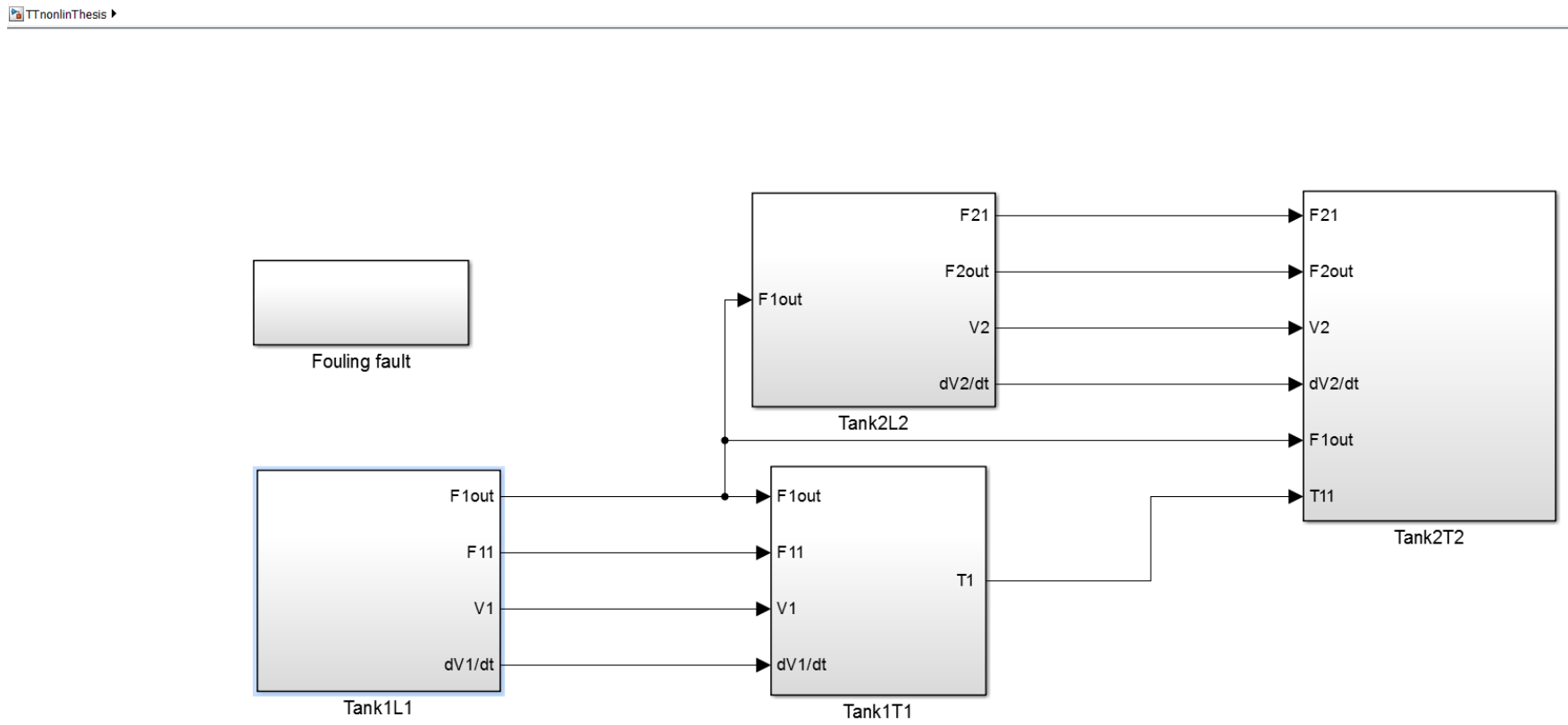

Figure A-2: Top level of Simulink model

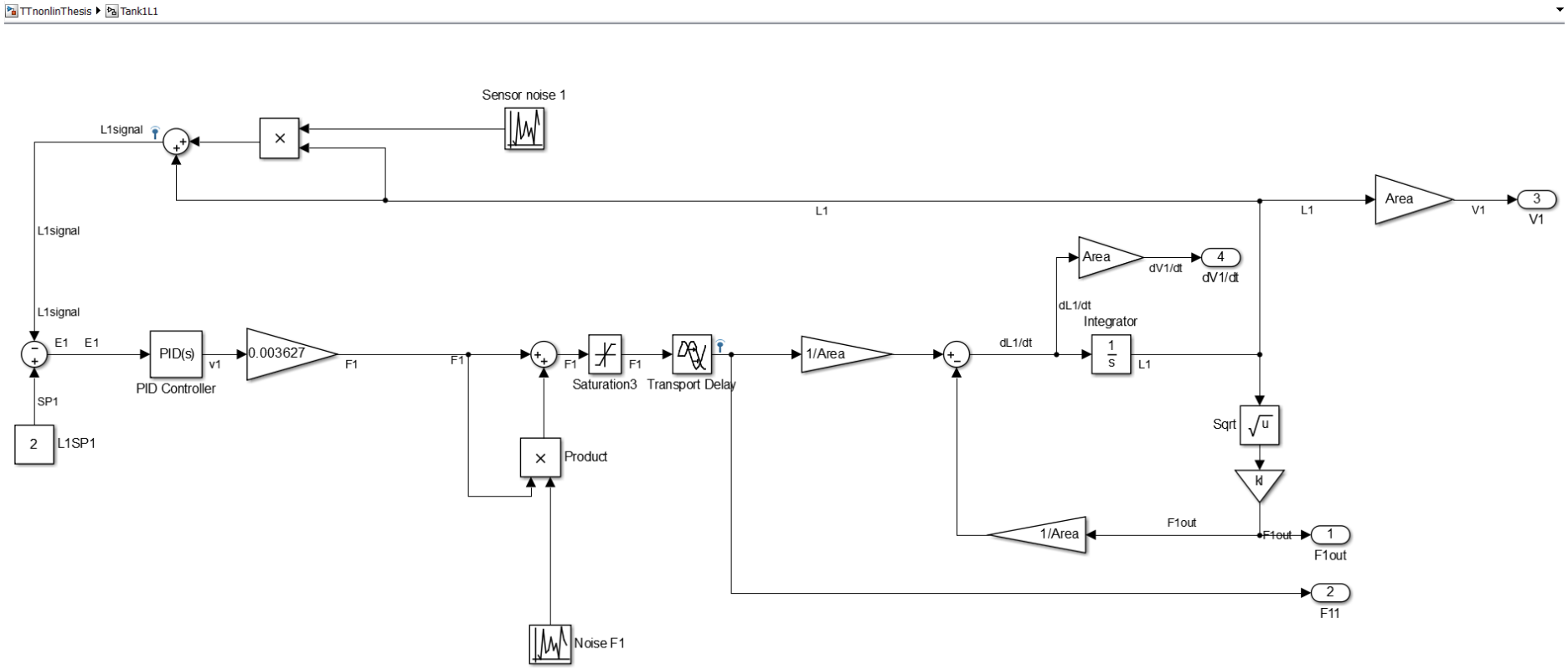

Figure A-3: First tank's level subsystem

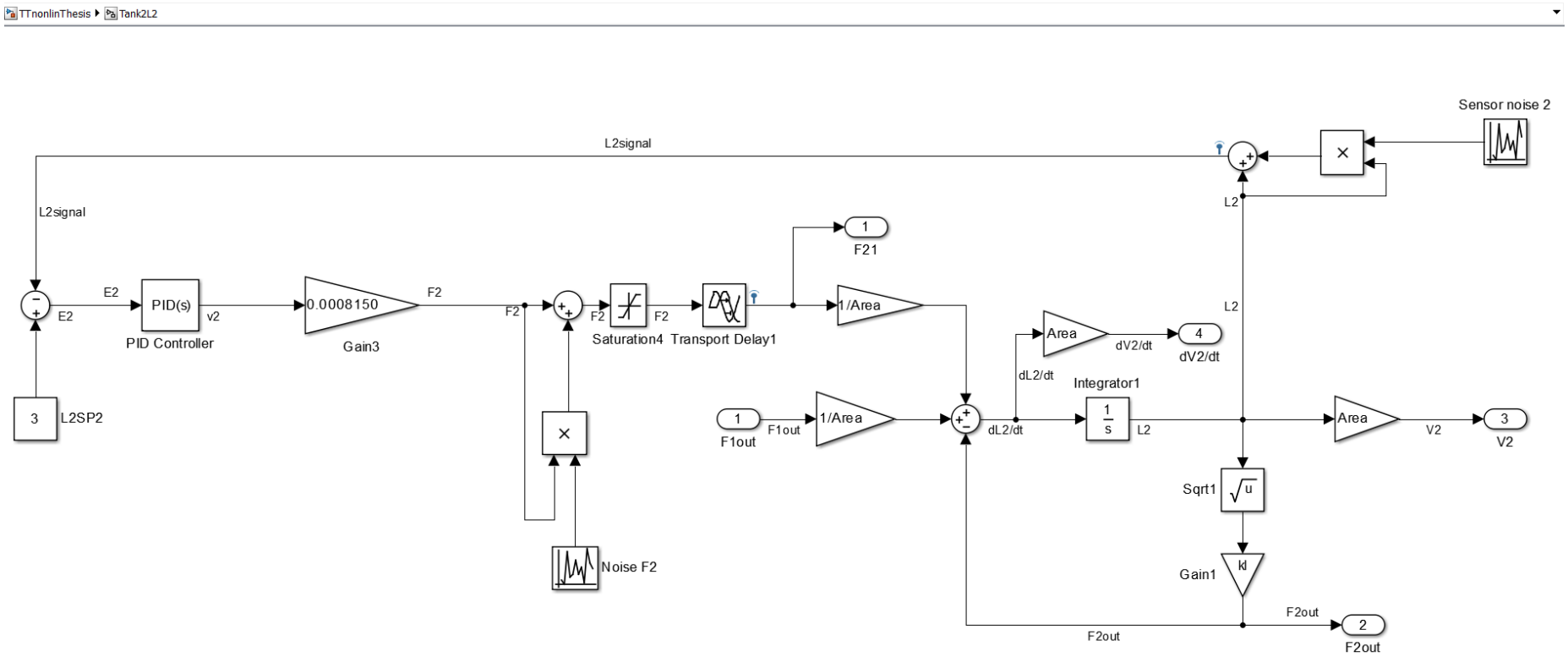

Figure A-4: Second tank's level subsystem

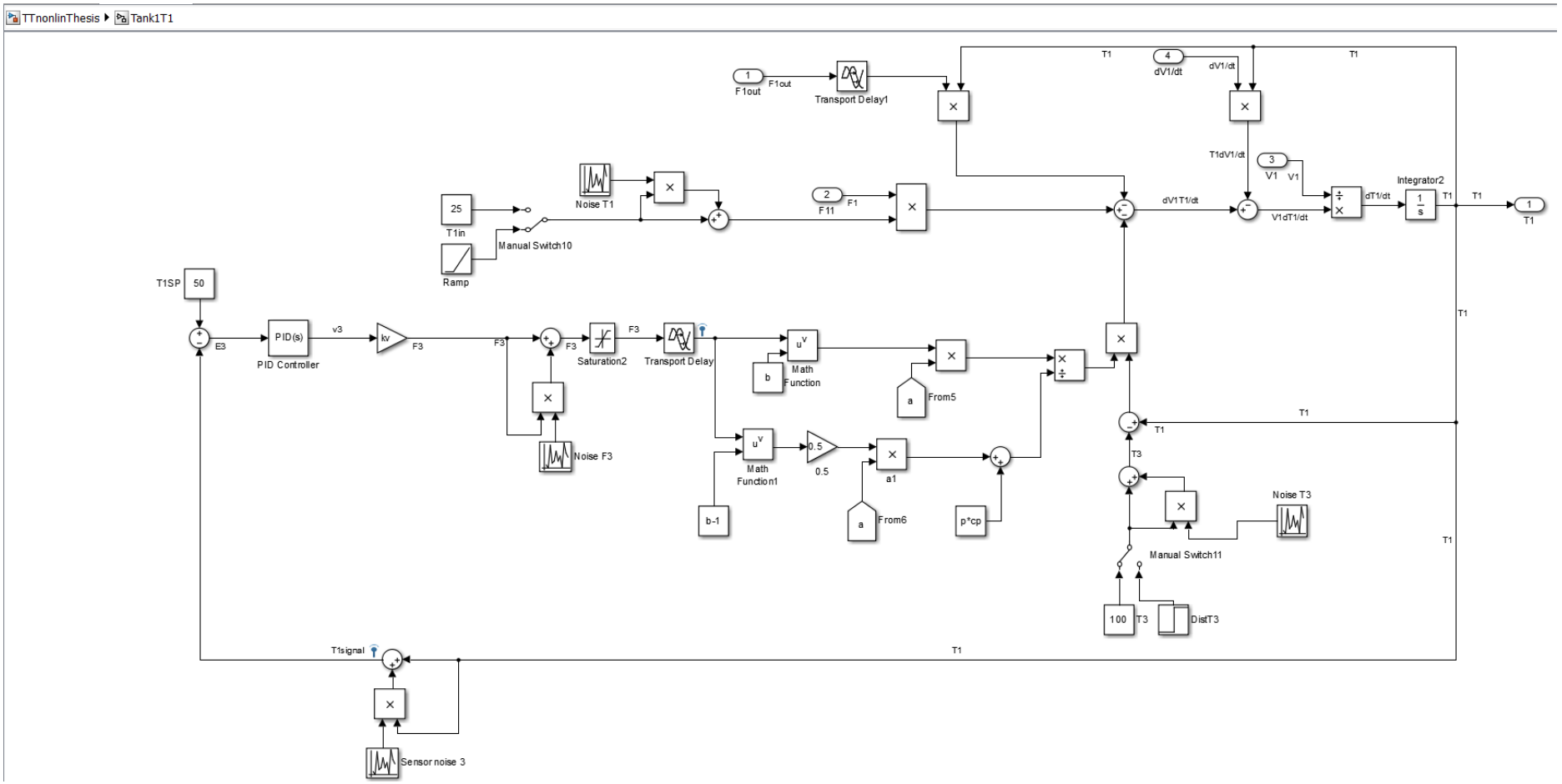

Figure A-5: First tank's temperature subsystem

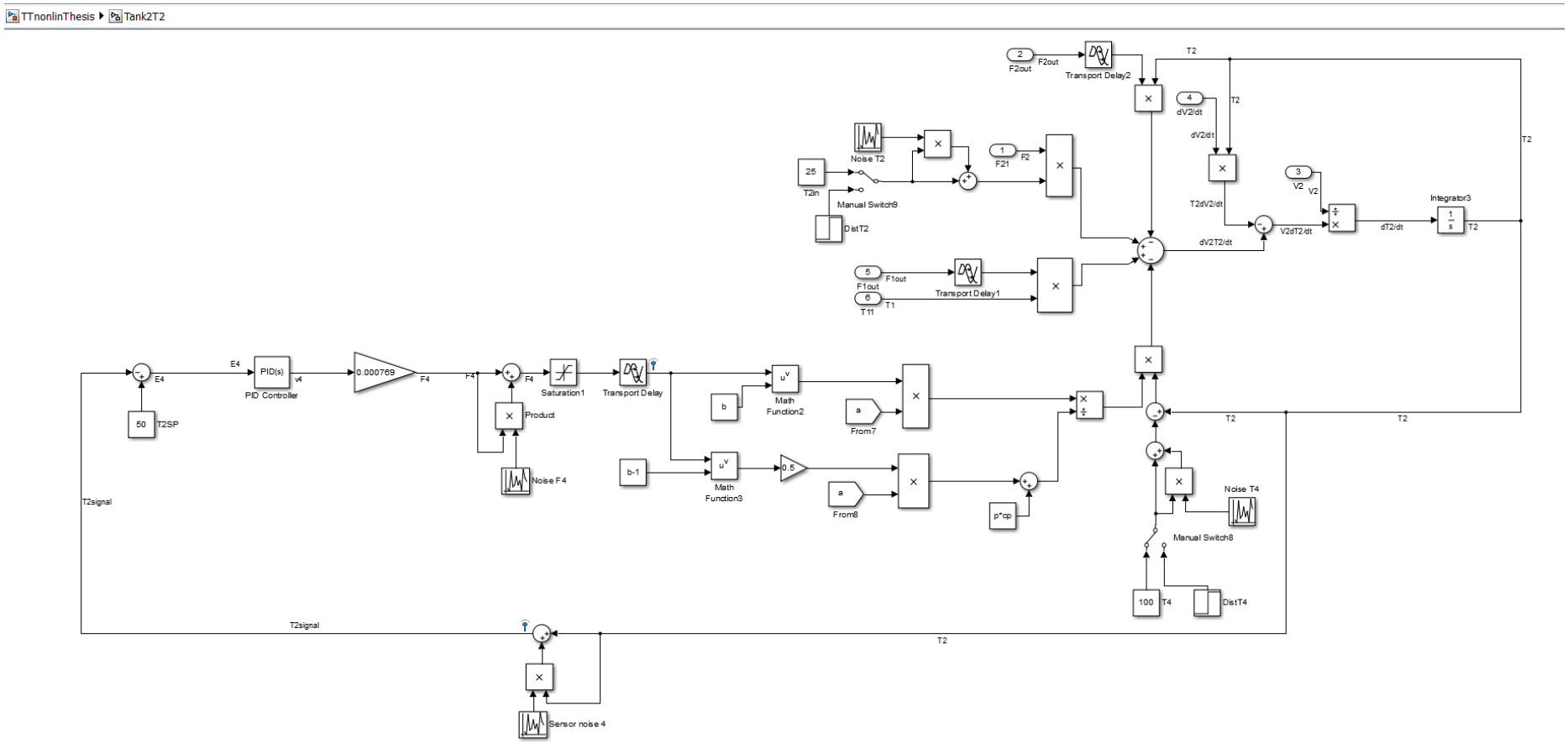

Figure A-6: Second tank's temperature subsystem

Appendix B- Two-Tank Case Study Fault Identification Results

B.1. Fault 1: Step $T_{1,in}$

For the first case the contributions identified L1, F2 T1 and F3 as possible symptom nodes. Despite the fact that L1 and F2 is present in this, the identification of T1 and F3 is a very good indication that a temperature fault has occurred in the first tank

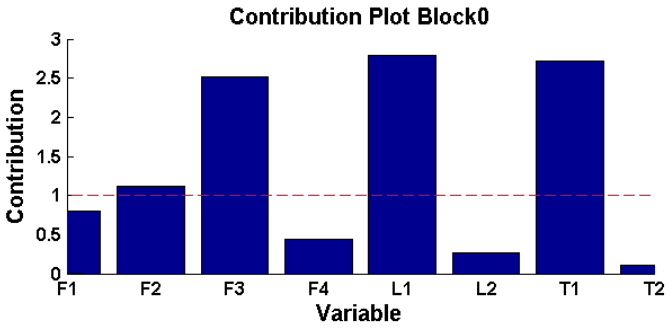

Figure B-1: Contribution plot for fault 1

The root nodes identified applying back propagation to the LC connectivity graph resulted in F1 and T1 being identified as possible root nodes: So symptoms yes, roots maybe.

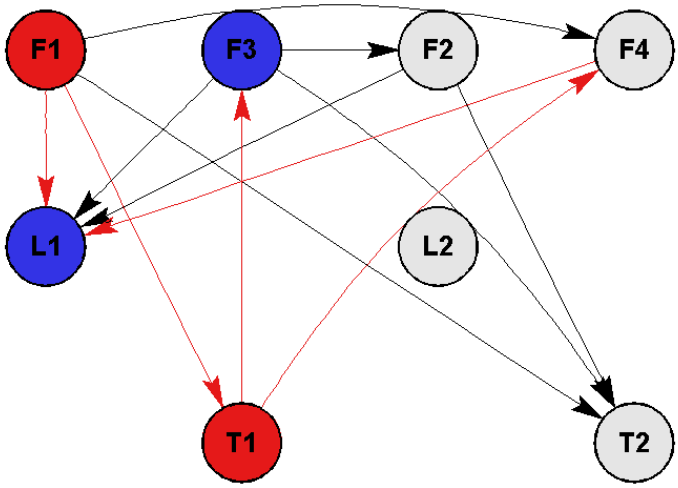

Figure B-2: Back propagation applied to LC graph from symptoms identified by contributions for fault 1

For the second case the connectivity change identified F3 and F4 as possible symptom nodes, which is very promising

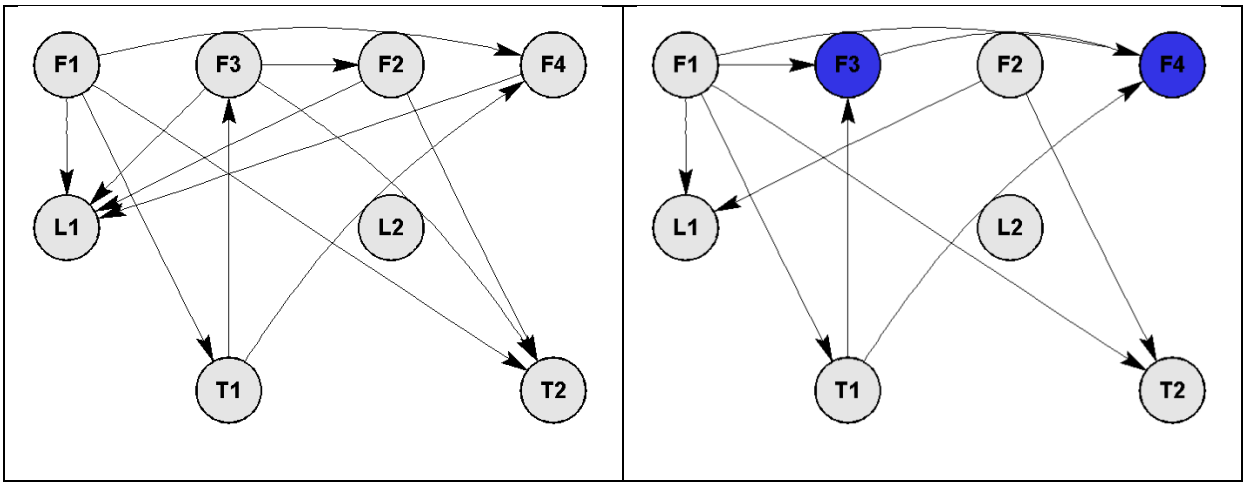

Figure B-3: Connectivity change for LC for fault 1

Applying back propagation from these two symptoms gave T1 as the only possible root node. This gives a very good indication that the fault lies somewhere with the first tank's temperature. So symptoms yes, roots yes.

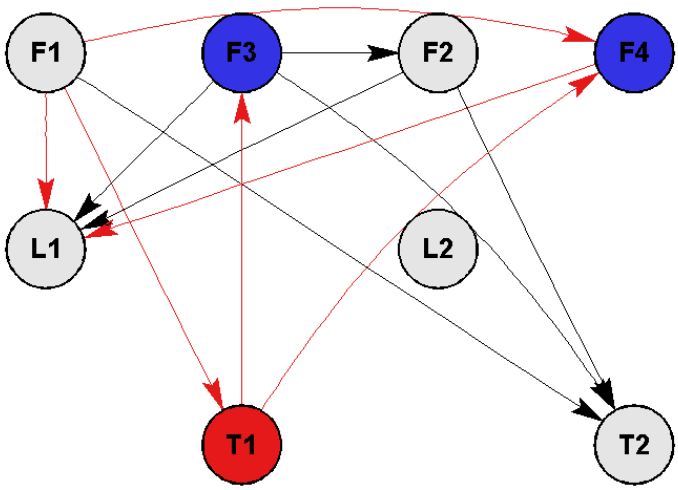

Figure B-4: Back propagation applied to LC graph from symptoms identified by connectivity change for fault 1

For the 3rd case applying back propagation from the symptom nodes identified from the contribution plots in the PC connectivity graph gave F3, F1, and F4 as possible root nodes. Since both F3 and F4 were identified this is a good indication that a temperature fault has occurred. So symptoms yes and roots yes.

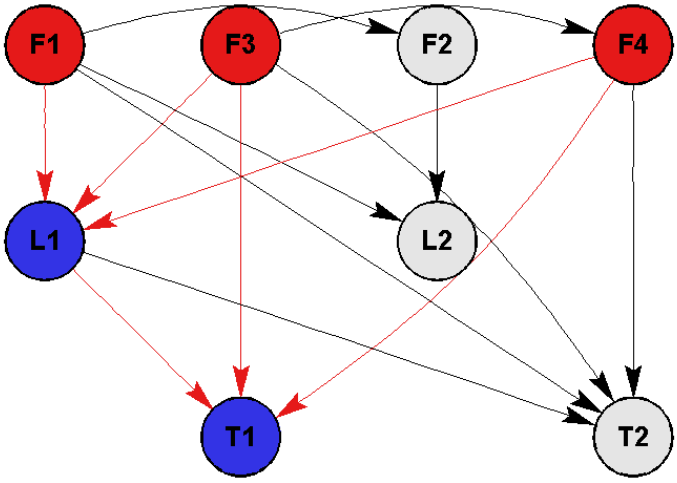

Figure B-5: Back propagation applied to PC graph from symptoms identified by contributions for fault 1

For the 4th case the connectivity change in the PC graph identified T1 as a possible symptom. This is a very good indication that something has occurred to affect the first tank's temperature

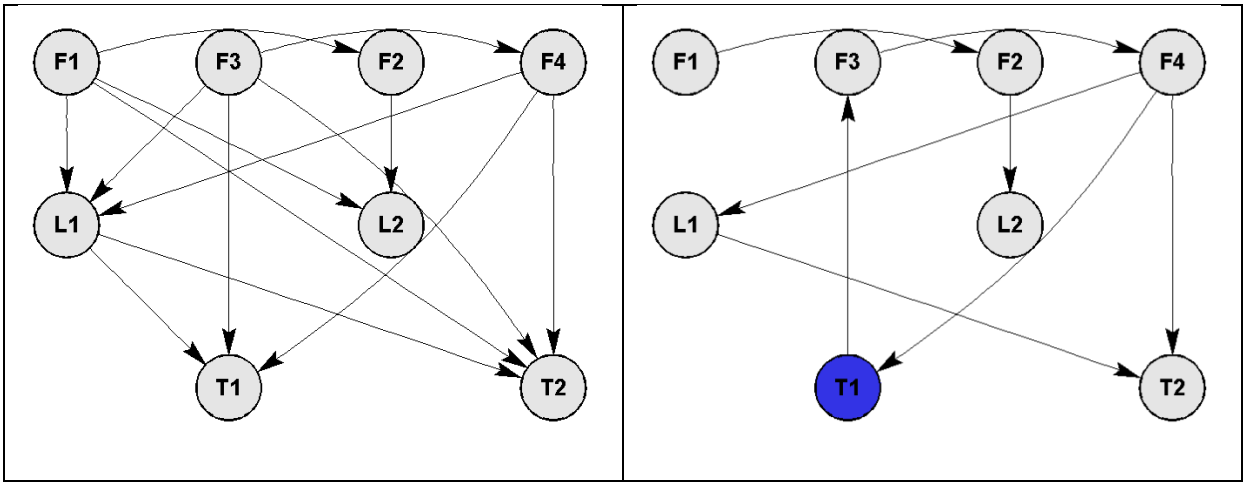

Figure B-6: Connectivity change for PC for fault 1

Applying back propagation on the PC connectivity graph then gives F3 , F4 and L1 as possible root nodes. With the exception of L1 this gives a very good indication that a temperature fault in the first tank has occurred. So symptoms yes, roots maybe.

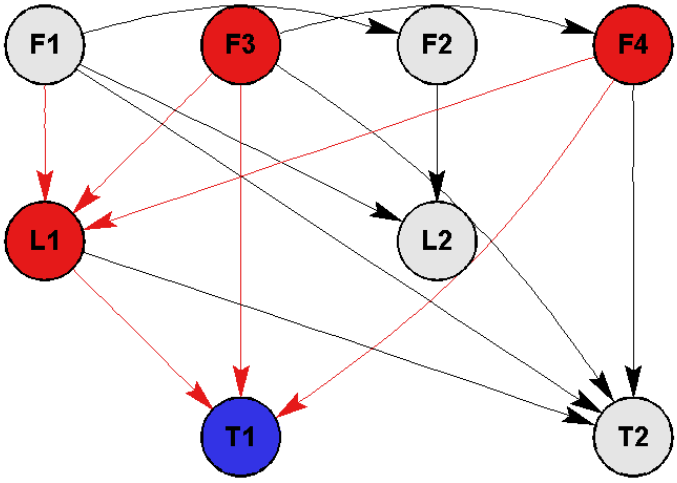

Figure B-7: Back propagation applied to PC graph from symptoms from connectivity change for fault 1

For the 5th case applying back propagation to the TE graph gives T2 T1 and L2 as possible root nodes. This gives a clear indication that a temperature fault in the first tank has occurred. So symptoms yes, roots yes.

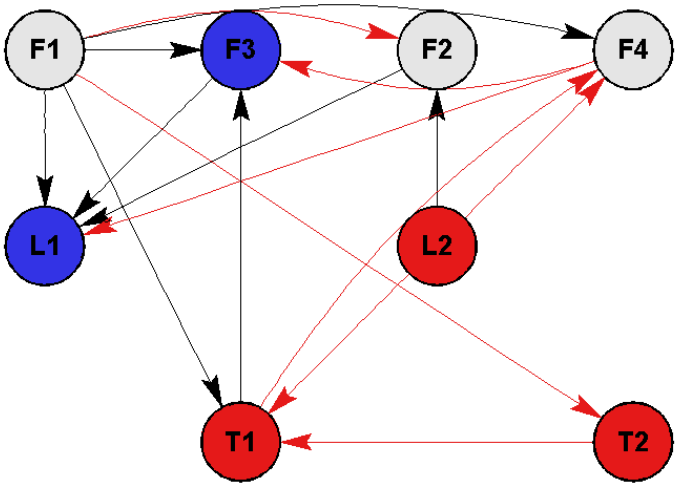

Figure B-8: Back propagation applied to TE graph from symptoms identified by contributions for fault 1

For the 6th case the TE connectivity change identified F2 and t2 as possible symptom nodes. This doesn't really give a good indication of a temperature fault in the first tank, although it does indicate a temperature fault.

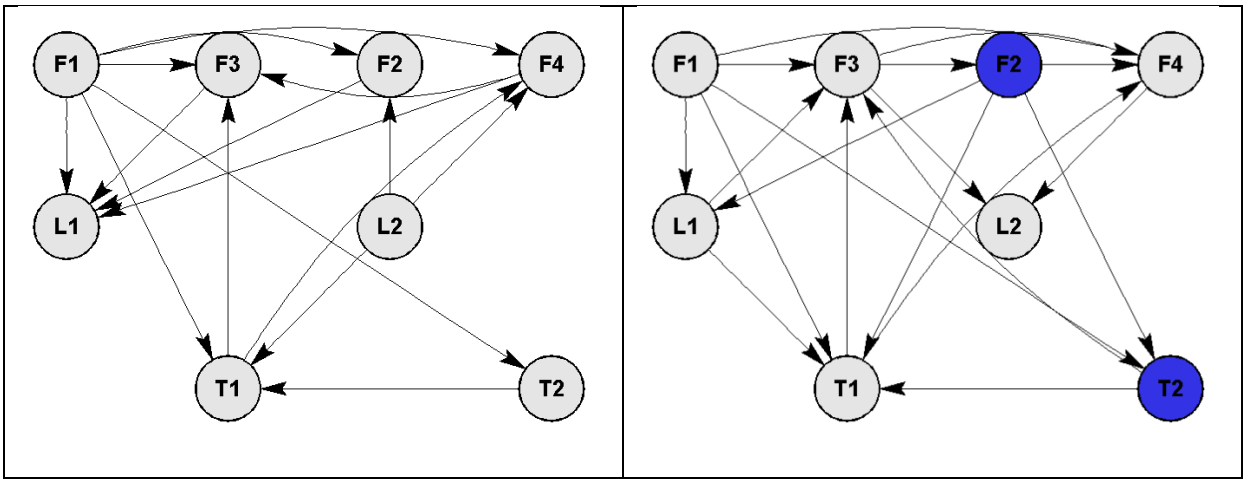

Figure B-9: Connectivity change for TE for fault 1

Applying back propagation on the TE graph then gives F1 as a possible root node. So symptoms maybe, roots no.

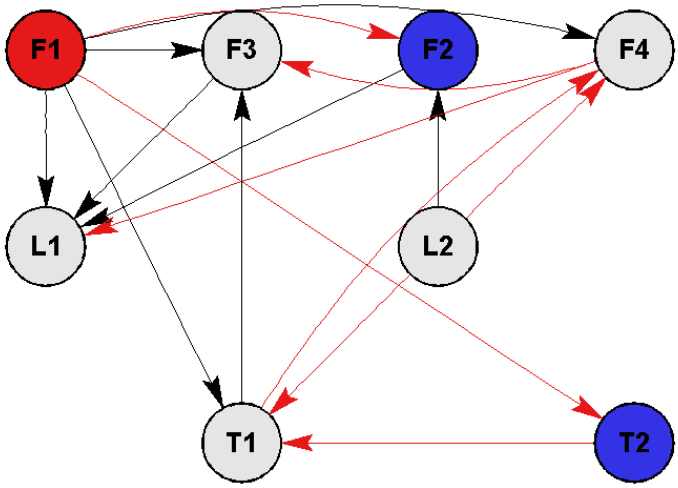

Figure B-10: Back propagation applied to TE graph from symptoms from connectivity change for fault 1

B.2. Fault 2: Ramp $T_{2,in}$

The contribution plot for the ramp T1 fault identified T1 f2, f3 and F4 as possible symptom nodes. It is clear that T1 showed the largest contribution though. This gives a very good indication that the fault has something to do with the temperature in the first tank

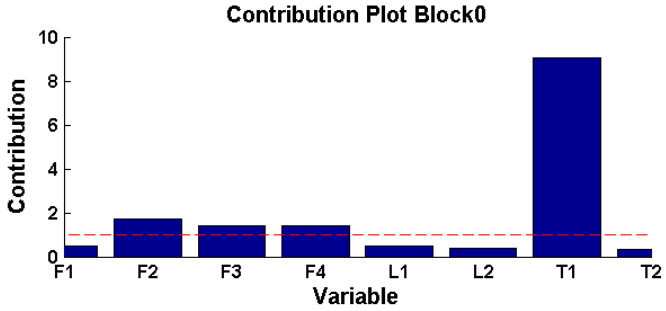

Figure B-11: Contribution plot for fault 2

For the first case applying back propagation in the LC graph from the contribution symptoms gives F1 and T1 as possible root nodes. This does indicate that tank 1 had some kind of a fault, but the presence of F1 as a possible root node complicates the results. So symptoms yes, roots maybe.

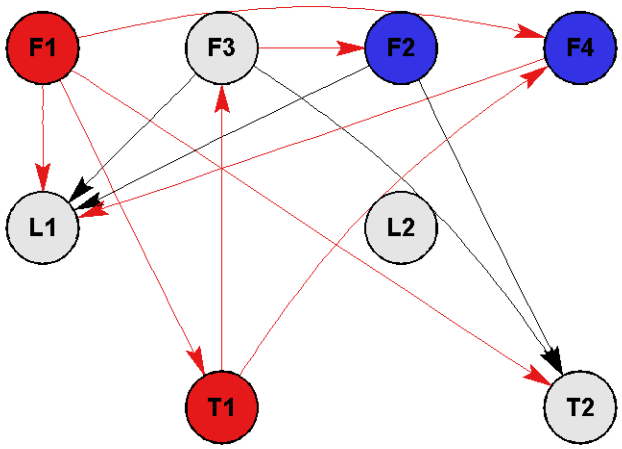

Figure B-12: Back propagation applied to LC graph from symptoms identified by contributions for fault 2

For the 2nd case the LC connectivity change identified T1 and T2 as possible root nodes, This gives a very good indication that a temperature fault has occurred that affect the first tank.

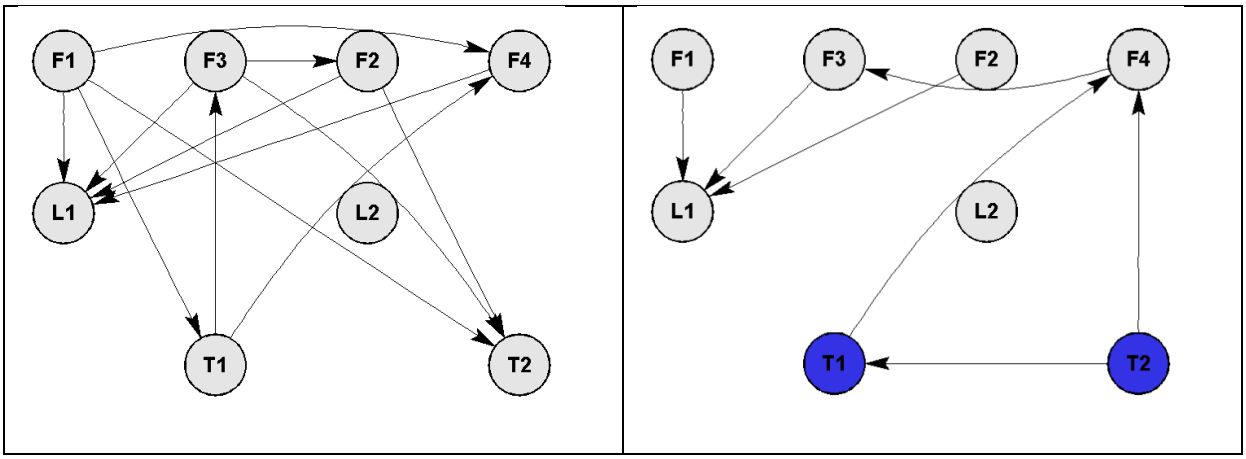

Figure B-13: Connectivity change for LC for fault 2

Applying back propagation in the LC connectivity graph from the symptoms identified by connectivity change gives F1 as a possible root node. This gives no indication that a temperature fault has occurred. So symptoms yes, roots no.

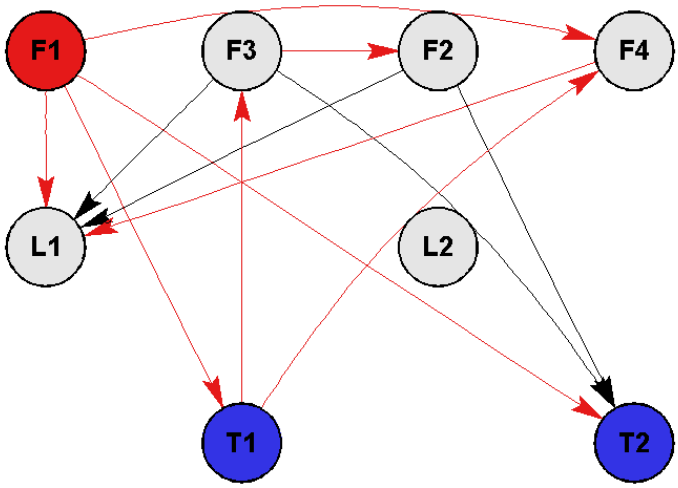

Figure B-14: Back propagation applied to LC graph from symptoms from connectivity change for fault 2

For the 3rd case applying back propagation to the PC connectivity graph from the symptoms identified by contributions gives no possible root nodes. However, if F2 were not present as a symptom node, F3 would have been the furthest ancestor of all the symptoms. So symptoms yes, roots maybe.

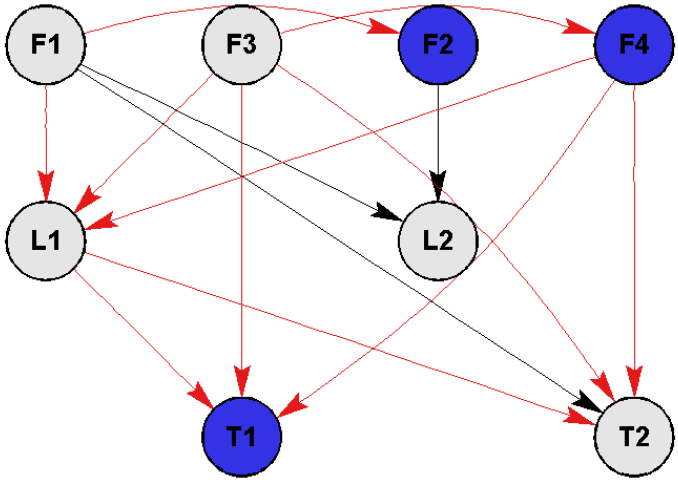

Figure B-15: Back propagation applied to PC graph from symptoms identified by contributions for fault 2

For the 4th case the symptoms identified by the connectivity change in the PC graph were t1 and t2. This gives a good indication that the fault has something to do with the temperatures in the first tank:

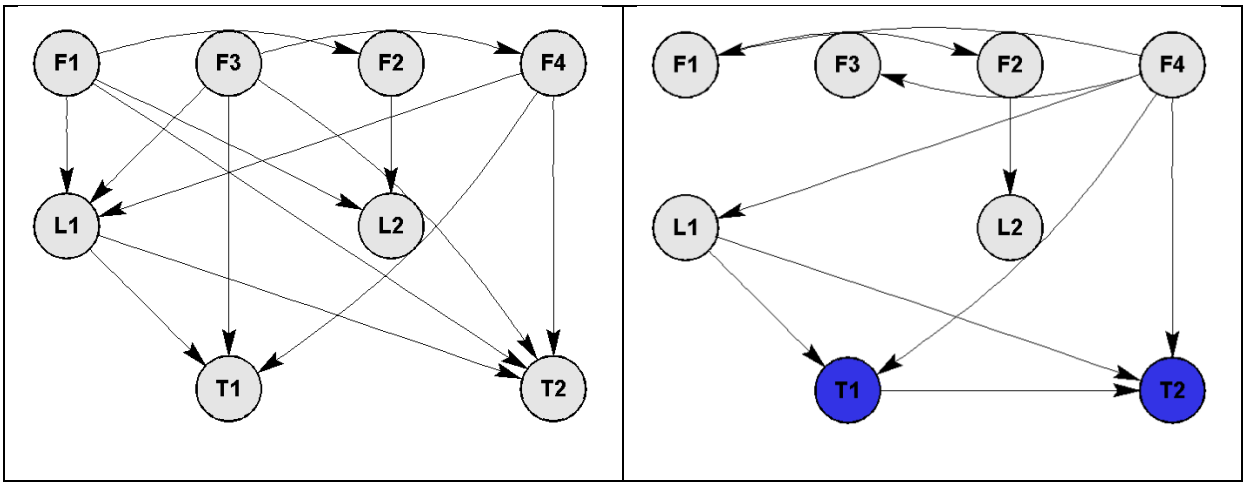

Figure B-16: Connectivity change for PC for fault 2

Applying back propagation to the PC graph from the symptoms identified by connectivity change results in L1, F4 and F3 being identified as possible root nodes. Apart from the presence of L1, this gives a good indication that a temperature fault in the first tank occurred. So symptoms yes and roots yes.

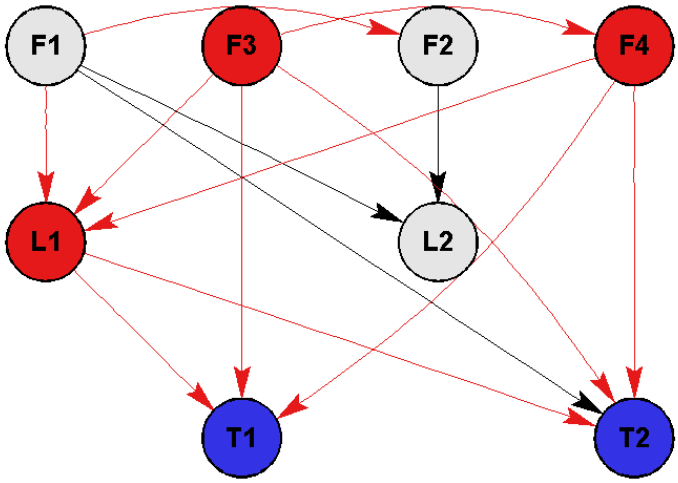

Figure B-17: Back propagation applied to PC graph from symptoms from connectivity change for fault 2

For the 5th case applying back propagation to the TE graph from the symptoms identified by Contributions resulted in F1 and L2 being identified as possible root nodes. This gives no indication that a temperature fault has occurred. So symptoms yes, roots no.

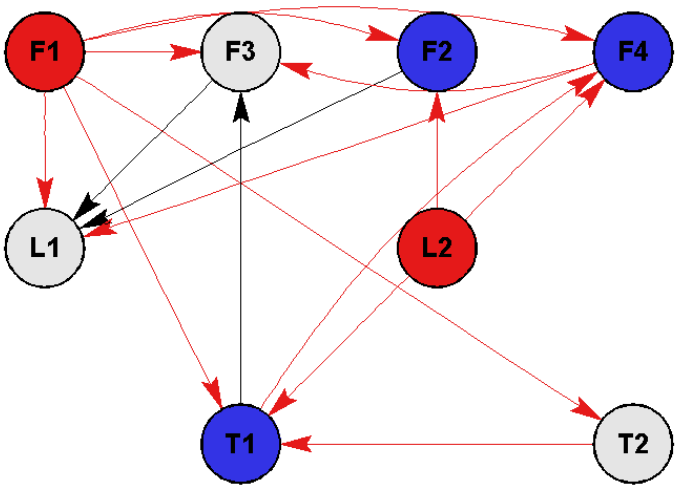

Figure B-18: Back propagation applied to TE graph from symptoms identified by contributions for fault 2

For the 6th case the change in connectivity for the TE graph identified L1 and T2 as possible symptoms. The fact that T2 was identified indicates that a temperature fault occurred, but the presence of L1 doesn't really make sense:

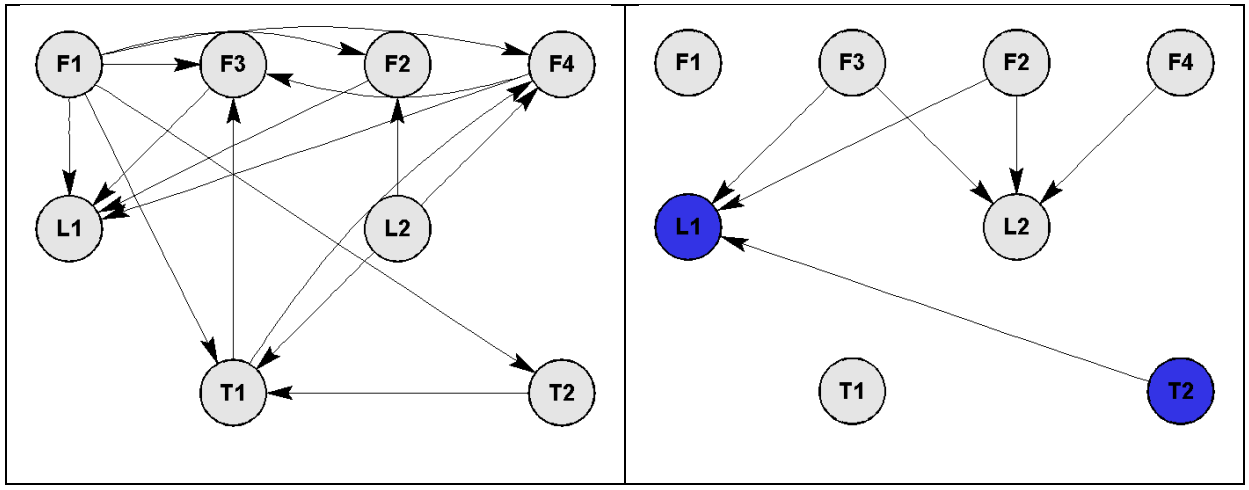

Figure B-19: Connectivity change for TE for fault 2

Applying back propagation in the TE graph from the symptoms identified by TE connectivity change resulted in F1 being identified as a root node. So symptoms maybe, roots no.

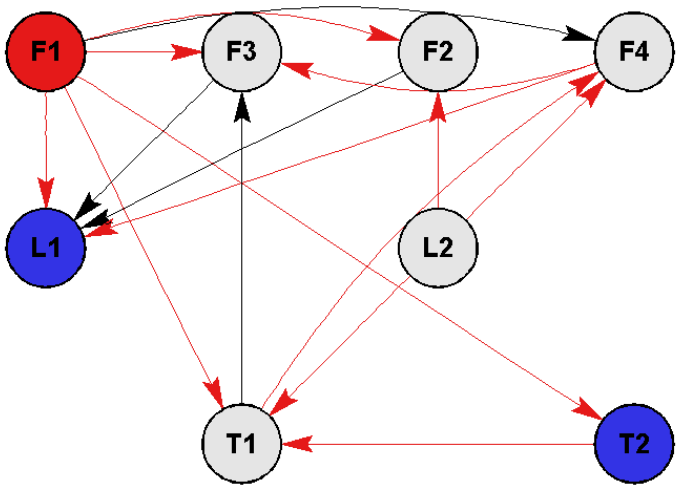

Figure B-20: Back propagation applied to TE graph from symptoms from connectivity change for fault 2

B.3. Fault 3: Step $T_{2,in}$

For this fault the contributions plots showed large contributions for T1 F4 and L1. The contribution of F4 makes sense for this fault, but L1 and T1 don't.

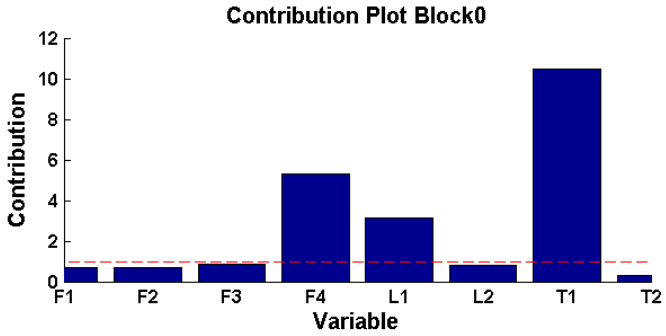

Figure B-21: Contribution plot for fault 3

For the 1st case applying back propagation in the LC graph from the contributions symptoms gives T1 and F1 as possible roots. This doesn't really give a good indication of a temperature fault in the second tank. So symptoms maybe, roots no.

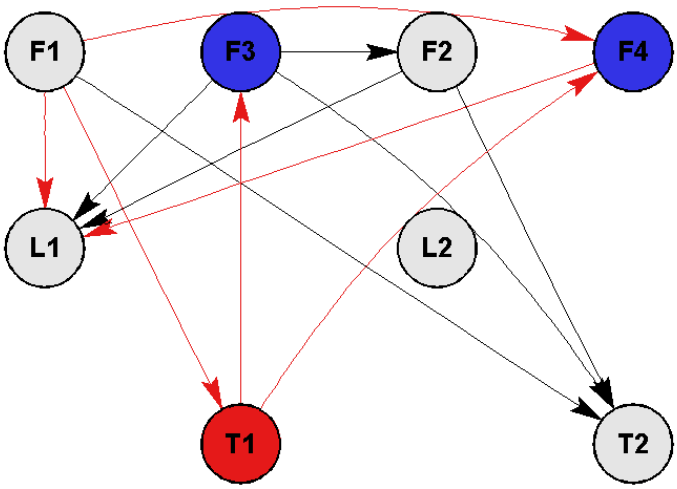

Figure B-22: Back propagation applied to LC graph from symptoms identified by contributions for fault 3

For the 2nd case the change in the LC identified F3 and F4 as possible symptoms. This is promising since it does indicate a temperature fault, although the presence of F3 may lead one to believe the fault is from the first tank.

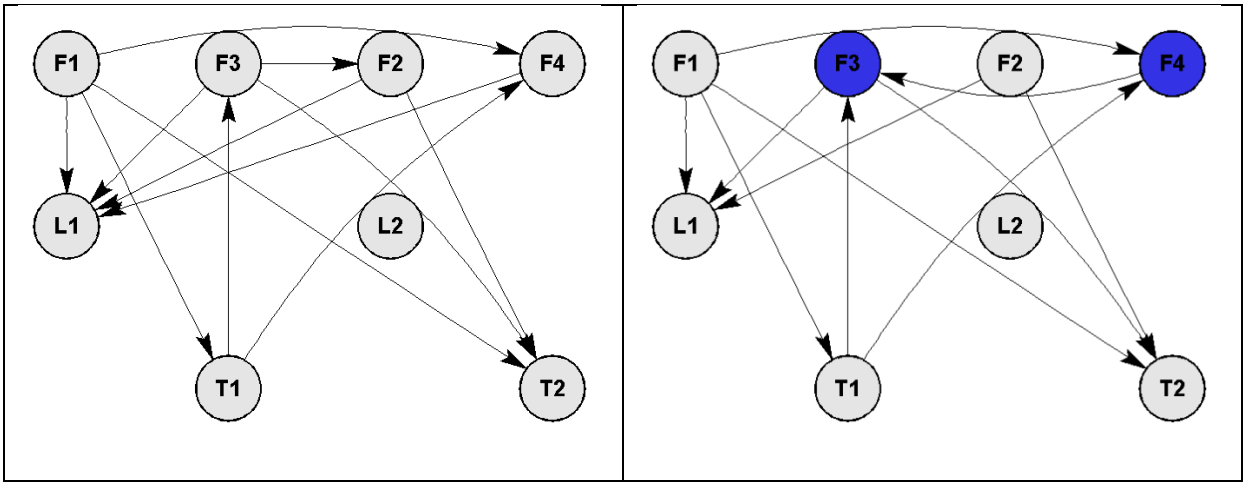

Figure B-23: Connectivity change for LC for fault 3

Applying back propagation to the LC graph from the symptoms identified by connectivity change results in T1 being identified as a possible root node. Although this does indicate a temperature fault it would lead one to believe the fault is from the first tank. So symptoms yes, roots maybe.

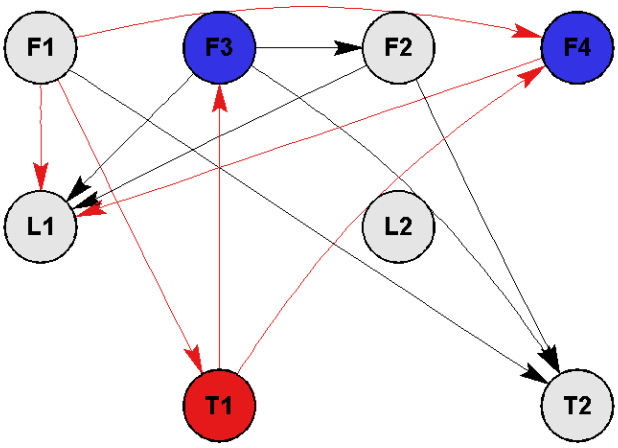

Figure B-24: Back propagation applied to LC graph from symptoms from connectivity change for fault 3

For the 3rd case applying back propagation in the PC graph from the symptoms identified by contributions results in F3 and F4 being identified as possible root nodes, Since thes both indicate that a temperature fault has occurred this is a good result. So symptoms maybe, roots yes.

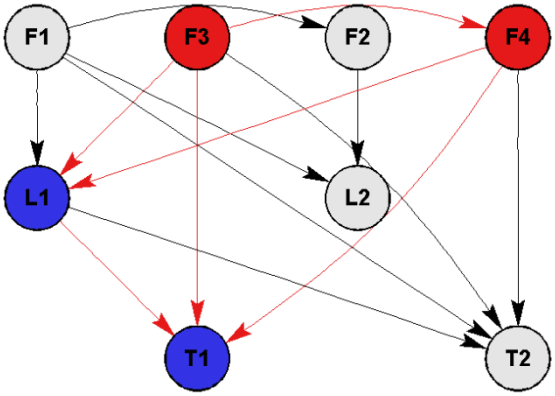

Figure B-25: Back propagation applied to PC graph from symptoms identified by contributions for fault 3

For the 4th case the change in the PC identified no symptom nodes.

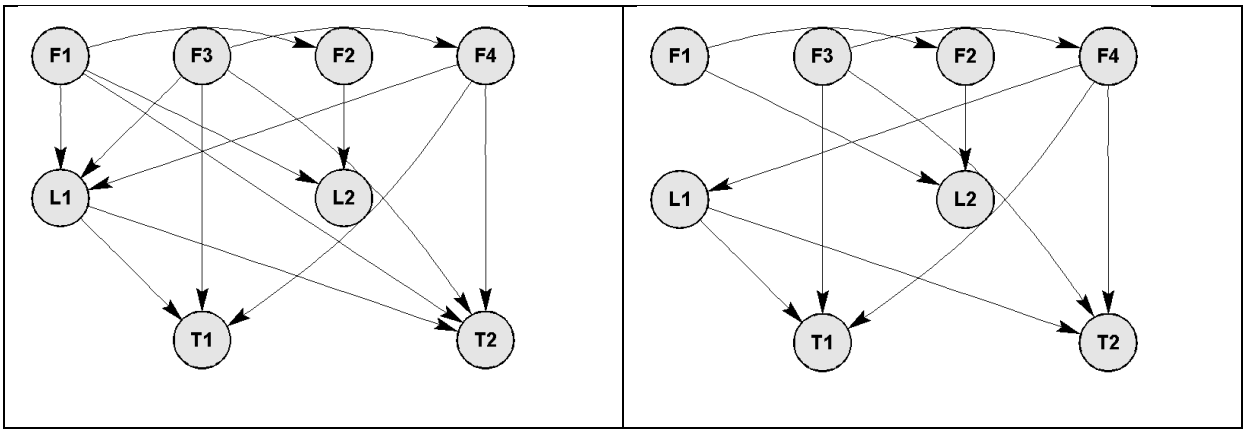

Figure B-26: Connectivity change for PC for fault 3

The reason why no symptom nodes were identified is that the only change in connectivity was some of the connections falling below the thresholds, and there were only a couple of them that changed.

So symptoms no, roots no.

For the 5th case applying back propagation in the TE graph from the symptoms identified by contributions resulted in T2, T1 and L2 being identified as possible root nodes. This does indicate that a temperature fault occurred, however the presence of L1 is confusing and the T1 as well. However, looking at the connectivity graph, t2 is clearly a predecessor of T1. So symptoms maybe, roots yes.

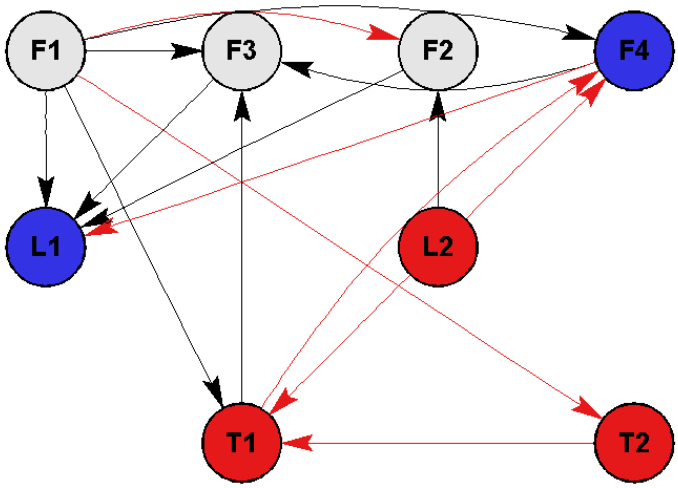

Figure B-27: Back propagation applied to TE graph from symptoms identified by contributions for fault 3

For the 6th case the change in TE identified F2 and T2 as possible symptoms. This is promising since the temperature was identified:

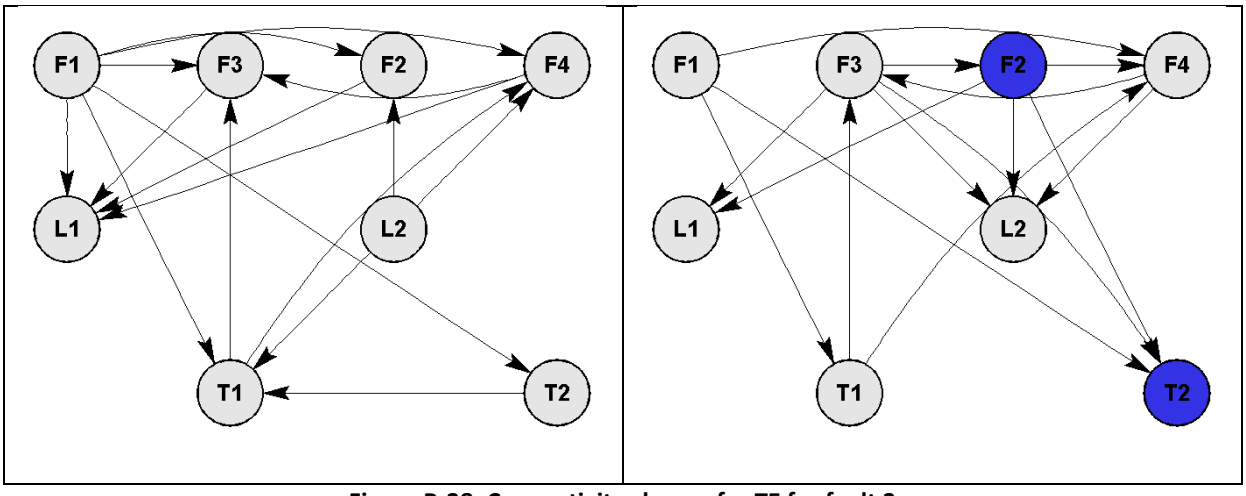

Figure B-28: Connectivity change for TE for fault 3

Applying back propagation in the TE graph from the symptoms identified by connectivity change resulted in F1 being identified as a root node. This gives no indication that the fault occurred in the temperature of the second tank. So symptoms yes, roots no.

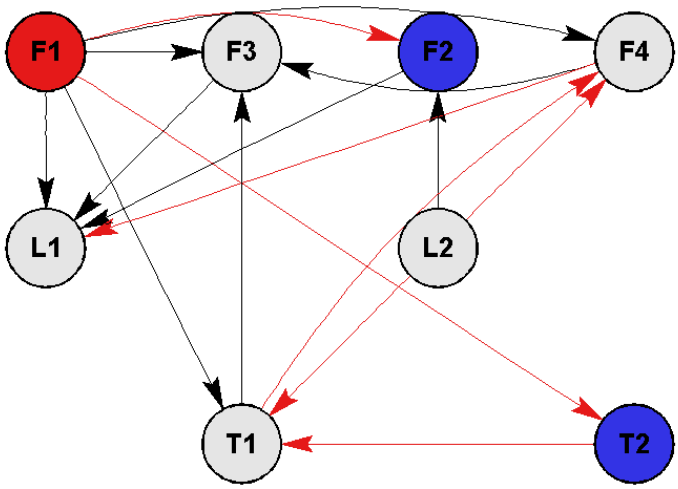

Figure B-29: Back propagation applied to TE graph from symptoms from connectivity change for fault 3

B.4. Fault 4: Fouling

The contributions of the individual variables to the PCA SPE for the fouling fault are shown in . The relative contributions of F3 and T1 were greater than 1, which is consistent with the fouling fault since fouling would influence the temperatures in the tanks (T1) which would cause the controller to change F3. The contributions of F2 and L1, however, are not consistent with the fault, since the temperatures cannot affect the levels or flow rates of the cold water into the tanks. The fact that T2 and F4 are not shown as giving large contributions also doesn't give a good indication of the fouling fault, since these variables should be affected by it. The results of this contribution plot are suspect, however, considering that PCA performed poorly for the detection of this fault.

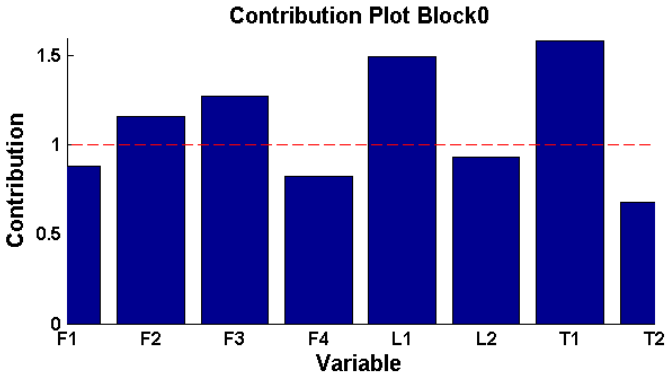

Figure B-30: Contribution plot for fault 4

For the first case applying back propagation from the symptoms identified by contributions to the LC graph resulted in F1 and T1 being identified as possible root nodes. This at least gives an indication of the temperature in the first tank being associated with the fault, but the presence of F1 complicates the result. So symptoms maybe, roots maybe.

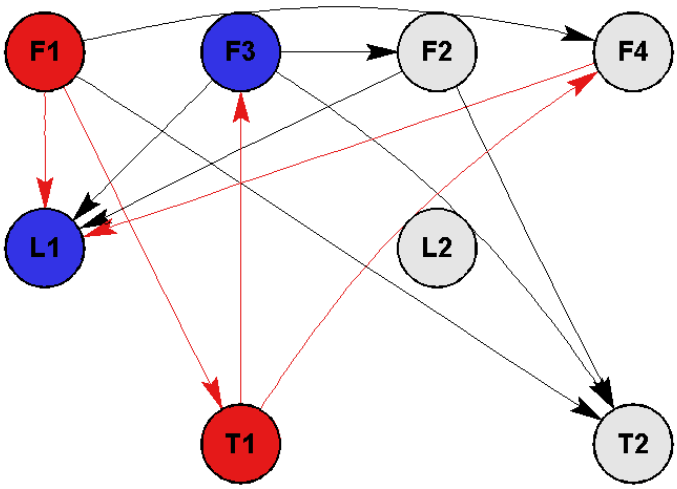

Figure B-31: Back propagation applied to LC graph from symptoms identified by contributions for fault 4

For the 2nd case the change in the LC connectivity resulted in F3 being identified as a symptom node. This is a positive result since the fault would affect this variable significantly. The only change in connectivity was F1 to F3 appearing, f3 to F2 disappearing and F4 to L1 disappearing. The fact that not much change was observed also indicates that this fault was not very noticeable.

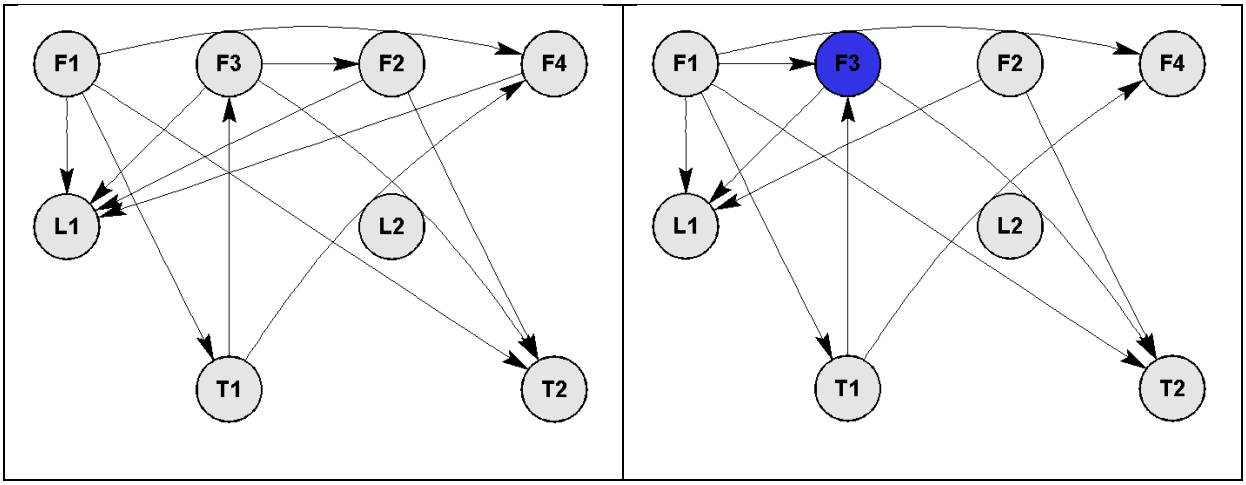

Figure B-32: Connectivity change for LC for fault 4

Applying back propagation in the LC graph from the symptom nodes identified by connectivity change resulted in F1, T1 and F3 being identified as possible root nodes. This gives a good indication of a temperature fault. So symptoms yes, roots yes.

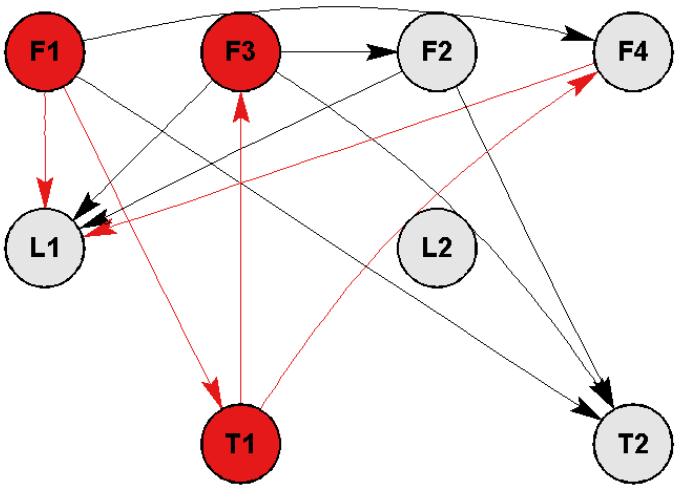

Figure B-33: Back propagation applied to LC graph from symptoms from connectivity change for fault 4

For the 3rd case applying back propagation in the PC graph gave F3, F1 and F4 as possible root nodes. This is a very good indication of the fouling fault since both F3 and F4 would be affected by it. Especially considering that if L1 wasn't a symptom node then F1 wouldn't have been identified as a root node. So symptoms maybe, roots yes.

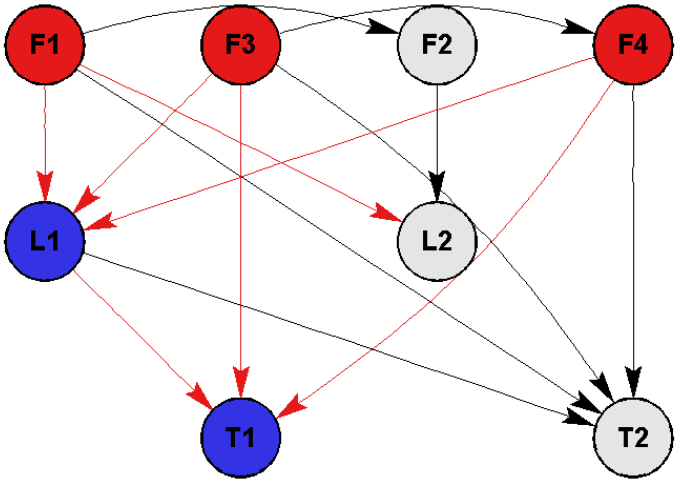

Figure B-34: Back propagation applied to PC graph from symptoms identified by contributions for fault 4

For the 4th case the change in the PC connectivity identified T1 as a symptom node. This gives a very good indication that a temperature fault has occurred. The only change in connectivity is that F1 to T1 appears, while F1 to T2 disappears.

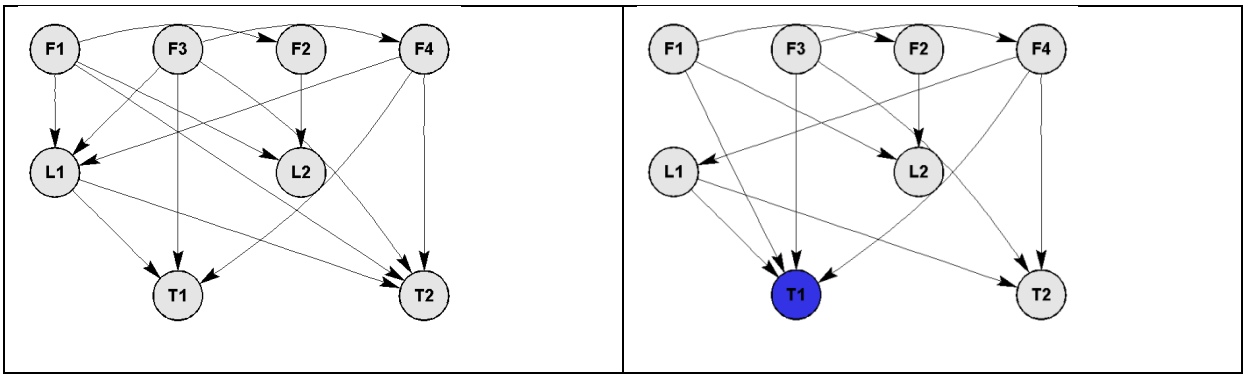

Figure B-35: Connectivity change for PC for fault 4

Applying back propagation in the PC graph from the symptoms identified by connectivity change resulted in F1, F3, F4 and L1 being identified as possible root nodes. Although F3 and F4 are identified, the presence of F1 and L1 confuse the result. So symptoms yes, roots maybe.

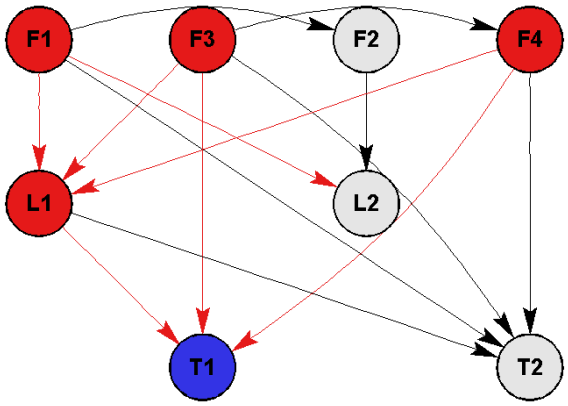

Figure B-36: Back propagation applied to PC graph from symptoms from connectivity change for fault 4

For the 5th case applying back propagation in the TE graph from the symptoms identified by contributions results in T2, t1 and L2 being identified as possible root nodes. This gives a very good indication of the fouling fault since both T1 and T2 are identified. So symptoms maybe, roots yes.

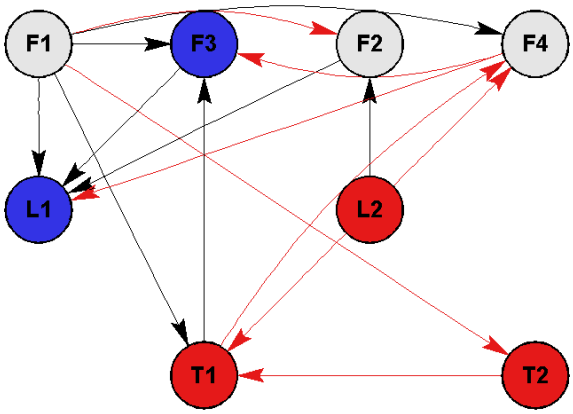

Figure B-37: Back propagation applied to TE graph from symptoms identified by contributions for fault 4

For the 6th case the connectivity change of the TE identified F2 and T2 as symptom nodes. It can be seen the the connectivity change resulted in a lot of changed connections with F2 and T2. The presence of F2 is a good indication of the fouling fault, but the presence of F2 confuses this.

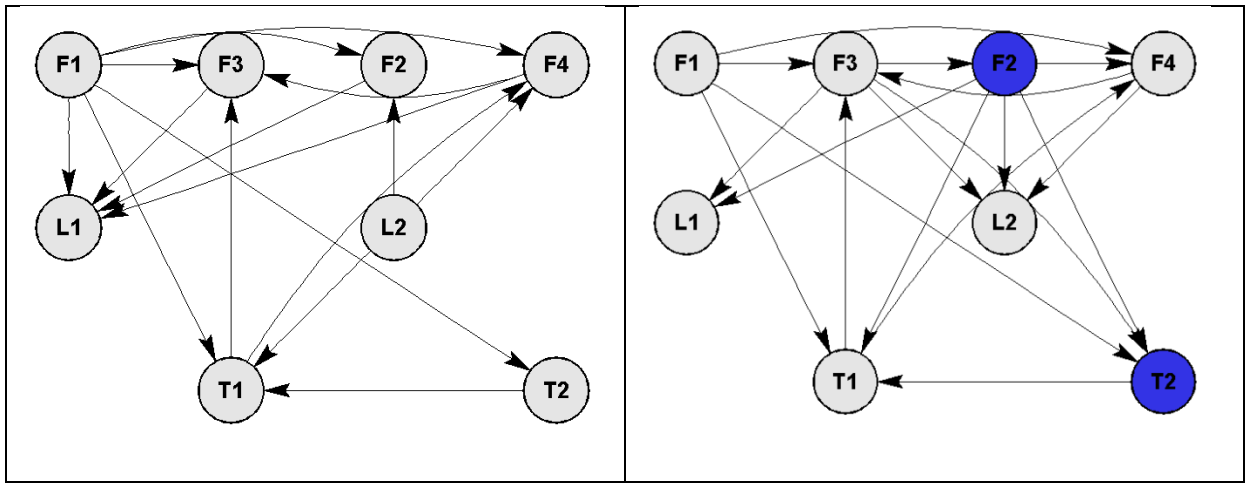

Figure B-38: Connectivity change for TE for fault 4

Applying back propagation in the TE graph using the symptoms identified from connectivity change resulted in F1 being identified as a possible symptom node. This doesn't give an indication of the fouling fault. So symptoms maybe, roots no.

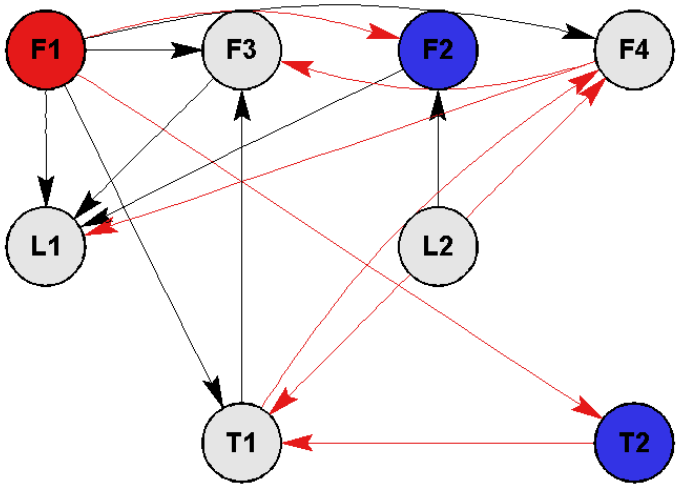

Figure B-39: Back propagation applied to TE graph from symptoms from connectivity change for fault 4

Appendix C- Autoclave Case Study Results

C.1.Fault Detection

C.1.1. Fault 1

LC

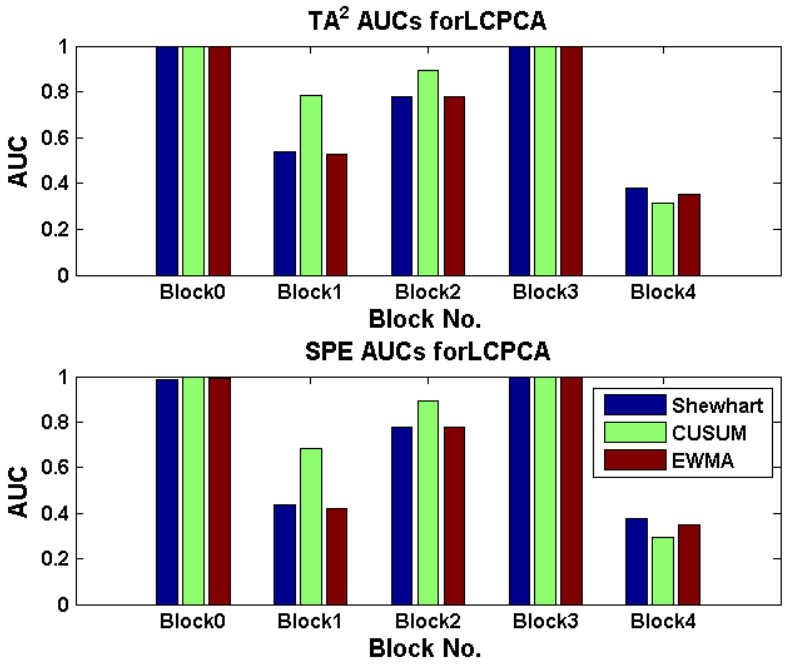

Figure C-1: AUCs for each LC block from PCA for fault 1

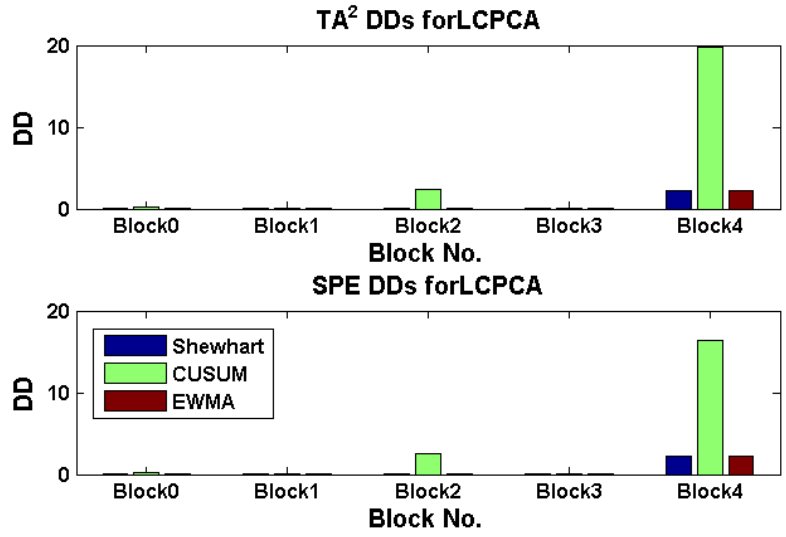

Figure C-2: DDs for each LC block from PCA for fault 1

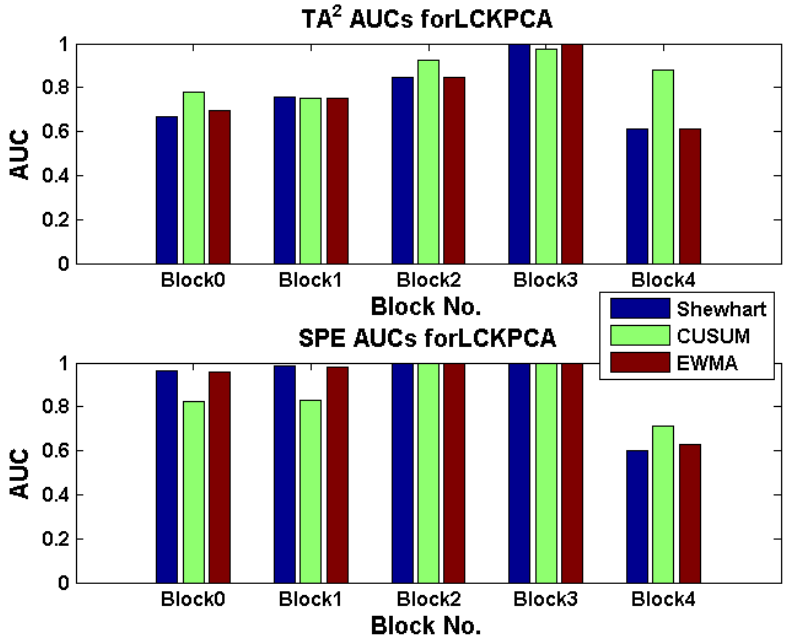

Figure C-3: AUCs for each LC block from KPCA for fault 1

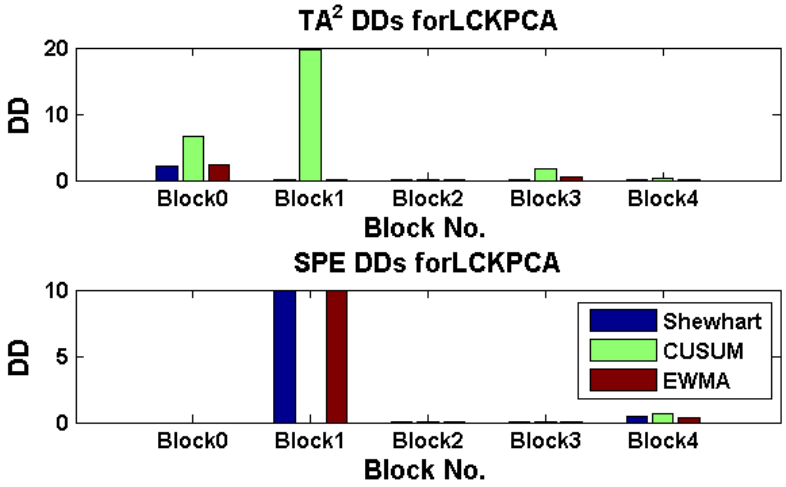

Figure C-4: DDs for each LC block from KPCA for fault 1

PC

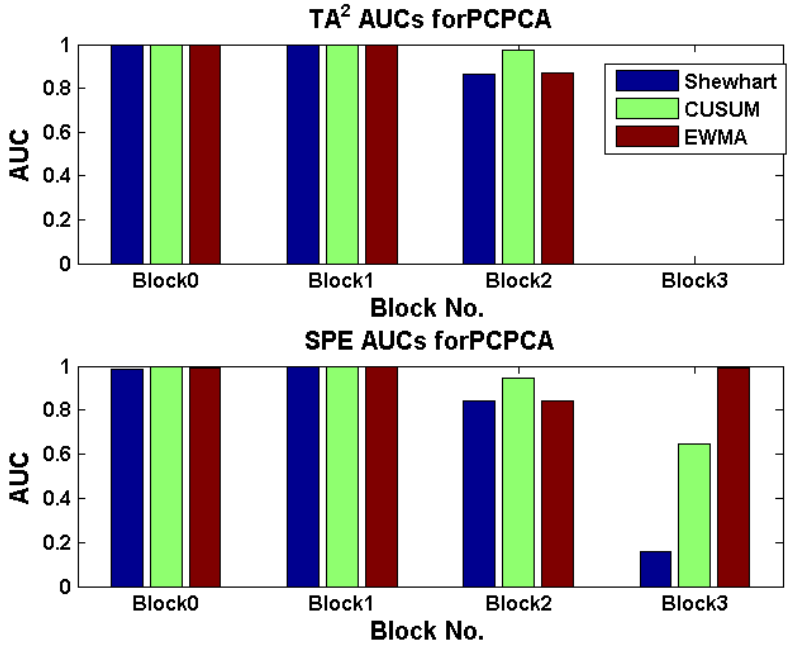

Figure C-5: AUCs for each PC block from PCA for fault 1

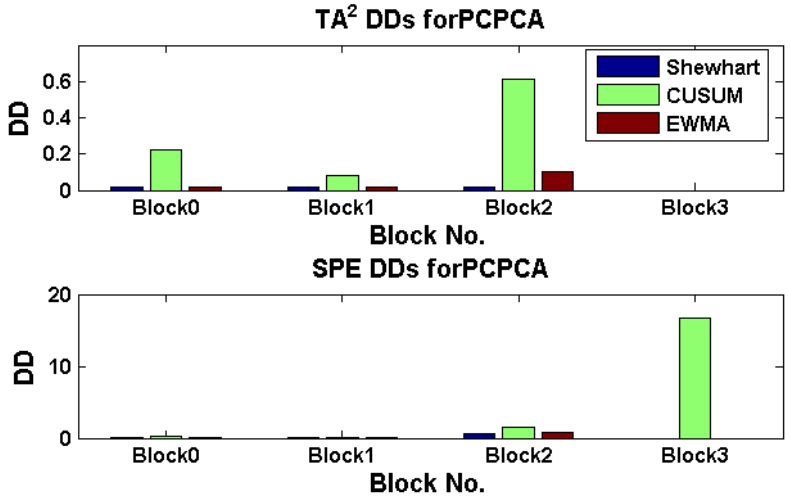

Figure C-6: DDs for each PC block from PCA for fault 1

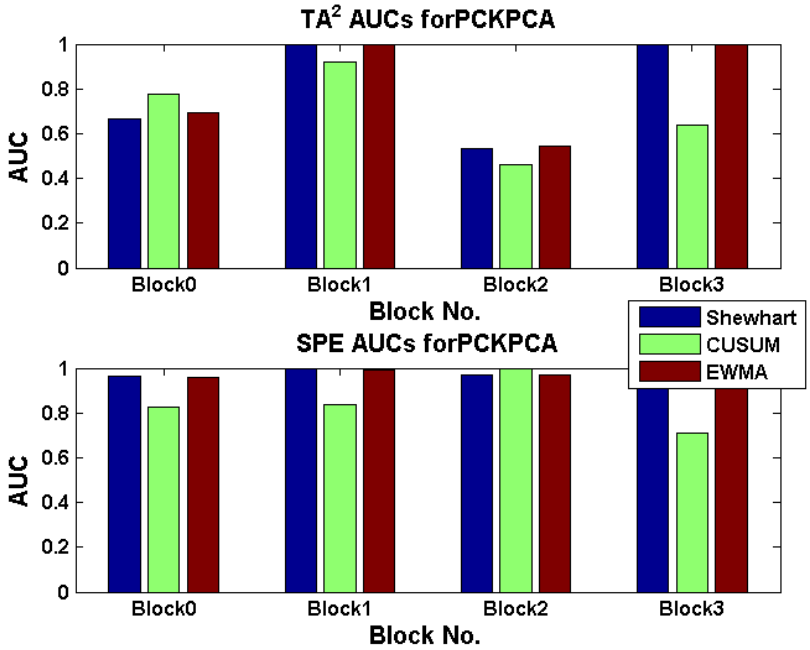

Figure C-7: AUCs for each PC block from KPCA for fault 1

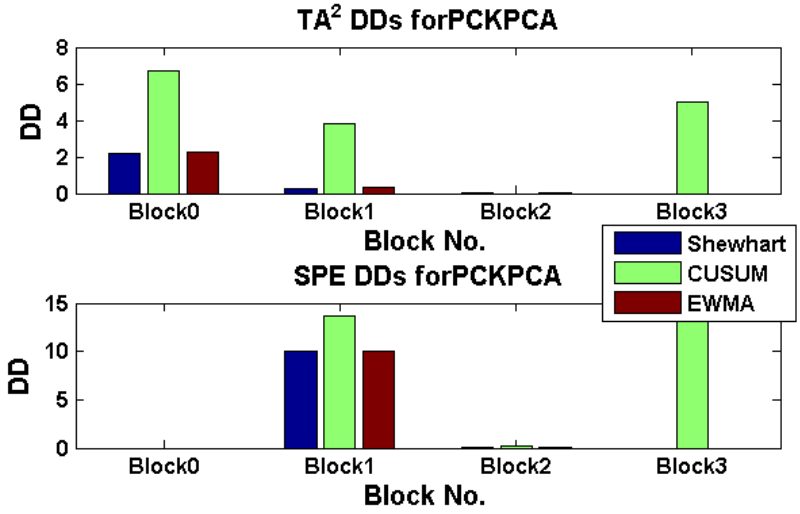

Figure C-8: DDs for each PC block from KPCA for fault 1

TE

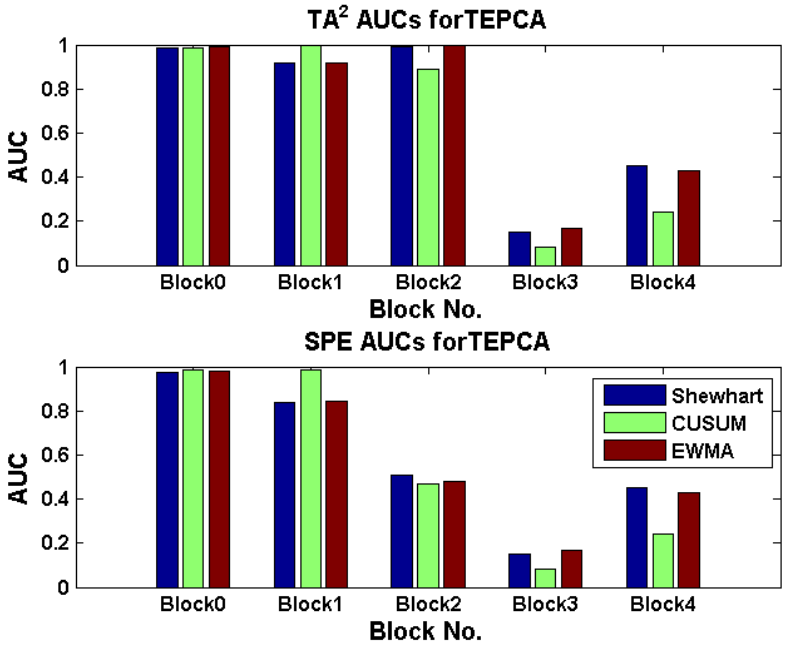

Figure C-9: AUCs for each TE block from PCA for fault 1

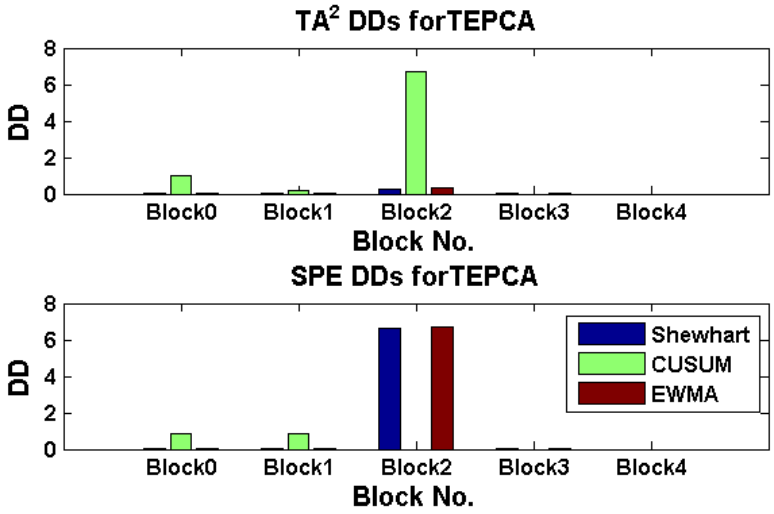

Figure C-10: DDs for each TE block from PCA for fault 1

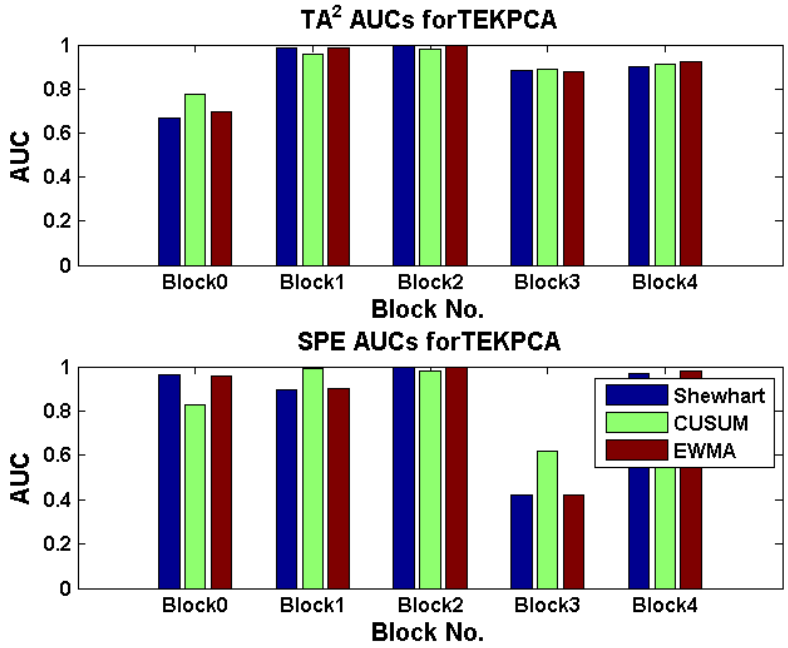

Figure C-11: AUCs for each TE block from KPCA for fault 1

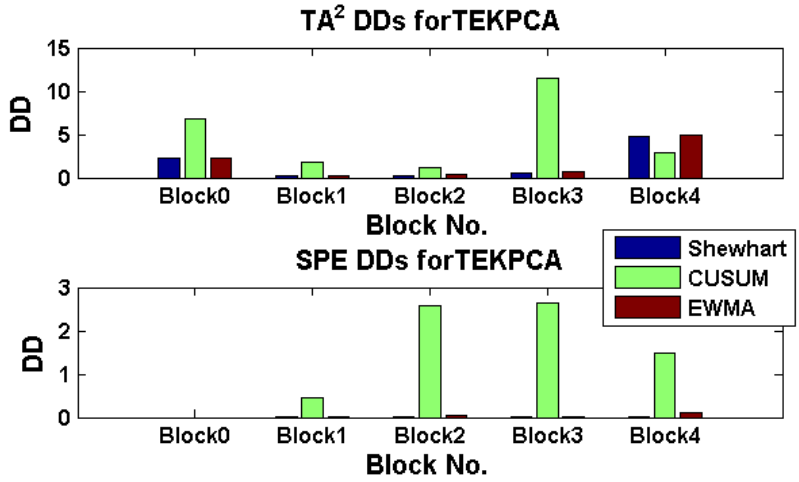

Figure C-12: DDs for each TE block from KPCA for fault 1

C.1.2. Fault 2

LC

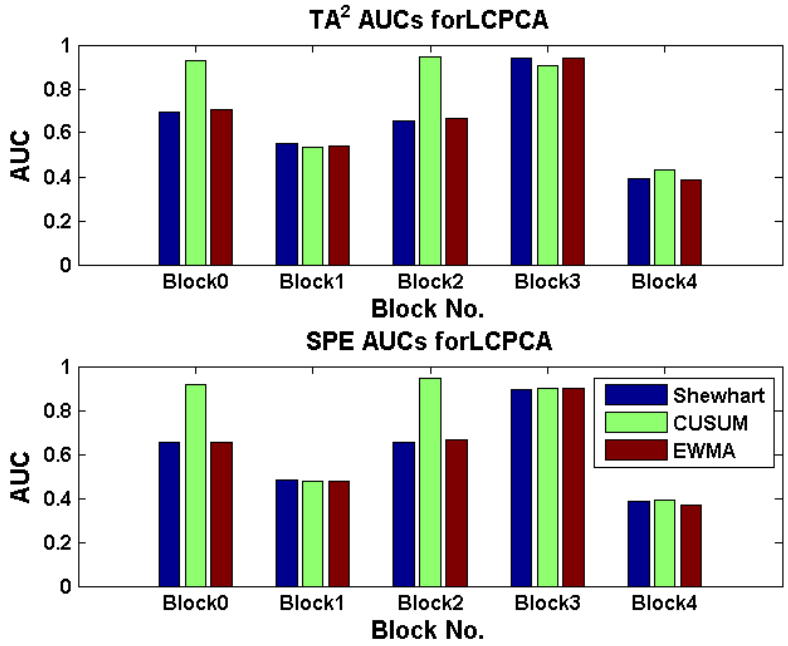

Figure C-13: AUCs for each LC block from PCA for fault 2

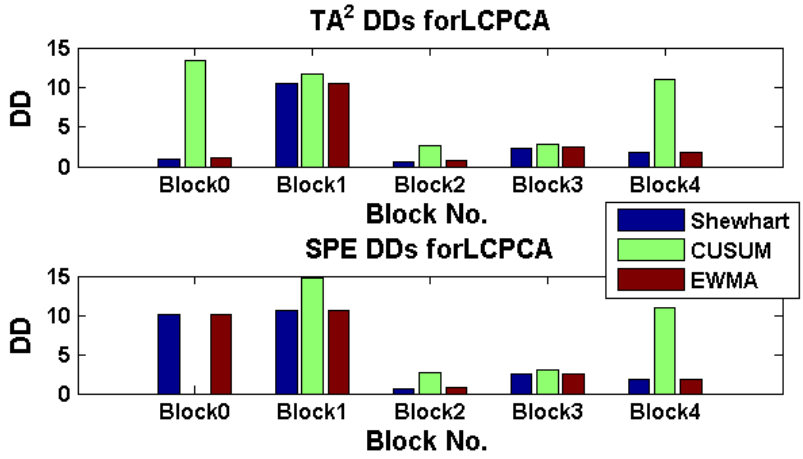

Figure C-14: DDs for each LC block from PCA for fault 2

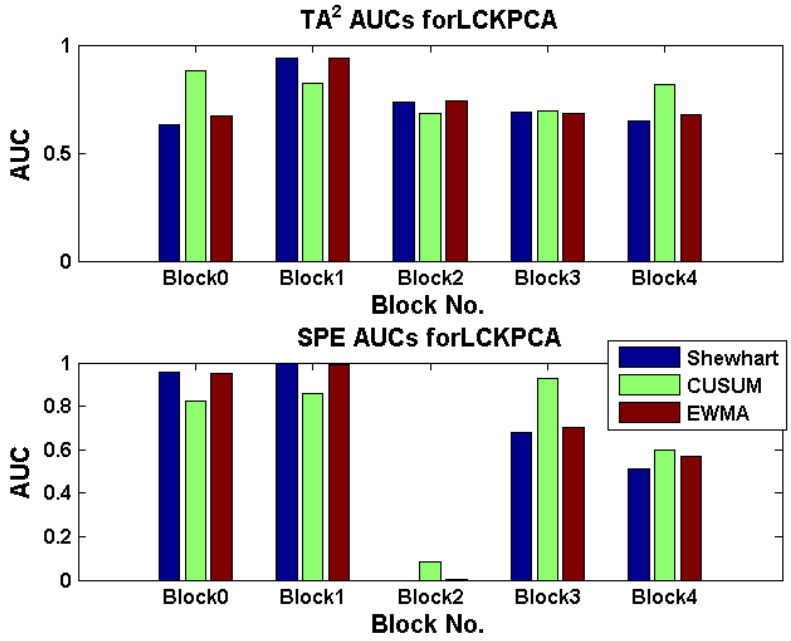

Figure C-15: AUCs for each LC block from KPCA for fault 2

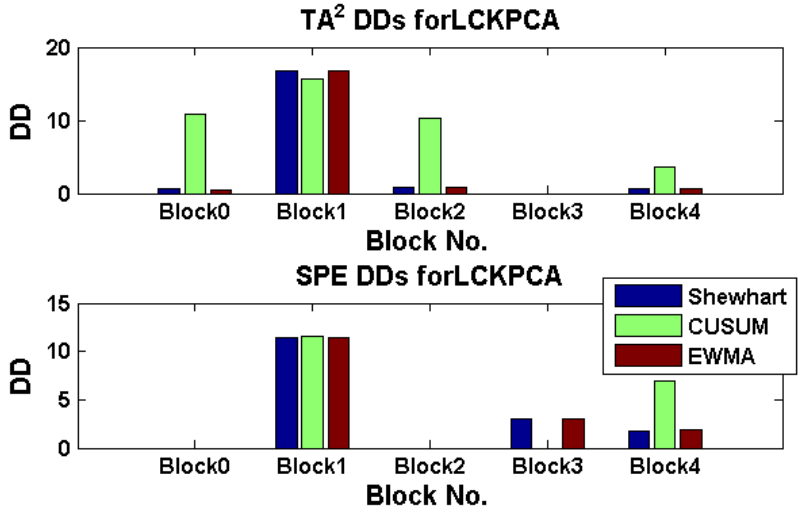

Figure C-16: DDs for each LC block from KPCA for fault 2

PC

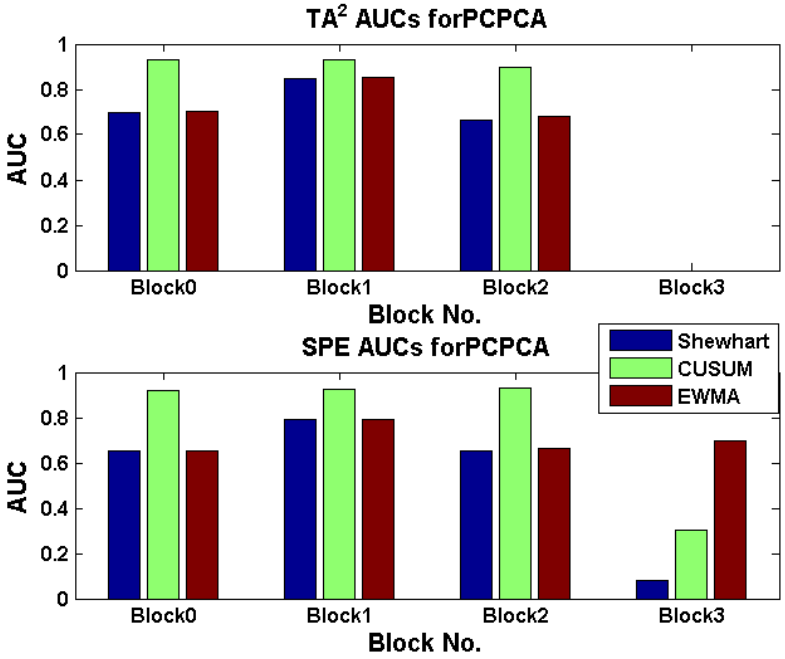

Figure C-17: AUCs for each PC block from PCA for fault 2

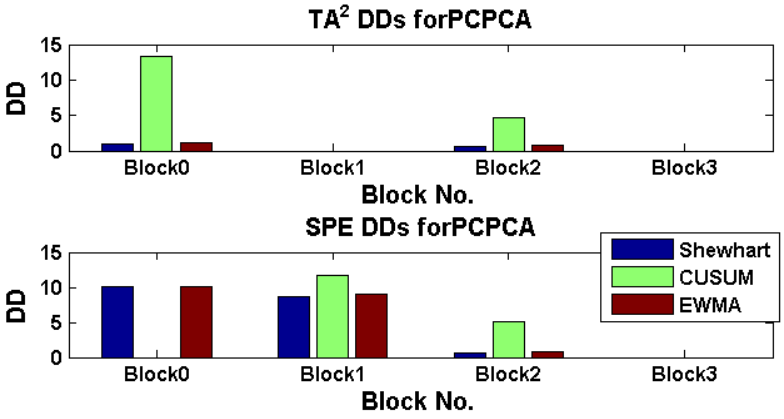

Figure C-18: DDs for each PC block from PCA for fault 2

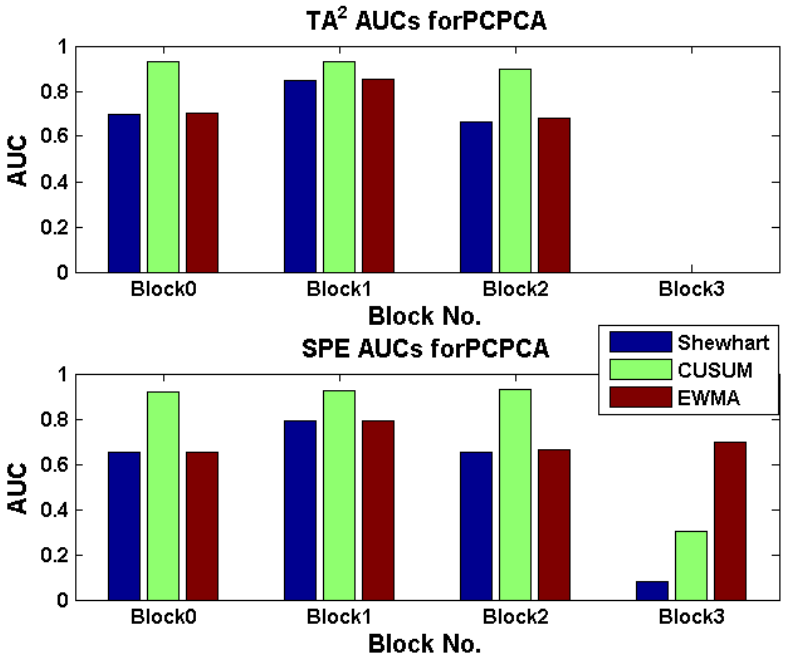

Figure C-19: AUCs for each PC block from KPCA for fault 2

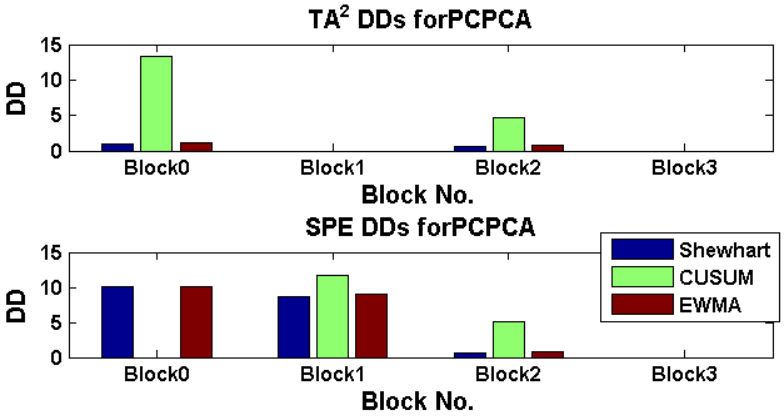

Figure C-20: DDs for each PC block from KPCA for fault 2

TE

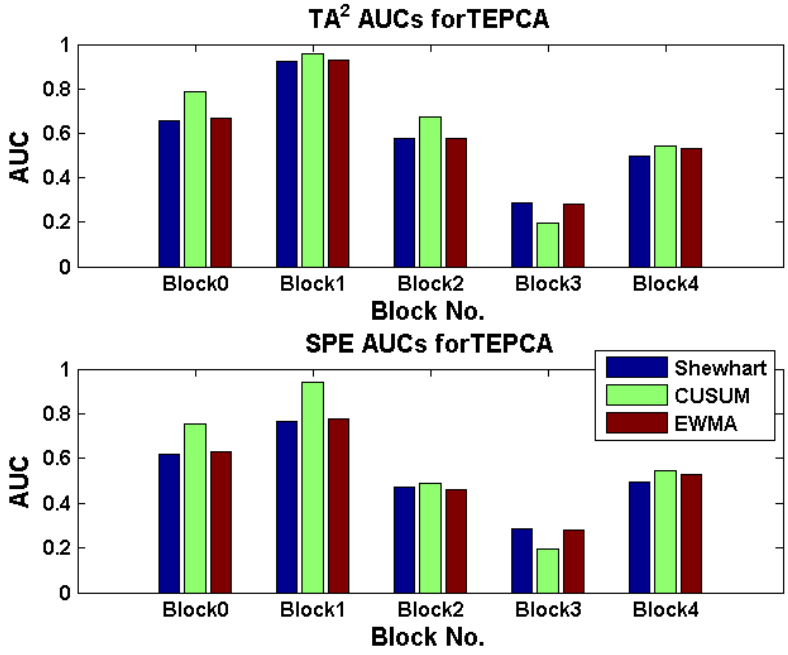

Figure C-21: AUCs for each TE block from PCA for fault 2

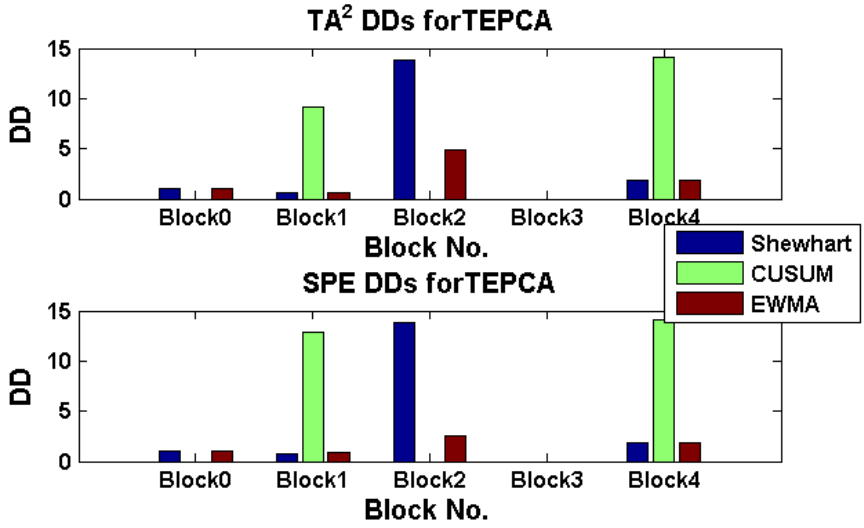

Figure C-22: DDs for each TE block from PCA for fault 2

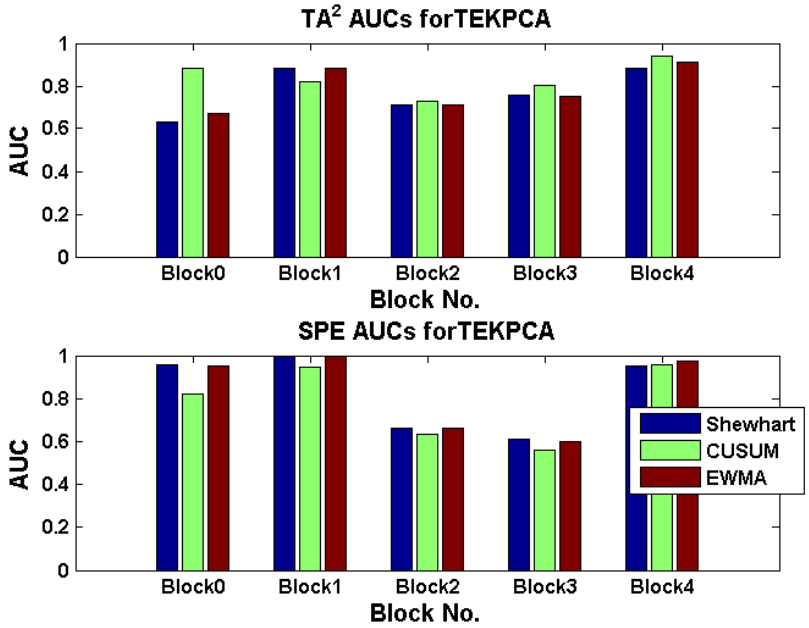

Figure C-23: AUCs for each TE block from KPCA for fault 2

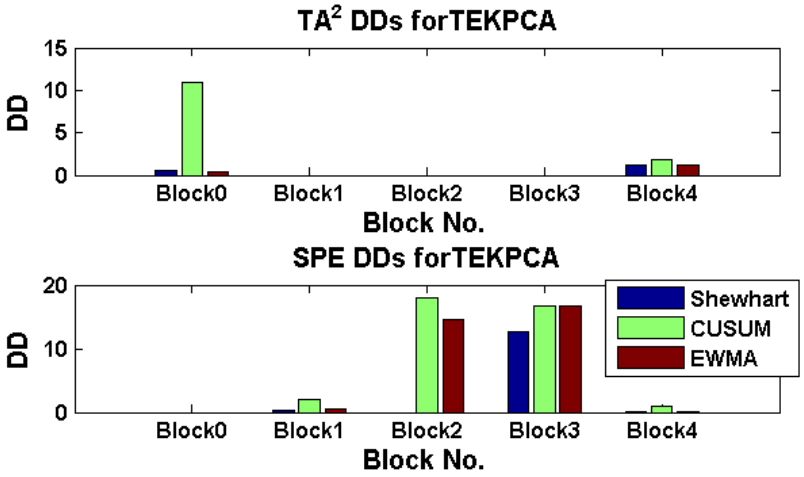

Figure C-24: DDs for each TE block from KPCA for fault 2

C.2.Fault Identification

C.2.1. Fault 1

In the first case the symptom nodes were closer to the fault than the identified root nodes. So symptoms yes, roots no.

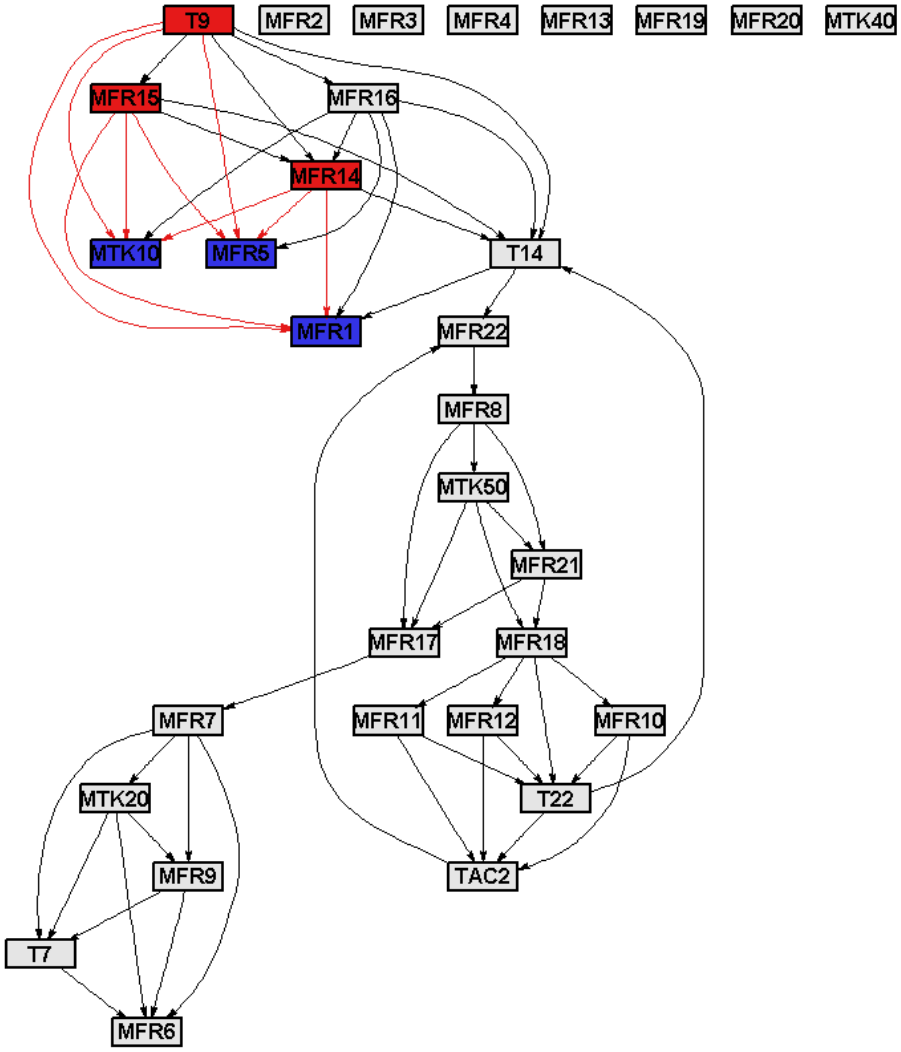

Figure C-25: Back propagation in the unblocked LC connectivity graph using the symptoms identified from contributions

In the second case, using connectivity change in the unblocked LC graph, many symptom nodes were identified, including MFR1, MFR5 and MTK10, but no roots were identified. So symptoms yes, roots no.

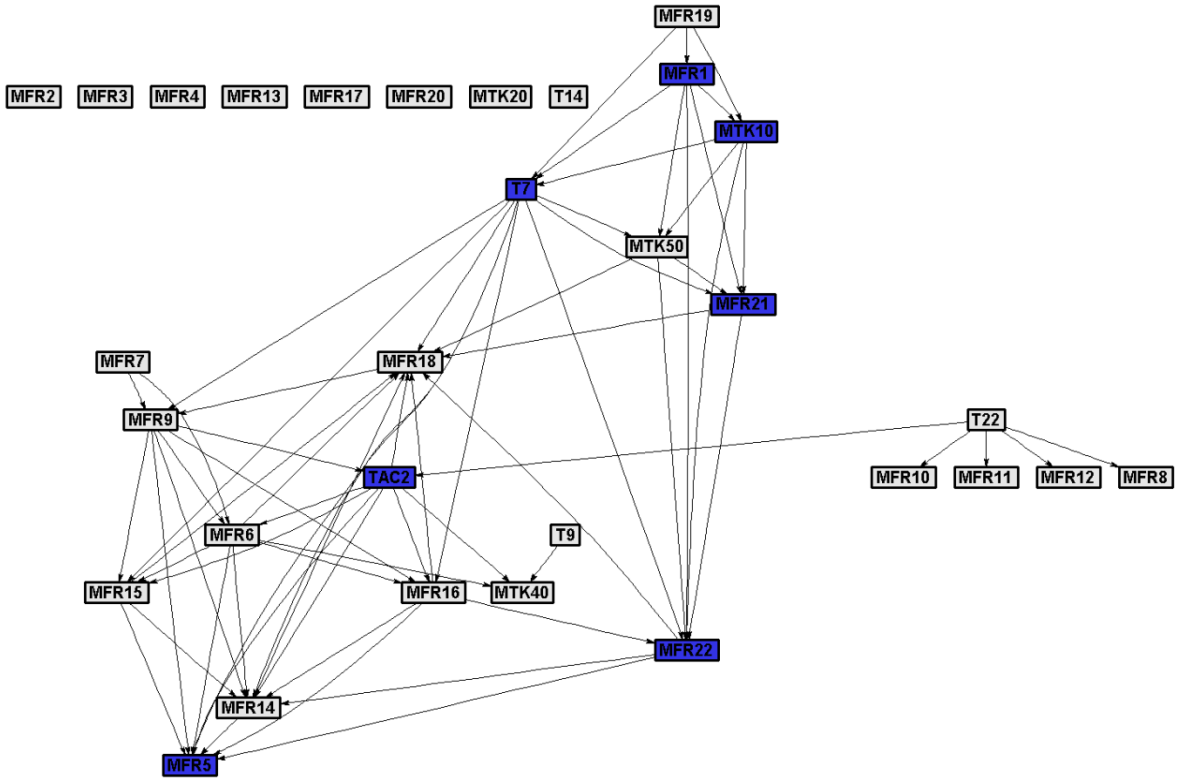

Figure C-26: Change in connectivity for Unblocked LC for fault 1

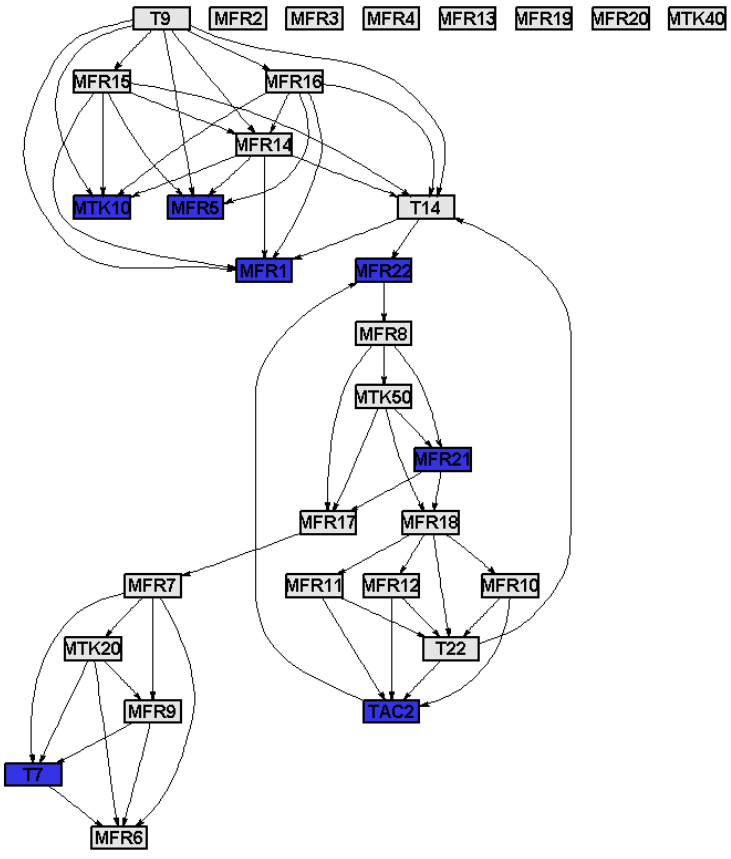

Figure C-27: Back propagation in the unblocked LC graph using the symptoms identified by connectivity change

In the third case MFR7 is identified as symptom, which makes sense, MFR7 and MFR17 were possible roots.

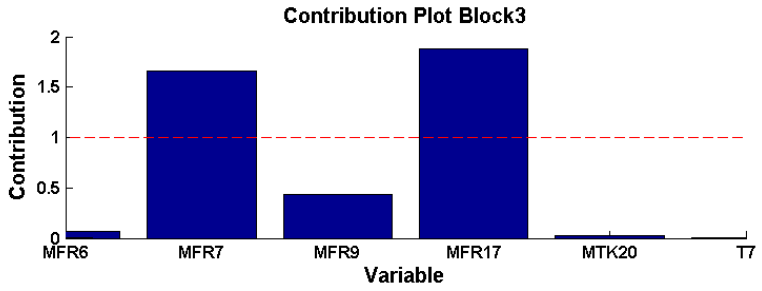

Figure C-28: Contribution plot for LC block 3 for PCA SPE for fault 1

Applying back propagation results in MFR7 being identified as a possible root node, as shown in Figure 6-17. Since this is directly downstream of the blockage, this is a very accurate indication of the fault conditions. So symptoms yes, roots yes.

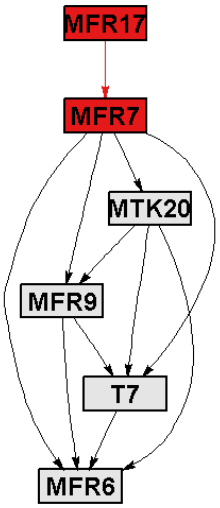

Figure C-29: Back propagation in LC graph for block 3 using the symptoms identified from contributions

For the 4th case MFR9 and T7 are identified as symptom nodes and MFR7.

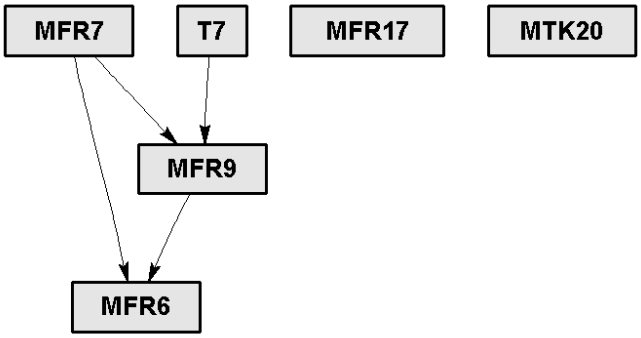

Figure C-30: Change in connectivity for LC block 3 for fault 1

MFR7, MTK20 and MFR9 are possible roots, as shown in Figure 6-21.This gives a very good indication of the fault conditions since this affects the tank directly downstream form the blockage. So symptoms yes and roots yes.

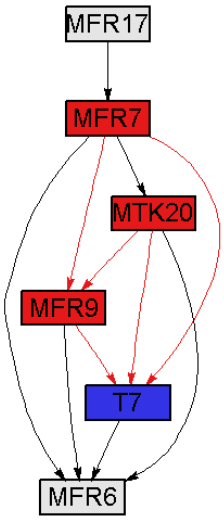

Figure C-31: Back propagation applied to the LC graph for block 3 using the symptoms identified from connectivity change

Case 5 results are the same as case 4 since KPCA found best detection in same block.

For case 6 MTK10 and MFR1 identified as symptoms, and MFR5 is one of the possible root node. So symptoms yes, roots yes.

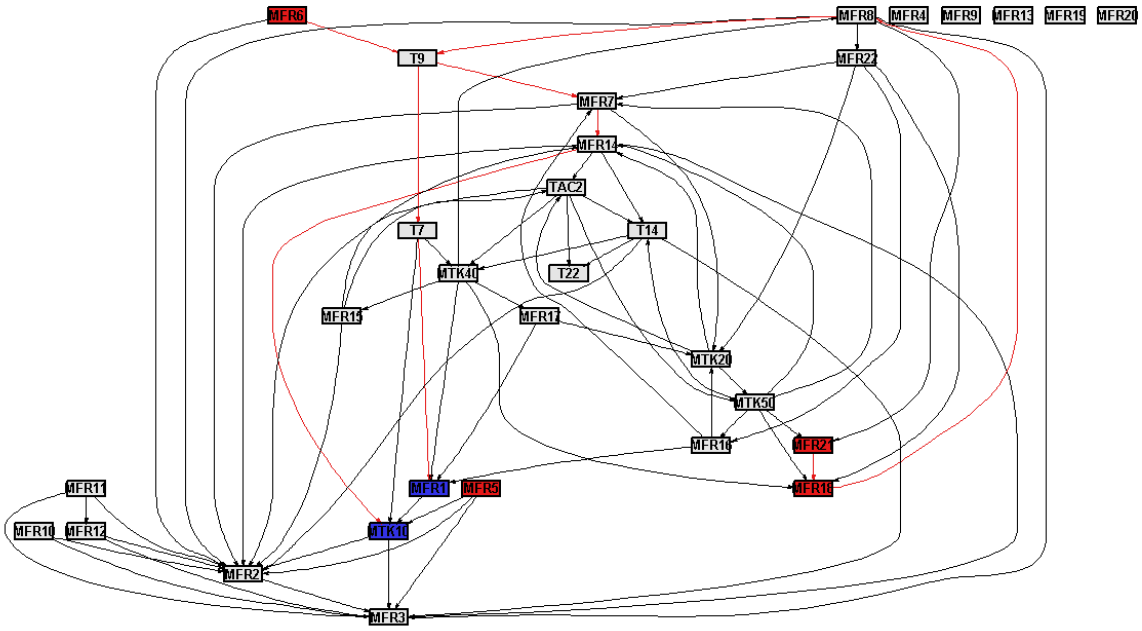

Figure C-32: Back propagation applied to the unblocked PC graph using the symptoms identified from contributions

For the 7th case a bunch of symptoms are identified, not really representative, except for MTK20, but MFR5 and MFR9 are possible root nodes. So symptoms maybe, roots yes.

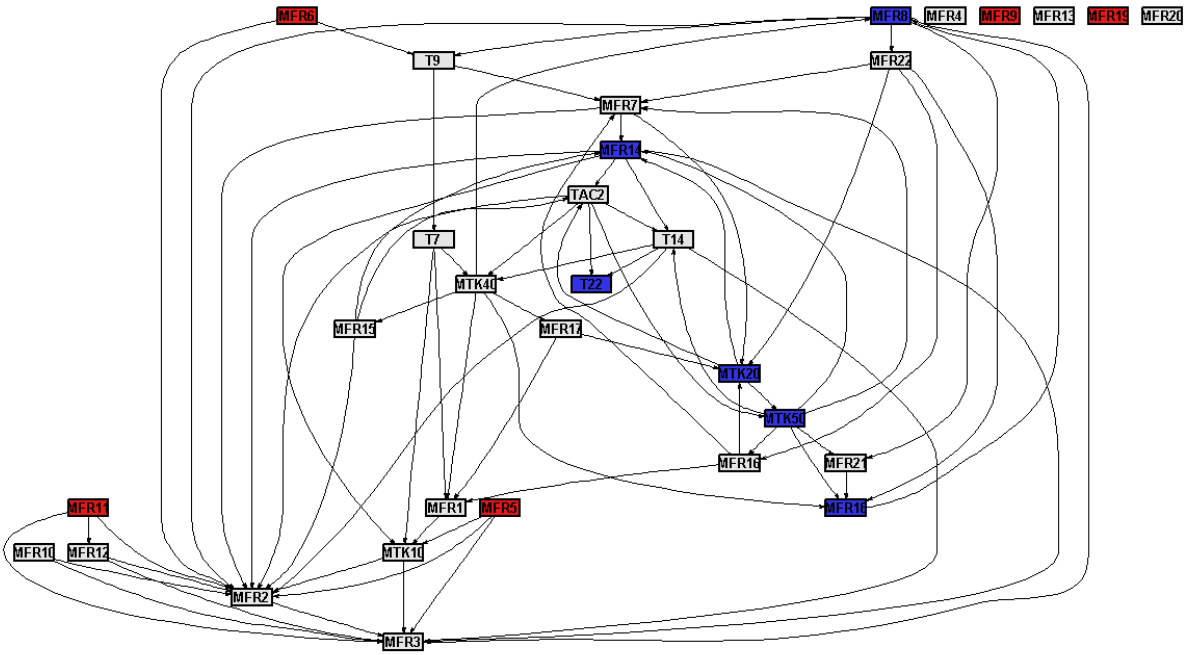

Figure C-33: Back propagation applied to the unblocked PC graph using the symptoms identified from connectivity change

For the 8th case a few symptoms are identified, not really representative, with the roots of MFR7 being a good identification of fault. So symptoms maybe, roots yes.

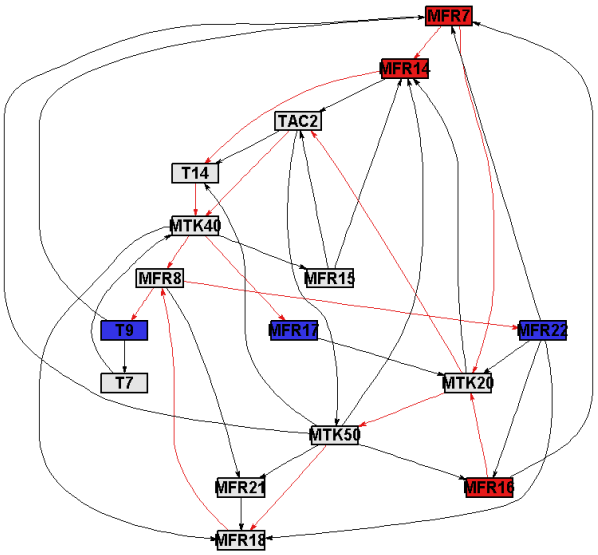

Figure C-34: Back propagation applied to the PC graph for block 1using the symptoms identified from contributions

For the 9th case a lot of symptoms are identified, none of them representative and no roots identified. So symptoms no, roots no.

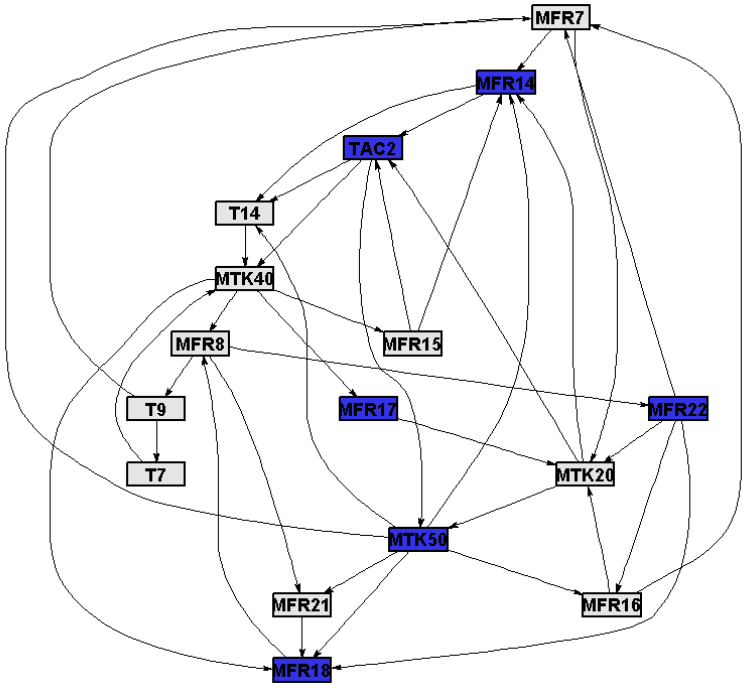

Figure C-35: Back propagation applied to the PC graph for block 1 using the symptoms identified from connectivity change

For the 10th case FMR 5and MFr11 identified as symptoms, both as possible roots. This points directly to MFR 5. So symptoms yes, roots yes.

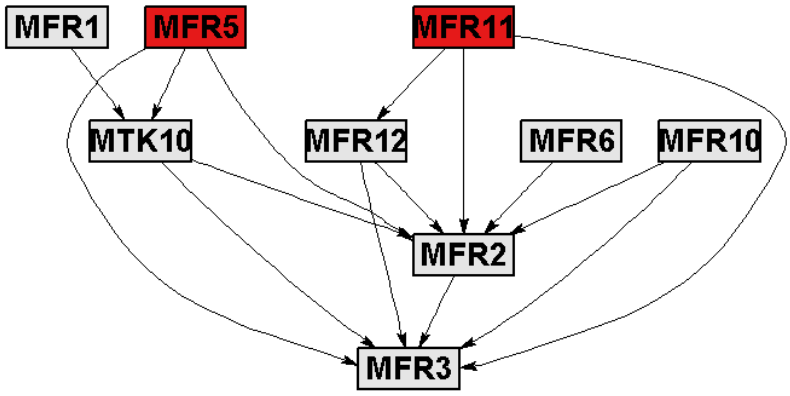

Figure C-36: Back propagation applied to the PC graph for block 2 using the symptoms identified from connectivity change

For the 11th case MFR1, MTK10 and MFR5 identified as symptoms, with T14, TAC2 and MTk40 as possible roots. So symptoms yes, roots no.

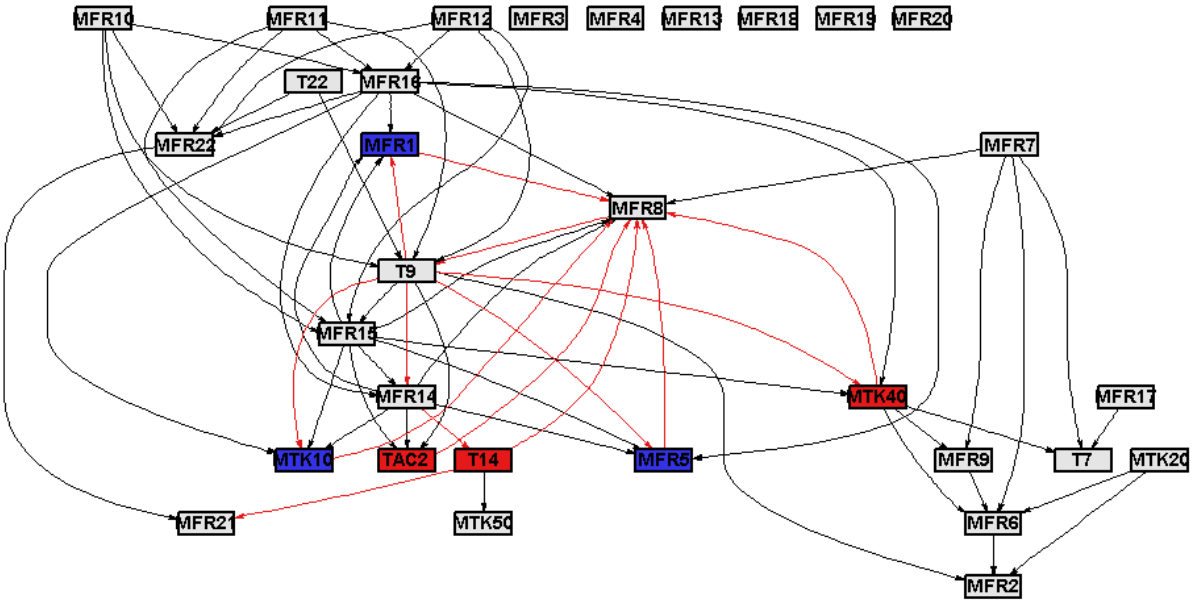

Figure C-37: Back propagation applied to the unblocked TE graph for using the symptoms identified from contributions

For the 12th case MFR2 and MFR8 were identified as symptoms with MFR10,11 and 12 being roots. So symptoms no, roots no.

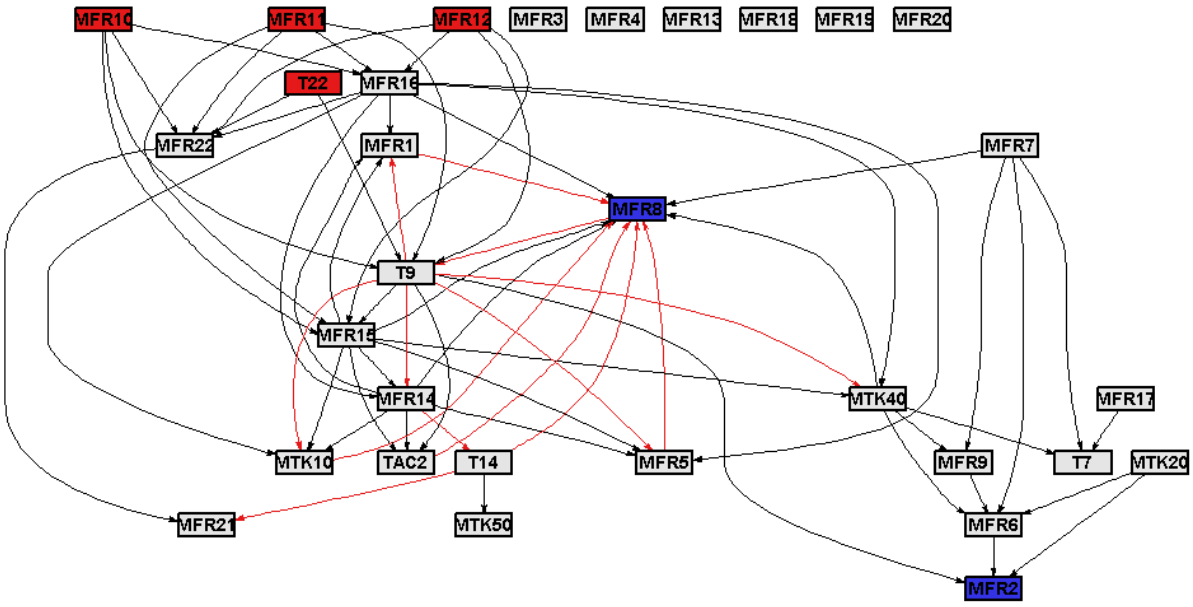

Figure C-38: Back propagation applied to the unblocked TE graph the symptoms identified from connectivity change

For the 13th case MTK10 and MFR 5 were symptoms, which is great, and MFR1 was a possible root node. So symptoms yes and roots yes.

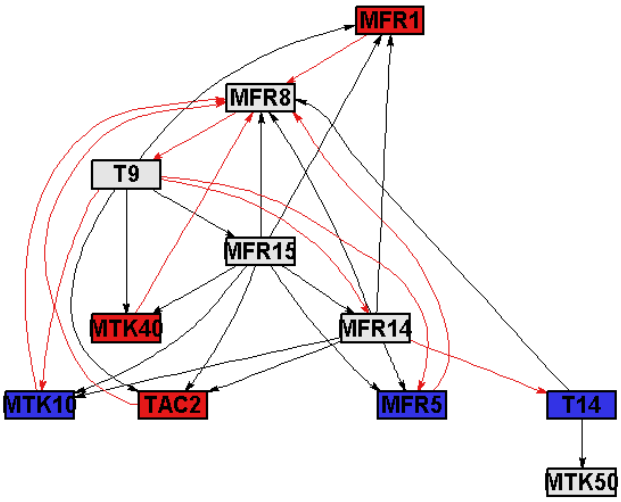

Figure C-39: Back propagation applied to the TE graph for block 1 using the symptoms identified from contributions

For the 14th case T14 and MTK40 were symptoms, not really representative, but MFr1 was identified as possible root. So symptoms maybe, roots yes.

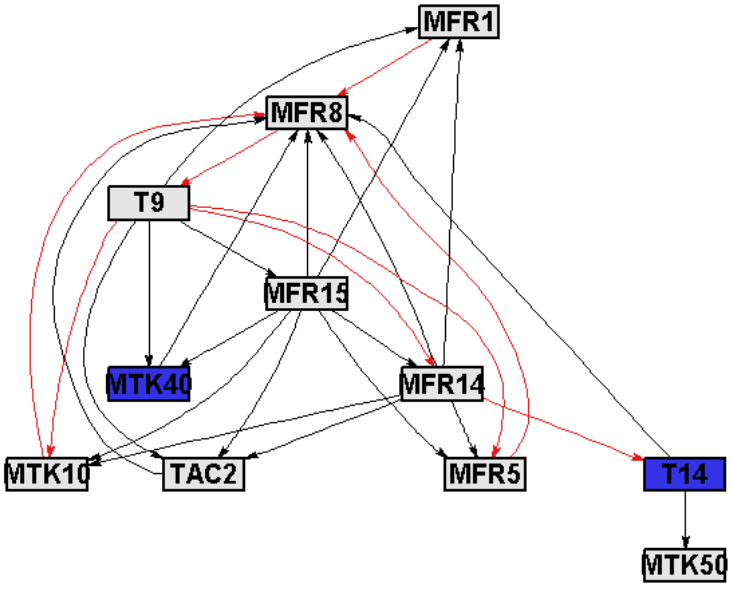

Figure C-40: Back propagation applied to the TE graph for block 1using the symptoms identified from connectivity change

For the 15th case it would be the same as the 14th.

C.2.2. Fault 2

For the first case the only symptom identified from the contributions was T14, this shows a remarkably accurate representation of the fault conditions since the cooling coil blockage would directly affect this temperature.

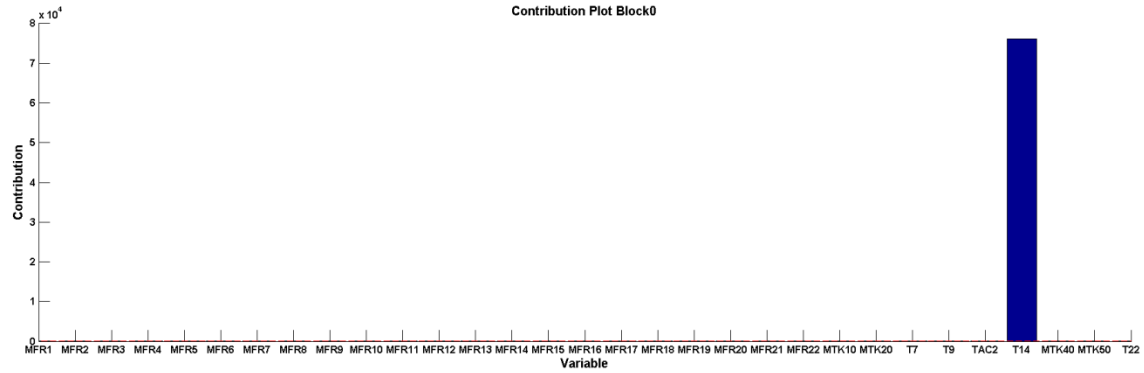

Figure C-41: Contributions to the PCA SPE for the unblocked data for the second fault

The root nodes identified include T9 and TAC2, which is also a very good representation of the possible root cause of the fault. So symptoms yes and roots yes.

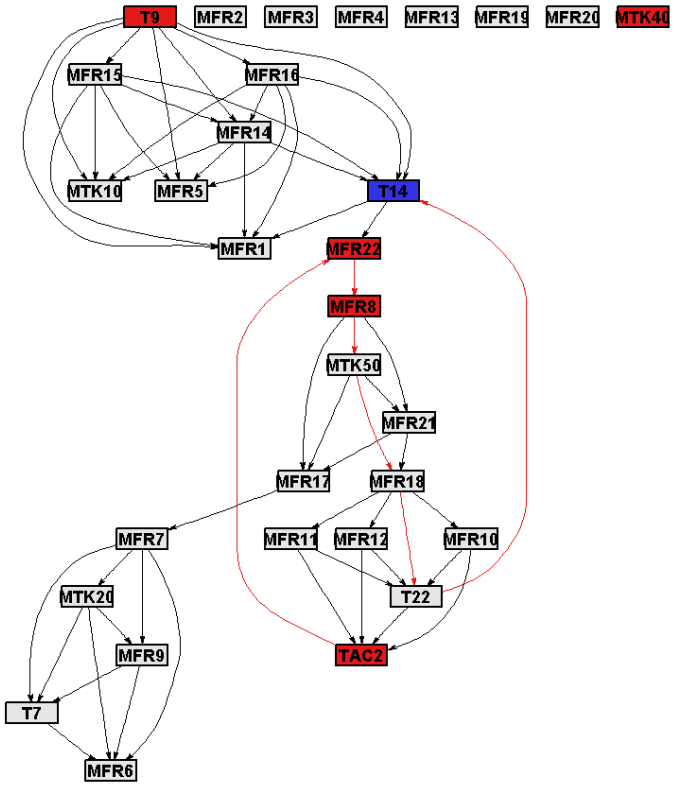

Figure C-42: Back propagation applied to the Unblocked LC graph using the symptoms identified from contributions

For the second case only a number of mass flow rates were identified as possible symptom nodes, which makes sense considering the effect of the recycle loop on the process. And the roots identified were MFR19 and MTK40, which gives no indication that there was a fault in the cooling coils.

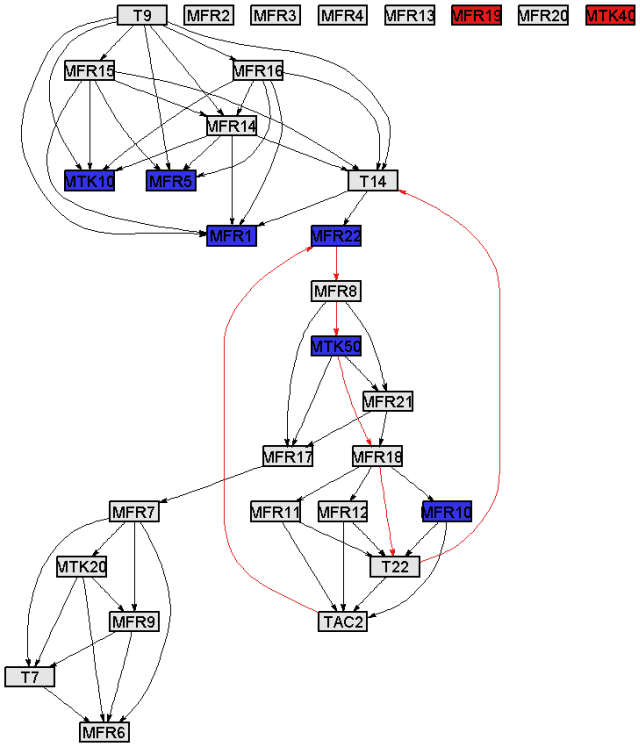

Figure C-43: Back propagation applied to the unblocked LC graph using the symptoms identified from contributions

So symptoms no and roots no. However, the reasons why the connectivity change identified these symptoms nodes is clear by looking at the graph: these variables are highly connected to the temperatures, T9, T22 and TAC2. This means that when the fault occurred there was a change in these connectives since the temperature behaved differently. Regardless, the connectivity change didn't show representative results for this case.

For the 3rd case the contributions showed MFR7 and MFR17 as symptom nodes. Since the temperatures in the autoclave would have been affected by the fault the recycle of MFR9 would have been manipulated to control the temperature, affecting MFR7 and MFR17 downstream.

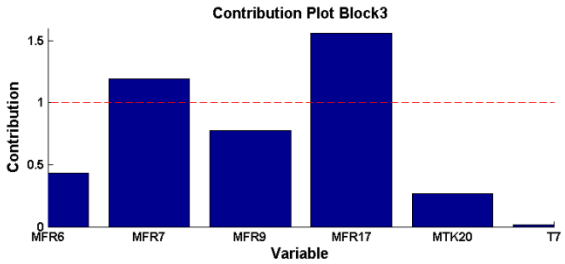

Figure C-44: Contributions for the PCA SPE for LC block 3

Applying back propagation gave MFR17 and MFR7 as possible root nodes. The symptoms could maybe be argued to be representative of this fault, but the roots don't really give any indication that

the fault had something to do with the temperatures within the autoclave. So symptoms maybe, roots no.

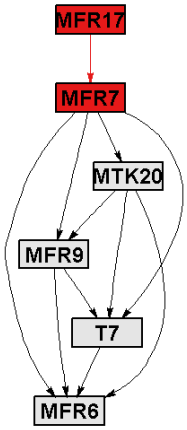

Figure C-45: Back propagation applied to the LC graph for block 3 using the symptoms identified from contributions

For the 4th case connectivity change in this block for LC gave mostly unchanged connections and no connections that rose above the significance threshold, so no symptoms were identified and no roots either.

For the 5th case, LC block1 gave the best results for KPCA. The connectivity change in this block gave a number of symptom nodes, including T14, which is promising, and MFR12, which would make sense since the amount of oxygen in the system is linked closely to the temperature. No root nodes were identified with this method, however by inspections it seems that TAC2 can be a furthest common ancestor. So symptoms yes and roots no.

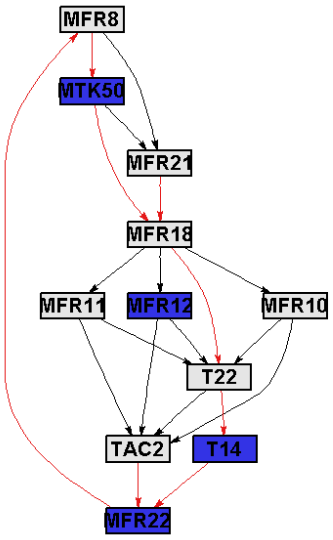

Figure C-46: Back propagation applied to the LC graph for block 3 using the symptoms identified from connectivity change

The contribution plots identified T14, MTk40 and T9 as symptom nodes, which gives a very good indication that a cooling coil fault occurred since T14 and T9 have been highlighted. Applying back propagation in the PC connectivity graph:

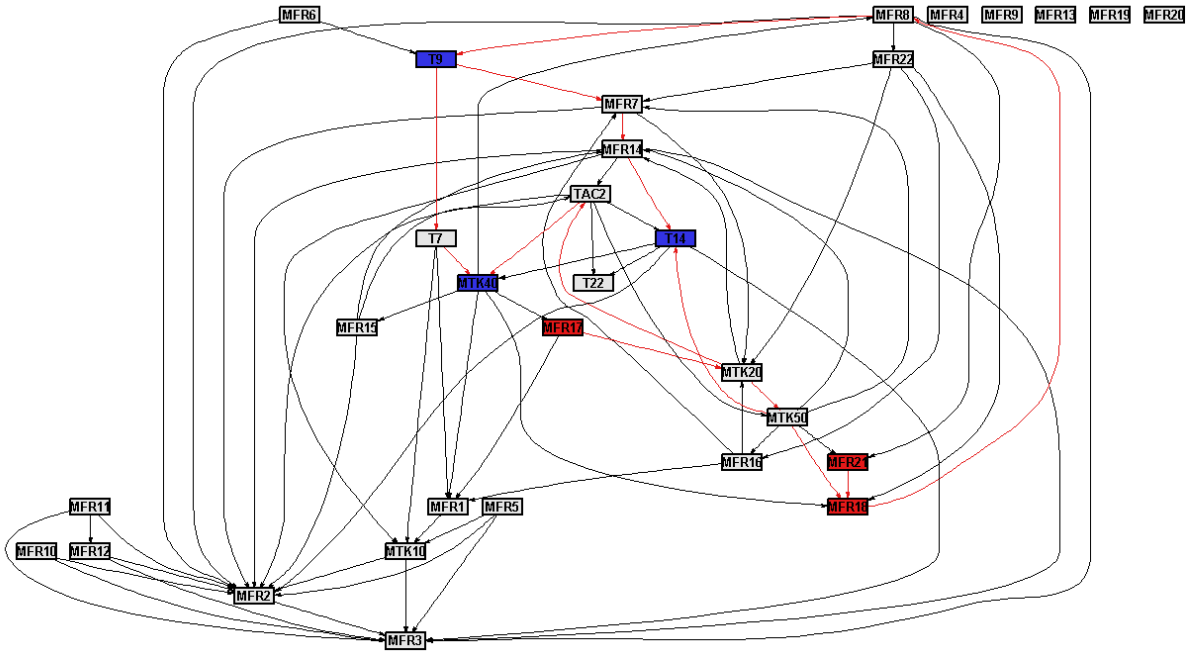

Figure C-47: Back propagation applied to the unblocked PC graph using the symptoms identified from contributions

The identified root nodes were MFR17, MFR18 and MFR21. This gives no indication that a cooling coil fault occurred. So symptoms yes, roots no.

For the 7th case connectivity change for the unblocked PC graph identified a lot of symptom nodes, most of which are not really representative of the fault. However, considering the three nodes that gave most symptom of connectivity change, MFR9, MFR7 and MFR12 it can be reasoned that the fault affected the autoclave temperature, causing the controller to change MFR9, which would affect MFR7. Alos the oxygen flow rates, MFr12, are highly connected to the autoclave temperatures, so this gives a very good indication that a cooling coil fault occurred. Applying back propagation:

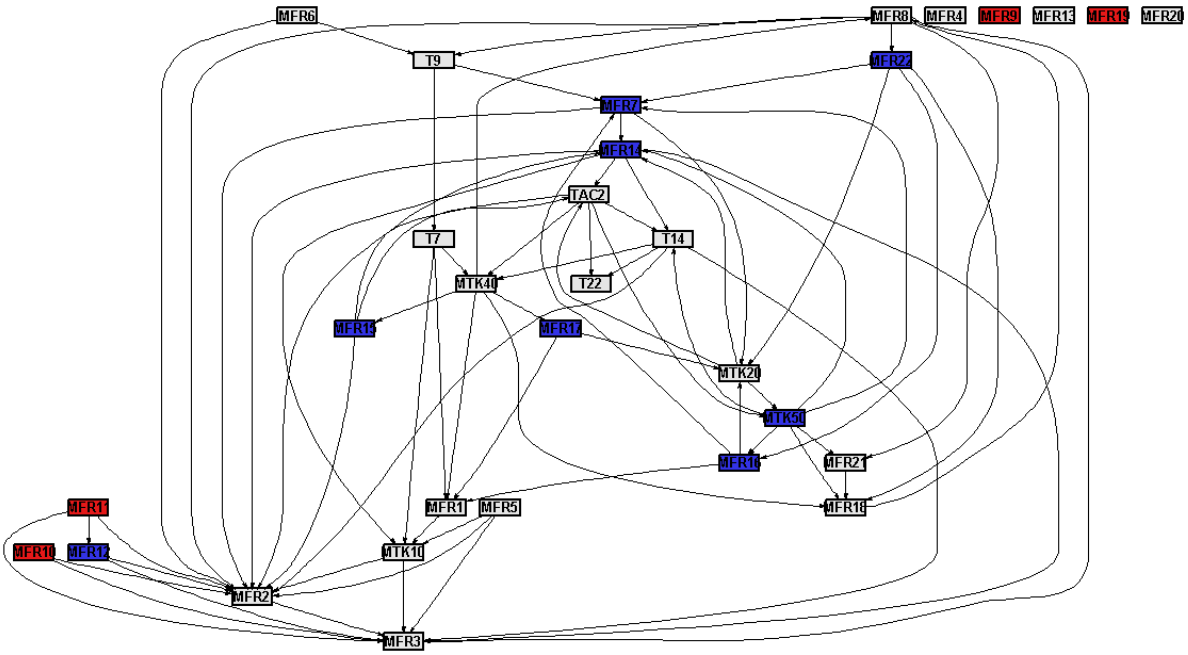

Figure C-48: Back propagation applied to the unblocked PC graph using the symptoms identified from connectivity change

The identified root nodes were MFR9,10 and 11 and MFR19. This actually gives a pretty good indication that a temperature fault occurred. So symptoms yes, roots maybe.

For the 8th case contributions in block2 of the PC blocking gives MFR1,6 and MTK10 as possible symptom nodes. It can be argued that MFR6 would be affected by the temperature in the autoclave since the vapour space in the autoclave is affected by its temperature, and also the flow rate of the recycle stream MFR9 is affected, which changes MFR6 since some of it evaporates.

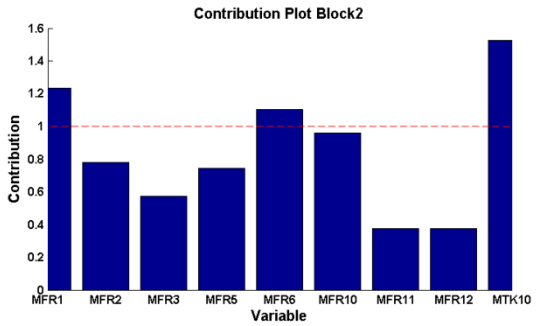

Figure C-49: Contribution plot for PCA SPE for PC block 2

Applying back propagation gives MFR1,5 and 6 and MTK10 as possible root nodes. This doesn't give any indication that a temperature fault has occurred. So symptoms maybe and roots no.

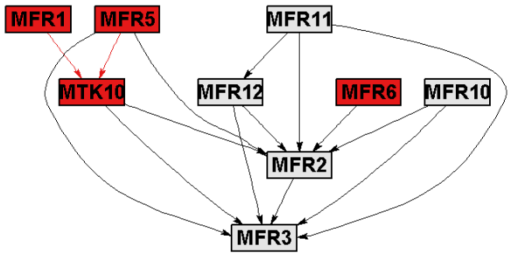

Figure C-50: Back propagation applied to PC graph for block 2 using symptoms identified from contributions

For the 9th case MFR 5 and MFR6 were identified as symptom nodes and root nodes. Although it could be argued that MFR6 would be affected by the fault since the vapour space in the autoclave could be greatly affected by the temperature, which would affect MFR6 greatly. So symptoms maybe and roots maybe.

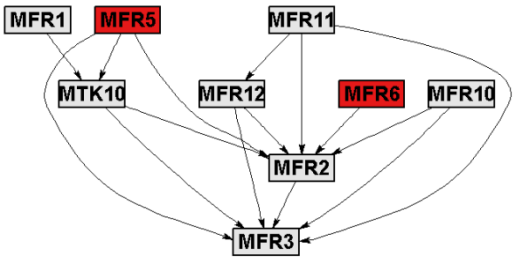

Figure C-51: Back propagation applied to PC graph for block 2 using symptoms ified from connectivity change

For the 10th case, KPCA showed the best results in the 1st block of PC. The connectivity change identified MFR15,16,17,22 and MTK50 as possible symptoms. This doesn't really give any indication that a cooling coil fault occurred. So symptoms no and roots no.

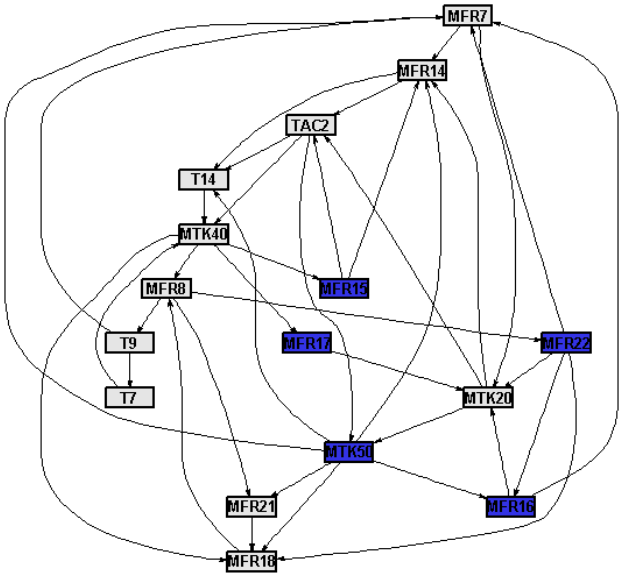

Figure C-52: Back propagation applied to the PC graph for block 1 using the symptoms identified from connectivity change

For the 11th the contribution plots identified T14, MTk40 and T9 as symptom nodes, which gives a very good indication that a cooling coil fault occurred since T14 and T9 have been highlighted. Applying back propagation in the TE connectivity graph. The main root node identified was T22, which gives a good indication that a cooling coil fault occurred. So symptoms yes and roots yes.

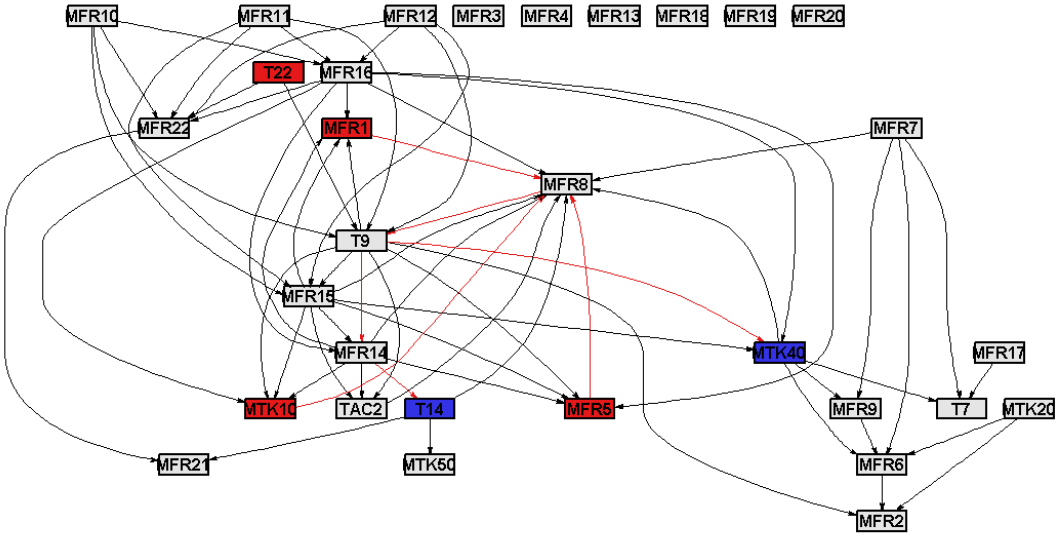

Figure C-53: Back propagation applied to the unblocked TE graph using the symptoms identified from contributions

For the 12th case the TE connectivity change highlighted some very promising symptom nodes, MFR2 and MTK40 are not really representative of the fault, but MFR6 and MFR8 would be affected by a temperature fault within the autoclave since the temperature affects its vapour space greatly, which changes MFR8 and MFR6 and also it would change MFR9 which would greatly affect MFR6. Also T9 and TAC2 were identified which directly points to a temperature fault. Applying back propagation. This identified T22 as a possible root node. This, along with the symptoms gives a very good indication that a temperature fault has occurred, which points to a cooling coil fault. So symptoms yes and roots yes.

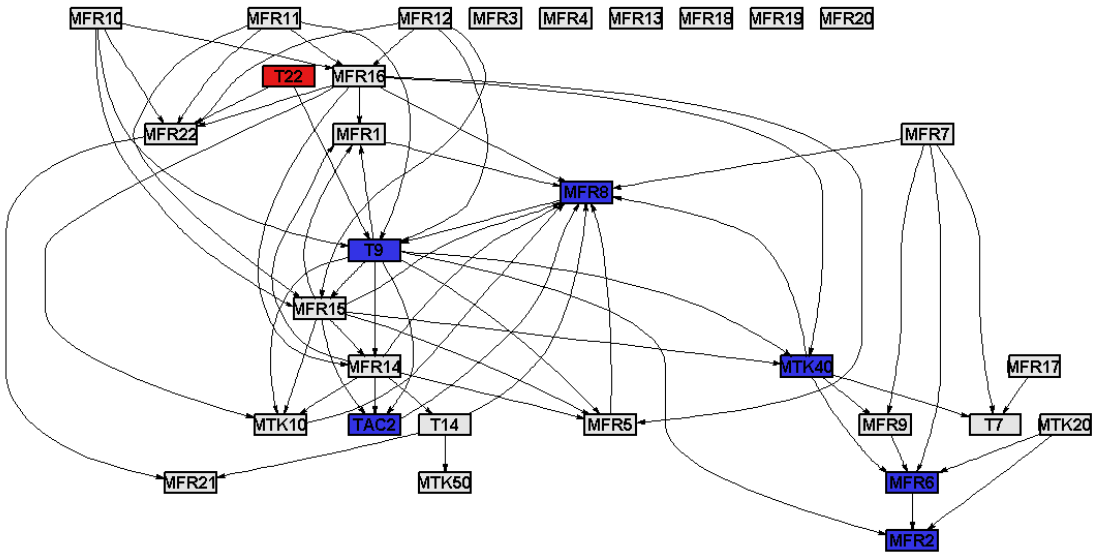

Figure C-54: Back propagation applied to the unblocked TE graph using the symptoms identified from connectivity change

For the 13th case PCA gave best results in block1. The contribution plot in this block identified T9, TAc2 and T14 and MTK40 as possible symptom nodes. This is very promising since the three autoclave temperature for the first 3 compartments have been flagged as symptoms, which clearly points to a temperature fault.

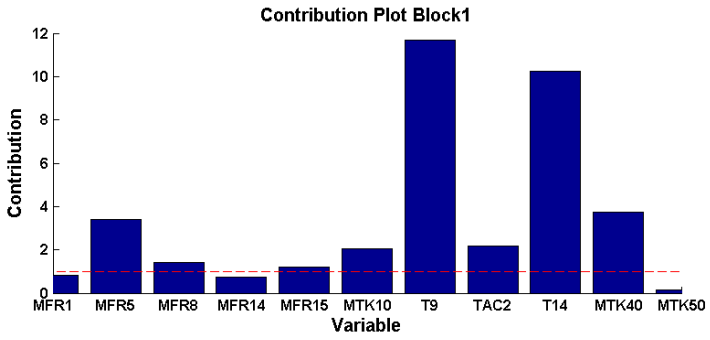

Figure C-55: Contributions to the PCA SPE for TE block 1

Applying back propagation with TE gives MFR1, FMR5 and MTK10 as possible root nodes, which really gives no indication of a temperature fault. So symptoms yes, roots no.

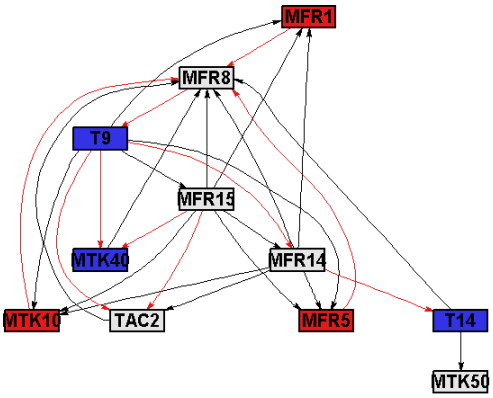

Figure C-56: Back propagation applied to the TE graph for block 1 using the symptoms identified from contributions

For the 14th case looking at the connectivity change identifies TAC2 and MTK40 as possible symptoms. Since TAC2 is present it gives a good indication that a temperature fault in the autoclave has occurred. Applying back propagation in the TE graph for block1 gives T9 and MFR15 as possible root nodes. Since T9 is identified it is a good indication that a temperature fault in the cooling coils has occurred. So symptoms yes, roots yes.

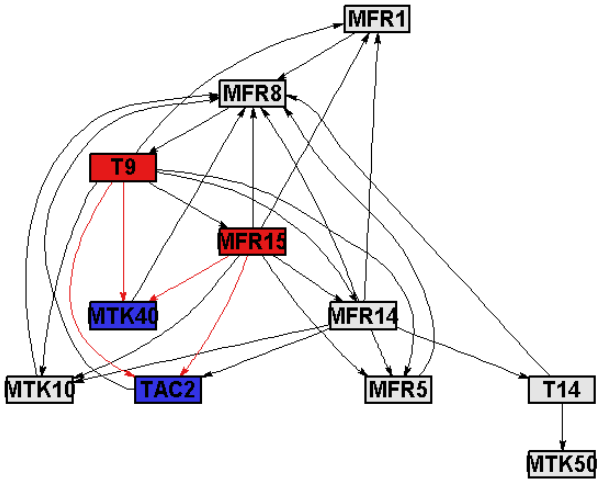

Figure C-57: Back propagation applied to the TE graph for block 1 using the symptoms identified from connectivity change

For the 15th case the results would be the same as case 14 since KPCA also gave best results in block1

Appendix D- Concentrator Case Study Results

D.1. Fault Detection

D.1.1. LC

PCA

Figure D-1 and Figure D-2 illustrate the results of using LC for blocking and then applying PCA for fault detection in each block as well as for the unblocked case. Inspection of the figures reveals that blocking in this case did not present a significant improvement for fault detection. This is because the blocking using LC resulted in one very large strongly connected component, with 31 variables, which means that tat blocks data was not much different from the full, unblocked data set. Because of this, the rest of the blocks mostly only have two variables each, meaning that they do not capture much of the process behaviour.

Block 6 showed slightly better performance, especially when considering the EWMA and CUSUM charts, but its detection delays were very high. Block 1 shows good results for the T_A^2 statistic, but bad results for the SPE. When considering both statistics and both the AUCs and DDs it can be concluded that Block 4 gave the best detection results of all the blocks. This block contained the final concentrate grade, which is linked strongly to the recovery, and the primary mill variables. This indicates that the final grade and the primary mill were strongly associated with the fault.

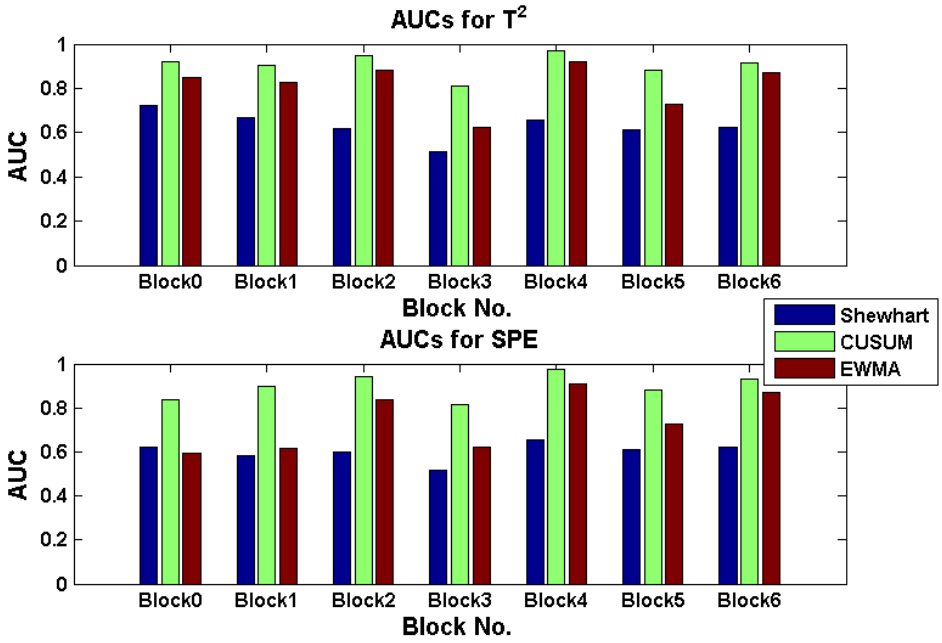

Figure D-1: AUCs for the each block as well as the unblocked case using PCA and LC for blocking

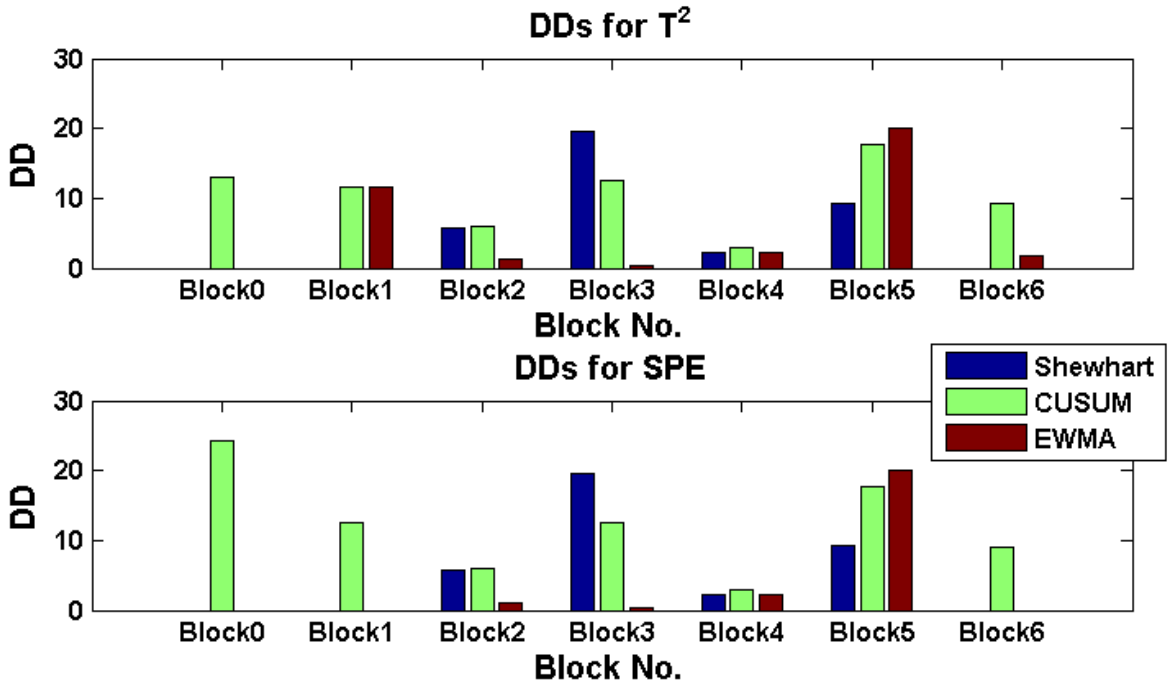

Figure D-2: DDs for the each block as well as the unblocked case using PCA and LC for blocking

KPCA

Figure D-3 and Figure D-4 illustrate the detection results using KPCA with LC blocking. Once again the cross validation just showed a decreasing trend for increasing kernel width for this data. Therefore a kernel width of 50 was chosen again, since by this value the SPE had levelled off. Even when using the data for individual blocks the same trend was observed

For the KPCA results it can be seen that for the unblocked case performed similarly to PCA in terms of AUCs, although it gave significantly better DDs. The SPE gave better results for the KPCA in the unblocked case than it did for PCA.

For the KPCA detection blocking still didn't show much improvement using the LC blocking. Again this is because the blocking gave one very large block and a number of very small ones. For KPCA Block 1 gave the best detection, with the highest AUCs and the lowest DDs. This block was the largest block obtained, with a lot of variables associated with the Mill23 mills, but also a collection of variables from other units. This does indicate that the Mill23 mills are strongly associated with this fault.

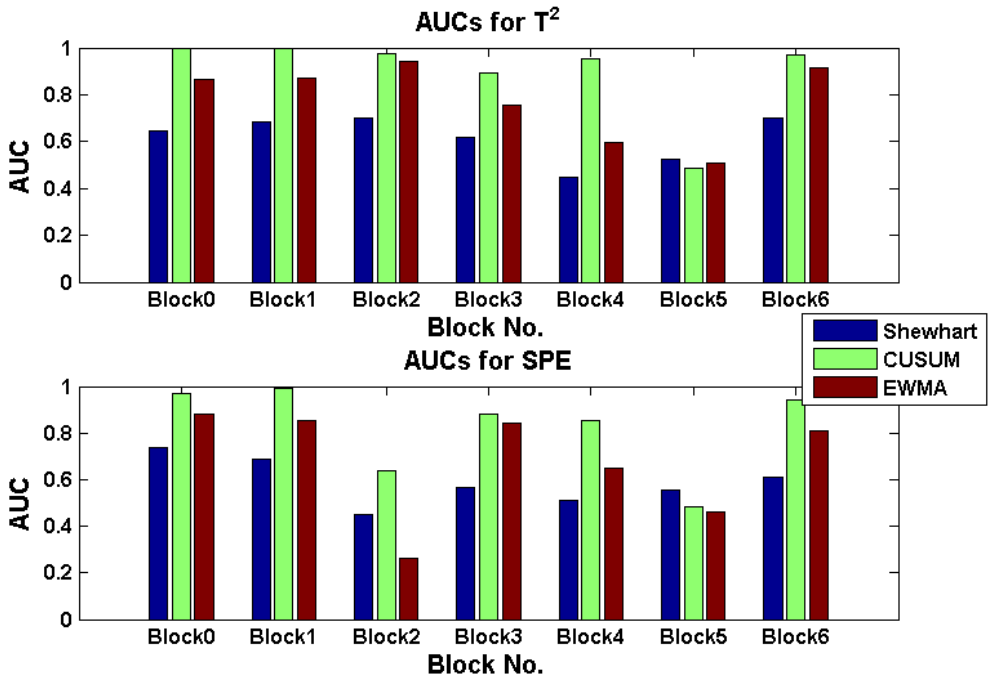

Figure D-3: AUCs for the each block as well as the unblocked case using KPCA and LC for blocking

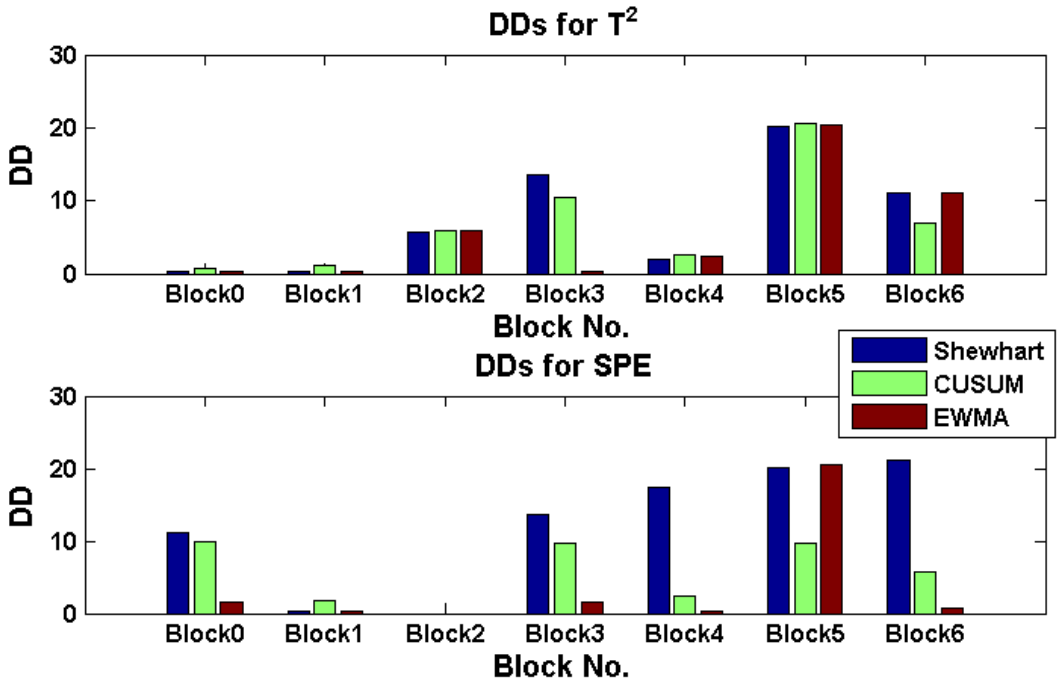

Figure D-4: DDs for the each block as well as the unblocked case using KPCA and LC for blocking

D.1.2. PC

PCA

Figure D-5 and Figure D-6 illustrate the results of using PC for blocking and then applying PCA for fault detection in each block as well as for the unblocked case. The figures clearly show that for this case blocking significantly improved the fault detection results. The AUCs for block 1 are much higher than those for any other block and much higher than for the unblocked case. The DDs are also much

lower than the others. Block1 contains the variables around the Mill23 mills, as well as the chrome cyclone classification splitting. The results here indicate very strongly that the Mill23 mills are strongly affected by the fault occurring. Block8 showed the second best results. Block 8 contains the chrome cyclone variables, so this indicates that the fault may be upstream of the Mill23 mills, affecting the cyclone as well. This is the block that deals the most with the Mill23 mills, indicating that the fault is somehow associated with these mills

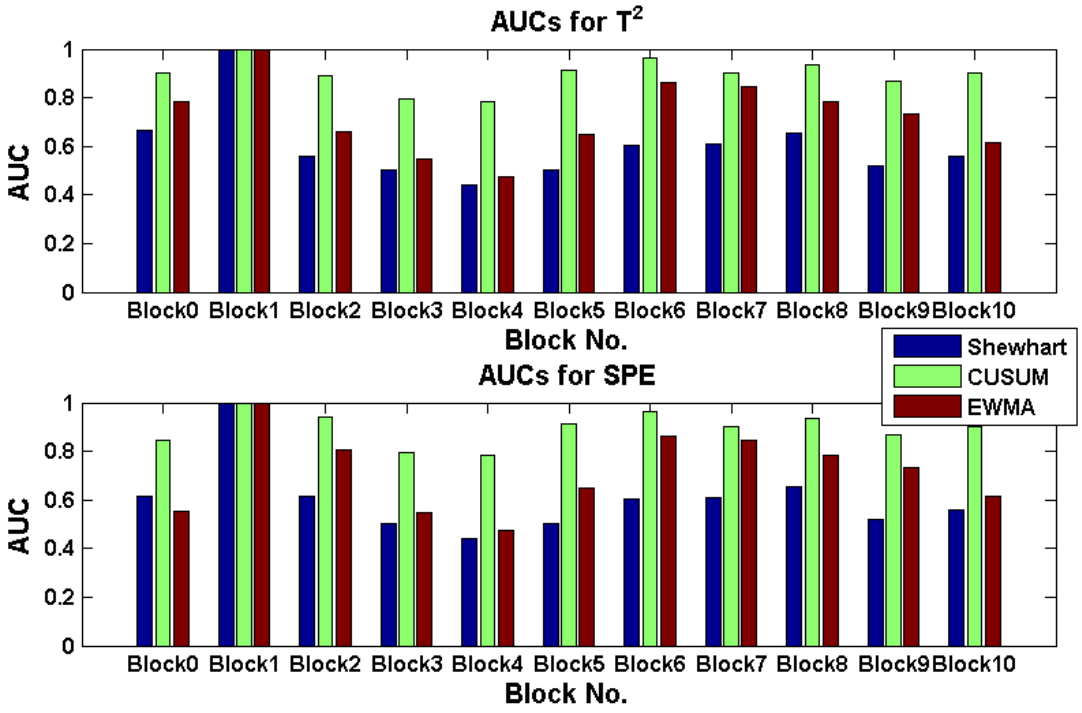

Figure D-5: AUCs for the each block as well as the unblocked case using PCA and PC for blocking

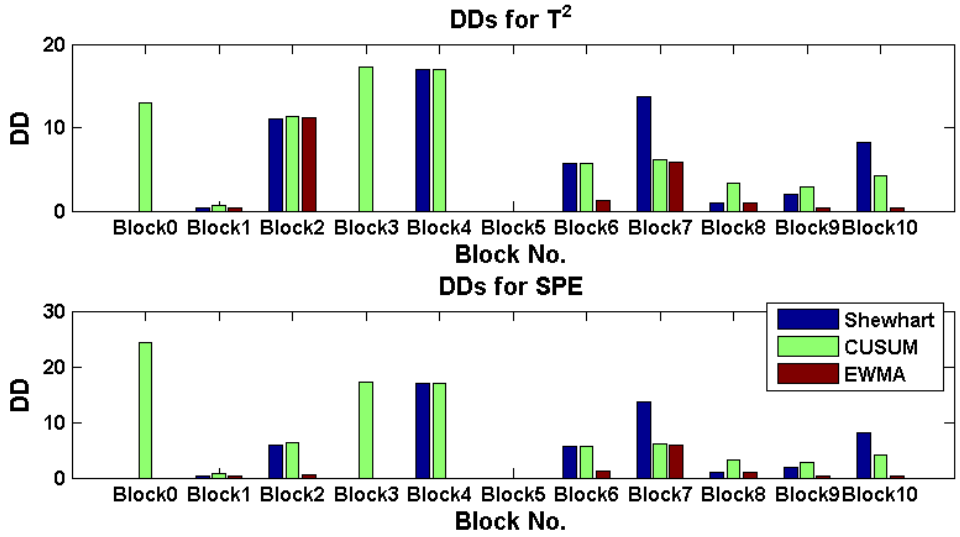

Figure D-6: DDs for the each block as well as the unblocked case using PCA and PC for blocking

KPCA

Figure D-7 and Figure D-8 illustrate the detection results using KPCA with PC blocking. Once again the cross validation just showed a decreasing trend for increasing kernel width for this data. Therefore a kernel width of 50 was chosen again, since by this value the SPE had levelled off. Even when using the data for individual blocks the same trend was observed. For the KPCA results it can be seen that for the unblocked case performed similarly to PCA in terms of AUCs, although it gave significantly better DDs. The SPE gave better results for the KPCA in the unblocked case than it did for PCA. For KPCA it was Block 8 that showed the highest AUCs and relatively low detection delays, with block 1 showing the second best results. This supports the conclusion that both the cyclone and the Mill23 mills are greatly affected by the fault conditions.

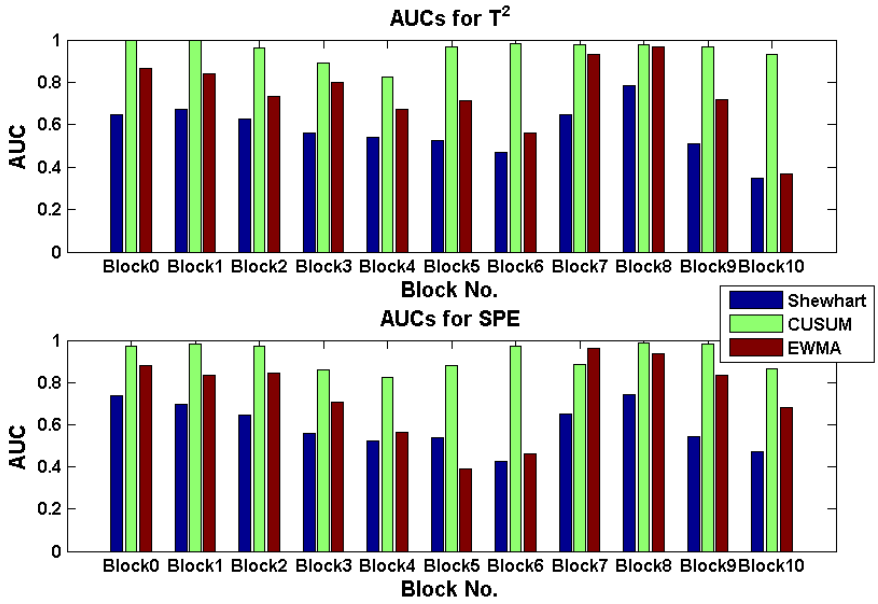

Figure D-7: AUCs for the each block as well as the unblocked case using KPCA and PC for blocking

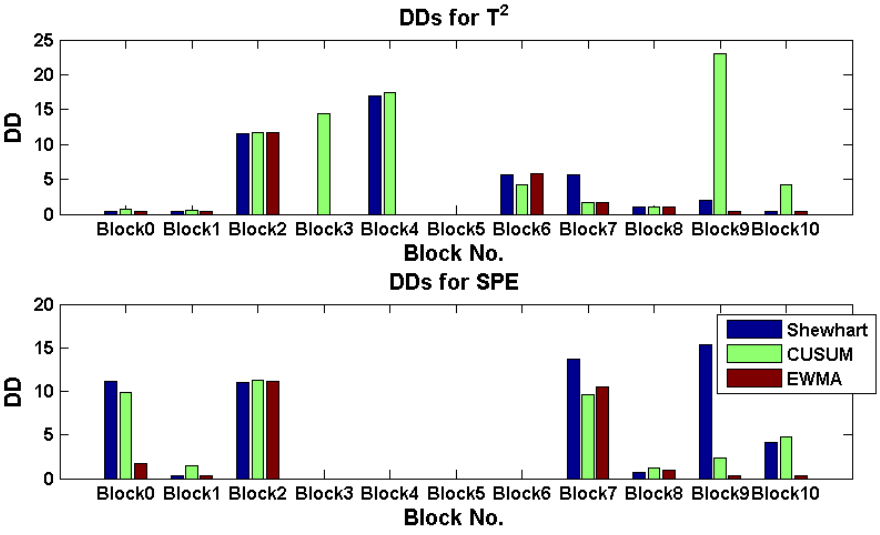

Figure D-8: DDs for the each block as well as the unblocked case using KPCA and PC for blocking

D.2. Fault Identification

In the unblocked case contributions to SPE of the PCA model showed Mill23O2Power, Split2 and Recovery as the largest contributors to this fault, as illustrated in Figure 7-14. Since the recovery was the symptom of the fault that was recognised by the operators observing the time series trend in the data, this is very accurate.

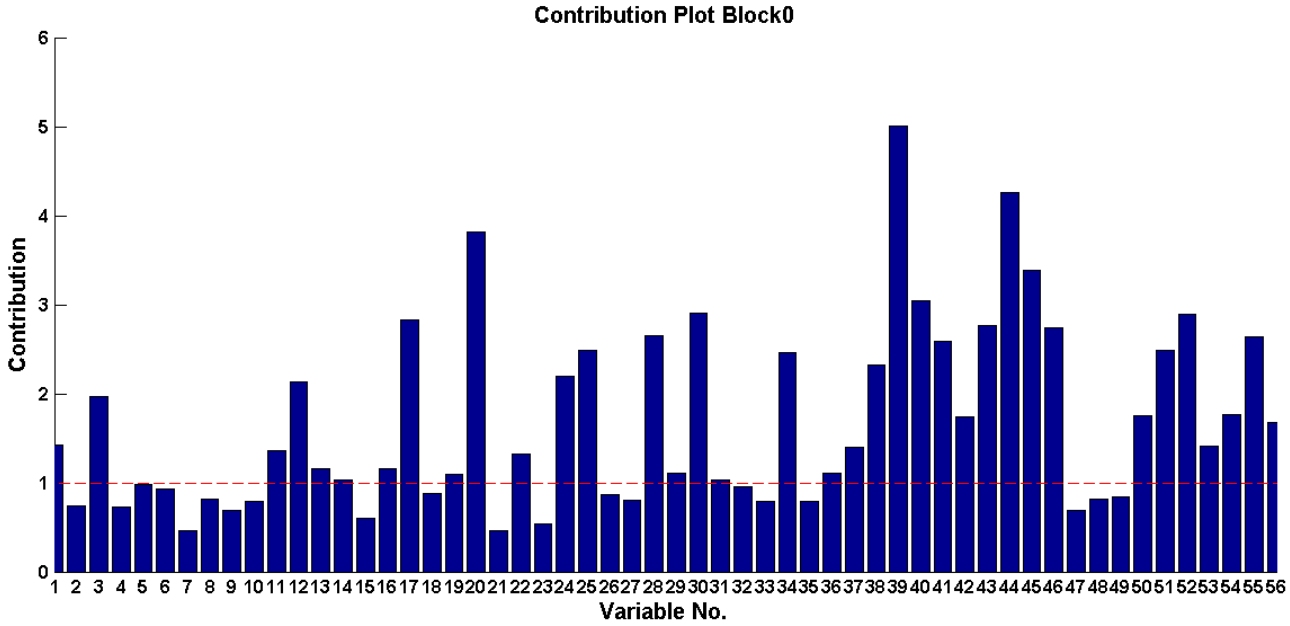

Figure D-9: Contribution plot for PCA SPE for Concentratore recovery fault for unblocked data

D.2.1. LC

For the first case using the contributions obtained from the unblocked PCA model for symptom node identification and applying back propagation in the unblocked connectivity graph showed the following results for possible roots. The main possible root was the primary mill's load

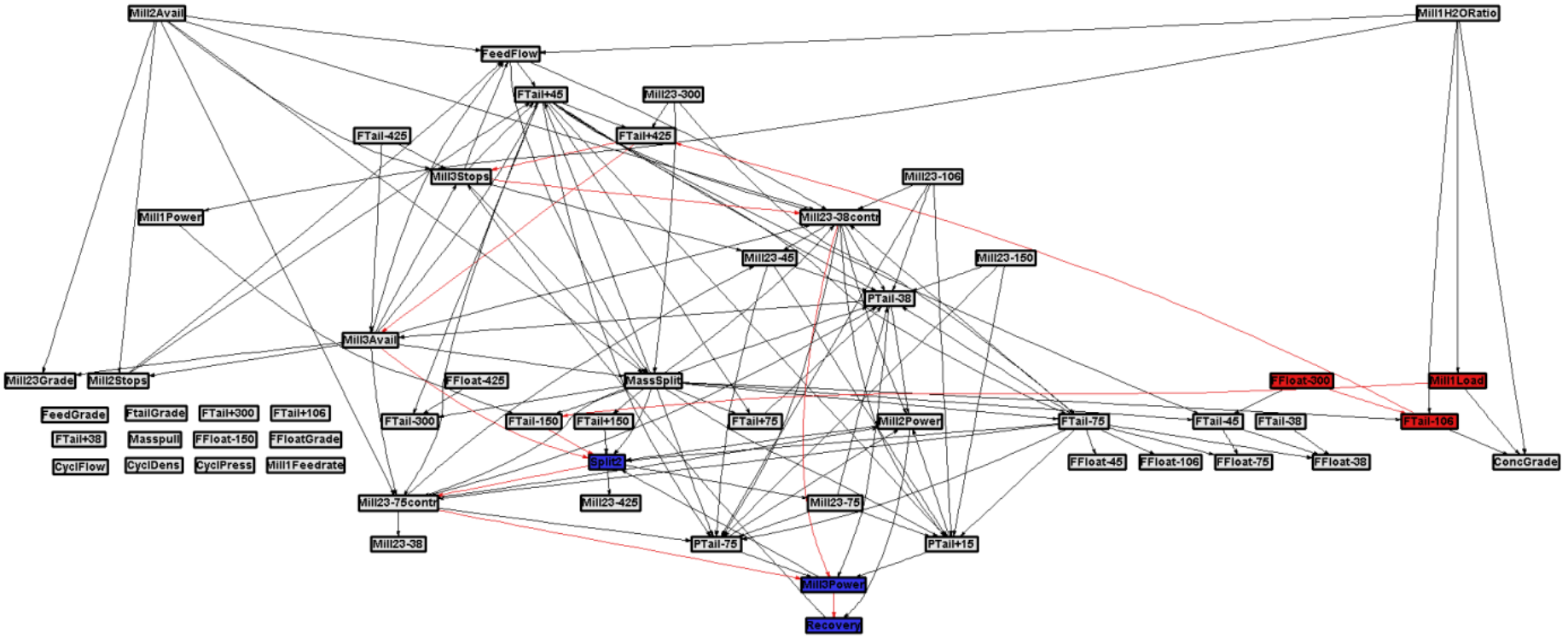

Figure D-10: Back propagation applied in the unblocked LC graph from the symptoms identified by contributions

For the second case, using the change in LC to identify possible symptom nodes resulted in Ftail PSD and Mill2 power and Smil02Stops being identified as symptoms. This indicates an effect on the Mill23 mills. Observing the change in connectivity shows that Mill232Stops underwent a significant transformation, becoming an apparent driving factor for many other variables.

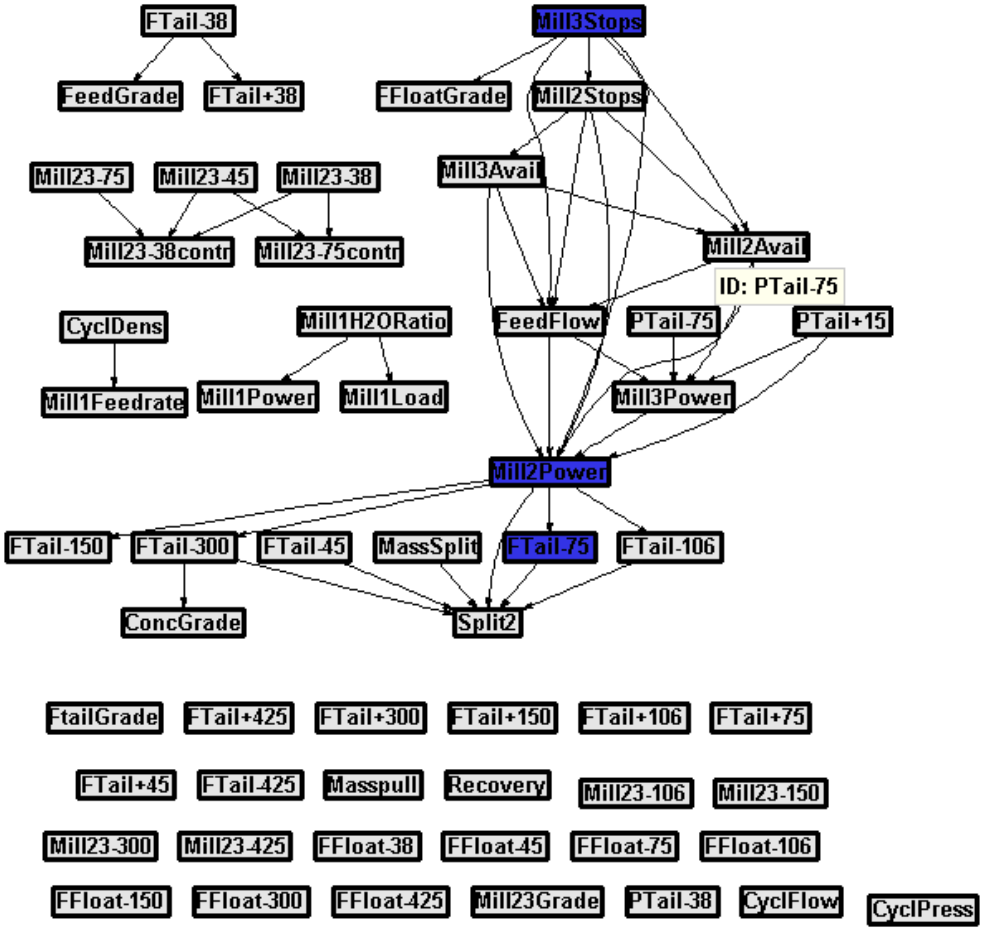

Figure D-11: Connectivity change for unblocked LC graph

Applying back propagation in the unblocked connectivity graph using the symptoms identified by connectivity change resulted din the results shown in Figure D-12. This resulted in Mill2Avail being identified as the possible root node. This indicates some fault associated with the Mill23 mills or something just upstream thereof.

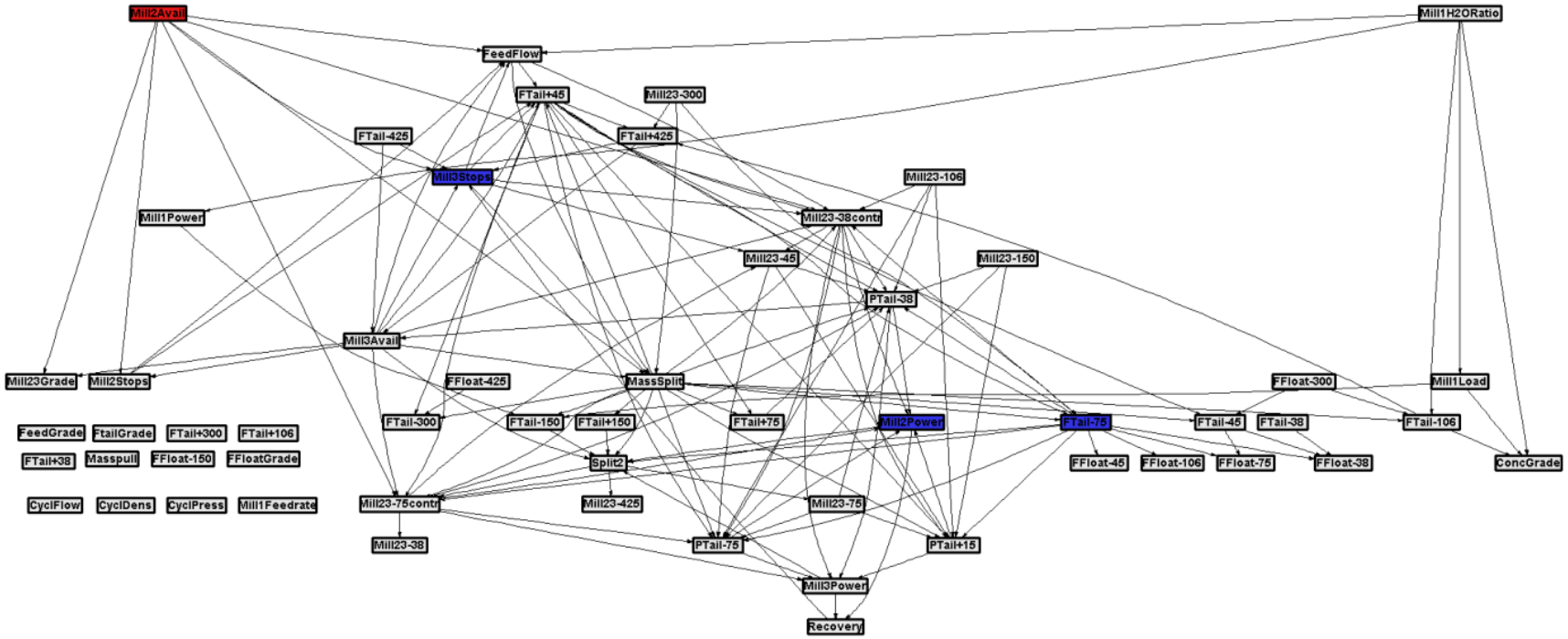

Figure D-12: Back propagation applied in the unblocked LC graph from the symptoms identified by connectivity change

For the 3rd case the contributions in Block 4, which gave the best detection results for LC, are shown in Figure D-13. This block contains few variables, and the three of them that showed major contributions were the primary mill's power, its load and its inlet water ratio.

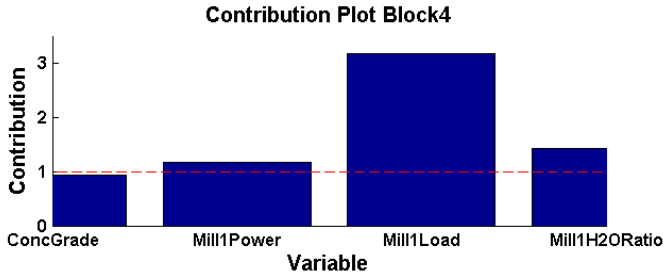

Figure D-13: Contributions for LC block 4 for PCA SPE

Applying back propagation in the LC graph for Block 4 using the symptoms identified by contributions resulted in Mill1H2OinRatio being identified as the possible root, as shown in Figure D-14.

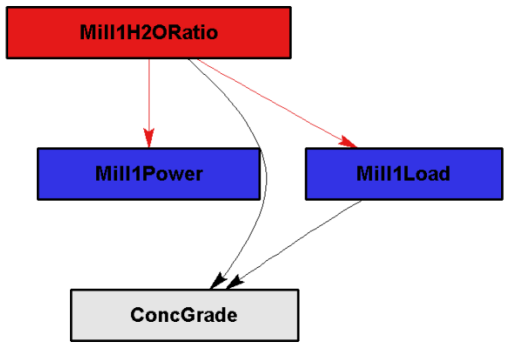

Figure D-14: Back propagation applied in block 4 of the LC graph from the symptoms identified by contributions

For the 4th case the change in LC in block 4 was used to determine possible symptom nodes. However, no symptoms were identified and therefore no roots could be identified. The reason no symptoms were identified is that only two edges disappeared, the edges to ConcGrade

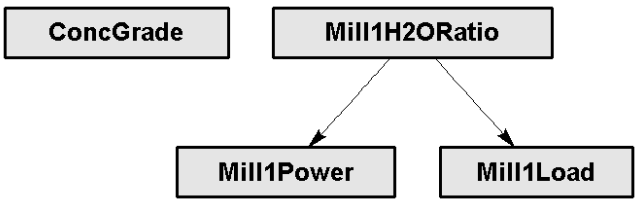

Figure D-15: Connectivity change for LC in block 4

For the 5th case connectivity change was used to identify symptom nodes in the block that gave the best detection results for KPCA, Block 1. This resulted in Ftail-75, Mill2Power and Mill3Stops being

identified as possible symptom nodes. These are exactly the same node that were identified for the unblocked graph's connectivity change.

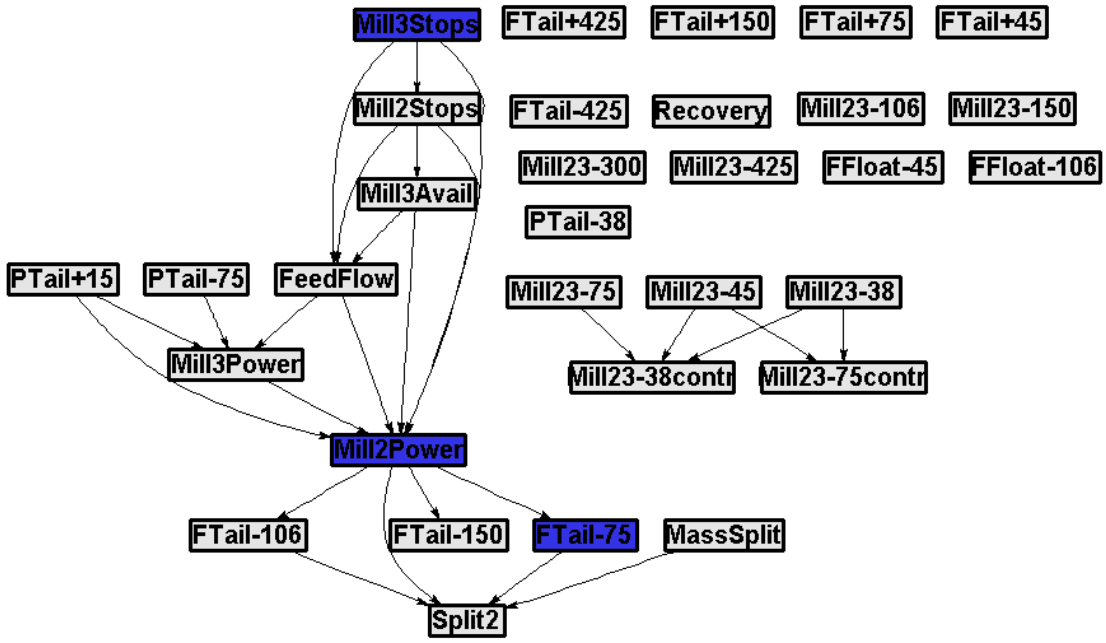

Figure D-16: Connectivity change for LC in block 1

Applying back propagation in the LC graph for Block1 resulted in no root nodes being identified.

D.2.2. PC

For the 6th case applying back propagation in the unblocked PC graph using the symptoms identified from contributions resulted in FtailGrade being identified as a possible root node, as shown in Figure 7-15.

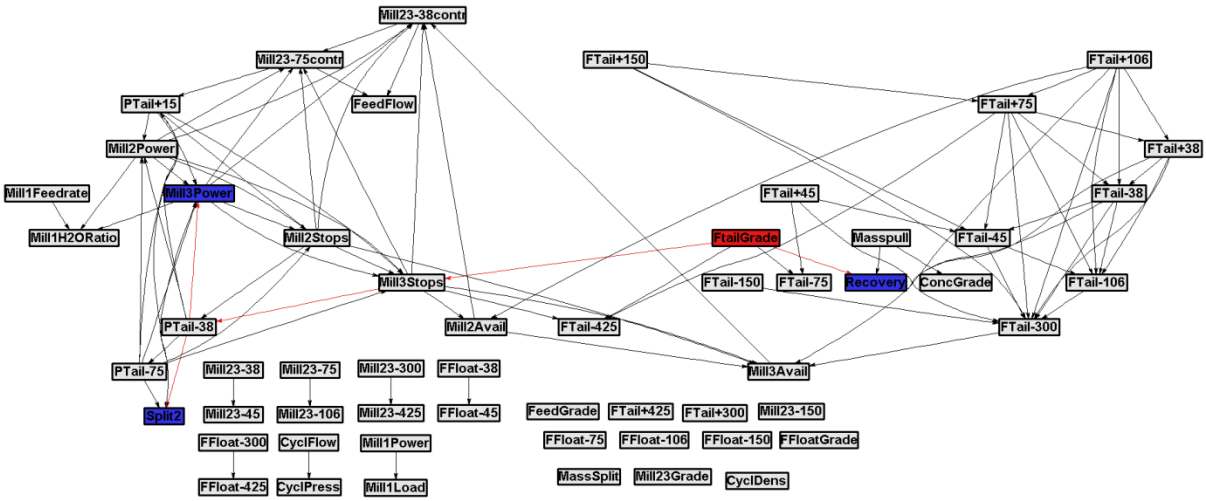

Figure D-17: Back propagation applied in unblocked PC graph from the symptoms identified by contributions

For the 7th case the change in PC was used to identify possible symptoms.

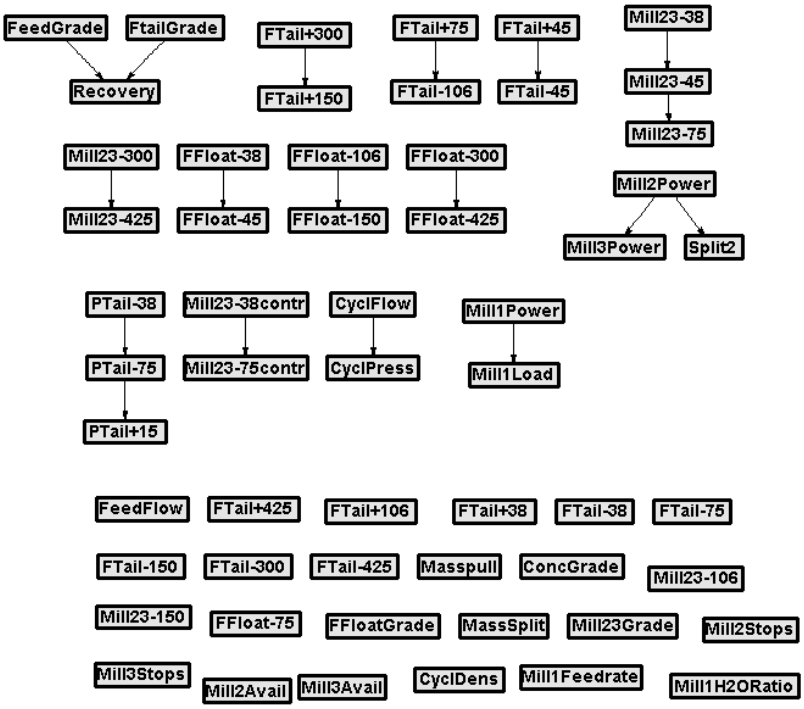

Figure D-18: Connectivity change for unblocked PC

FFloat-106, FFloat-150 FeedGrade and FtailGrade being identified as possible symptoms and possible roots.

For the 8th case looking at the contributions of individual variables in th block that gave the best detection results for PCA in the PC blocking method gave Mill3Power, Mill3Stops and Mill3Avalil as the largest contributors to the SPE, as shown in Figure 7-17. In fact, with the exception of PTail+15, all the variables that showed increased contributions had to do with the Mill23 mills. These symptoms are similar to those for cases 1, 2, and 5 and 6.

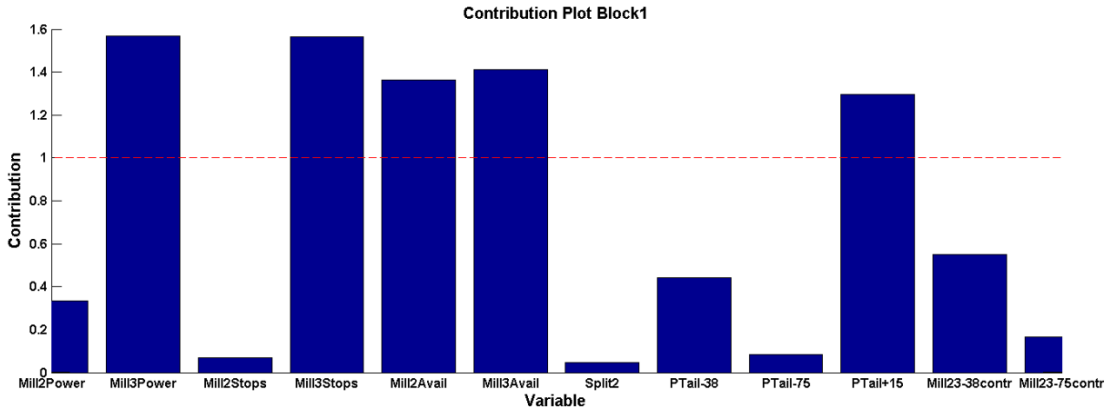

Figure D-19: Contribution plot for PCA SPE in PC Block 1

Applying back propagation in the PC graph for Block1, using the symptoms identified by contributions then resulted in Mill23-38contr, Mill2Avail and Mill3Avail being identified as possible

root nodes, as shown in Figure 7-18. This is similar to the results obtained by using LC unblocked connectivity change

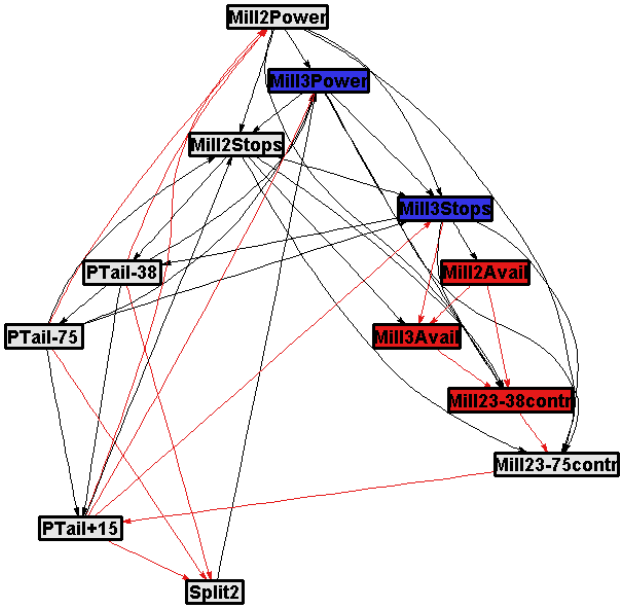

Figure D-20: Back propagation applied in block 1 of the PC graph from the symptoms identified by contributions

For th 9th case looking at the change in PC in the block that showed the best detection results for PCA, Block 1, identified Mill2Power and Split2 as possible symptom nodes. This again indicates that the Mill23 mills are associated with the fault.

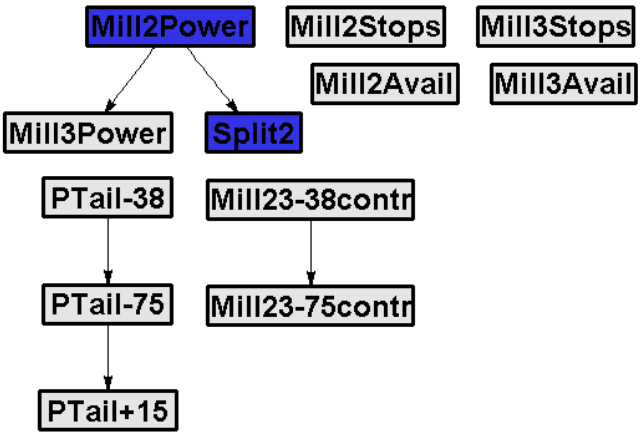

Figure D-21: Connectivity change for PC in block 1

Applying back propagation in the PC graph for block 1 using the symptoms identified by connectivity change resulted in the PTails PSD being identified as possible root nodes, as shown in Figure 7-20.

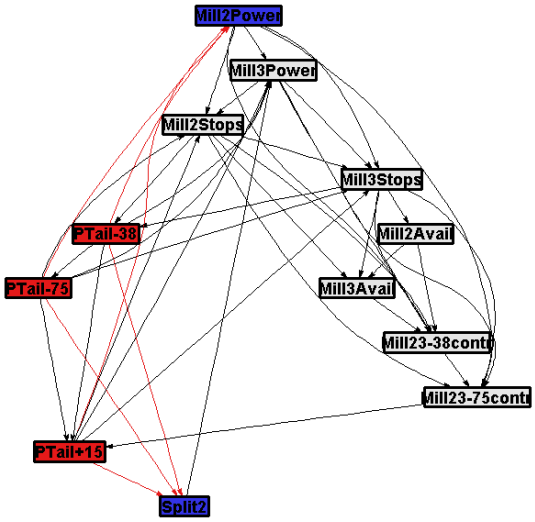

Figure D-22: Back propagation applied in block 1 of the PC graph from the symptoms identified by connectivity change

For the 10th case the change in PC in block8, which showed the best results for KPCA was used to determine the symptoms. However, block 8 only has two variables, as shown in Figure 7-21:. Therefore connectivity change gave no results. However, since the fault is in this block and there are only two nodes, and only one of them is a root node it can be concluded that CyclFeedFlow was the identified root node in this case.

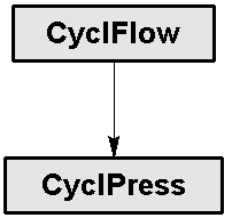

Figure D-23: PC block 8

D.2.3. TE

For the 11th case applying back propagation in the unblocked TE graph using the symptoms identified by PCA SPE contributions the possible root nodes identified wereFtail-106 and SplitCr, as shown in Figure D-24.

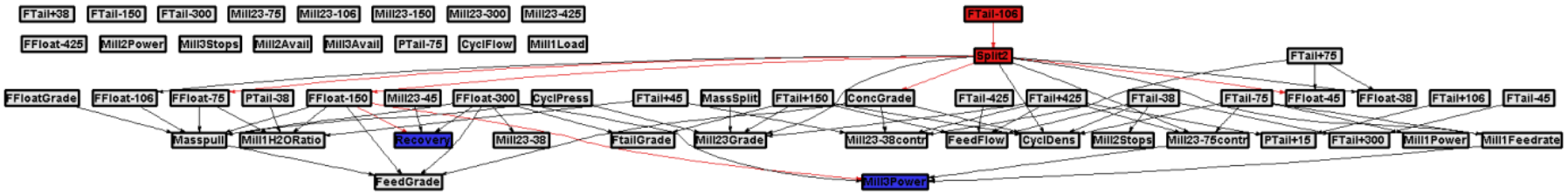

Figure D-24: Back propagation applied in the unblocked TE graph from the symptoms identified by contributions

For the 12th case, looking at the change in connectivity of the unblocked TE graph identified ConcGrade and the FFloat PSD as possible symptoms. Interestingly the TE is the only graph that became better connected using fault rather than NOC data

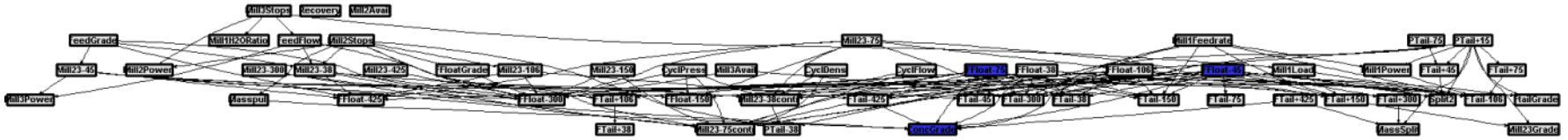

Figure D-25: Connectivity change for unblocked TE

Applying back propagation in the TE graph using the symptoms identified by connectivity change resulted in the Ftail PSD, Mill23 PSD and Split2 being identified as possible roots of the fault.

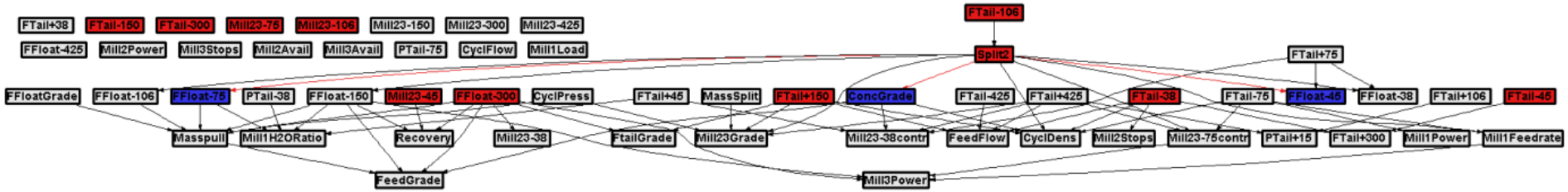

Figure D-26: Back propagation applied in the unblocked TE graph from the symptoms identified by connectivity change

Appendix E- Publications Based on this Thesis

Two peer-reviewed conference papers based on work performed for this thesis were submitted and accepted:

1) The first was for the International Federation of Automation and Control's (IFAC) conference in Cape Town, 2014, and was based on the work performed for the two-tank simulation case study. Title: Data driven fault detection with process topology for fault identification.
2) The second was for the International Mineral Processing Conference (IMPC) in Santiago, Chile, 2014, and was based on the work performed for the autoclave leaching simulation case study. Title: Exploiting process topology for fault diagnosis in a simulated pressure leaching system.